AN ABSTRACT OF THE THESIS OF

Kevin J. Tillotson for the degree of Master of Science in Oceanography presented on December 21, 1994. Title: Wave Climate and Storm Systems on the Pacific Northwest Coast.

Redacted for Privacy

Abstract Approved: _____

Paul D. Komar

A diverse assortment of wave measurement systems have been used along the Northwest coasts of Oregon and Washington. The present study compares wave data derived from these measurement systems to obtain a representative ocean wave climate for the region. Wave measurements have been derived from deep-water buoys of the National Data Buoy Center (NDBC) of NOAA, and from shallow-water pressure sensor arrays and deep-water buoys of the Coastal Data Information Program (CDIP) of Scripps Institution of Oceanography. Data have also been obtained for the past 20 years from a microseismometer system, a technique based on measuring seismic vibrations produced by ocean waves. Finally, the Wave Information Study (WIS) of the U.S. Army Corps of Engineers has produced 20+ years of wave data spanning 1956-75 from hindcasts based on daily weather charts.

The deep-water wave climate is essentially uniform along the Pacific Northwest coastline, though there are some systematic differences between data sets. The NDBP buoy yields wave heights that are roughly 8% higher than the two CDIP buoys. The microseismometer system yields wave heights in good agreement with the buoy data, but no trend is found when comparing wave periods which are systematically too high when derived from the microseismometer. Significant wave heights derived from WIS hindcast techniques are roughly 30-60% higher than measurements by the buoys.

The data sets indicate a marked seasonality in the annual wave climate of the Pacific Northwest, with mean-monthly significant wave heights in the summer months ranging from 1.25 to 1.75 meters, increasing to 2 to 3 meters in the winter months. Major Individual storms have yielded significant wave heights from 6 to 7 meters, with corresponding calculated wave breaker heights of 9 to 10 meters on Northwest beaches. Mean-monthly dominant wave periods range from 7 to 9 seconds during summer months, increasing to 11-13 seconds in winter months.

Due to the systematic differences between measured and hindcast wave heights, the WIS data could not be used to predict extreme-wave parameters. The largest storm waves measured during the 23-year continuous record of microseismometer and deep-water buoy measurements had a deep-water significant wave height of 7.3 meters. The projection of the 50- and 100-year extreme wave heights for storms with heights exceeding 5 meters yields deep-water significant wave heights of 8.2 and 8.8 meters respectively.

WAVE CLIMATE AND STORM SYSTEMS ON THE PACIFIC NORTHWEST COAST

by

Kevin J. Tillotson

A THESIS

submitted to

Oregon State University

in partial fulfillment of
the requirements for
the degree of

Master of Science

Completed December 21, 1994
Commencement June 1995

Master of Science thesis of Kevin J. Tillotson presented on December 21, 1994.

APPROVED:

Redacted for Privacy

Major Professor, representing Oceanography

Redacted for Privacy

Dean of College of Oceanography

Redacted for Privacy

Dean of Graduate School

I understand that my thesis will become part of the permanent collection of Oregon State University libraries. My signature below authorizes release of my thesis to any reader upon request.

Redacted for Privacy

Kevin J. Tillotson, Author

ACKNOWLEDGMENTS

Faced with the frightening prospect of actually having to find a job, I entered the graduate program in physics at OSU in the fall of 1990. As it turned out, graduate physics was harder than working. Given my natural affinity for things of a fluid nature - beer and wine - I decided to pursue a masters degree in oceanography.

I was fortunate to take a course from Dr. Paul Komar where I immediately gained an interest in coastal science. I was also fortunate that Paul decided to take me on as his graduate student. I want to thank Paul for all his guidance and help in the writing of this thesis. I would also like to thank Dr. Rob Holman for allowing me to be a permanent fixture in his lab.

John Stanley, a guru among gurus, helped immensely in the completion of this work. Though he always threatened that he could destroy my data at the mere push of a button, in the interest of science he decided only to hassle me for his own amusement. Thanks, John.

Special thanks go out to all the folks who made my stay in Corvallis memorable and fun. In particular: Mark L., Tom A., Mark M., Brady, Diane, Nathaniel, Todd, Dylan, Diana, and Chris. Thanks most of all to Darcy for love, support, and enduring many, many hours of my preoccupation with this thesis. My fine friend Mark Lorang was always around to provide the necessary distractions, and to remind me (through the words of Jimmy Buffet) of what really matters.

Finally, I want to express my deepest love and gratitude for all the support and friendship given to me by my parents, Lyn and Jerry. Without them, none of this work and fun would have happened. I love them dearly.

If it were not for the help of all these people, I wouldn't be able to say with pride: I avoided the job market for a quarter of a century!

"We take a handful of sand from the endless landscape of awareness around us and call that handful of sand the world."

Robert M. Pirsig

TABLE OF CONTENTS

TABLE OF CONTENTS (Continued)

LIST OF FIGURES

LIST OF FIGURES (Continued)

LIST OF FIGURES (Continued)

LIST OF FIGURES (Continued)

LIST OF FIGURES (Continued)

LIST OF FIGURES (Continued)

LIST OF FIGURES (Continued)

LIST OF FIGURES (Continued)

LIST OF FIGURES (Continued)

LIST OF FIGURES (Continued)

LIST OF FIGURES (Continued)

LIST OF TABLES

LIST OF TABLES (Continued)

LIST OF TABLES (Continued)

WAVE CLIMATE AND STORM SYSTEMS ON THE PACIFIC NORTHWEST COAST

CHAPTER 1
INTRODUCTION

The extreme wave climate of the Northwest coast, including the ocean shores of Oregon and Washington, creates a highly dynamic and variable nearshore environment. Storm systems in the North Pacific typically have large fetch areas and strong winds, the two factors that account for the large heights and long periods of the generated waves. Extreme storm events can cause catastrophic erosion on public beaches, sea cliffs, sand spits, and private properties. Most susceptible to the resulting erosion have been the sand spits along the Oregon coast, several of which are heavily developed with homes constructed within foredunes backing the beach (Komar, 1978, 1983, 1986; Komar and Rea, 1976; Komar and McKinney, 1977). Along much of the Northwest coast the beach is backed by sea cliffs, but they are generally composed of non-resistant sandstones which easily succumb to wave attack (Komar and Shih, 1993).

Analyses of specific instances of dune or cliff erosion have relied on direct measurement of the waves, the primary factor causing erosion. To understand the causes of erosion and movement of sediment in the nearshore zone, one needs to know the wave climate not only during extreme events, but also on a daily and seasonal basis. Waves are capable of moving sediment at depths of up to 200 meters on the continental shelf (Komar, Neudeck, and Kulm, 1972), so a knowledge of wave climate is also important in studying the fate of dredged harbor sediments dumped on the shelf, and investigating the origin of mineral placers known to exist offshore. Long-term wave records also allow for statistical predictions of extreme wave conditions, essential for the sound engineering design of jetties, seawalls, and riprap revetments. The broad objective of this study, therefore, is to better characterize the wave climate of the Northwest coast.

Due to the exceptional wave climate of the Northwest, conventional in-situ wave gauges have been only marginally successful. Pressure transducers are frequently covered with sand or cables are broken by large waves, making continuous low-maintenance recording of waves difficult. Visual observations can only be made in

daylight and under favorable weather conditions, and are subject to observer error. Pressure-sensor array and buoy data sets are available for the Northwest coast, and have yielded daily measurements of waves since the 1980's. Data are available from the National Data Buoy Center (NDBC) of NOAA (deep-water buoys), and the Coastal Data Information Program (CDIP) of the Scripps Institution of Oceanography (deep-water buoys and shallow-water directional arrays). A hindcast wave data set of the Wave Information Study (WIS) of the Corps of Engineers (based on analyzing daily weather charts), is also available but only for 1956 to 1975. The microseismometer system at the OSU Mark Hatfield Marine Science Center (HMSC) in Newport has been recording wave heights and periods four times daily for the past 22 years, a technique based on the measurement of microseisms produced by ocean waves. According to theoretical analyses, the microseisms are generated by the pressure field associated with standing waves produced by wave reflection from the coastline. The development of this microseismometer wave measurement system allows the instrument to be deployed in a remote, sheltered location, where it measures vertical ground oscillations produced by ocean waves.

There are two primary goals of this study:

(1) To directly compare wave measurements for the Northwest coast derived from the available sources. These include the microseismometer system, NOAA deep-water buoys (NDBC), Scripps Coastal Data Information Program (CDIP) deep-water buoys and shallow water directional arrays, and wave hindcast information from the Wave Information Studies of the US Army's Corps of Engineers.

(2) To analyze the combined wave data from the various measurement systems to determine the extreme design-wave conditions for the Northwest coast.

In the course of this study various aspects of the microseism analysis are discussed, and means of improving the analysis methods are addressed.

The body of this thesis has been divided into seven parts. Chapter 2 is a discussion of wave measurement techniques and available data sources. Various in-situ and remote measurement systems are described, with the chief focus being on data types used in this study: pressure sensors, deep-water buoys, and the microseismometer system. This chapter will address the basic principles behind the measurement of waves with a microseismometer system, its implementation and calibration, as well as past utilization of the measurements. In addition to these direct wave measurements, wave data derived

from the WIS wave hindcasts will be discussed. Finally, a summary of available wave data for the Northwest coast is presented.

Chapter 3 consists of comparisons of the buoy and array data from the CDIP and NDBC programs. The data sets will be assessed as to whether they represent true deep-water wave statistics, and north-south variations in significant wave heights and dominant (peak spectral) wave periods will be examined. Deep-water monthly wave climate statistics are presented and compared with various mathematical distributions. Finally, wave breaker heights are calculated from the deep-water measurements.

Chapter 4 will discuss the conversion of the microseismometer from a strip chart recorder to an automated digital recorder. The microseismometer data are analyzed and presented in the same manner as the buoy and array data. Data obtained from the microseismometer before and after computerization will be compared with the deep-water buoy data for daily wave conditions during the winter and summer.

Chapter 5 evaluates the WIS wave hindcast data set for the Pacific Northwest. Direct comparisons of hindcast estimates with microseismometer data are made, and wave climate statistics from the WIS data are presented and analyzed as per the buoy and microseismometer data. The wave hindcast techniques are then assessed.

Chapter 6 presents the extreme-wave analyses performed on the various data sets. In this chapter, extreme significant wave heights are calculated for various return periods using data from the two Scripps deep-water buoys, the microseismometer system, and the WIS hindcast data. The microseismometer and buoy data are joined together to produce a 23-year data set from which extreme wave heights are calculated. Also, calculations of extreme run-up heights and wave power are presented for various data sets.

Chapter 7 summarizes the main conclusions of this study, and presents implications of the results and discusses possible applications.

CHAPTER 2
WAVE MEASUREMENT TECHNIQUES AND DATA SOURCES

The objective of this chapter is to outline various wave measurement techniques, with the focus being on those used in this study. The two basic methods of ocean wave measurement are in-situ and remote observations. In-situ wave measurement systems include pressure sensors, accelerometer buoys, acoustic sensors, and wave staffs. Remote sensing wave measurement systems include aerial photography, radar, and microseismometer wave sensors. Wave data can also be obtained from hindcasting techniques using surface wind data. The following sections will outline the general characteristics of these diverse measurement systems. Since a major objective of this study is a comparison of wave data sets spanning Oregon and Washington, a listing of available data is provided. Those data will be analyzed in detail in the subsequent chapters.

In-Situ Measurement Systems

Pressure Sensors

Pressure sensors measure the time-dependent pressure field beneath waves. Pressure fluctuations due to progressive ocean waves decrease exponentially with increasing depth below the water surface. Further, the pressure field attenuates more rapidly for short, high-frequency waves than under long, low-frequency waves. The pressure depth attenuation factor (between surface elevation and pressure), K(f), is:

$$K(f) = \cosh[k(z + D)]/\cosh(kD) \qquad (1)$$

or for deep-water: $K(f) = e^{kz}$

where k is the wave number (2π/wavelength), z is the depth of the sensor below the surface, and D is the total water depth. The depth below the surface at which pressure

sensors can be successfully deployed is dependent on the ratio between signal intensity (wave pressure) and noise (instrument and analysis characteristics). The limiting water depth of pressure sensors measuring progressive waves is typically 20 meters (Earle and Bishop, 1984). In high energy coastal environments such as the Northwest, pressure sensors are typically unable to cope with extreme wave conditions because they are frequently covered with sand, or cables are broken in the turbulent surf. Another disadvantage of subsurface pressure sensors is the need to utilize frequency-dependent correction factors to convert from measured pressures to sea surface elevations. Pressure sensors can be configured in an array to obtain directional information about the waves by using the phase information between the different sensors in the array. Array data of this type have been collected by the Coastal Data Information Program (CDIP) of Scripps Institution of Oceanography off the Coquille River (Bandon) in southern Oregon and Long Beach in southern Washington. The pressure sensor arrays used by CDIP consist of four bottom-resting pressure transducers placed at roughly 10 meters depth which is outside the surf zone under all but the most extreme wave conditions. Three brands of pressure transducers have been used (Kulite, Paros Press, and Sensotec). The standard sampling rate of these sensors is 1Hz and the sampling interval is 1024 seconds (approximately 17 minutes). These array data will be analyzed in Chapter 3 to characterize the wave climate of the Pacific Northwest.

Buoys

Deep-water in-situ wave measurements are often obtained with accelerometer buoys. An accelerometer buoy is moored to a fixed location offshore and measures the imposed vertical acceleration from passing waves. This measurement of acceleration is then converted to wave elevation by a double integration, and the time-dependent signal can be spectrum-analyzed to obtain wave variance vs. frequency. Data produced from buoys is usually transmitted to shore-based receiving stations where the information is transformed into a spectrum (Steele and Johnson, 1977). Since the vertical component of acceleration is all that is required, several methods have been developed to maintain the accelerometer in a vertical orientation, including the use of gyroscopes, gimbals, and pendulums. A commonly-used example of an accelerometer buoy is the WAVERIDER^{tm} buoy by Datawell. The WAVERIDER buoy is moored using an elastic rubber cord so that the buoy is able to follow the water surface. Datawell claims that the buoy can

reliably measure waves up to 20 meters in height with a maximum error of 1.5%. The accelerometer in the WAVERIDER buoy is maintained in a vertical orientation mechanically, and horizontal accelerations are less than 3% of the total signal intensity. Measurements derived from this type of buoy are collected by CDIP off Bandon, Oregon, and off Grays Harbor, Washington.

Directional wave information can also be obtained from specially designed buoys. Buoys shaped as discs respond to the local slope of the wave surface, and the measurement of this time-varying slope together with the acceleration can be analyzed to yield a directional spectrum. Traditional accelerometer buoys can be modified to monitor small horizontal accelerations, which are then converted into directional spectra (Earle and Bishop, 1984).

The NOAA National Data Buoy Center (NDBC) collects marine meteorological, oceanographic, and wave data from C-MAN (Coastal-Marine Automated Network) stations. The C-MAN data used in this study are collected from a 3-M discus buoy located offshore from Newport, Oregon. This buoy has a discus-shaped hull 3 meters in diameter with a 2-metric ton displacement. The buoy employs a DACT (Data Acquisition, Control, and Telemetry) payload which measures significant wave heights (0 to 35 m), and average and dominant periods (3 to 30 s) computed from spectra produced by an accelerometer. The spectra are calculated from 20 minute time-series sampled at 2.56 Hz. Wave direction and meteorological data are also collected by this buoy.

Other In-Situ Wave Measurement Systems

An acoustic sensor is a subsurface, upward-looking device which transmits sound pulses to the ocean surface which are then reflected and received at the instrument. The time interval between transmission and reception gives the elevation of the sea surface, and thus wave height, assuming the speed of sound between the instrument and surface is known (a function of temperature, salinity, and pressure). Acoustic sensors are not frequently used for wave measurement as they are more expensive and complicated than other, equally reliable measurement systems (buoys, pressure sensors, and wave staffs).

Wave staffs are often an effective, low-cost method of obtaining wave measurements. A wave staff needs to be attached to a fixed structure exposed to all incoming wave directions. The typical wave staff acts as one component of an electrical

circuit whose resistance varies in time as a function of the amount of staff submerged (wave height). Although fairly inexpensive and reliable, wave staffs require maintenance to prevent biological fouling. New staffs have been designed to reduce this problem.

Remote Wave Measurement Systems

Photography and Radar Systems

Aerial photographs can be used to remotely measure some aspects of ocean waves. Although it is not possible to determine wave heights from simple aerial photographs, wave lengths and directions can be resolved. Aerial photographs are primarily used for the study of wave refraction and diffraction near the coast, and can sometimes determine the existence of multiple wave trains not resolvable by other measurement techniques. Stereo photography has been used to determine the distribution of wave energy as a function of frequency or wave number, although this method is complex (Ross, 1979).

Narrow-beam laser or radar profilometers mounted on aircraft have been used effectively to measure wave height and/or wave directional information. Satellite based synthetic aperture radars produce images similar to aerial photographs, which can be analyzed to determine wave number and direction. Shore-based radar systems (called skywave or over-the-horizon radar) have been developed to determine wave heights and directions near the coast (Earle and Bishop, 1984).

Microseismometer System

The microseismometer wave gauge is a remote wave measurement system. Theory predicts that ocean waves traversing a sloping beach will be partially reflected and the interaction of incident and reflected waves will result in the formation of standing waves which produce a pressure field on the ocean bottom. According to Longuet-Higgins (1950), this pressure field generates small seismic waves (microseisms) propagating in the horizontal plane which can be detected many kilometers from their source. It was shown theoretically by Longuet-Higgins that the amplitude of the resulting seismic

motion is linearly related to the pressure from the standing waves, and that the frequency of seismic motion is twice the ocean wave frequency. Theoretical work by Hasselman (1963) suggests that both the fundamental ocean wave period and the half period component should be present in the microseism signal, with the former being the much weaker of the two by a factor of about 10 (some of the microseism time series in this study contain both components). The mechanism of primary frequency generation, though not firmly established, is a pressure force exerted on the ocean floor from wave shoaling.

Analysis of microseisms (strip-chart recordings) have produced useful estimates of nearshore significant wave heights and zero-crossing periods which correlate well with observations during large wave conditions (Zoph, Creech, and Quinn, 1976). The system is less reliable for the measurement of small waves. Further, estimates of wave periods have been much less accurate than estimates of wave heights since there is typically more than one wave train incident to the coast at any given time, and the analysis of a zero-crossing ocean wave period does not resolve this. The microseismometer at the Hatfield marine Science Center (HMSC) in Newport was computerized in 1992 and now records microseism time series for statistical analysis. This allows for less human error in wave height estimates, and makes it possible to resolve both the dominant and zero-crossing wave periods.

The microseismometer system at Newport consists of four stages: a seismometer, an amplifier, a filter (to attenuate signals outside the frequency band of interest), and a recorder. The seismometer is a Teledyne-Geotech Model SL-210 designed for geophysical surveys, and has an adjustable natural frequency of 10-30 seconds. An electrical signal proportional to the vertical ground velocity is produced by a motion-sensitive (moving-coil) transducer. The transducer is connected to a damping resistor so that the system behaves as an approximately critically-damped spring-mass system with a natural period of about 18 seconds. From May 1971 to May 1992, the seismometer signal was recorded directly on a strip-chart recorder for manual analysis of the prevailing wave conditions. As of May 5, 1992 the signal is now digitally stored in a personal computer located at HMSC to facilitate automated spectral analysis of the wave records.

From the theory of Longuet-Higgins (1950), it can be shown that:

$$P = C\, a^2\, \omega^2 \cos(2\omega t) \qquad (2)$$

where P is the mean pressure fluctuation on the sea floor, a is the ocean wave amplitude, ω is the wave frequency, and C is a constant. This pressure variation is not attenuated with depth, and ultimately predominates over first order effects at large depths. Assuming that ground displacement is linearly related to this forcing pressure field on the ocean bottom, Zoph, Creech, and Quinn (1976) derived the following relationship between the ocean wave height (H_{ocean}), peak-to-peak seismometer deflection (H_{seis}), and the period of the seismic signal(T_{seis}):

$$H_{seis} = K\,(H^2_{ocean}/T^3_{seis}) \qquad (3)$$

where K is an empirical constant. The seismometer signal is modified by a low-pass filter with a break point at 0.7 Hz to eliminate ambient seismic noise. Another filter with a ($1/\omega^3$) response between 0.1 and 0.4 Hz is used to remove the wave period dependence in Eq. 2. The filters are designed to give an effectively flat energy spectrum between 0.1 and 0.4 Hz (corresponding to wave periods from 20 to 5 seconds). Therefore, in the filtered signal:

$$H_{ocean} = (KH_{seis})^{1/2} \qquad (4)$$

The empirical constant K is determined by simultaneously measuring the seismic signal deflection and the ocean wave height. For the initial calibration in 1971, visual observations of wave heights were made from shore against a 4 meter high buoy in 20 meters water depth (Zoph, Creech, and Quinn, 1976). The observer, Clay Creech, watched waves pass the buoy and estimated the height (to the nearest foot) and period (to the nearest second) of the highest 10% of waves. The errors associated with these visual observations are discussed by Enfield (1973). The visual observations were augmented by occasional pressure sensor and fathometer data. During the period July 1971 to June 1972, 403 observations were made, leading to a K=32 value in equation (3). The correlation between observed wave height and microseismometer wave height was found to be $R^2 = 0.87$, with a standard error of 1.61 ft. Correlation diagrams are shown in Figure 1. A similar analysis of ocean wave period and seismic period confirmed the expected 2:1 frequency relationship (Zoph, Creech, and Quinn, 1976).

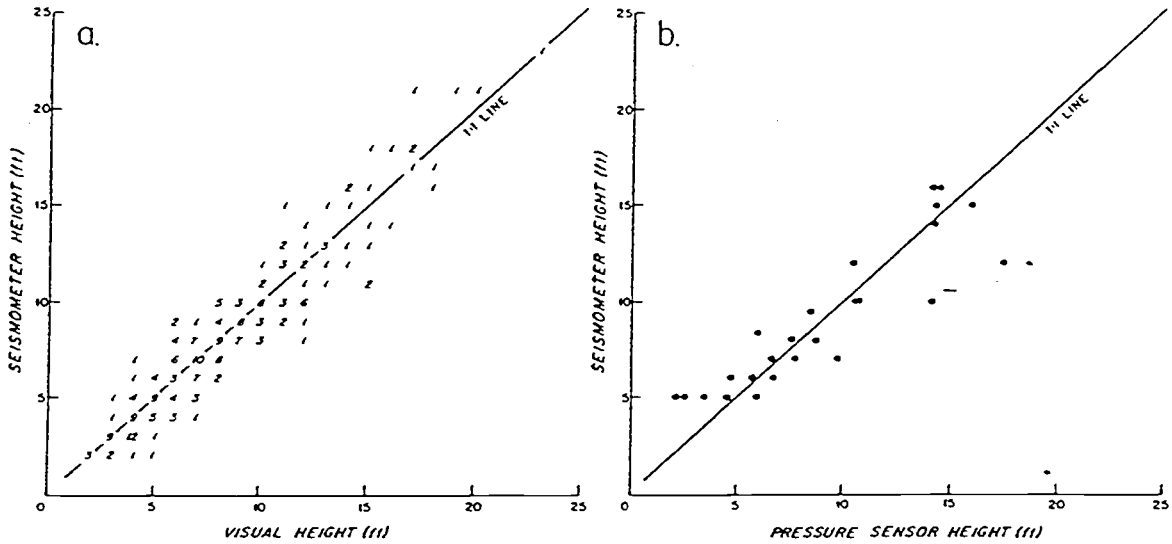

Figure 1. Calibration of the OSU microseismometer wave gage based on (a) the visually observed wave heights, and (b) pressure-sensor wave heights. [from Quinn et. al., 1974; Zoph et. al., 1976]

Manual analysis of the strip-chart seismic signal requires a visual estimate of the largest wave packet (group) in the 10-minute record. A template (prepared from calibration) is then placed over the wave group and the peak-to-peak deflection of the largest wave in the group is recorded (as an estimate of the highest 10 percent of waves during that period), which can then be modified to a significant wave height (the mean of the highest 1/3 of waves) by multiplying by 0.79 (Shore Protection Manual, 1984). The zero-crossing wave period is determined from counting the number of zero-upcrossings, dividing the length of the record by this value, and multiplying the result by 2 (because of the 2-to-1 relationship between seismic period and wave period).

Bodvarsson (1975) analyzed the OSU microseismometer system and theoretical generation mechanisms. A roughly linear relationship was found between the root-mean-square (rms) amplitudes of the microseisms and the squared product of the local ocean wave heights and frequencies. Calculations were made according to the Longuet-Higgins (1950) theory which showed microseisms could be quantitatively accounted for by a

narrow (roughly 400 meter wide) standing-wave generation region along the coast, assuming wave reflection coefficients on the order of 0.01 to 0.1. Microseism energy at the incident ocean wave frequency was rarely present, and 10 to 100 times weaker than the double-frequency energy.

Creech (1981) compiled the wave data collected by the microseismometer system for the decade between 1971 and 1981, and provided an analysis of the wave climate. As part of the present study, the unprocessed data from 1981 to 1992 were analyzed in order to yield 20 years of measurements upon which to base the wave climate and to identify the most extreme storms during that period. Komar et. al. (1976) used the microseismometer data to calculate the corresponding breaking waves in the nearshore, documenting the seasonal variations and discussing the ramifications to nearshore processes. Thompson et. al. (1985) compared two months of OSU microseismometer data with pressure-sensor data off the Coquille River near Bandon on the southern Oregon Coast. Estimates of wave height were found to be significantly better than wave period estimates. Further, wave height measurements were found to be in best agreement during high-energy winter wave conditions. Howell and Rhee (1990) investigated the use of computer analysis of the microseism signal to obtain more reliable wave period estimates from the system. Again, the system was found to be most reliable during extreme wave conditions, and spectral estimates of wave periods were judged to be at least as good as estimates derived from zero-crossing analysis.

A similar microseismometer system has been used successfully on the coast of New Zealand to measure wave conditions (Ewans, 1984; Kibblewhite and Ewans, 1985; Brown, 1991; Kibblewhite and Brown, 1991). Their analyses provide further confirmation of the Longuet-Higgins (1950) theory of microseism generation by reflected waves.

Wave Hindcasting

The Wave Information Study (WIS) of the US Army Corps of Engineers was undertaken to generate 20 years of hindcast wave data spanning the period 1956 to 1975 (Hemsley and Brooks, 1989). The WIS data analyses have been divided into three phases. In Phase I barometric weather charts were analyzed for a spatial grid on the order of 2 degrees along the coast every three hours to obtain significant wave heights, periods, and directions for both sea and swell conditions. The spectral wave information

is determined by the wind speed, and is then truncated at its low-frequency end according to fetch length or duration, whichever is limiting. The wave energy is then divided into frequency bands and propagated at their group velocities to the hindcast point (taking into account refraction and diffraction for nearshore locations). Phase II utilized the same meteorological information, but at a finer scale (0.5 degrees) to better resolve the sheltering effects of continental bathymetry. Phase II wave estimates are available for 17 stations along the ocean coasts of Oregon and Washington. Station 42 (Phase II) positioned in deep-water offshore from Newport, Oregon (Figure 2), is employed in the analyses of this study. The details of the hindcast method are discussed in Corson et. al. (1987). Due to the extensive nature of this data set, annual and long-term statistics are also provided by the WIS reports. The hindcast wave measurements from the WIS program yield both deep and shallow-water wave estimates for sites along the US coastline.

Of note is that the peak wave period reported by WIS is not the same as the peak spectral wave period derived from buoy measurements. It is actually the weighted average wave period because it is defined as the reciprocal of the weighted average frequency. This fact is of no consequence, however, in the following analyses.

Data Available for the Northwest Coast

One of the major objectives of this study is to compare wave data for the Northwest coast of Oregon and Washington derived from the various measurement systems. A listing of this data, as well as times of availability, is given in Table 1, and their positions are identified in Figure 2. A deep-water buoy operated by the National Data Buoy Center (NDBC) of NOAA (Steele and Johnson, 1979; NDBC, 1992) has been collecting data offshore from Newport on the mid-Oregon coast on a daily basis since May 1987 (Table 1). Deep-water buoys have also been installed by the Coastal Data Information Program (CDIP) of Scripps Institution of Oceanography (Seymour, et. al., 1985), and are located offshore from the Grays Harbor, Washington, and the Coquille River at Bandon on the southern coast of Oregon. Both have been in operation since November 1981 (Table 1).

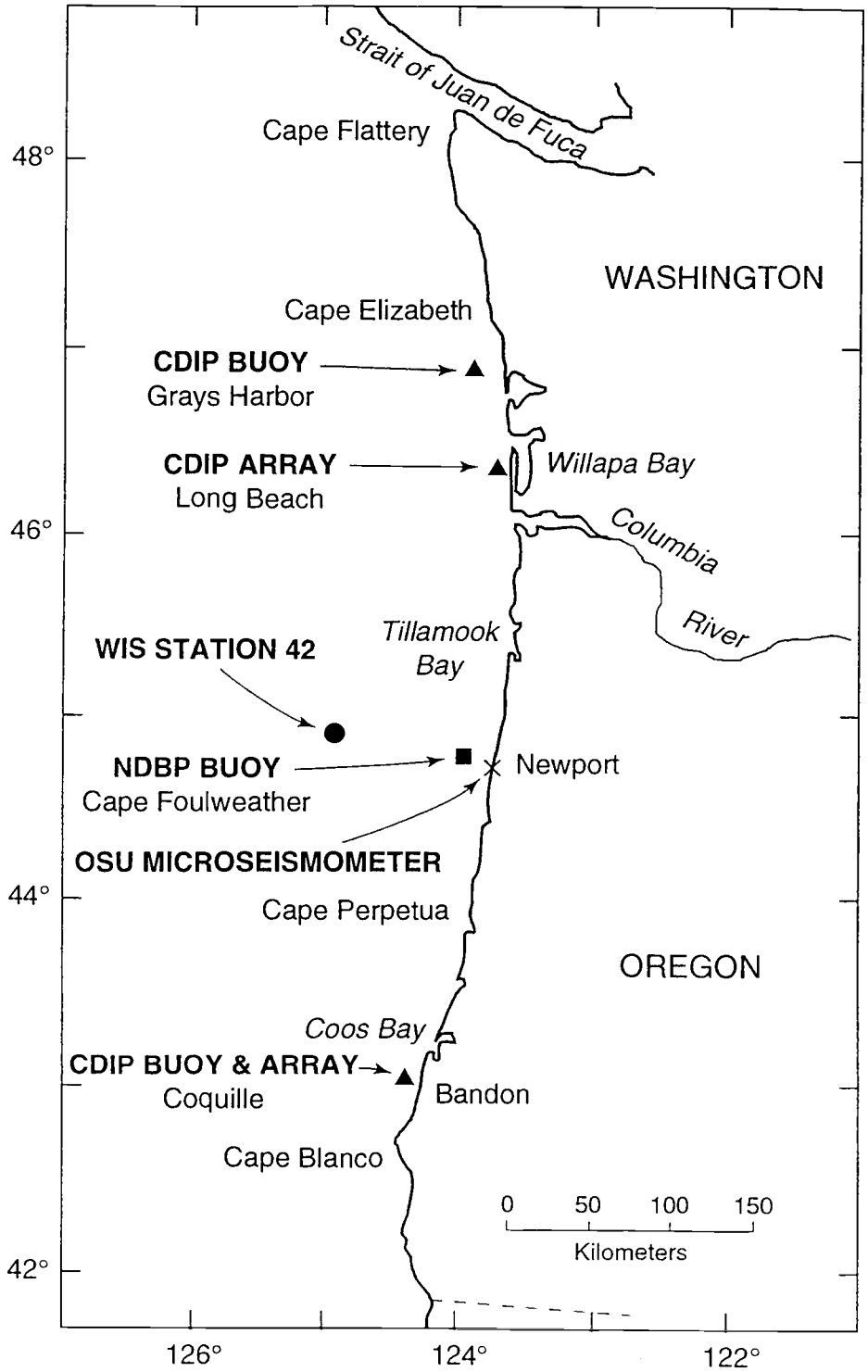

Figure 2. Locations along the coastline of the Pacific Northwest of wave-measurement systems and the positions of WIS Phase II hindcast data.

Table 1. List of Northwest data sources and time periods of availability.

Data Source	Time Periods	Location N. Lat.	Location W. Long	Depth (M)
Scripps Coastal Data Information Program (CDIP)				
Buoy, Coquille Bay, OR	Daily, 12/81-pres. (NC)	43 06.4'	124 30.4'	64
Buoy, Grays Harbor, WA	Daily, 12/81-pres. (NC)	46 51.2'	124 14.8'	42.6
Pressure-sensor Array, Coquille Bay, OR	Daily, 8/83-pres (NC)	43 07.4'	124 26.5'	11
Pressure-sensor Array, Long Beach, WA	Daily, 9/83-pres (NC)	46 23.4'	124 04.6'	9.8
NOAA				
Buoy, Cape Foulweather, OR	Daily, 5/87-pres (NC)	44 40.2'	124 18.4'	112
Wave Information Studies (WIS), Corps of Engineers				
Hindcast Estimates - Station 42	Daily, 9/56-75	44.8	125	Deep-Water
Oregon State University				
Microseismometer Wave Guage	Daily, 5/71-pres.	Newport, Oregon		20 (Calibration)*

(NC) - Not Continuous

*Depth to which original calibration corresponds (from Zoph, Creech, and Quinn, 1976)

The CDIP has also installed pressure-sensor arrays to monitor wave conditions along the U.S. coastline (Seymour, et. al., 1985). Sensor arrays have been in operation since 1983 at a water depth of 9.8 meters offshore from Long Beach, Washington, and in 11 meters of water offshore from the Coquille River at Bandon (Figure 2). The arrays consist of four pressure-sensors arranged on the corners of a square, held in place by supports that follow the diagonals. This arrangement permits the determination of directions of wave energy propagation as well as the periods and heights of the waves. This system is used in water depths less than 15 meters, and has a cable from the array to the shore to provide power and to deliver the measured data to a land-based recorder. In the standard mode of operation, each instrument array reports once every six hours, when the central station at SIO initiates a telephone call to the shore station using an autodialer and normal telephone lines. The shore station responds by answering the call, and then transmits the collected data. All wave sensor records collected by CDIP stations are analyzed by Fast Fourier Transform. The Fourier coefficients from shallow-water pressure sensor arrays are depth corrected by linear wave theory to represent deep-water wave parameters. The Fourier coefficients are used to produce an energy spectrum grouped into various period bands published in CDIP monthly reports. Since January, 1993, CDIP directional wave records have been presented in the form of daily two-

dimensional energy spectra, and wave parameters such as total spectral energy, significant wave height, peak period, and weighted direction. Also, the mean direction and energy is reported for each period band.

The microseismometer wave measurement system of Oregon State University has been in operation since 1971 at the Hatfield Marine Science Center in Newport, Oregon. Since May, 1992, the microseismometer has produced measurements of significant wave height, zero-crossing wave period, and dominant wave period. Prior to May 1992, only the significant wave height and zero-crossing period obtained from manual analysis are available.

The WIS hindcast data are listed in the report by Corson et. al. (1987), and include directional wave spectra as well as significant wave parameters hindcast at 3 to 6 hour intervals for the 20 years from 1956 to 1975. The report also contains summary statistics such as average monthly wave heights and periods, and probabilities of extreme wave statistics such as the projected significant wave height and period of the 100-year storm. Those data are not employed in the present analyses as preference is given to the deep-water conditions provided by the Phase II hindcast data.

With the exception of the WIS hindcast data, all of the data sets listed in Table 1 are concurrent from May 1987 to the present. This concurrence permits direct comparisons, which are undertaken in Chapters 3 and 4. The microseismometer data overlap with 4 years of WIS data, allowing for direct verification of the hindcast estimates for the Northwest coast (Chapter 5). Collectively, the data sets used in this study (WIS data (1956-1975), microseismometer data (1971-present), and buoy and array data (1981-present) represent 38 years of Northwest wave climate information from which more reliable estimates of future extreme events can be predicted (Chapter 6).

CHAPTER 3
BUOY AND ARRAY DATA

In this chapter, deep-water buoy and array-derived data sets are analyzed (see Figure 2 for locations). The buoy measurement systems are first examined to determine whether they represent true deep-water wave parameters. Next, monthly mean significant wave heights and dominant wave periods are compared for the three offshore buoys to determine if they yield comparable results and whether north-south variations in wave climate exist along the coast. Linear regressions of mean daily significant wave heights and dominant periods are undertaken to compare buoy measurements. A joint frequency distribution of wave heights and periods is presented for each buoy as the basic form of data representation. Histograms of measured wave heights and periods are then presented and compared with statistical distributions. Pressure-sensor array data collected in intermediate to shallow water depths are examined and compared with the corresponding offshore buoy measurements in deep water. This involves the application of wave transformation analyses and the validity of those analyses. Finally, wave breaker heights are calculated from the deep-water wave parameters.

Assessment of Deep-Water Wave Measurements

The deep-water wave climate is most directly determined from the NDBC and CDIP buoys. These buoys are deployed in water depths of 42.6 to 128 meters, and for the most part the data can be assumed to represent true deep-water wave conditions. The depths of the various wave sensors used in this study are given in Table 2. None of the sensors are in true deep-water under all measured wave conditions. In rare instances the wave periods are in excess of 20 seconds, such that these buoy depths actually represent intermediate water according to the $D/L > 1/4$ criterion where D is the water depth and L is the deep-water wave length (Komar, 1976; CERC, 1984). It was therefore necessary to evaluate the factors for converting the measured wave heights to deep-water wave heights for more accurate comparisons between the sensors. Table 2 lists the range of measured mean daily significant wave periods for the different sensors, as well as the range of conversion factors. The conversion factors were calculated using the Shore Protection Manual (CERC 1984) of the U.S. Army Corps of Engineers. Appendix 1 of

the SPM provides a table listing measured values of D/Lo (where D is the measurement depth and Lo is the deep-water wavelength) to H/Ho' (where H is the measured wave height, and Ho' is the un-refracted deep-water wave height) based on linear wave theory. The conversion factors were judged to be close enough to unity as to not require corrections of the data sets of measured waves. Due to the similarities in conversion factors between the deep-water buoys, systematic differences in wave height observations are not due to sensor depth differences.

Table 2. Buoy depths, range of dominant period observations, and conversion factors to convert to deep-water significant wave heights.

Sensor	Depth (m)	Range of MD Td (s)	Hs Conversion factor to deep-water
CDIP Coquille River Buoy	64	5 to 20	0.9148 to 0.9997
NDBC 46040 Buoy	112	5 to 20	0.9553 to 0.9998
NDBC 46050 Buoy	128	5 to 20	0.9667 to 0.9997
CDIP Grays Harbor Buoy	42.6	5 to 20	0.9130 to 0.9998
Microseismometer Calibration Obs.	20	10 to 16	0.9175 to 1.0230

MD Td - Mean Daily Dominant Wave Period
Hs - Significant Wave Height

Offshore Buoy Comparisons

Data from the three offshore buoys were first analyzed to produce mean daily significant wave heights and mean daily dominant wave period statistics. This produced statistics spanning roughly six years of wave measurements (See Table 1). Direct comparisons between measured wave parameters are not possible because the measurements are not simultaneous in time, and the buoys sample at different intervals. The NDBC buoy located off Newport, Oregon, samples hourly, whereas the CDIP stations sample roughly every three hours. Further, the use of mean daily statistics helps to eliminate any phase shifts in the wave signal measured by the three buoys. Differences in measurements made by the individual buoys at any given time could potentially be due to the time it takes the wave signal to propagate from one buoy location to another (i.e. the buoys could be measuring identical wave climates at slightly

different times). Since the predominant wave signal is nearly shore-normal, phase shifts in the measured signal are much less than 24 hours, and sub-sampling the data by daily averaging makes it impossible to resolve phase information. Mean daily statistics were then averaged to produce mean monthly statistics for the entire record of overlapping measurements made by the various buoys. This gives representative wave climate statistics for each location over the duration of measurement.

Figures 3a and 3b compare monthly mean and maximum values of significant wave heights derived from the offshore buoy measurements. The best agreement in mean and maximum wave height occurs between the two Scripps buoys located off the Coquille River, OR and Grays Harbor, WA. The NDBC buoy located approximately mid-way between the Scripps buoys, measures slightly higher (O(0.5m)) mean and maximum wave heights, though the annual trends in buoy measurements are remarkably similar. It is clear from these figures and the locations of the buoys that there is little north-south variation in the wave climate measured by the offshore buoys. There is, however, a distinct seasonality to the deep-water wave climate. The CDIP data indicate that mean daily significant wave heights range from 1.25 to 1.75 meters during the summer, increasing on average to 2.0 to 3.0 meters during the winter. There is a gradual transition in the spring, showing a progressive decrease in wave heights from December and January to a minimum in July to August. The fall transition to larger wave heights is more abrupt, with a sharp jump between October and November with the arrival of the first winter storms. This annual trend is seen best in the mean monthly statistics, less so in the maximum monthly mean statistics. According to the CDIP data, individual winter storms generate waves having deep-water mean daily significant wave heights of 5 to 6 meters, while the NDBC data show storm wave heights up to nearly 7 meters (Figure 3b). Differences in the magnitudes of measured wave heights are most likely due to differences in instrumentation between the NDBC and CDIP systems. The method of analysis used by each system is the same. Both the NDBC and CDIP buoys take the Fast Fourier Transform of the time series of surface elevation, calculate the zeroth spectral moment, and then calculate the significant wave height as 4 times the square root of this value. Given identical wave environments, the differences between systems must lie in the black box electronics which perform the analyses (i.e. the WDA (Wave Data Analyzer) of CDIP systems, and the DACT (Data Acquisition, Control, and Telemetry) payload onboard the NDBC buoy).

Figures 4a and 4b show similar comparisons between measurements of dominant (peak-spectral) wave periods. Again, the two Scripps buoys agree extremely well in

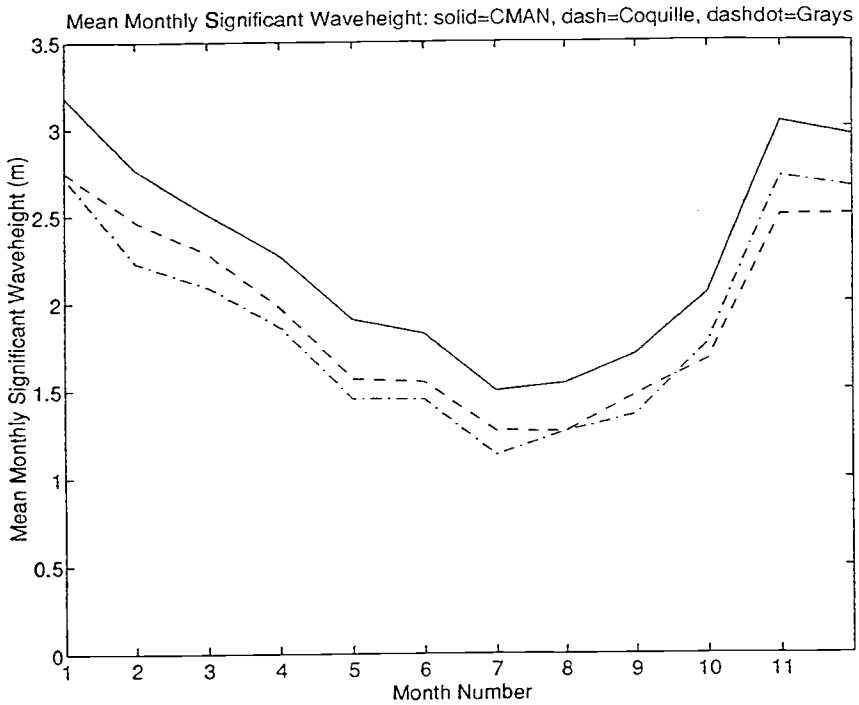

Figure 3A. Seasonality of the deep-water wave climate in terms of the mean monthly significant wave height measured by the CDIP and NDBC deep-water buoys.

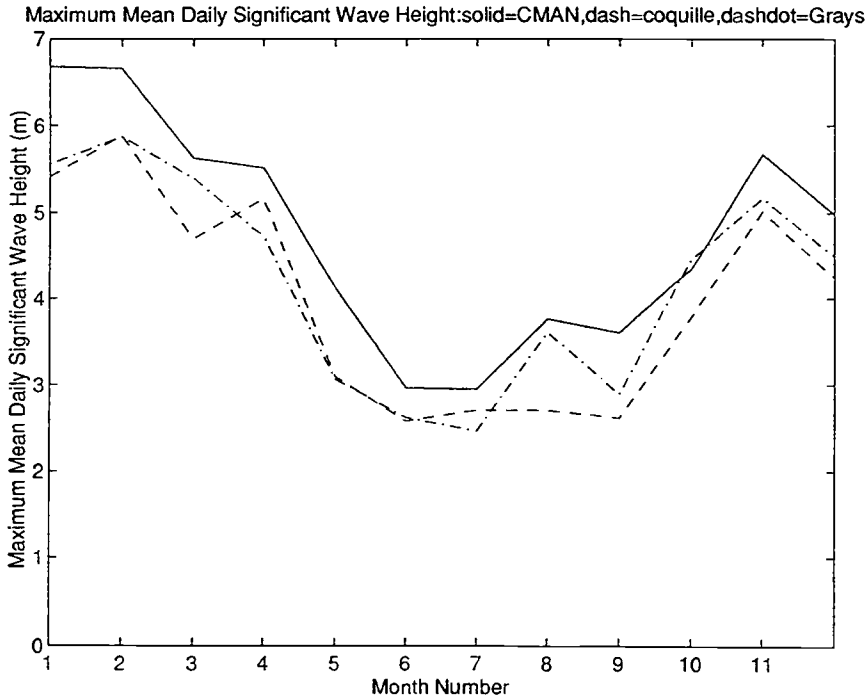

Figure 3B. Seasonality of the deep-water wave climate in terms of the maximum mean monthly significant wave height measured by the CDIP and NDBC buoys.

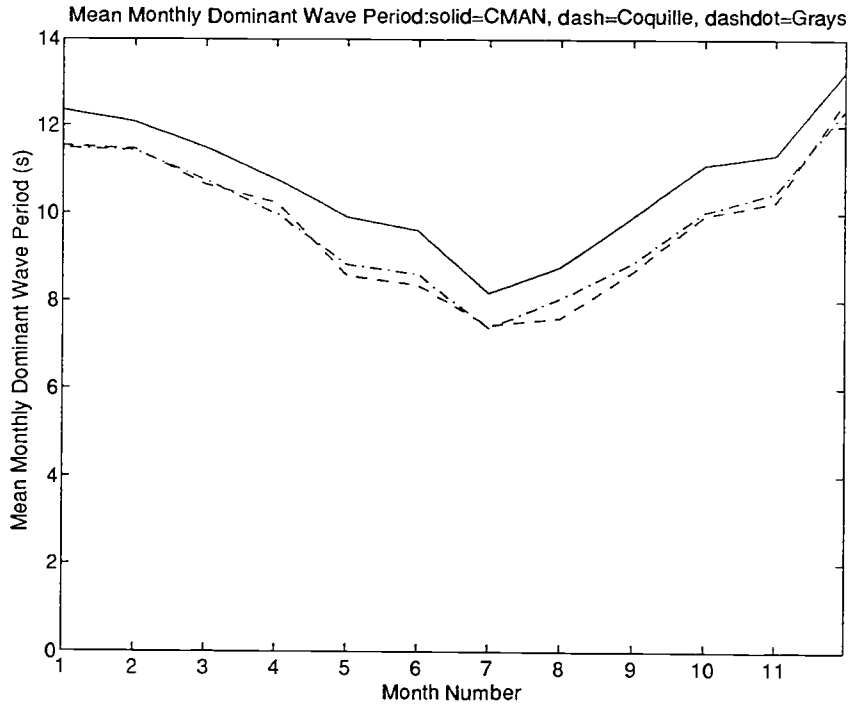

Figure 4A. Seasonality of the deep-water wave climate in terms of the mean monthly dominant wave period measured by the CDIP and NDBC deep-water buoys.

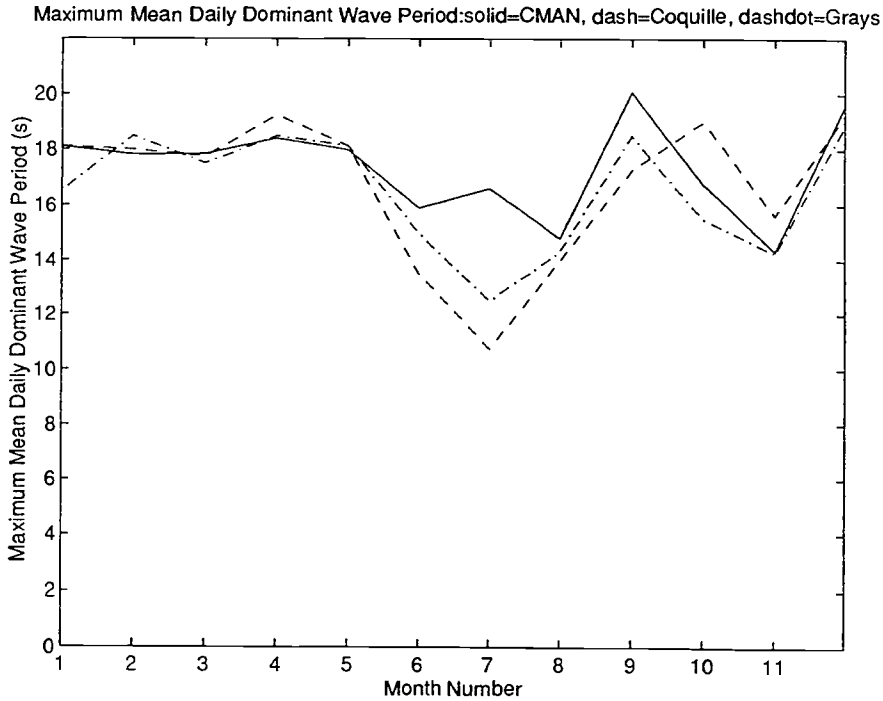

Figure 4B. Seasonality of the deep-water wave climate in terms of the maximum mean monthly dominant wave period measured by the CDIP and NDBC buoys.

monthly mean and maximum (mean daily) wave period measurements, whereas the NDBC buoy measurements of periods are slightly higher. There is a similar annual trend in the period data which follows the pattern of the annual wave height trend. Due to the close agreement in dominant periods between the Scripps buoys, and the fractionally larger wave period signal of NDBC, differences in measurement magnitudes must again be due to differences in signal analysis procedures and instrumentation. Tables 3a, b, and c list statistics of monthly mean and maximum (mean daily) significant wave heights and dominant periods upon which Figures 3 and 4 are based. Wave height and period variances are also included, as well as the number of observations (days) upon which each monthly value is based.

Table 3a. Coquille deep-water buoy wave statistics.

Month	MD Hs (m)	Hs Variance (m*m)	Max MD Hs (m)	MD Td (s)	Td Variance (s*s)	Max MD Td (s)	Observations
January	2.75	0.86	5.41	11.54	4.55	18.12	117
February	2.47	0.89	5.88	11.46	6.22	18	117
March	2.29	0.74	4.71	10.65	6.31	17.75	99
April	1.98	0.73	5.17	10.24	5.56	19.25	144
May	1.56	0.26	3.09	8.57	4.15	18.12	112
June	1.55	0.22	2.58	8.36	2.05	3.5	95
July	1.26	0.16	2.71	7.44	1.42	10.75	145
August	1.26	0.14	2.71	7.61	2.15	14	124
September	1.47	0.18	2.62	8.67	5.82	17.25	100
October	1.67	0.34	3.79	9.94	4.75	19	131
November	2.49	0.84	5.02	10.26	6.03	15.62	56
December	2.5	0.61	4.25	12.59	5.64	19.25	42

MD - Mean Daily; Td - Dominant Wave Period; Hs - Significant wave Height

The f-test comparison of variances and the t-test comparison of means were performed on monthly mean significant wave heights and dominant periods measured by the two Scripps buoys (Bandon and Grays Harbor). Nearly all of these tests (performed by month), are below the critical test value at the 95% confidence limit (45 of 48), so there is no evidence to conclude that the monthly means or variances of the two buoys are different. Therefore, there is no evidence to conclude that the Coquille and Grays Harbor buoys are measuring different wave climates in either summer or winter. Similar tests on monthly mean significant wave heights and dominant periods were performed

between the Coquille and NDBC buoy measurements. Wave height and period variances test near the critical value for equal variances, whereas wave height and period means

Table 3b. NDBC deep-water buoy wave statistics.

Month	MD Hs (m)	Hs Variance (m*m)	Max MD Hs (m)	MD Td (s)	Td Variance (s*s)	Max MD Td (s)	Observations
January	3.18	1.52	6.68	12.35	5.09	18.11	117
February	2.77	1.29	6.66	12.08	5.45	17.83	118
March	2.51	0.88	5.62	11.49	4.6	17.84	99
April	2.27	0.7	5.51	10.77	4.47	18.41	144
May	1.91	0.37	4.13	9.9	4.57	17.98	112
June	1.82	0.3	2.96	9.6	4.26	15.9	95
July	1.49	0.18	2.95	8.19	3.22	16.6	146
August	1.54	0.26	3.77	8.77	2.46	14.8	124
September	1.7	0.31	3.61	9.92	6.41	20.08	101
October	2.05	0.5	4.35	11.09	3.73	16.76	133
November	3.03	1.14	5.67	11.32	3.57	14.33	56
December	2.95	0.94	4.98	13.23	4.1	19.6	42

Table 3c. Grays Harbor deep-water buoy wave statistics.

Month	MD Hs (m)	Hs Variance (m*m)	Max MD Hs (m)	MD Td (s)	Td Variance (s*s)	Max MD Td (s)	Observations
January	2.72	1.25	5.55	11.48	3.86	16.5	117
February	2.23	1.1	5.87	11.42	6.53	18.5	118
March	2.09	0.88	5.4	10.75	5.54	17.5	99
April	1.87	0.57	4.73	9.98	5.58	18.5	144
May	1.45	0.25	3.06	8.82	4.7	18.13	112
June	1.45	0.21	2.62	8.61	3.12	15	95
July	1.13	0.12	2.47	7.38	2.03	12.5	145
August	1.26	0.24	3.61	8.06	2.35	14.33	124
September	1.36	0.23	2.9	8.87	5.76	18.5	100
October	1.77	0.45	4.47	10.03	3.72	15.5	133
November	2.72	1	5.17	10.47	2.84	14.25	55
December	2.65	0.87	4.5	12.36	5.57	18.87	42

test as statistically different. The same analysis was performed between the Grays Harbor and NDBC buoys. Not surprisingly, since Coquille and Grays Harbor measurements are statistically the same, the Grays Harbor/NDBC comparisons of wave heights and periods test the same as the Coquille/NDBC comparison.

Regressions of Deep-Water Buoy Wave Heights and Periods

Mean daily significant wave heights and dominant periods measured by the three buoys were regressed as a further comparison of the data sets. Tables 4 through 7 show the calculated least-squares regression slopes and y-intercepts for wave height and wave period correlations between the Coquille and Grays harbor buoys (Tables 4 & 5), and the Coquille and NDBC buoys (Tables 6 & 7). Also shown are the R-squared (goodness-of-fit) values, and the number of points (days) used in each regression. Plots of the

Table 4. Significant wave height regression statistics between the Coquille and Grays Harbor buoys.

Period	Least Squares Slope (Confidence Interval)	y-intercept (Confidence Interval)	R-Squared	Number of Points
All	0.96(0.0255)	0.0(0.1)	0.81	1280
Nov.1-Mar.1 (period 1)	1.01(0.0622)	0.1(0.3)	0.756	331
Mar.1-Jul.1 (period 2)	0.86(0.0399)	0.1(0.2)	0.8	450
Jul.1-Nov.1 (period 3)	0.95(0.0592)	0.0(0.2)	0.666	499

Table 5. Significant wave height regression statistics between the Coquille and NDBC buoys.

Period	Least Squares Slope (Confidence Interval)	y-intercept (Confidence Interval)	R-Squared	Number of Points
All	1.08(0.0218)	0.2(0.1)	0.881	1280
Nov.1-Mar.1 (period 1)	1.15(0.0517)	0.0(0.4)	0.853	331
Mar.1-Jul.1 (period 2)	0.95(0.0387)	0.4(0.2)	0.839	450
Jul.1-Nov.1 (period 3)	1.13(0.0444)	0.1(0.2)	0.835	499

Table 6. Dominant wave period regression statistics between the Coquille and Grays Harbor Buoys.

Period	Least Squares Slope (Confidence Interval)	y-intercept (Confidence Interval)	R-Squared	Number of Points
All	0.78(0.0312)	2.2(0.5)	0.654	1280
Nov.1-Mar.1 (period 1)	0.67(0.0687)	3.7(1.2)	0.529	331
Mar.1-Jul.1 (period 2)	0.80(0.0552)	2.0(0.9)	0.641	450
Jul.1-Nov.1 (period 3)	0.73(0.0592)	2.4(0.8)	0.54	499

Table 7. Dominant wave period regression statistics between the Coquille and NDBC Buoys.

Period	Least Squares Slope (Confidence Interval)	y-intercept (Confidence Interval)	R-Squared	Number of Points
All	0.75(0.0332)	3.3(0.5)	0.607	1280
Nov.1-Mar.1 (period 1)	0.68(0.684)	4.4(1.2)	0.536	331
Mar.1-Jul.1 (period 2)	0.68(0.0603)	4.0(0.9)	0.523	450
Jul.1-Nov.1 (period 3)	0.77(0.0653)	2.9(0.8)	0.521	499

regressions on which these tables are based are shown in Figures 5 through 8 (a, b, c, and d). The dashed lines in the figures show the 1:1 relationship along which the data should lie if the wave measurement systems agree perfectly and are measuring the same wave signal. The mean daily significant wave heights measured by the CDIP buoys at Bandon (Coquille) on the south coast of Oregon and at Grays Harbor, Washington, are nearly identical, as shown in the regression of Figure 5a. The measured mean daily dominant periods are also in close agreement (Figure 7a). This result represents a near uniformity of the deep-water wave climate along the length of the Northwest coast. However, it can be seen that mean daily significant wave heights agree more favorably than mean daily dominant periods. The least-squared regression slopes and R-squared values of the wave height regressions are closer to unity than are the wave period regressions. Also, wave height regression slope intercepts are nearer to zero than the wave period slope intercepts. Scatter, as represented by the R-squared value, is evident in all the regressions leading to less meaningful slope and intercept values for low R-squared values. This can be seen in the dominant wave period regression between Coquille and Grays Harbor in Figure 7b. Though the means in both sets of data are equal, the regression is less significant due to the large scatter in data. Analyses of the measurements by season [period 1(winter), period 2(spring), and period 3(summer)] also reveal a near uniformity on average of the wave climate. Period 1 (November 1 to March 1) regressions have the largest scatter in wave height and period, and correspond to a more broad banded wave signal than Periods 2 or 3. The scatter of data does allow for differences of daily wave conditions measured at Bandon versus Grays Harbor, in part due to the spatial extent of storms and weather conditions.

The measured periods derived from the NDBC buoy agree well with the CDIP measurements, except at times during summer months of low wave activity. However, significant wave height measurements by the NDBC buoy are systematically greater than

those measured by the CDIP buoys, a difference which has a seasonal dependence. Figures 6b and 6d are comparisons between the NDBC and CDIP Coquille station significant wave height measurements for winter months (November through February (6b)) and for the summer (July through October (6d)). Both figures show that the NDBC measurements are slightly greater than the CDIP measurements. On average, the difference is about 0.5 meters, but becomes greater with increasing wave heights such that it is about 1 meter during extreme storm conditions. In some cases the NDBC measurements are 1.5 to 2 meters larger than those measured by the CDIP systems. These apparently spurious measurements by the NDBC system cannot be accounted for by the locations of the respective buoys as the NDBC buoy is positioned approximately mid-way between the two CDIP stations. As mentioned above, since the signal analysis procedures are the same, the differences must be in the electronic systems which perform the data collection and analyses.

A frequently-used presentation of wave climate at a particular station is the joint frequency distribution of significant wave heights and periods (Herbich, et. al., 1990). Joint frequency tables were created for data from the three deep-water buoys, shown in Figures 9 a, b, and c. The contour lines represent the numbers of observations of significant wave heights and periods for the entire length of record measured by each buoy. The dashed lines in the figures denote significant wave steepness. All three distributions show the expected overall increase in wave period with increasing wave height. The greatest concentration of CDIP observations centers on significant wave heights of about 1.5 meters and corresponding periods around 7 seconds; the NDBC observations center closer to 2 meters wave height and around a 10 second wave period. This appears to represent local wave generation in the near-coastal zone of the Pacific Northwest. The joint frequency distributions of the two CDIP buoys (Figures 9a and 9c) are very similar in appearance, though no particular wave steepness best describes the data. The larger wave heights tend to correspond to longer wave periods, commonly in the range 12 to 16 seconds. According to the CDIP data, the longer period waves reaching the coast, greater than 16 seconds, tend to have slightly lower wave heights (between 1 and 4 meters). This must represent distantly generated swell, also indicated by the low values of wave steepness. The joint distribution of NDBC data, however, is unique in overall appearance and is best described by a significant wave steepness (H/L) of between 0.015 and 0.02. The differences in shapes between the three distributions reinforce other comparisons of the data sets (i.e. that the NDBC buoy reports slightly different wave conditions than the CDIP buoys).

A)

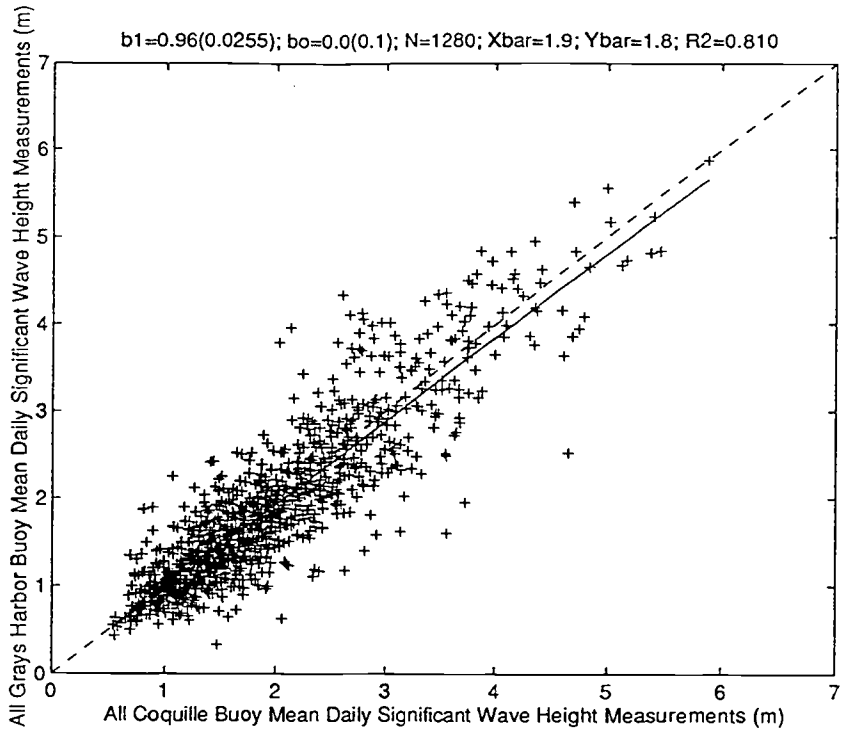

B)

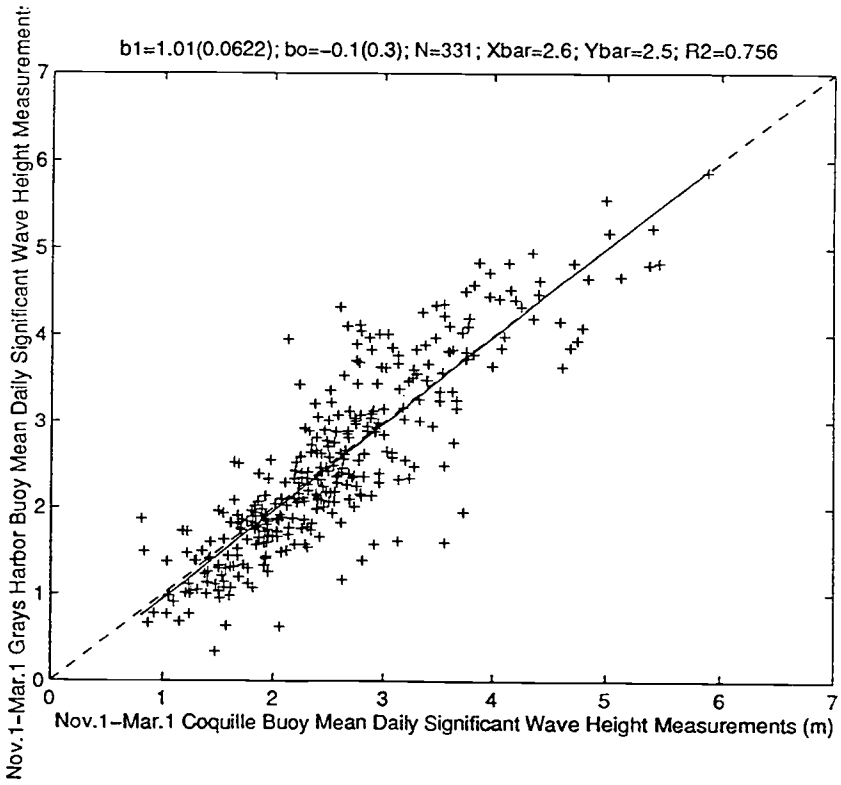

Figure 5 (A/B). A regression of Coquille (CDIP) and Grays Harbor (CDIP) deep-water buoy significant wave height measurements for A) ALL DATA, and B) WINTER MOS (Nov.-Feb.). The solid line is the best-fit least-squares regression line, and the dashed line is 1:1.

C)

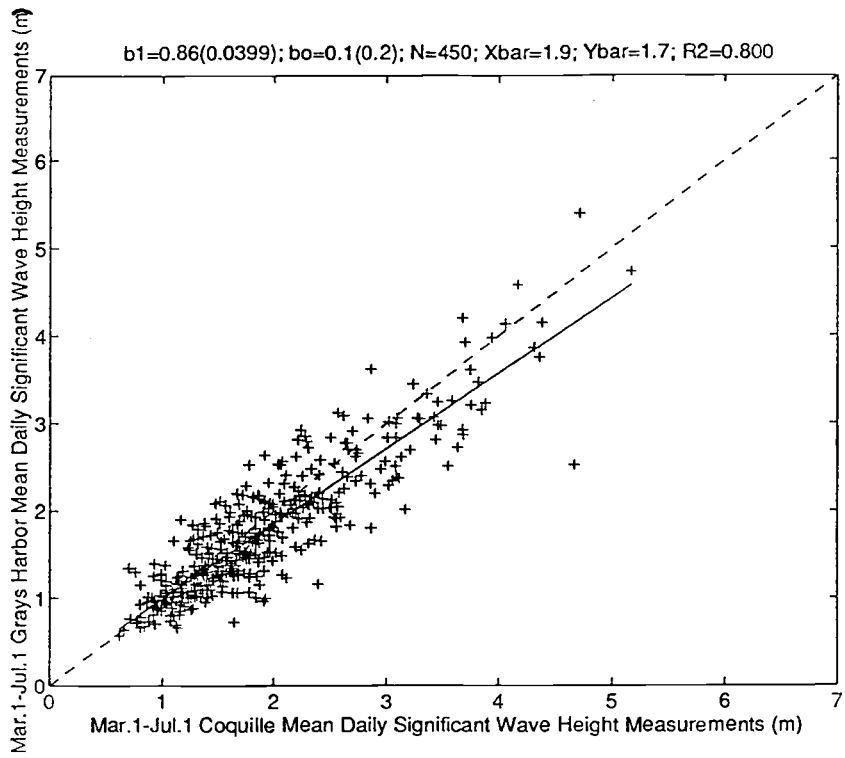

D)

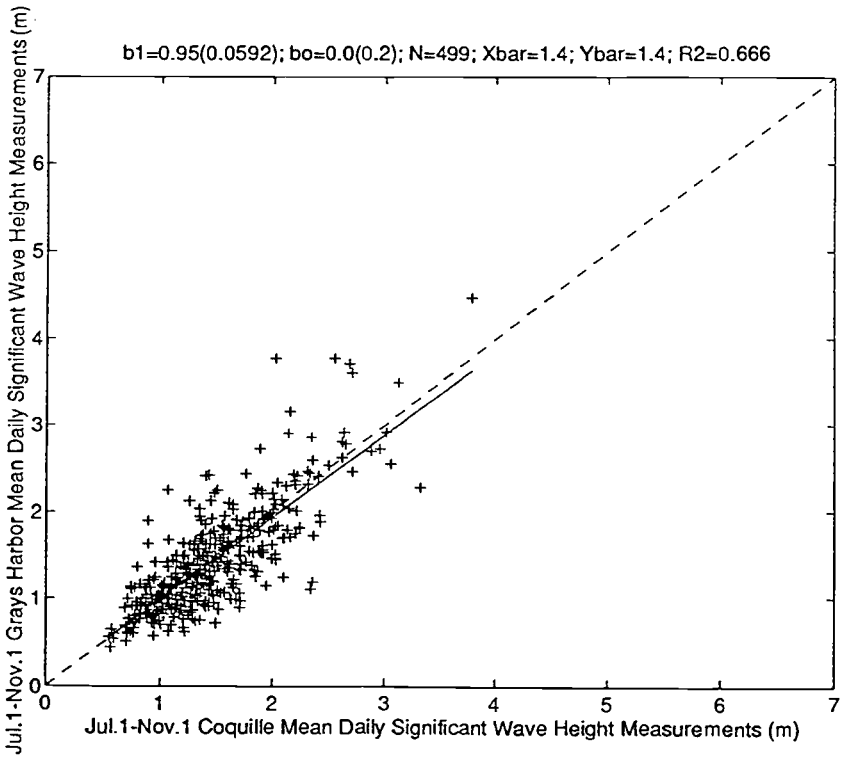

Figure 5 (C/D). A regression of Coquille (CDIP) and Grays Harbor (CDIP) deep-water buoy significant wave height measurements for C) SPRING (Mar.-Jun.) and D) SUMMER (Jul.-Oct.). The solid line is the best-fit least-squares regression line, and the dashed line is 1:1.

A)

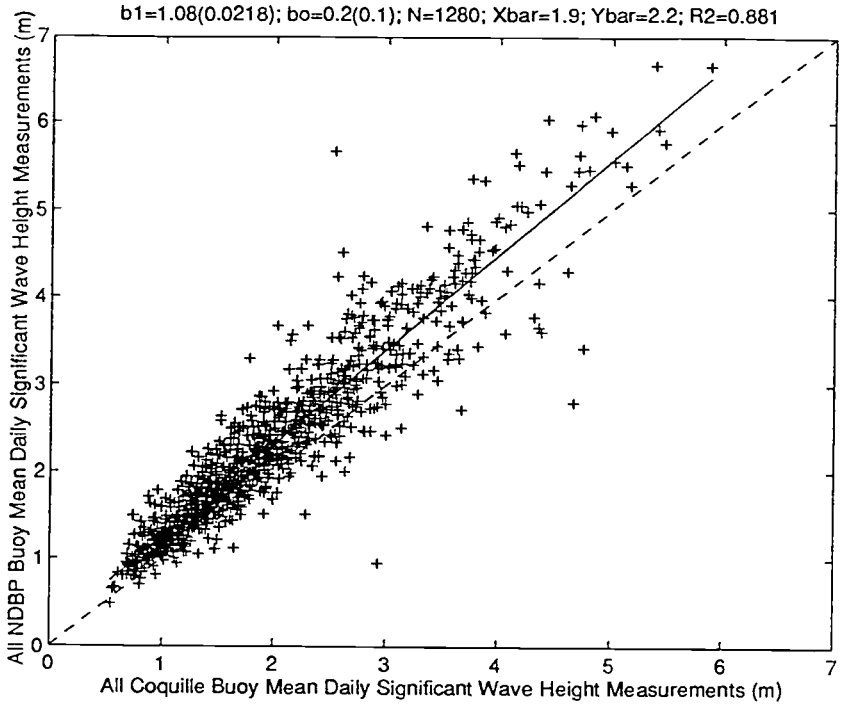

B)

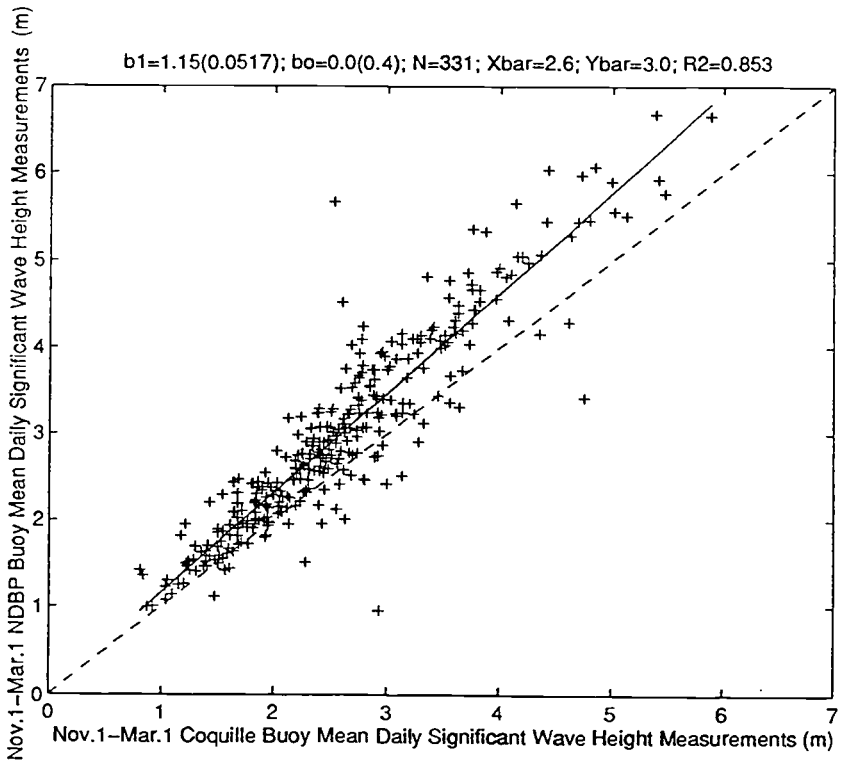

Figure 6 (A/B). A regression of Coquille (CDIP) and Newport (NDBC) deep-water buoy significant wave height measurements for A) ALL DATA, and B) WINTER MOS (Nov.-Feb.). The solid line is the best-fit least-squares regression line, and the dashed line is 1:1.

C)

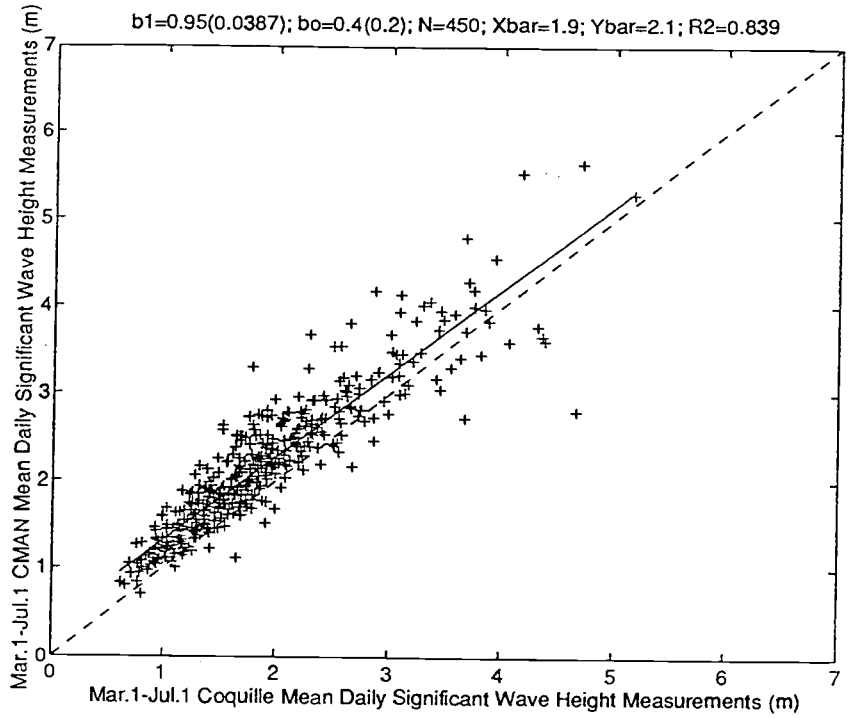

D)

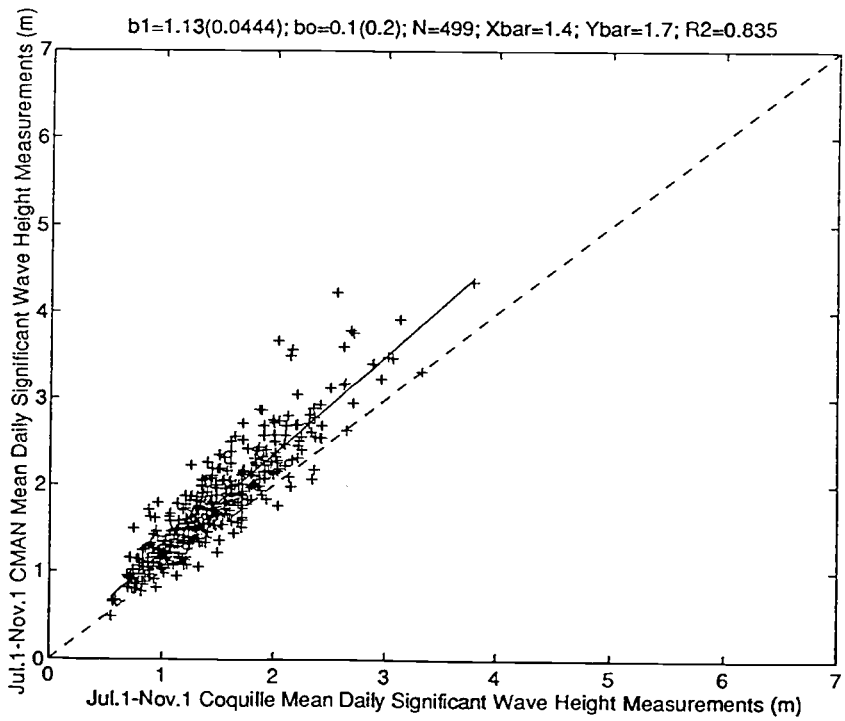

Figure 6 (C/D). A regression of Coquille (CDIP) and Newport (NDBC) deep-water buoy significant wave height measurements for C) SPRING (Mar.-Jun.) and D) SUMMER (Jul.-Oct.). The solid line is the best-fit least-squares regression line, and the dashed line is 1:1.

A)

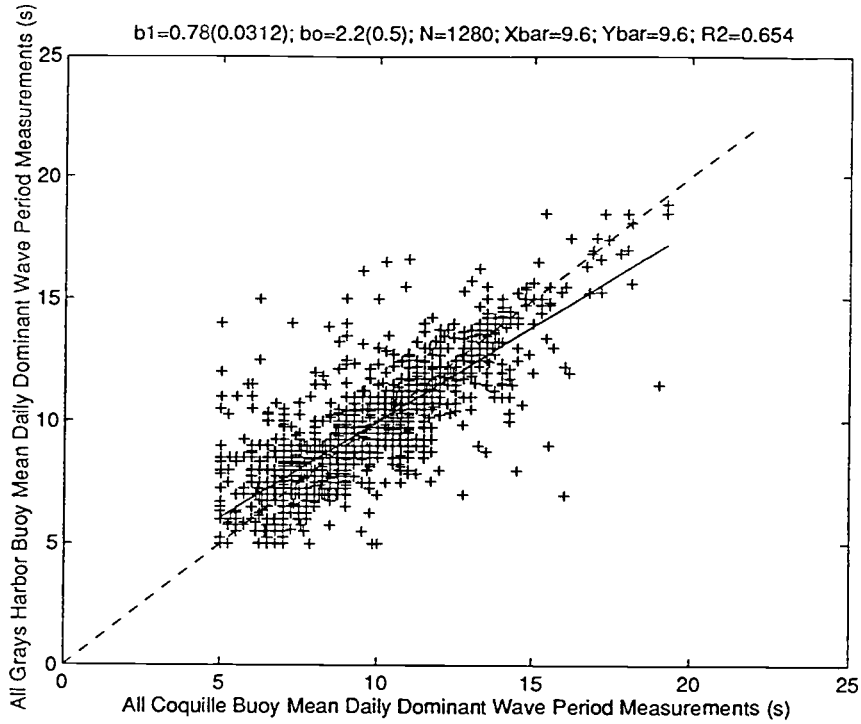

B)

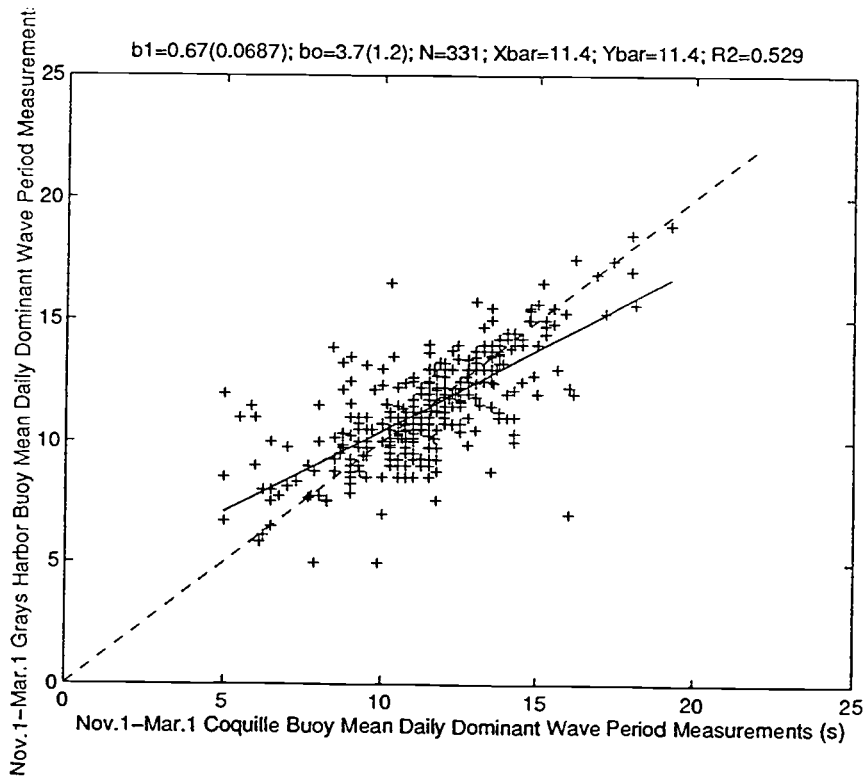

Figure 7 (A/B). A regression of Coquille (CDIP) and Grays Harbor (CDIP) deep-water buoy dominant wave period measurements for A) ALL DATA, and B) WINTER MOS (Nov.-Feb.). The solid line is the best-fit least-squares regression line, and the dashed line is 1:1.

C)

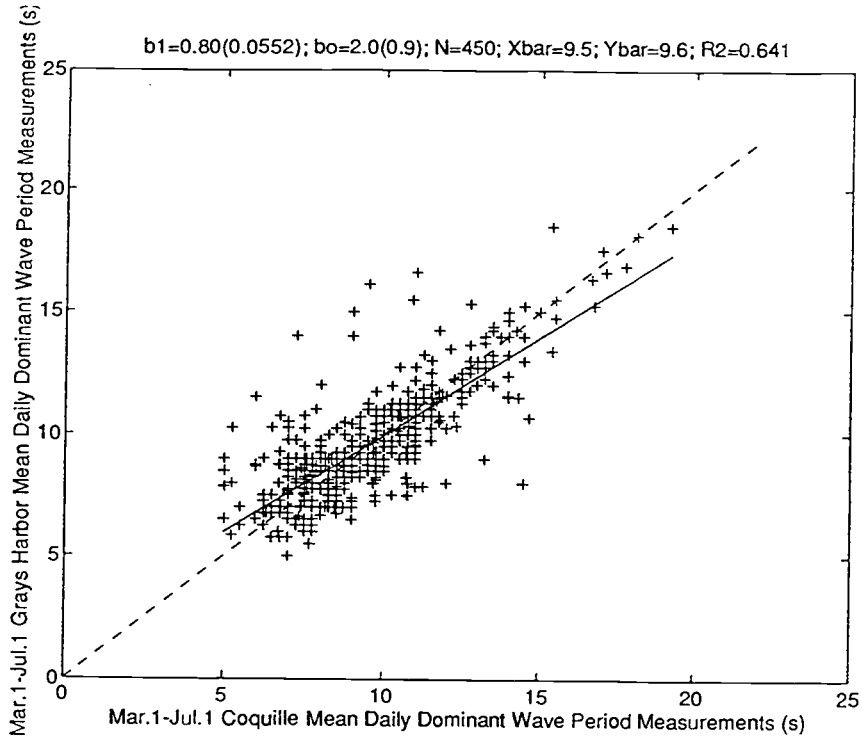

D)

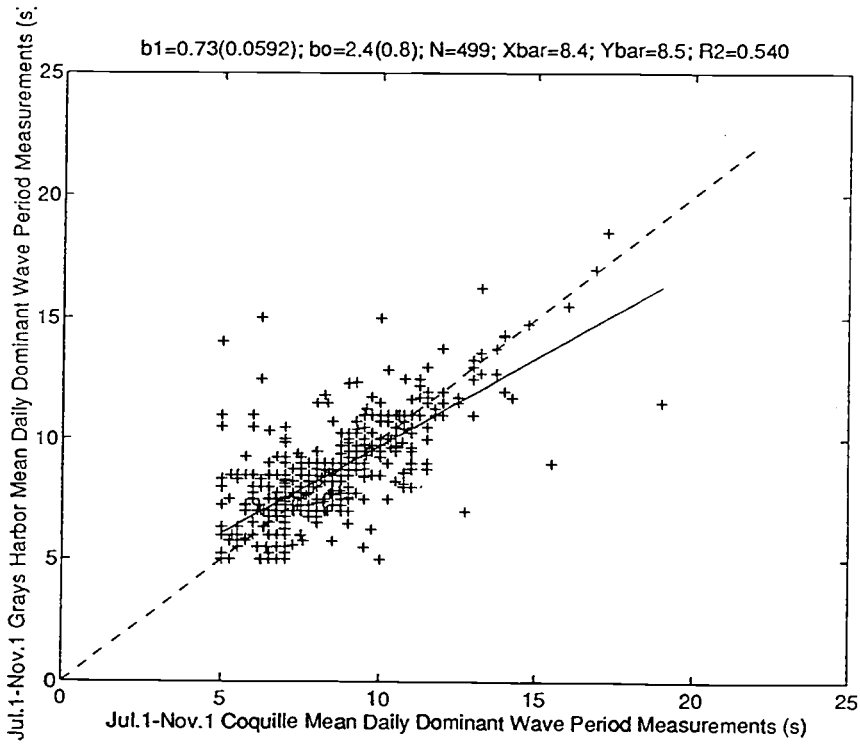

Figure 7 (C/D). A regression of Coquille (CDIP) and Grays Harbor (CDIP) deep-water buoy dominant wave period measurements for C) SPRING (Mar.-Jun.) and D) SUMMER (Jul.-Oct.). The solid line is the best-fit least-squares regression line, and the dashed line is 1:1.

A)

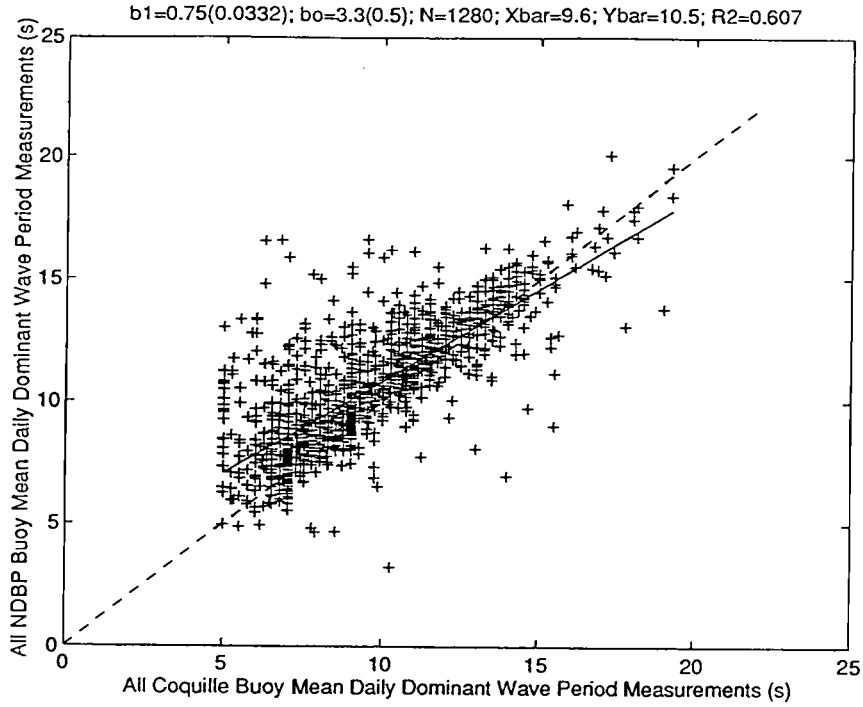

B)

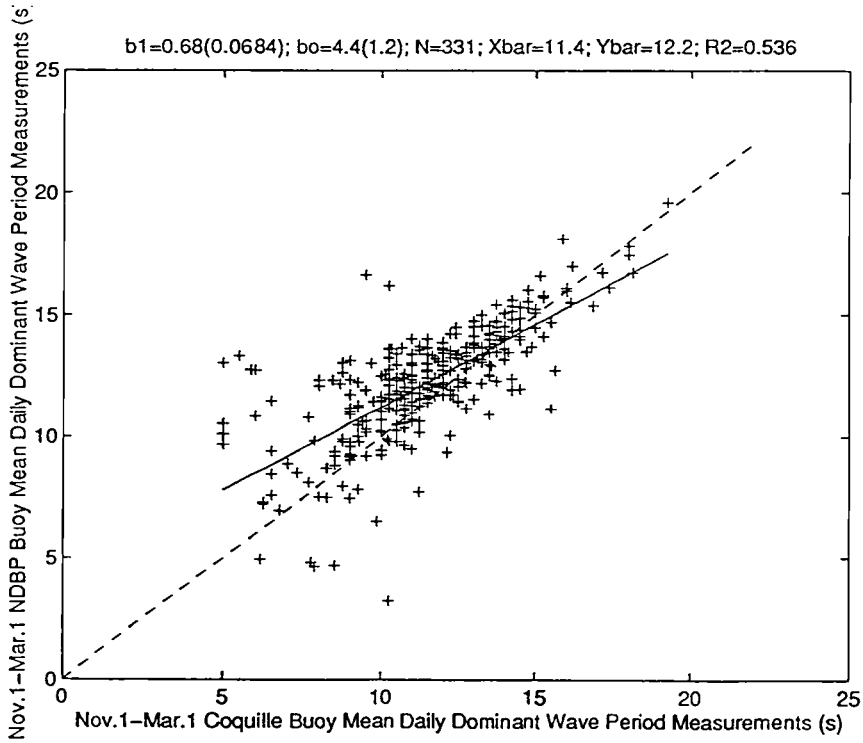

Figure 8 (A/B). A regression of Coquille (CDIP) and Newport (NDBC) deep-water buoy dominant wave period measurements for A) ALL DATA, and B) WINTER MOS (Nov.-Feb.). The solid line is the best-fit least-squares regression line, and the dashed line is 1:1.

C)

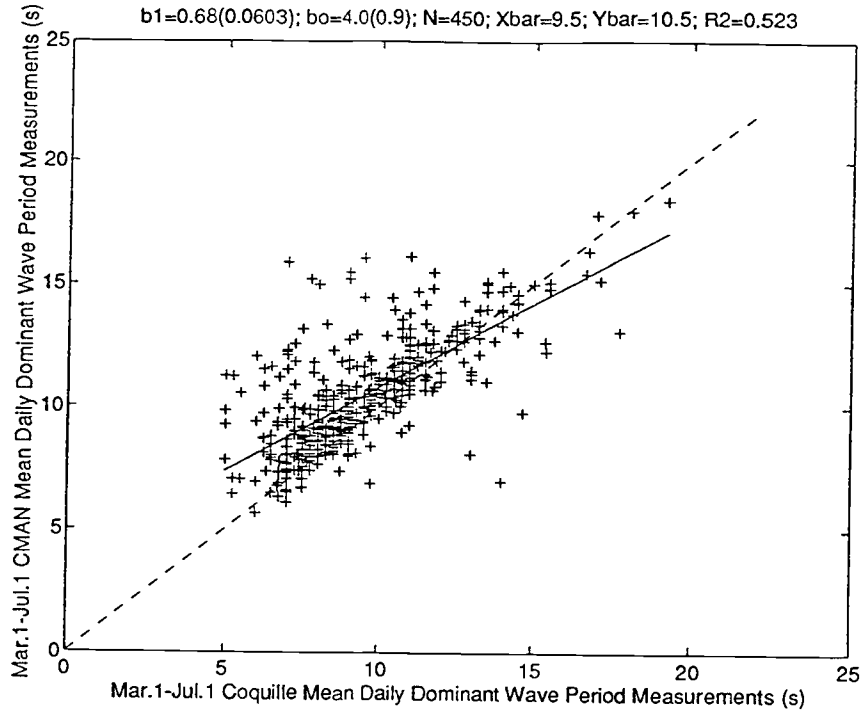

D)

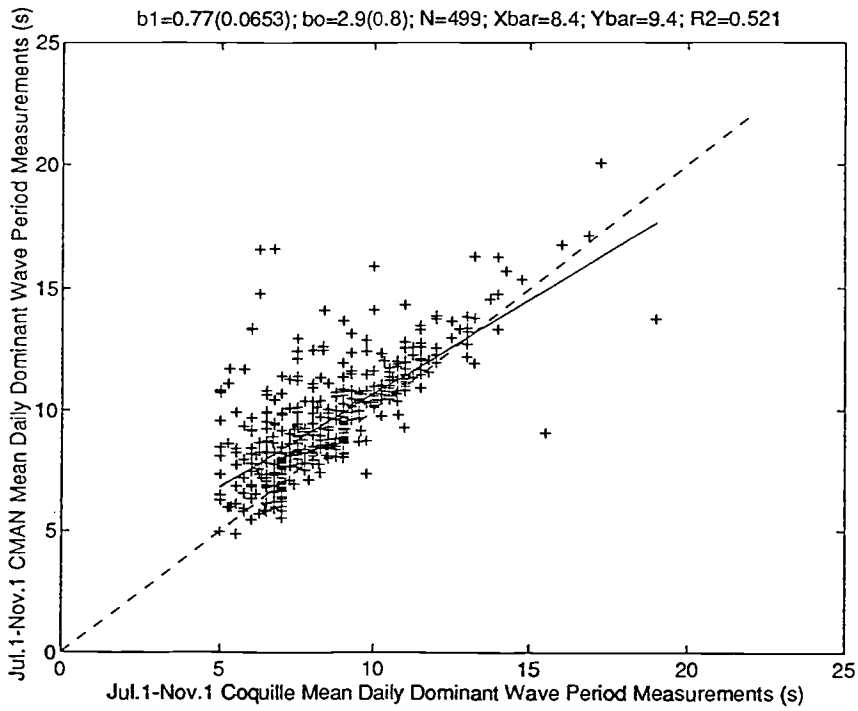

Figure 8 (C/D). A regression of Coquille (CDIP) and Newport (NDBC) deep-water buoy dominant wave period measurements for C) SPRING (Mar.-Jun.) and D) SUMMER (Jul.-Oct.). The solid line is the best-fit least-squares regression line, and the dashed line is 1:1.

Distributions of Deep-Water Buoy Data

Figures 10a, b, and c show the distributions of significant wave height measurements respectively for the Coquille, NDBC, and Grays Harbor buoys. These distributions represent all individual wave height measurements made by each buoy since deployment. Note that the NDBC distribution has far more observations (35K) than the Scripps buoy distributions (15-17K), a result of more frequent sampling by the NDBC buoy (hourly as opposed to every ~3 hours). All three distributions have the same shape (skewed towards smaller wave heights with rare large wave heights), indicating similar wave climates. The distributions are shifted right of zero since each point in the distribution is a significant wave height which is not likely to be near zero. Though the significant wave height measurements appear to be Rayleigh distributed, they fail the statistical goodness-of-fit test.

Wave height distributions were then plotted log-normally. Figures 11a, b, and c show the log-normal distributions of all significant wave height measurements for the Coquille, NDBC, and Grays Harbor buoys. Although the three distributions fail the Chi-squared goodness-of-fit test, they all appear log-normally distributed. The Chi-squared statistic was calculated using the number of bins and degrees of freedom shown in the figures. The number of bins could be altered so that the distributions have a better goodness-of-fit to the normal distribution, but then detailed information on the shapes of the distributions would not be resolvable. The distributions all appear to be equally broad-banded, indicating similar overall wave variability at each location. The distributions of NDBC data appear more irregular than the CDIP distributions, which may be due to differences in sampling intervals between the different systems. The NDBC buoy samples hourly, whereas the CDIP systems sample roughly every 3 hours. Wave data sampled hourly are more mutually correlated, and potentially violate the statistical assumption of independent random data. This may account for the NDBC distributions appearing more irregular.

The distributions were separated into three four-month segments to examine any seasonality in the wave climate at each location. Figure 12a, b, and c show the log-normal distributions of mean daily significant wave heights measured by the Coquille buoy for the periods November 1-March 1 (period 1 (a)), March 1- July 1 (period 2 (b)), and July 1- November 1 (period 3 (c)), respectively. Figures 13 and 14 (a, b, and c) show similar distributions for the NDBC and Grays Harbor buoys. For each buoy, period 1 contains 332 observations (days), period 2 contains 450 observations, and period 3 has

A)

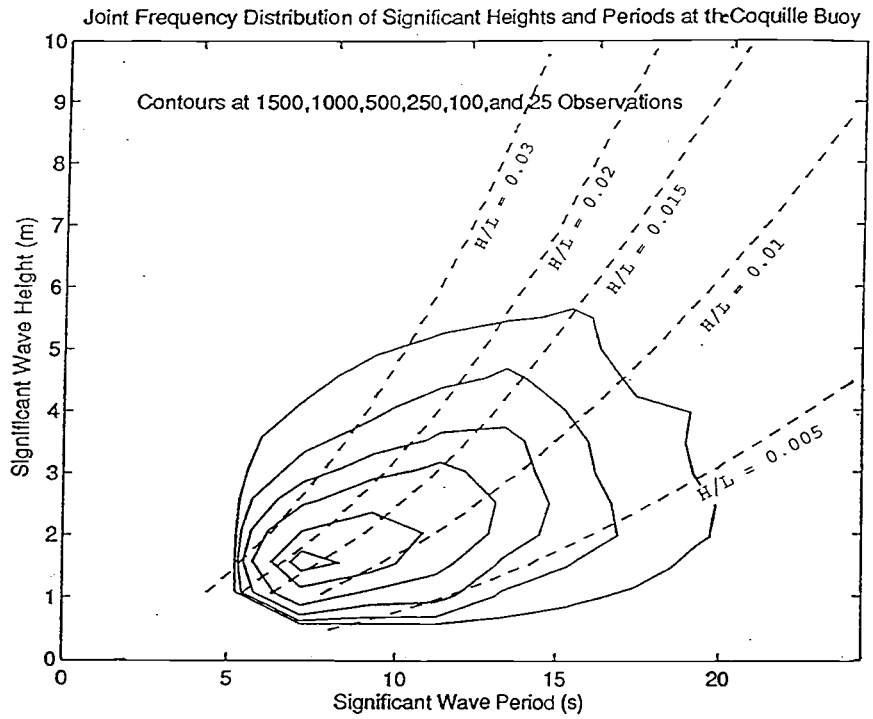

B)

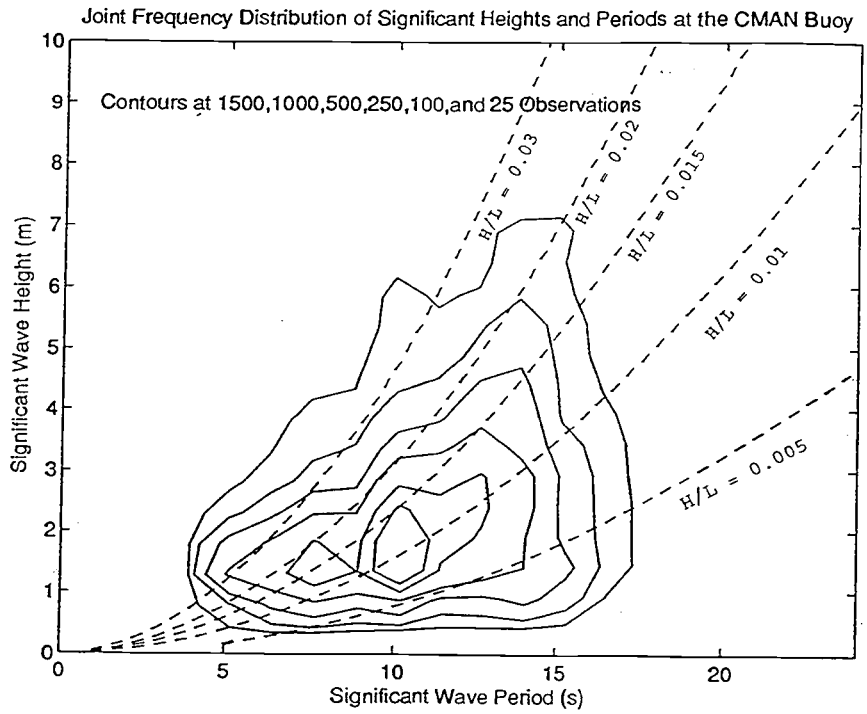

Figure 9 (A/B). The joint frequency plot of significant wave heights versus dominant wave periods for the measurements derived from A) the CDIP buoy offshore from Bandon, Oregon, and B) the NDBC buoy offshore from Newport, Oregon, approximately mid-way between the two CDIP stations.

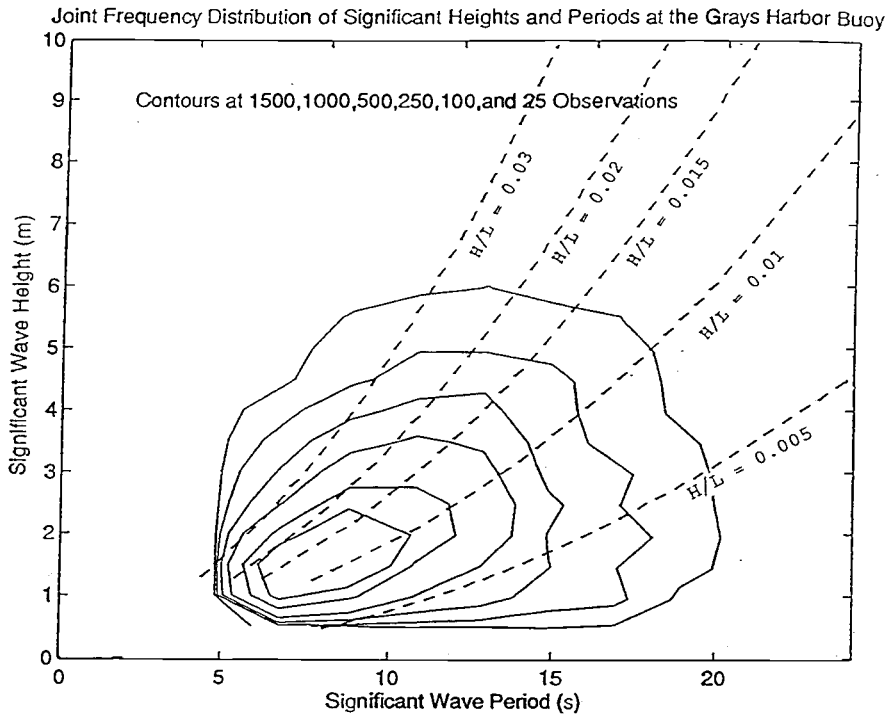

Figure 9 C. The joint frequency plot of significant wave heights versus dominant wave periods for the measurements derived from the CDIP deep-water buoy offshore from Grays Harbor, Washington.

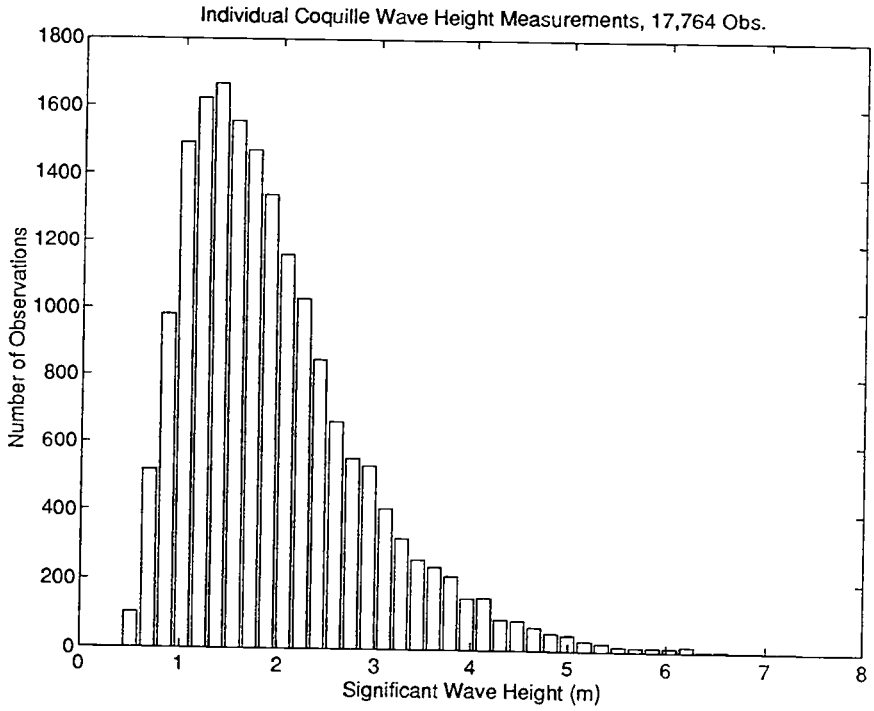

Figure 10A. Histogram of all CDIP Coquille Bay buoy significant wave heights.

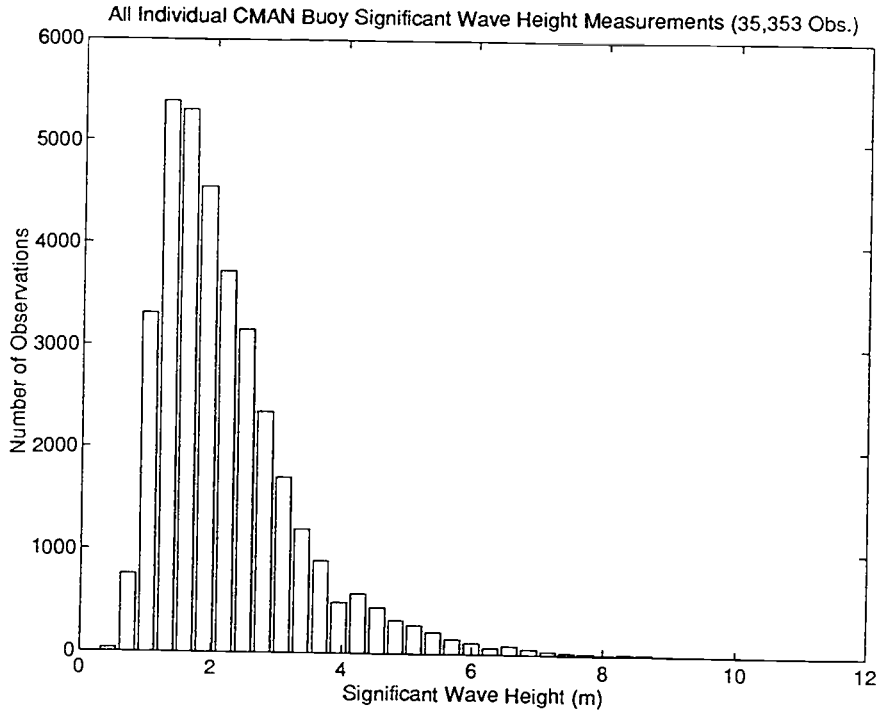

Figure 10B. Histogram of NDBC Newport buoy significant wave heights.

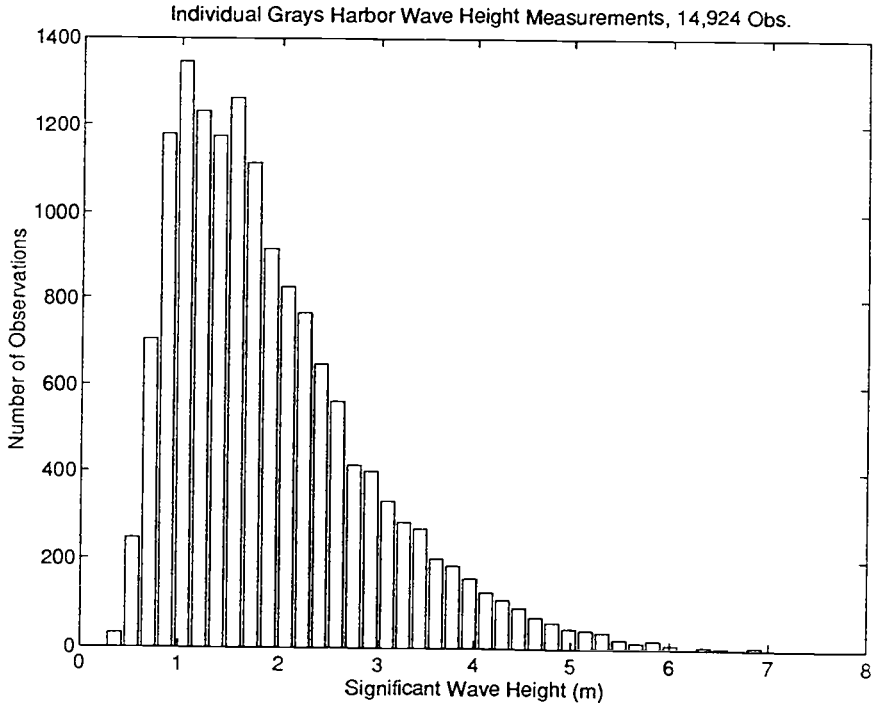

Figure 10C. Histogram of all CDIP Grays Harbor buoy significant wave heights.

499 observations. Differences noted in the tables of statistics already presented are evident in the distributions. The variance in wave heights between the three buoys, represented by the widths of the distributions, is similar. Also observable is that the distributions become more narrow-banded from period 1 to period 3, a reflection of the wave generation process (i.e. the seasonality of storm systems). The mean of the NDBC buoy wave height observations can also be seen in the distributions as being slightly larger than that of the other two buoys. Though none of the buoy wave height distributions pass the Chi-squared goodness-of-fit test, the Scripps buoy measurements appear more log-normally distributed. In fact, they appear to become more log-normally distributed from period 1 to period 3, which may reflect either an increasing narrow-bandedness, or simply an increasing number of observations.

Figures 15 a, b, and c show the distributions of all dominant wave period measurements for the three buoys. The lack of detail in the distributions (their large bin widths) is an artifact of the spectral calculation of dominant wave period. No attempts were made to try and fit these distributions to theoretical probability distributions.

Buoy and Pressure-Sensor Array Comparisons

Pressure-sensor array data from the Coquille Bay, OR and Long Beach, Washington stations were analyzed in the same manner as the offshore buoy data. Direct comparisons were made between data from each array and data from the nearest offshore buoy. This results in comparing Coquille array data with the Coquille deep-water buoy data (directly offshore), and Long Beach array data with the Grays Harbor deep-water buoy data (nearly 55 km north of the Long Beach station). Both arrays are operated by the CDIP of Scripps Institution of Oceanography. Wave heights measured by the arrays are depth-corrected using linear wave theory to represent deep-water wave heights (wave refraction effects are not included). This permits direct comparisons of buoy and array data, and offers something of a test of the linear wave transformation.
Data from the pressure-sensor arrays were analyzed to produce mean daily significant wave heights and mean daily dominant wave periods. Data for the array/buoy comparisons span roughly 8 years of discontinuous wave measurements (See Table 1). Figures 16a and 16b compare monthly mean and maximum (mean daily) values of significant wave heights for the Coquille Bay array and offshore buoy. There is excellent agreement between wave height monthly means for the two data sets, whereas wave

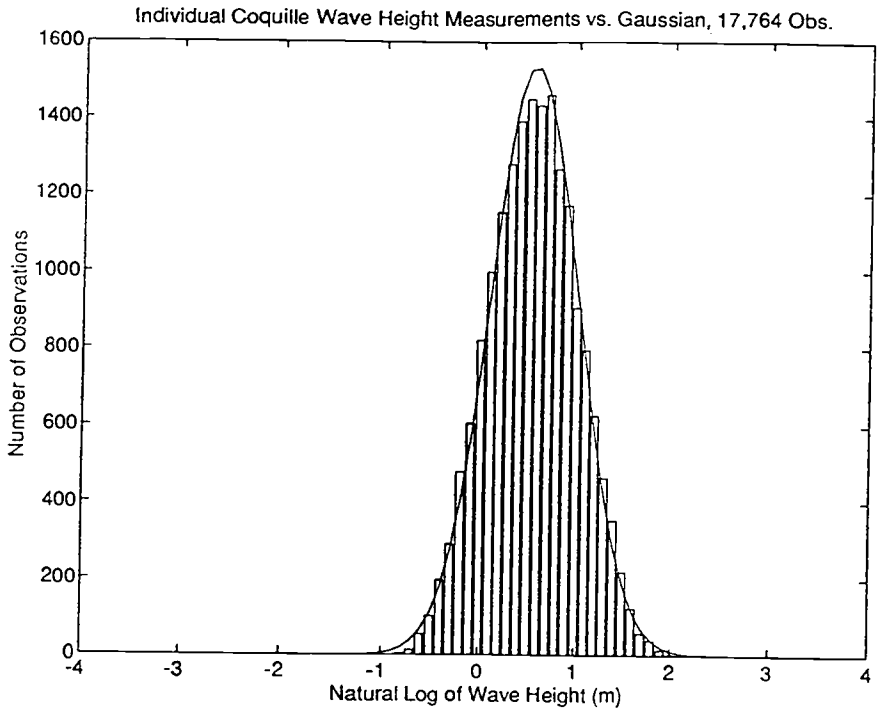

Figure 11A. The log-normal distribution of all CDIP Coquille Bay buoy significant wave height measurements versus the Gaussian distribution.

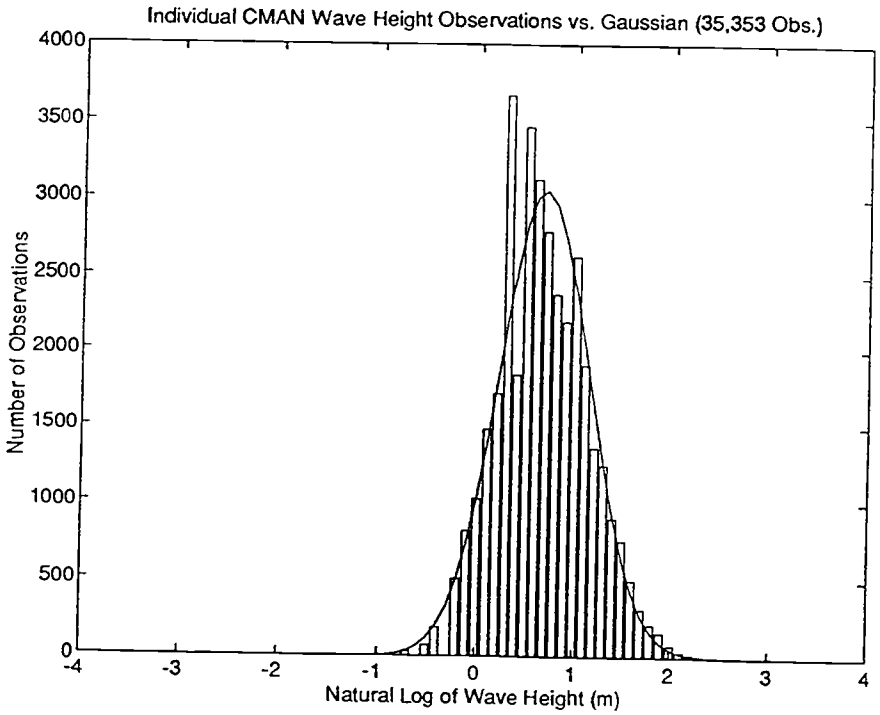

Figure 11B. The log-normal distribution of all NDBC Newport buoy significant wave height measurements versus the Gaussian distribution.

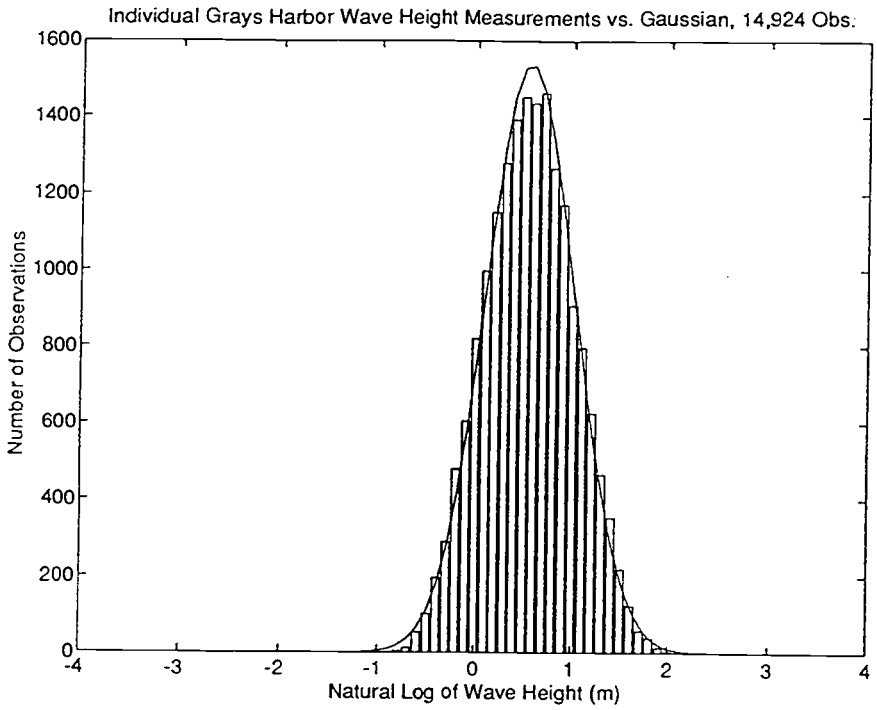

Figure 11C. The log-normal distribution of all CDIP Grays Harbor buoy significant wave height measurements versus the Gaussian distribution.

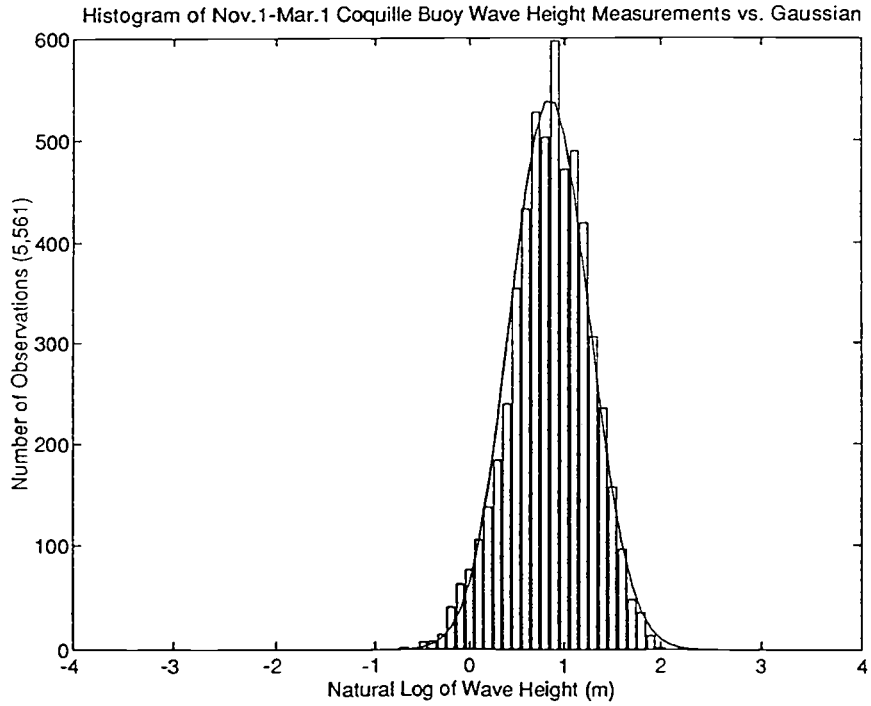

Figure 12A. The log-normal distribution of Winter (Nov.-Feb.) CDIP Coquille Bay buoy significant wave height measurements versus the Gaussian distribution.

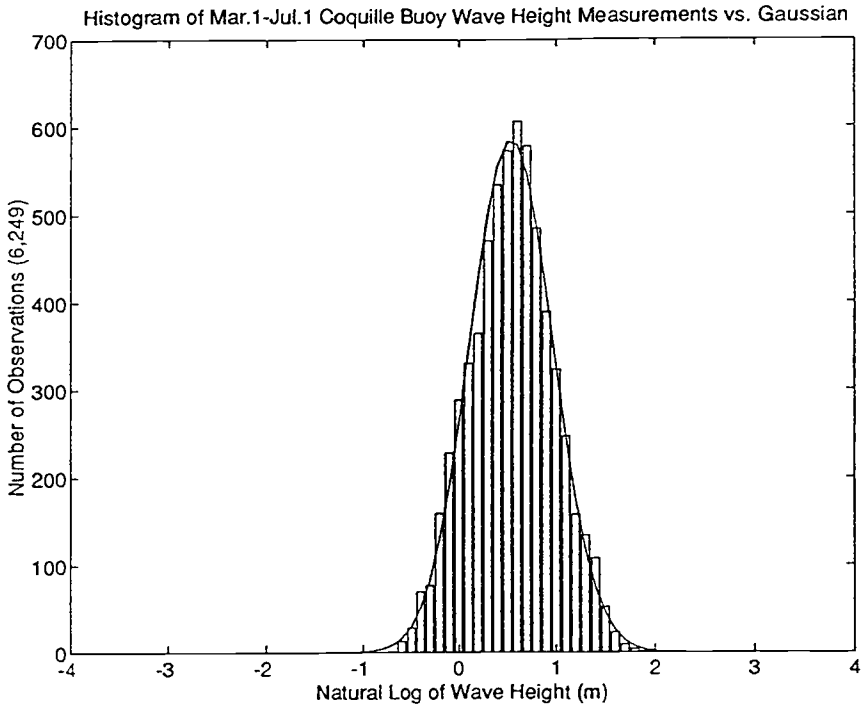

Figure 12B. The log-normal distribution of Spring (Mar-Jun.) CDIP Coquille Bay buoy significant wave height measurements versus the Gaussian distribution.

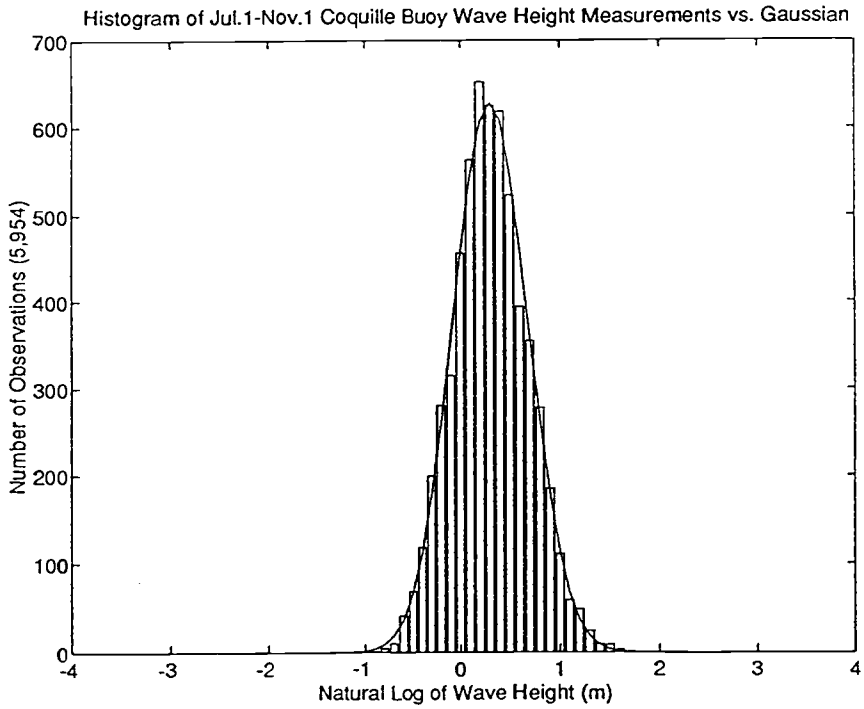

Figure 12C. The log-normal distribution of Summer (Jul.-Oct.) CDIP Coquille Bay buoy significant wave height measurements versus the Gaussian distribution.

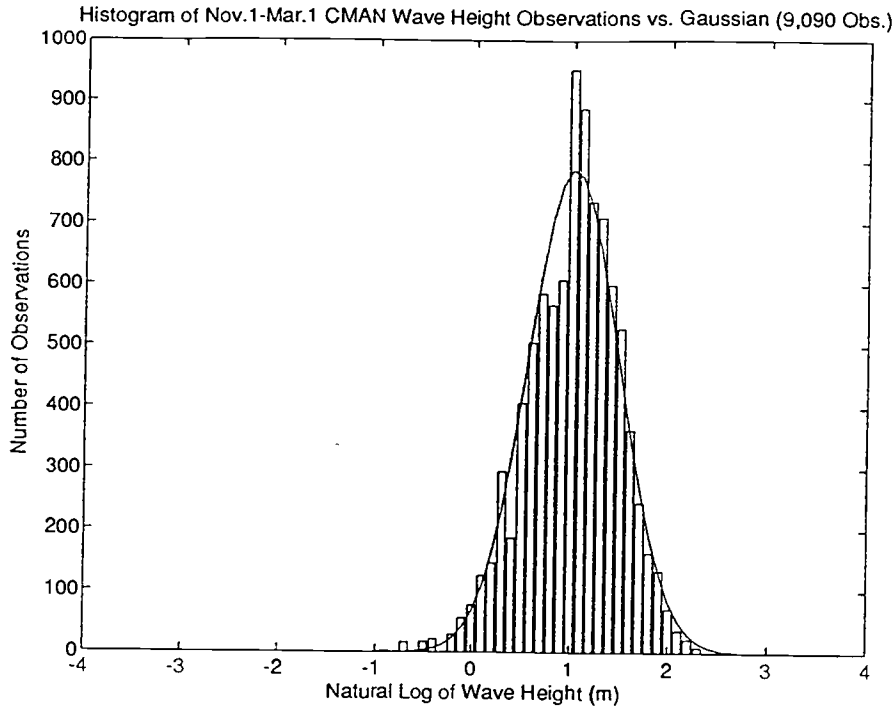

Figure 13A. The log-normal distribution of Winter (Nov.-Feb.) NDBP Cape Foulweather buoy significant wave height measurements versus the Gaussian distribution.

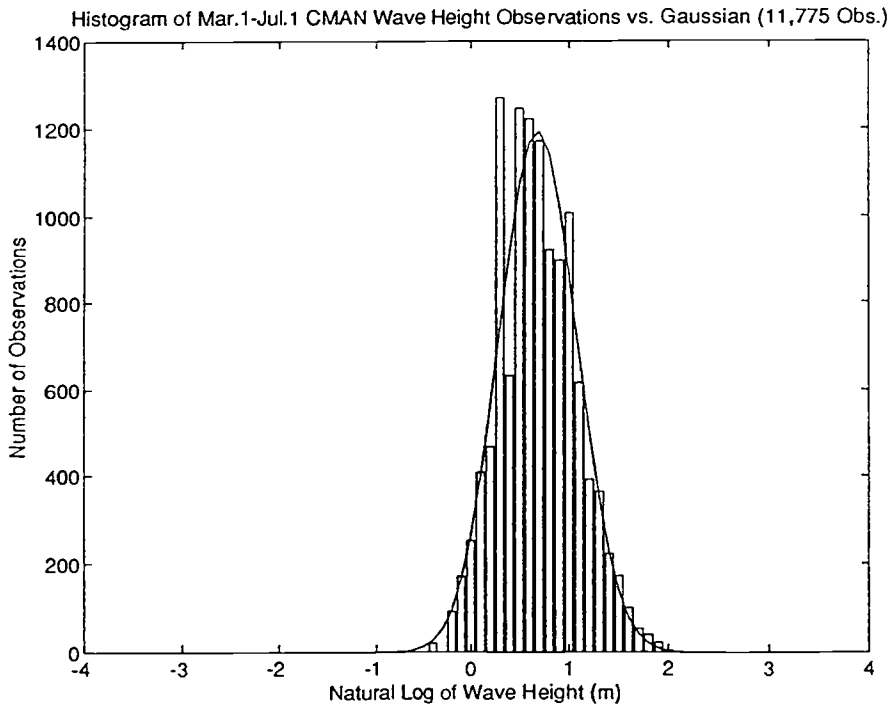

Figure 13B. The log-normal distribution of Spring (Mar.-Jun.) NDBC Cape Foulweather buoy significant wave height measurements versus the Gaussian distribution.

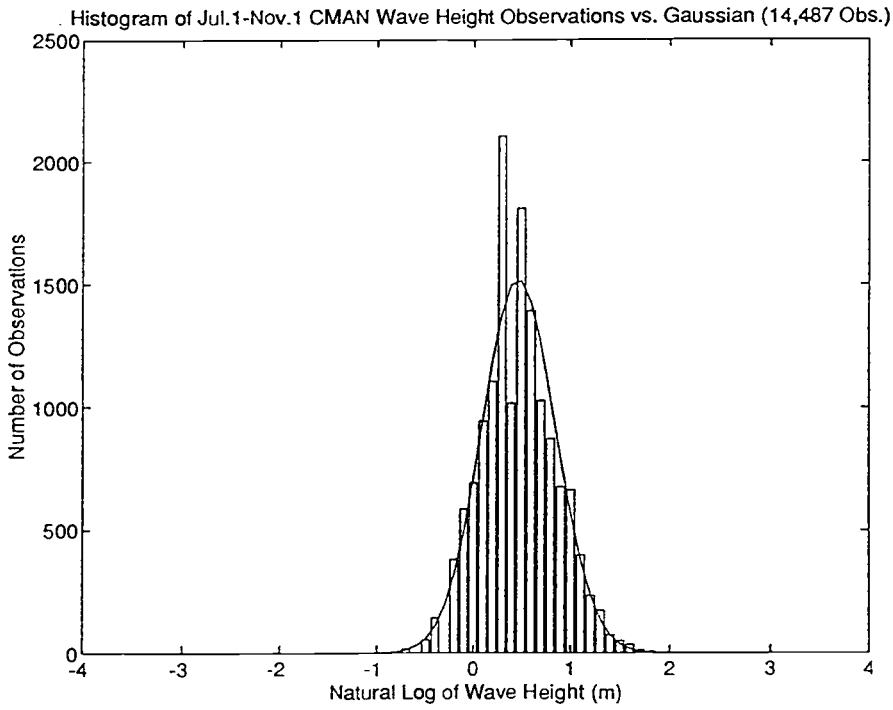

Figure 13C. The log-normal distribution of Summer (Jul.-Oct.) NDBC Cape Foulweather buoy significant wave height measurements versus the Gaussian distribution.

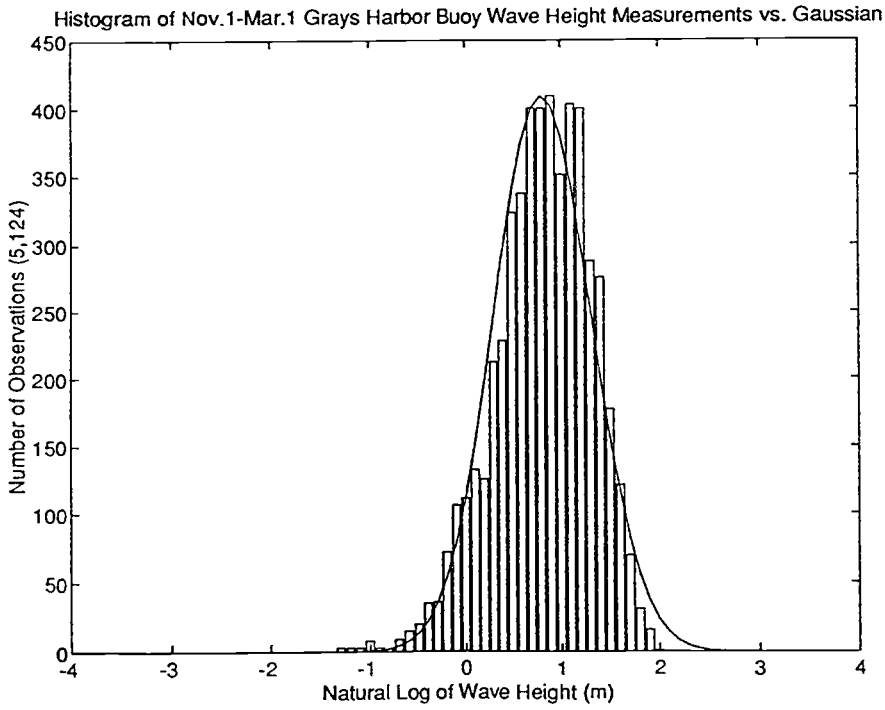

Figure 14A. The log-normal distribution of Winter (Nov.-Mar.) CDIP Grays Harbor buoy significant wave height measurements versus the Gaussian distribution.

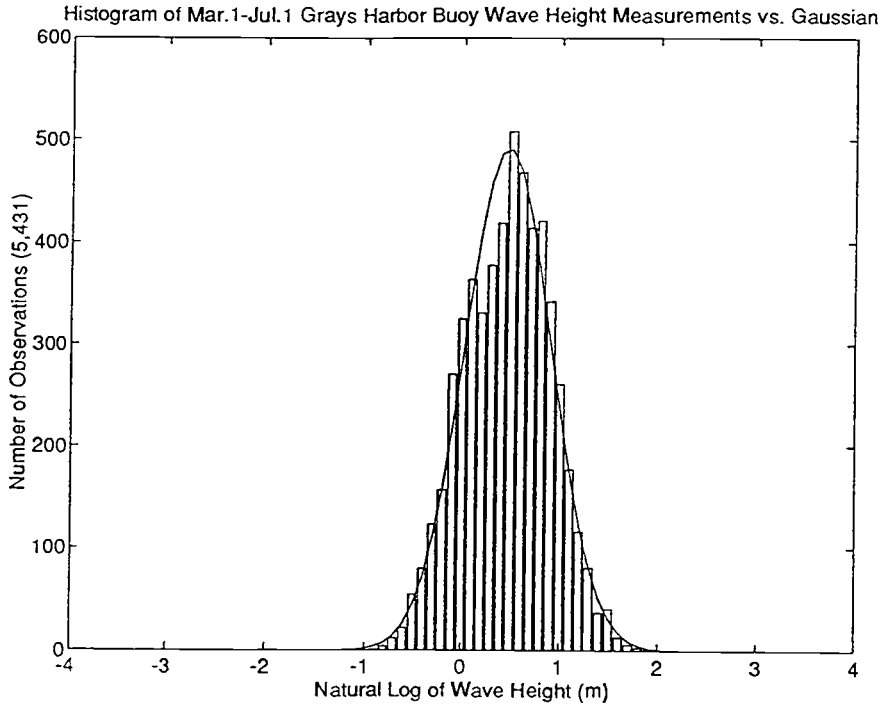

Figure 14B. The log-normal distribution of Spring (Mar.-Jun.) CDIP Grays Harbor buoy significant wave height measurements versus the Gaussian distribution.

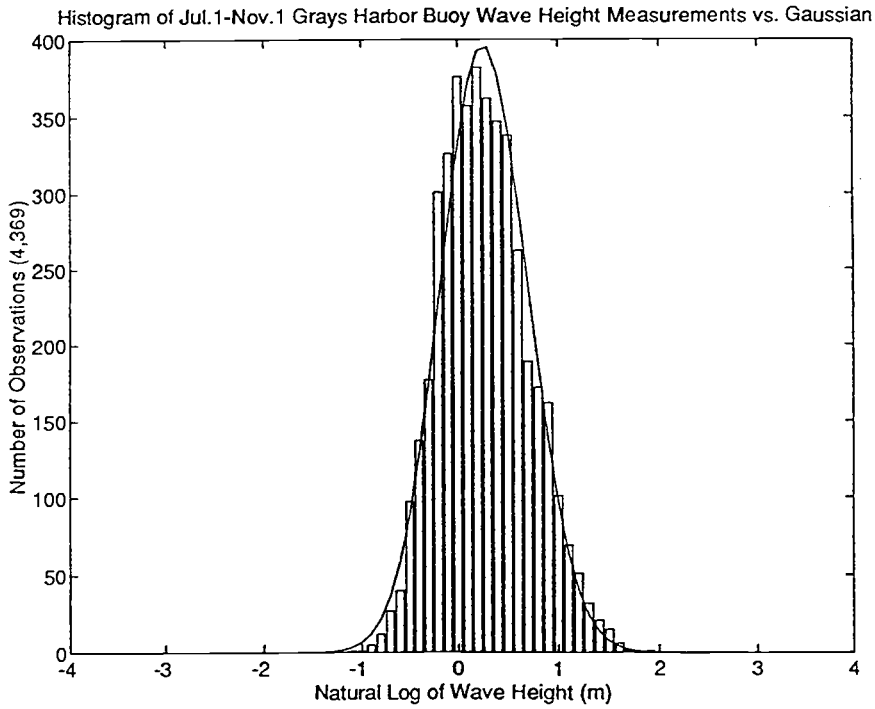

Figure 14C. The log-normal distribution of Summer (Jul.-Oct.) CDIP Grays Harbor buoy significant wave height measurements versus the Gaussian distribution.

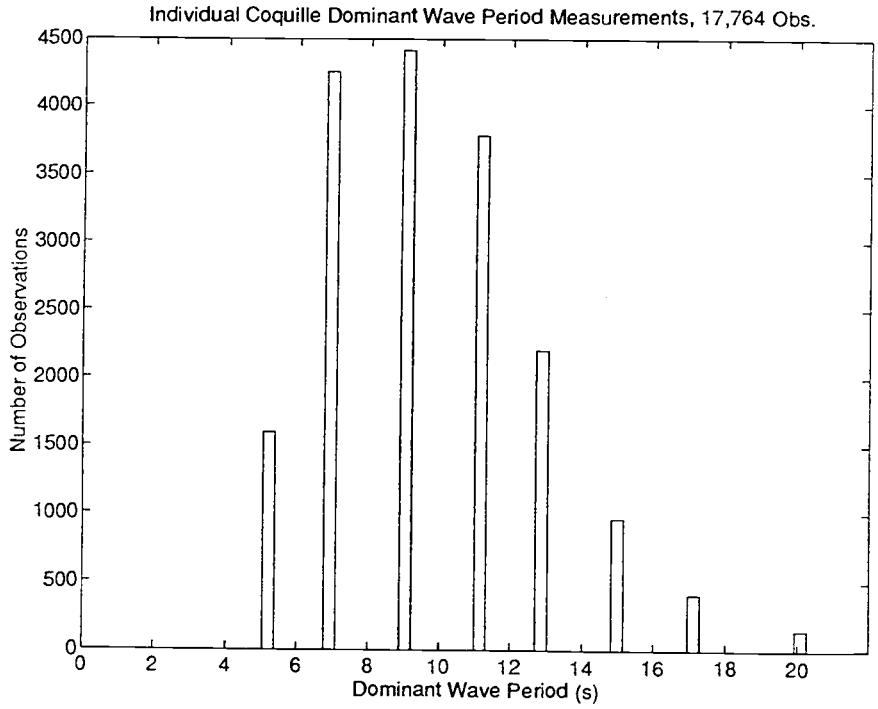

Figure 15A. Histogram of all CDIP Coquille Bay dominant wave period measurements.

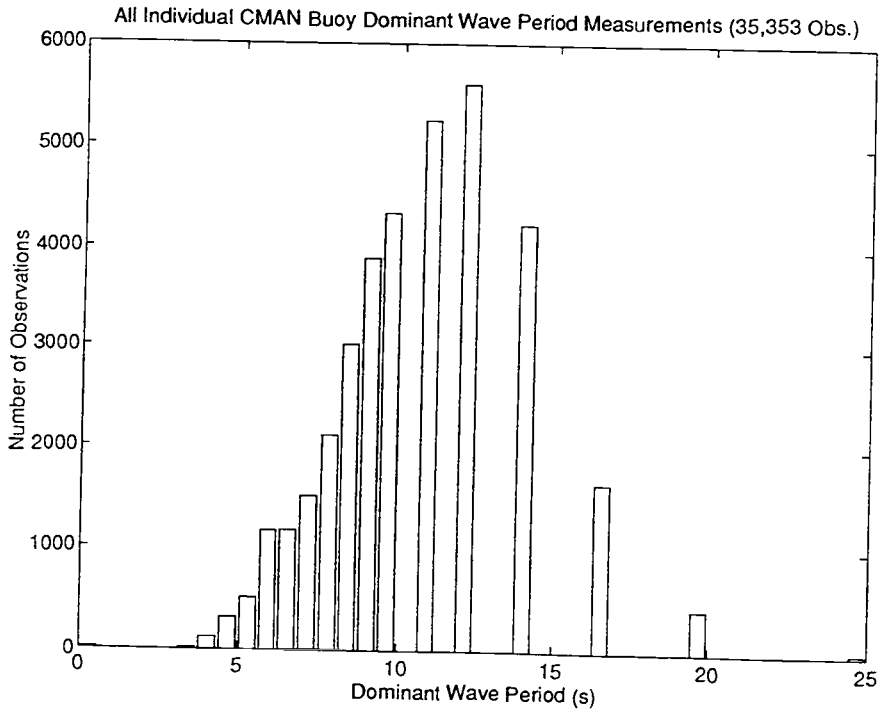

Figure 15B. Histogram of all NDBC Newport dominant wave periods.

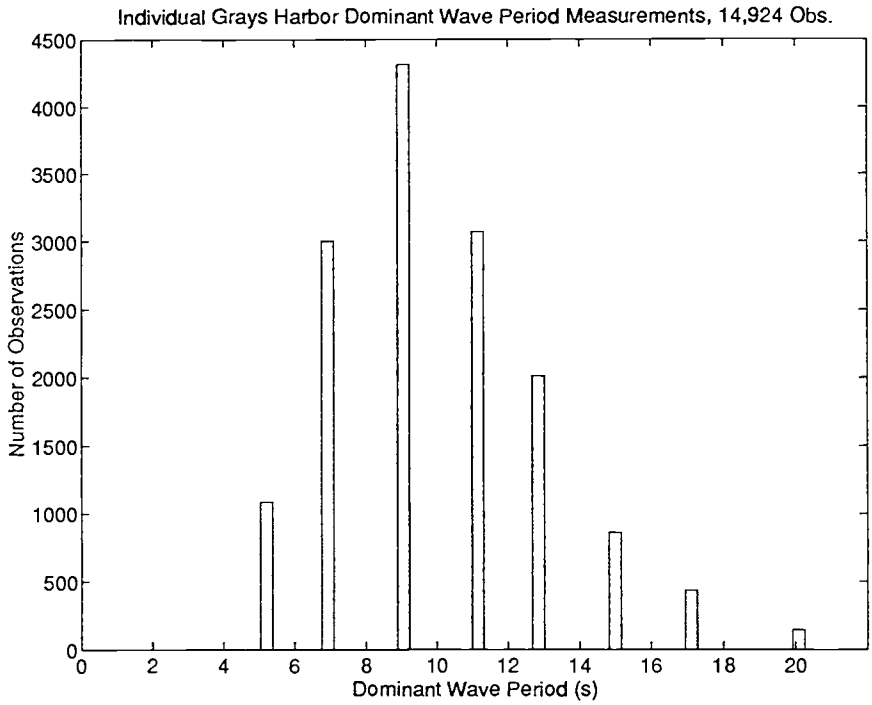

Figure 15C. Histogram of all CDIP Grays Harbor dominant wave period measurements.

height maxima do not agree as well (though they display the same annual trend). The array mean monthly significant wave heights are roughly O(0.5m) larger than the offshore buoy maxima, and the maximum mean-monthly values are O(1m) larger. Given the proximity of the two stations (and therefore the improbability of climatic differences), these observed differences in wave height must be due to the linear wave theory transformation of the array data and/or experimental errors.

Figures 17a and 17b show similar comparisons based on monthly mean and maximum dominant wave periods. Monthly mean and maximum dominant wave periods agree very well in magnitude as do significant wave heights, and the annual trend in means is similar and evident. There appears to be no annual trend in maximum reported values of dominant wave period, though they agree very well. There is little physical reason why measured dominant periods should be different between the Coquille buoy and array, since wave period is essentially conserved during shoaling (there are slight frequency shifts in the spectrum due to shoaling transformations and friction, which may account for the differences). Tables 8a and 8b contain the basic statistics of the Coquille array and buoy for the days of measurement overlap between the two stations on which Figures 16 and 17 are based. Wave height and period variances are also included, as well as the number of observations (days) upon which each monthly average is based.

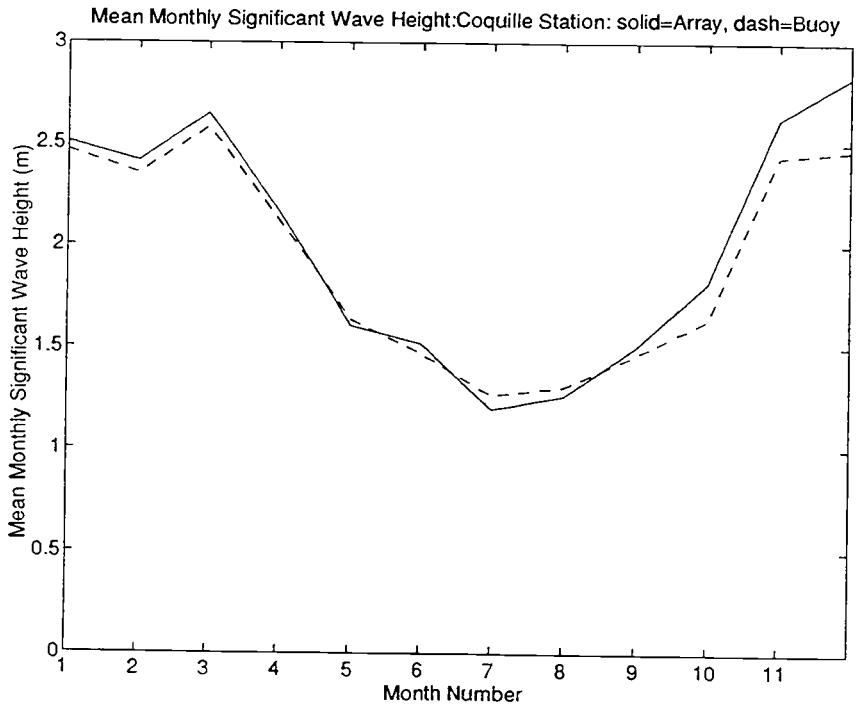

Figure 16A. Comparison of the mean monthly significant wave heights between the CDIP Coquille Bay deep-water buoy and shallow-water pressure sensor array.

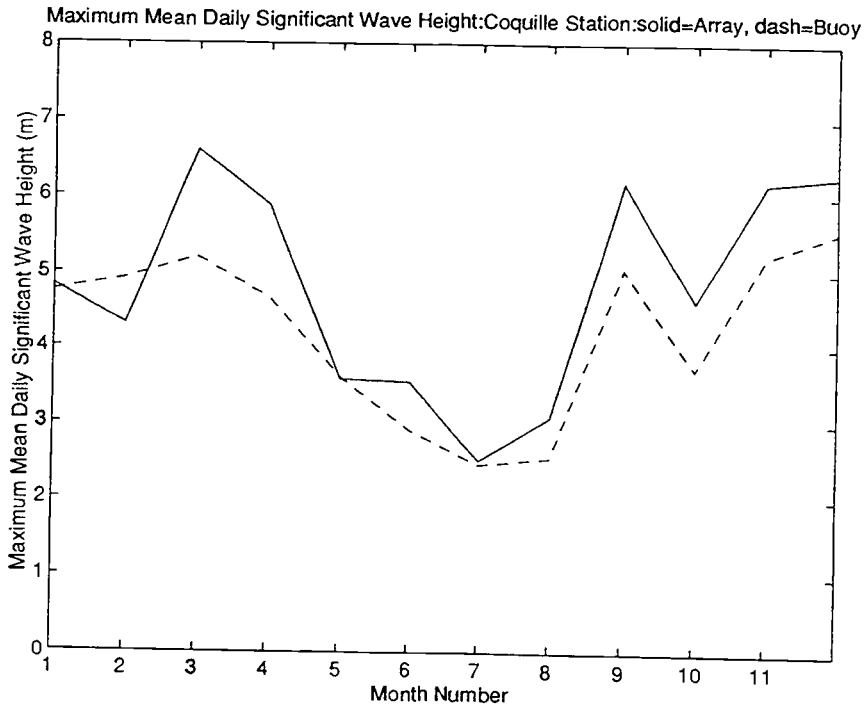

Figure 16B. Comparison of maximum monthly significant wave heights between the CDIP Coquille Bay deep-water buoy and shallow-water pressure sensor array.

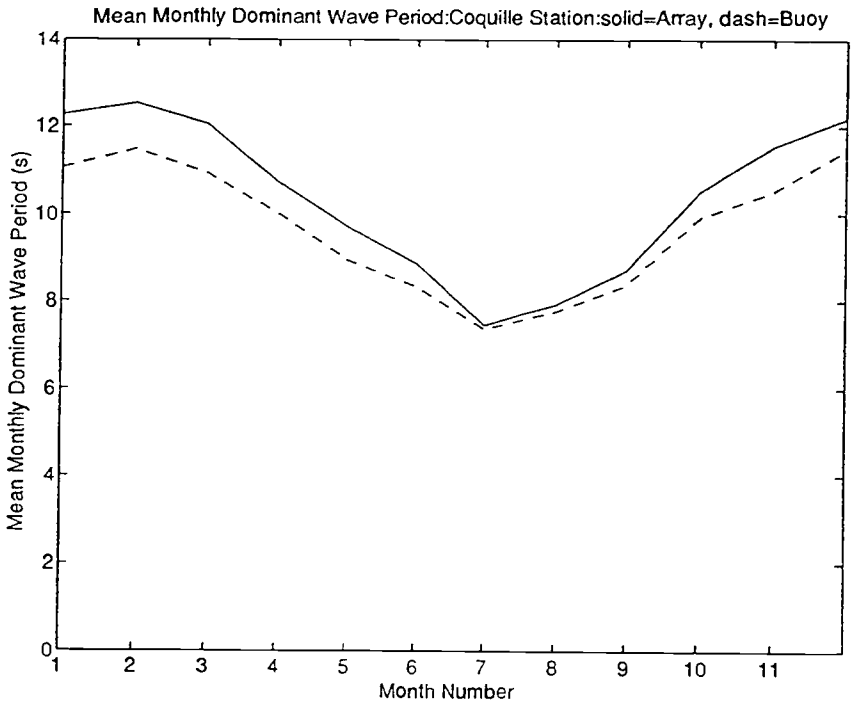

Figure 17A. Comparison of mean monthly dominant wave periods between the CDIP Coquille Bay deep-water buoy and shallow-water pressure sensor array.

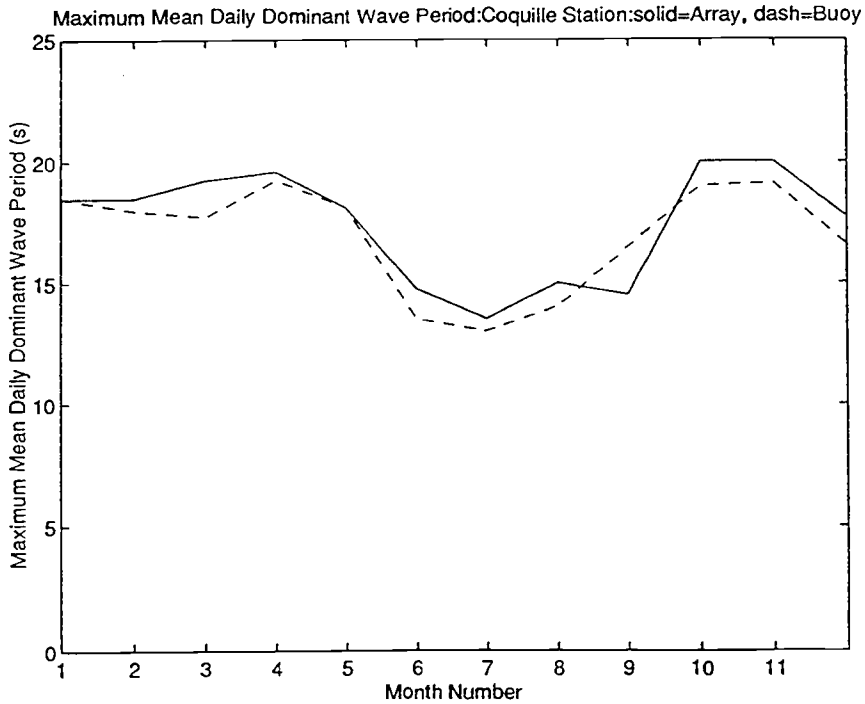

Figure 17B. Comparison of maximum monthly dominant wave periods between the CDIP Coquille Bay deep-water buoy and shallow-water pressure sensor array.

Table 8a. Coquille pressure-sensor array wave statistics.

Month	MD Hs (m)	Hs Variance (m*m)	Max MD Hs (m)	MD Td (s)	Td Variance (s*s)	Max MD Td (s)	Observations
January	2.51	0.64	4.83	12.26	4.92	18.5	119
February	2.41	0.57	4.31	12.52	6.38	18.5	121
March	2.64	1.22	6.6	12.04	7.61	19.25	122
April	2.16	0.96	5.88	10.72	5.36	19.6	101
May	1.61	0.34	3.57	9.7	5.5	18.13	91
June	1.52	0.31	3.54	8.87	4.13	14.75	102
July	1.19	0.18	2.51	7.44	2.46	13.5	131
August	1.26	0.21	3.08	7.92	2.99	15	163
September	1.5	0.48	6.18	8.71	4.46	14.5	167
October	1.82	0.51	4.62	10.49	5.92	20	173
November	2.62	0.99	6.17	11.55	5.49	20	103
December	2.83	1.47	6.27	12.2	5.43	17.75	100

MD - Mean Daily; Td - Dominant Wave Period; Hs - Significant wave Height

Table 8b. Coquille deep-water buoy wave statistics.

Month	MD Hs (m)	Hs Variance (m*m)	Max MD Hs (m)	MD Td (s)	Td Variance (s*s)	Max MD Td (s)	Observations
January	2.46	0.61	4.75	11.05	4.95	18.5	119
February	2.35	0.52	4.92	11.47	6.42	18	121
March	2.57	0.84	5.2	10.91	5.82	17.75	122
April	2.12	0.64	4.66	10.01	5.87	19.25	101
May	1.64	0.32	3.6	8.93	3.99	18.13	91
June	1.47	0.27	2.91	8.33	3.01	13.5	102
July	1.26	0.15	2.46	7.35	1.82	13	131
August	1.3	0.17	2.54	7.75	2.63	14	163
September	1.46	0.32	5.05	8.37	4.26	16.5	167
October	1.63	0.33	3.71	9.91	5.79	19	173
November	2.43	0.78	5.23	10.51	7.07	19.12	103
December	2.47	0.99	5.54	11.47	5.45	16.6	100

F-test and t-test comparisons for mean monthly significant wave heights and dominant periods were made between the Coquille pressure-sensor array and deep-water buoy. Significant wave height monthly means and variances, and dominant wave period variances test at or below the critical test value at the 95% confidence limit. Therefore, there is no evidence to conclude that these quantities are different between the two stations. However, dominant wave period means do not test as well, though all t-test

values are near or just above the critical test value in nearly every month. This suggests that period means are statistically different for certain months.

Figures 18a and 18b show comparisons of monthly mean and maximum values of significant wave heights between the Long Beach pressure-sensor array and Grays Harbor deep-water buoy. In Figure 17a it is evident that the array data has slightly larger (O(0.5m)) magnitudes of monthly mean wave heights, with very similar annual trends in both figures.

Figures 19a and 19b show comparisons of monthly mean and maximum values of dominant wave periods between the Long Beach pressure-sensor array and Grays Harbor deep-water buoy. Surprisingly, unlike the comparison with the Coquille data, dominant wave period means and maxima agree more favorably than do significant wave height means and maxima for these two sensors. Tables 8c and 8d contain the basic statistics (on which Figures 18 and 19 are based) of the Grays Harbor buoy and Long Beach array for the days of measurement overlap between the two stations. Monthly wave height and period variances, and the number of observations (days) on which each monthly measurement is based are presented there.

Table 8c. Grays Harbor deep-water buoy wave statistics.

Month	MD Hs (m)	Hs Variance (m*m)	Max MD Hs (m)	MD Td (s)	Td Variance (s*s)	Max MD Td (s)	Observations
January	2.68	1.31	6.17	11.67	4.56	17	95
February	2.27	0.62	4.4	11.92	5.13	17.75	112
March	2.1	0.58	4.21	11.41	6.19	18.13	124
April	2.07	0.54	4.18	10.71	5.51	18.5	98
May	1.51	0.34	2.8	9.37	5.82	17.88	68
June	1.37	0.23	2.66	8.37	3.71	15.5	53
July	1.2	0.12	2.35	7.97	3.05	14.5	85
August	1.27	0.24	2.39	8.27	3.34	14	73
September	1.51	0.41	3.89	9.65	6.54	18.5	86
October	1.87	0.51	3.72	10.25	4.36	16	112
November	2.26	0.87	5.17	10.38	3.74	16	109
December	2.78	1.65	6.01	12.53	4.4	18.88	70

MD - Mean Daily; Td - Dominant Wave Period; Hs - Significant wave Height

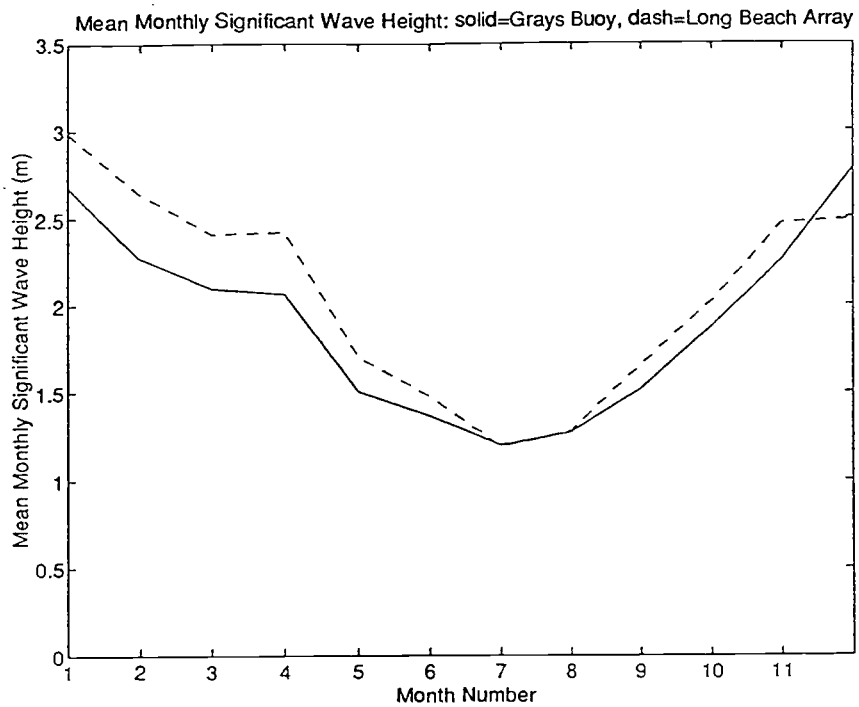

Figure 18A. Comparison of mean monthly significant wave heights between the CDIP Grays Harbor, OR buoy and Long Beach, WA shallow-water array.

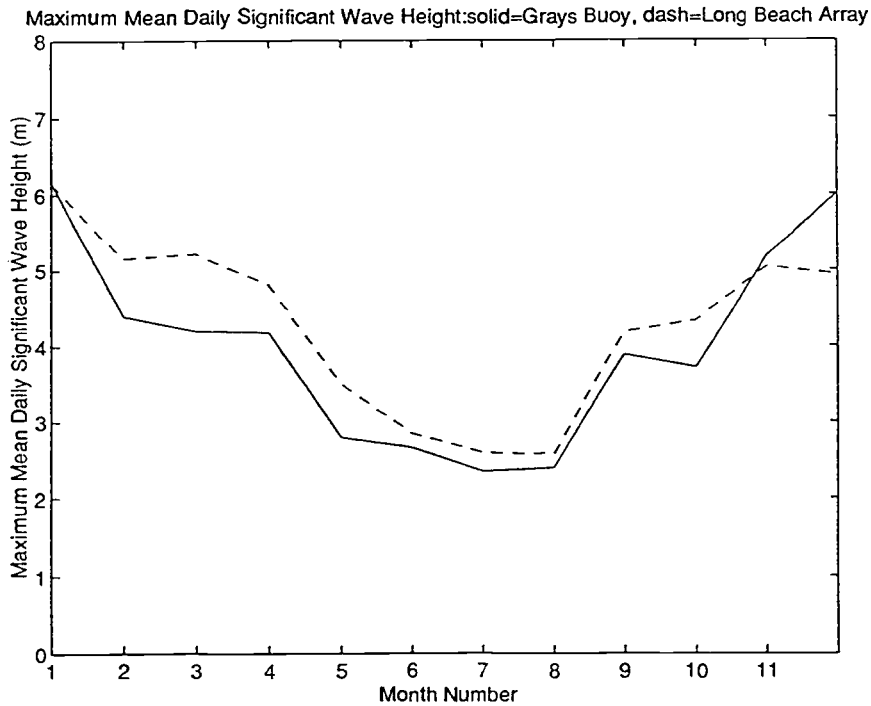

Figure 18B. Comparison of maximum monthly significant wave heights between the CDIP Grays Harbor, OR buoy and Long Beach, WA shallow-water array.

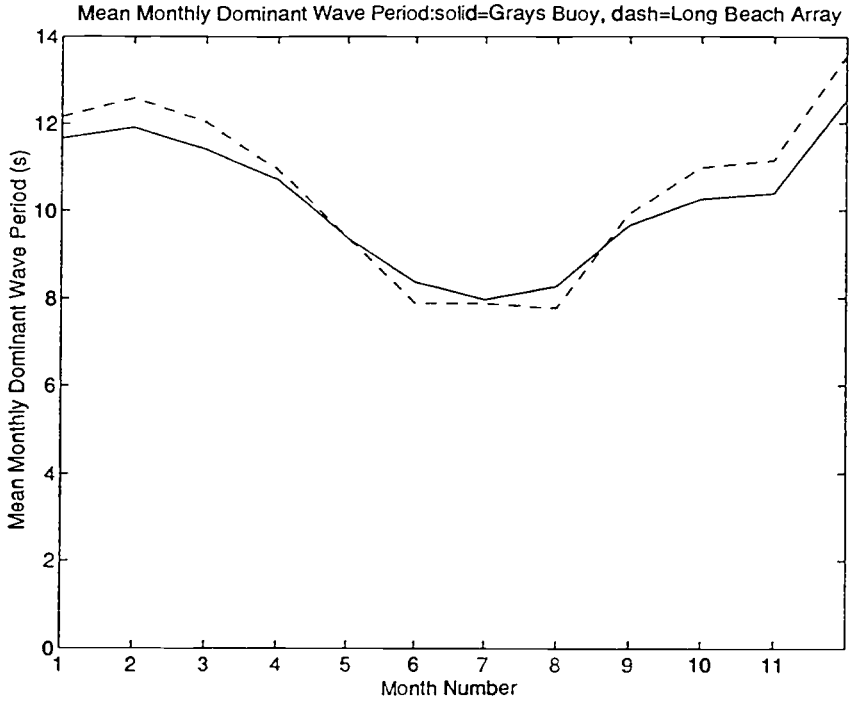

Figure 19A. Comparison of mean monthly dominant wave periods between the CDIP Grays Harbor, OR deep-water buoy and Long Beach, WA shallow-water array.

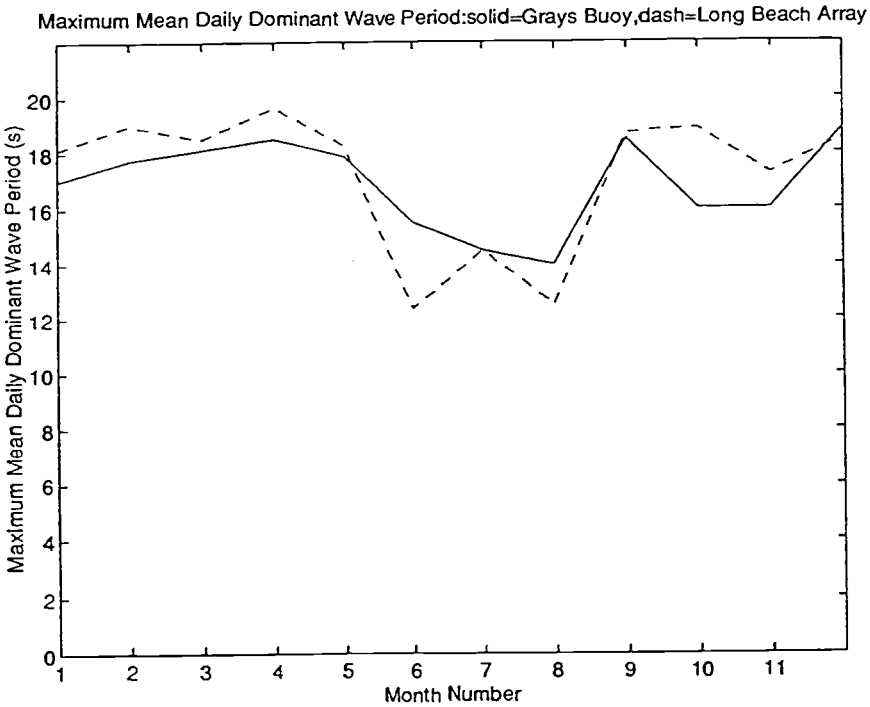

Figure 19B. Comparison of maximum monthly dominant wave periods between the CDIP Grays Harbor, OR buoy and Long Beach, WA shallow-water array.

Table 8d. Long Beach pressure-sensor array wave statistics.

Month	MD Hs (m)	Hs Variance (m*m)	Max MD Hs (m)	MD Td (s)	Td Variance (s*s)	Max MD Td (s)	Observations
January	2.99	1.41	6.15	12.16	5.95	18.13	95
February	2.64	0.79	5.16	12.58	5.81	19	112
March	2.41	0.86	5.21	12.04	7.11	18.5	124
April	2.42	0.86	4.8	10.93	7.16	19.63	98
May	1.7	0.53	3.5	9.38	7.37	18.25	68
June	1.48	0.23	2.85	7.88	2.9	12.33	53
July	1.19	0.14	2.59	7.88	4.11	14.5	85
August	1.28	0.22	2.57	7.78	3.29	12.5	73
September	1.65	0.58	4.19	9.91	8.5	18.71	86
October	2.02	0.69	4.34	10.98	5.43	18.88	112
November	2.47	0.96	5.04	11.14	4.88	17.25	109
December	2.49	0.94	4.94	13.56	3.87	18.5	70

F-test and t-test comparisons were made between the Grays Harbor buoy and Long Beach pressure sensor array. With few exceptions, both significant wave height and dominant wave period means and variances test below the 95% confidence test values to conclude that the means and variances are equal in these two data sets. Remarkably, using these statistical tests, the Long Beach/Grays Harbor stations are in better statistical agreement than the two Coquille Bay stations which are roughly 50 km closer together.

Regressions of Array and Deep-Water Buoy Data

Mean daily significant wave heights and dominant wave periods measured by the Coquille station array and buoy were regressed as a further comparison of the data sets. Regressions were also performed between the Grays Harbor buoy and Long Beach array. Tables 9 through 12 show the calculated least-squares regression slopes and y-intercepts for wave height and wave period correlations between the Coquille buoy and array (Tables 9 & 11), and the Grays Harbor buoy and Long Beach array (Tables 10 & 12). Also shown are the R-squared (goodness-of-fit) values, and the numbers of points (days) used in the regressions. Plots of the regressions upon which these tables are based are shown in Figures 20 through 23 (a, b, c, and d). The dashed lines in the figures show the 1:1 relationship along which the data should lie if the wave measurement systems agree perfectly and are measuring the same wave signal. The least-squared regression slopes

Table 9. Significant wave height regression statistics between the Coquille buoy and array.

Period	Least Squares Slope (Confidence Interval)	y-intercept (Confidence Interval)	R-Squared	Number of Points
All	1.06(0.0224)	0.0(0.1)	0.852	1493
Nov.1-Mar.1 (period 1)	1.02(0.0457)	0.1(0.3)	0.812	443
Mar.1-Jul.1 (period 2)	1.01(0.0519)	0.0(0.2)	0.777	416
Jul.1-Nov.1 (period 3)	1.15(0.0364)	0.2(0.1)	0.858	634

Table 10. Significant wave height regression statistics between the Grays Harbor buoy and Long Beach array.

Period	Least Squares Slope (Confidence Interval)	y-intercept (Confidence Interval)	R-Squared	Number of Points
All	0.97(0.0290)	0.2(0.1)	0.799	1085
Nov.1-Mar.1 (period 1)	0.79(0.0584)	0.7(0.3)	0.646	386
Mar.1-Jul.1 (period 2)	1.17(0.0402)	0.1(0.3)	0.906	343
Jul.1-Nov.1 (period 3)	1.10(0.0377)	0.1(0.2)	0.903	356

Table 11. Dominant wave period regression statistics between the Coquille buoy and array.

Period	Least Squares Slope (Confidence Interval)	y-intercept (Confidence Interval)	R-Squared	Number of Points
All	0.92(0.0305)	1.4(0.6)	0.701	1493
Nov.1-Mar.1 (period 1)	0.75(0.0563)	3.8(1.0)	0.601	443
Mar.1-Jul.1 (period 2)	0.86(0.0695)	2.2(1.1)	0.584	416
Jul.1-Nov.1 (period 3)	0.89(0.0463)	1.2(0.7)	0.695	634

Table 12. Dominant wave period regression statistics between the Grays Harbor buoy and Long Beach array.

Period	Least Squares Slope (Confidence Interval)	y-intercept (Confidence Interval)	R-Squared	Number of Points
All	1.01(0.0330)	0.3(0.7)	0.767	1085
Nov.1-Mar.1 (period 1)	0.89(0.0611)	2.0(1.3)	0.681	386
Mar.1-Jul.1 (period 2)	0.97(0.0629)	0.5(1.3)	0.728	343
Jul.1-Nov.1 (period 3)	1.04(0.0575)	0.2(1.2)	0.78	356

A)

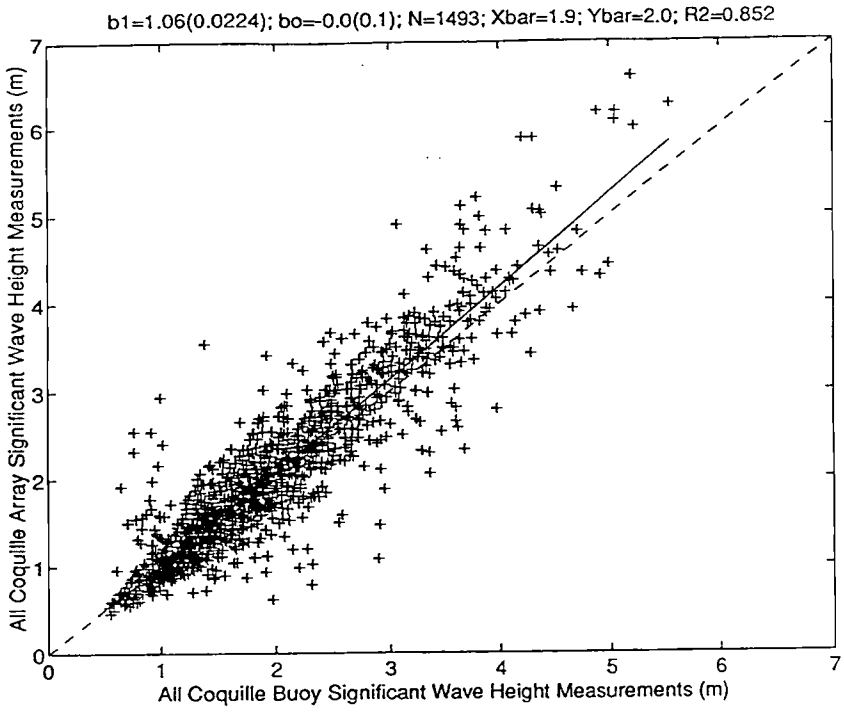

B)

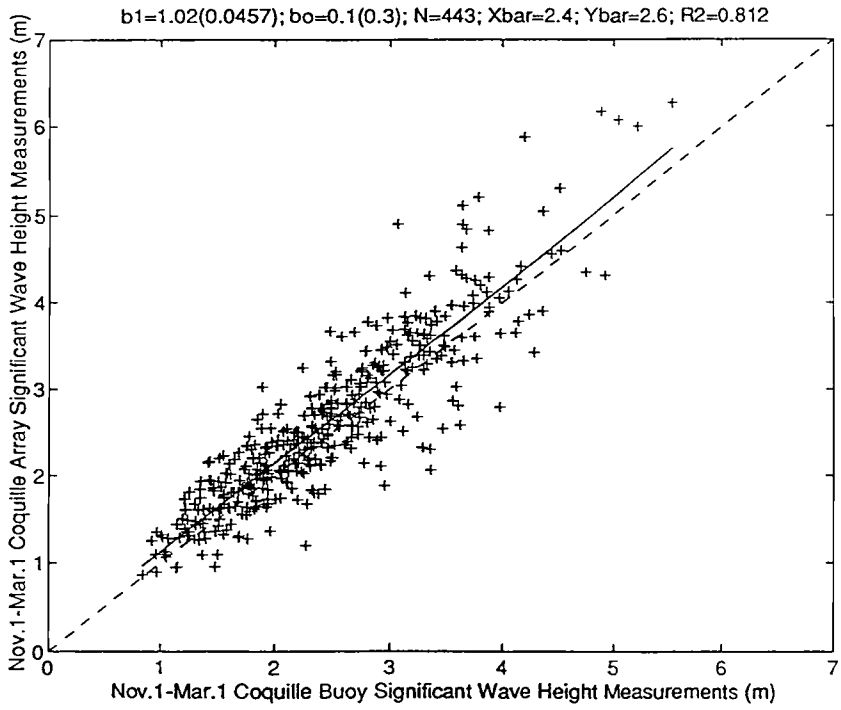

Figure 20 (A/B). A regression of Bandon, Oregon, CDIP array significant wave height measurements in 11 meters depth versus the offshore buoy measurements for A) ALL DATA and B) WINTER (Nov.-Feb.).

C)

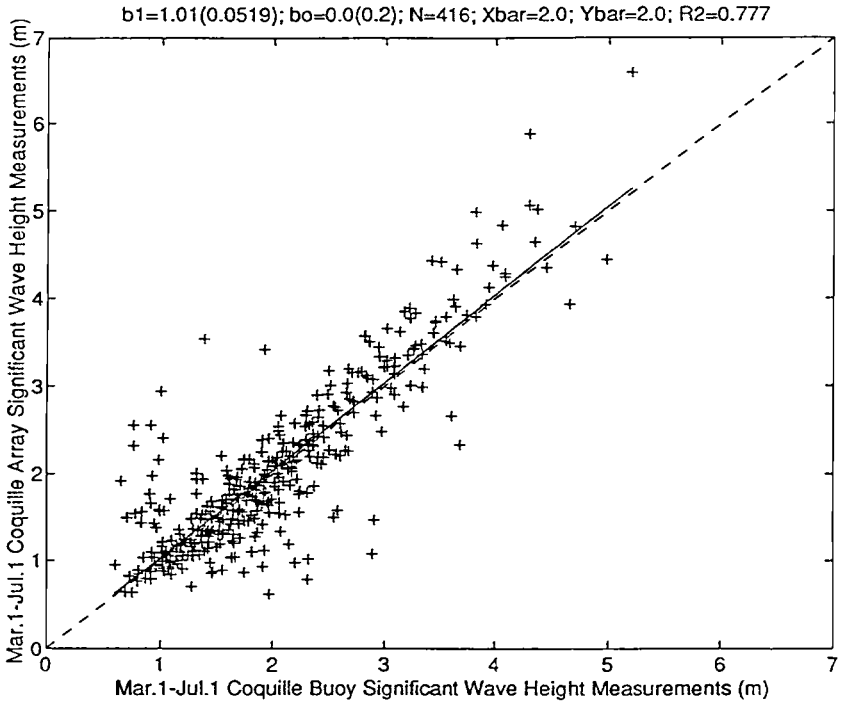

D)

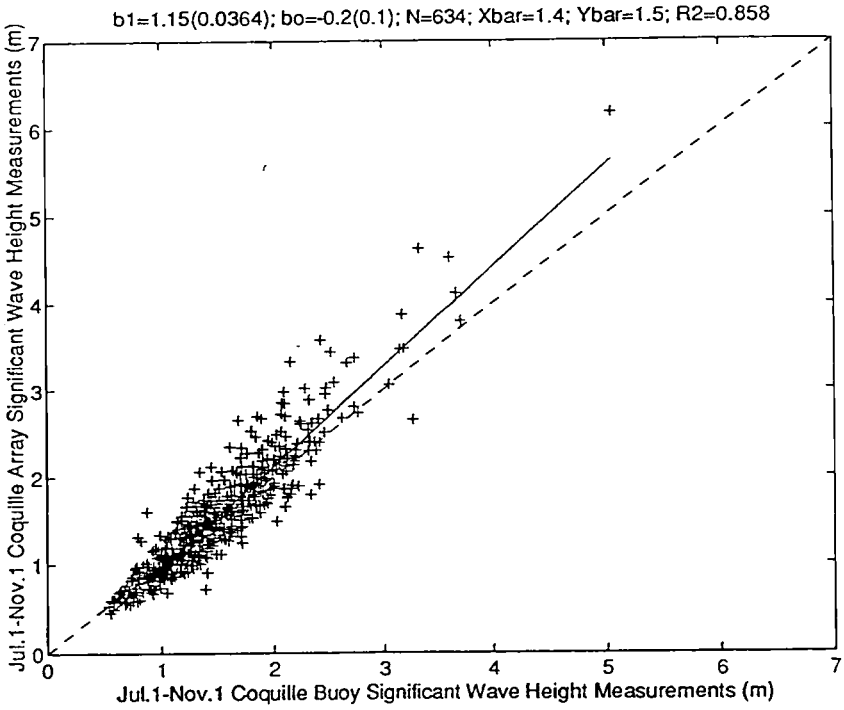

Figure 20 (C/D). A regression of Bandon, Oregon, CDIP array significant wave height measurements in 11 meters depth versus the offshore buoy heights for C) SPRING (Mar.-Jun.) and D) SUMMER (Jul.-Oct.).

A)

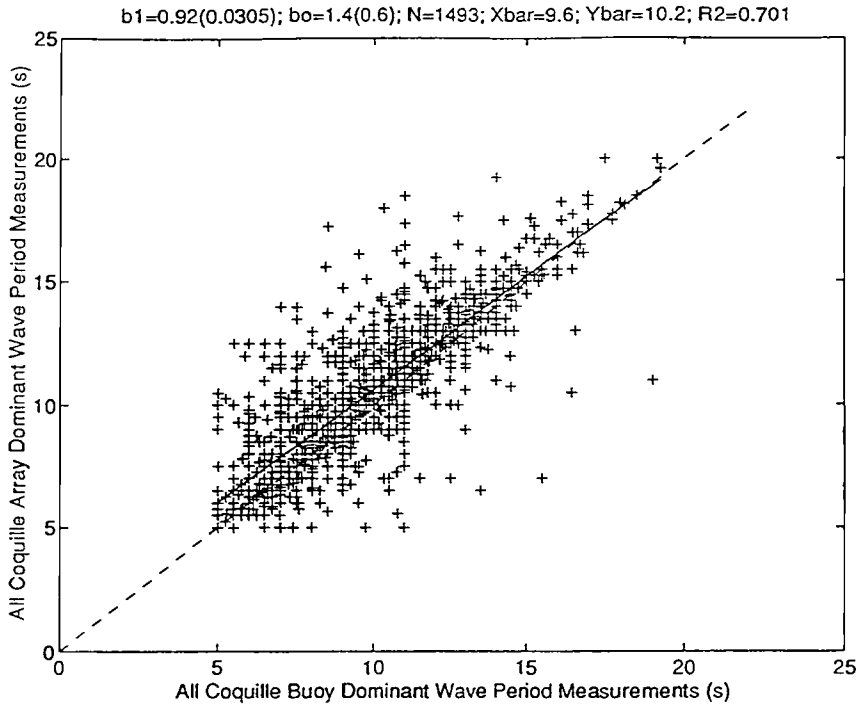

B)

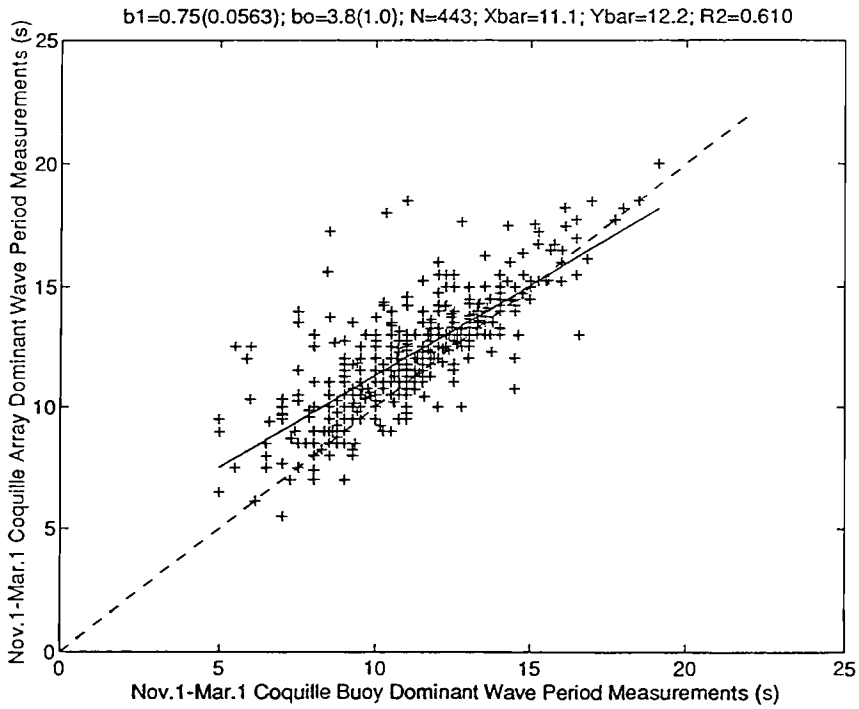

Figure 21 (A/B). A regression of Bandon, Oregon, CDIP array dominant wave period measurements in 11 meters depth versus the offshore buoy measurements for A) ALL DATA and B) WINTER (Nov.-Feb.).

C)

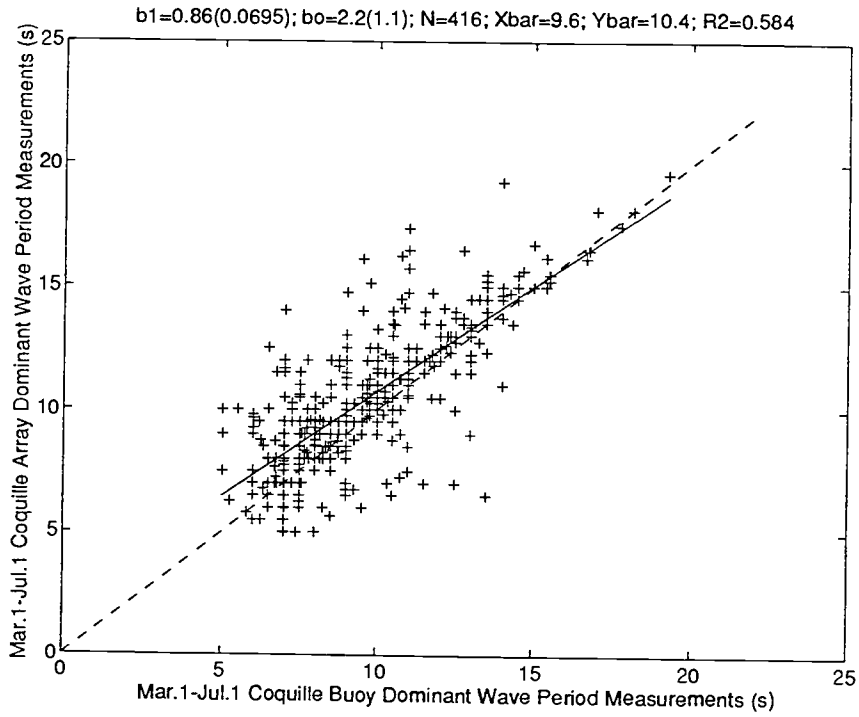

D)

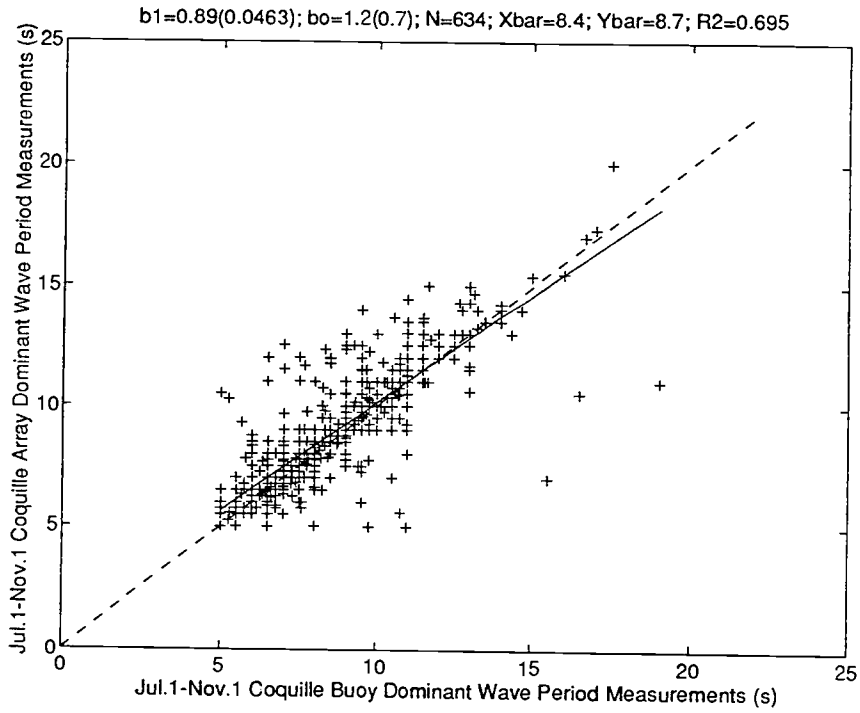

Figure 21 (C/D). A regression of Bandon, Oregon, CDIP array dominant wave period measurements in 11 meters depth versus the offshore buoy periods for C) SPRING (Mar.-Jun.) and D) SUMMER (Jul.-Oct.).

A)

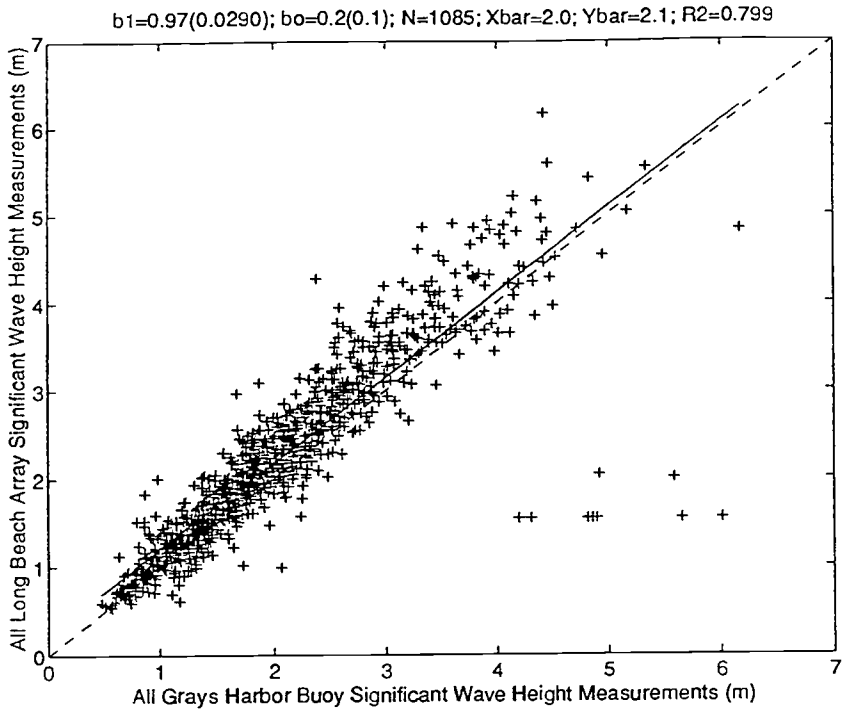

B)

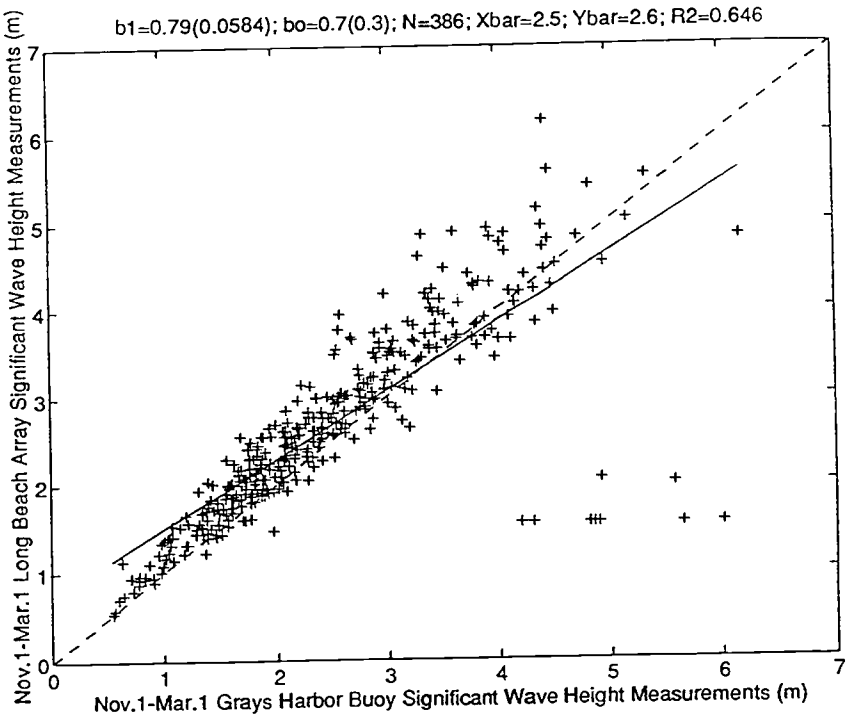

Figure 22 (A/B). A regression of Long Beach, Wa, CDIP array significant wave heights in 11.5 meters depth versus the Grays Harbor, Wa, buoy measurements for A) ALL DATA and B) WINTER (Nov.-Feb.).

C)

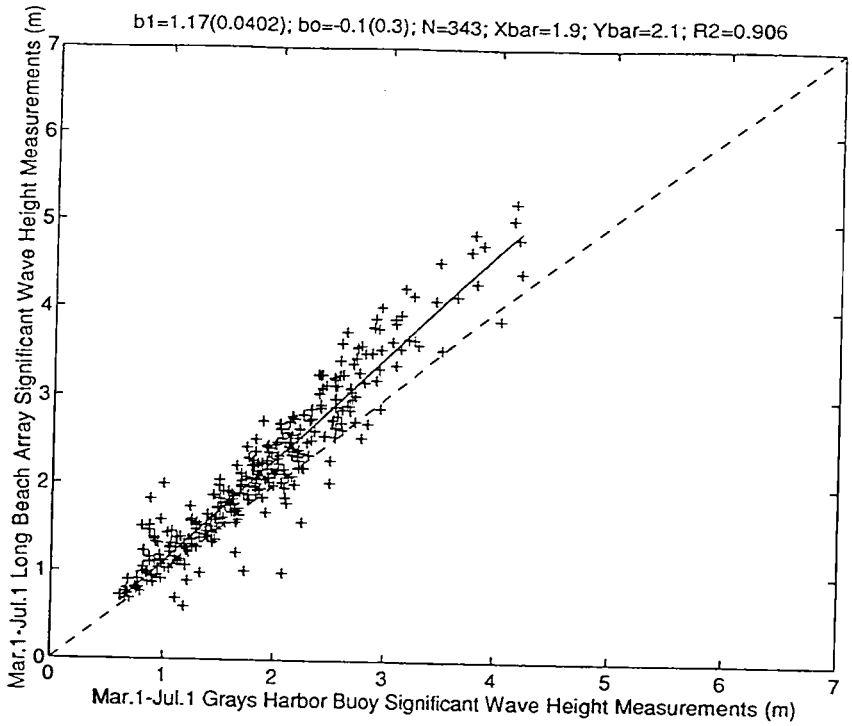

D)

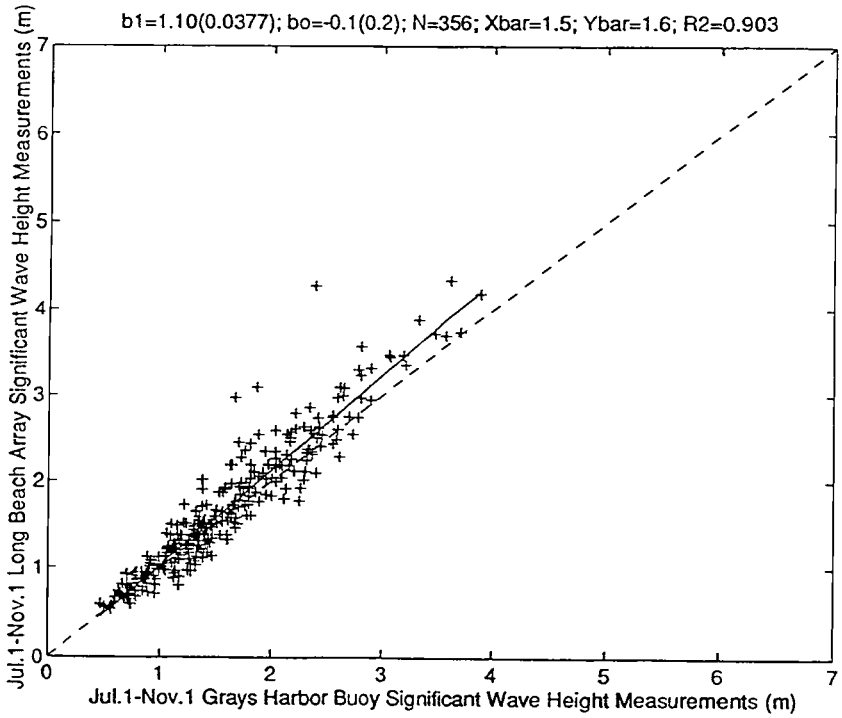

Figure 22 (C/D). A regression of Long Beach, Wa, CDIP array significant wave heights in 11.5 meters depth versus the Grays Harbor, Wa, buoy heights for C) SPRING (Mar.-Jun.) and D) SUMMER (Jul.-Oct.).

A)

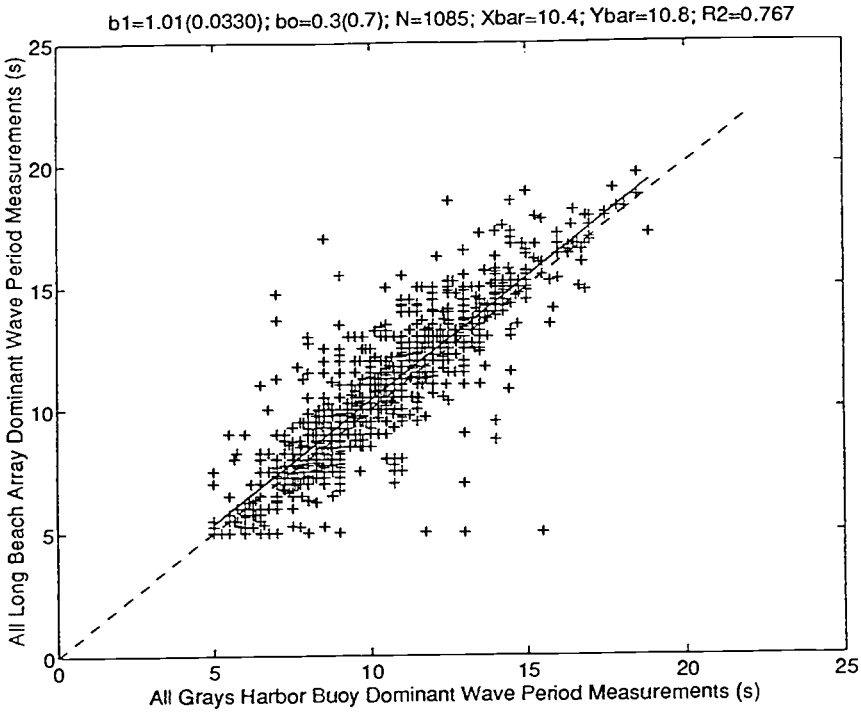

B)

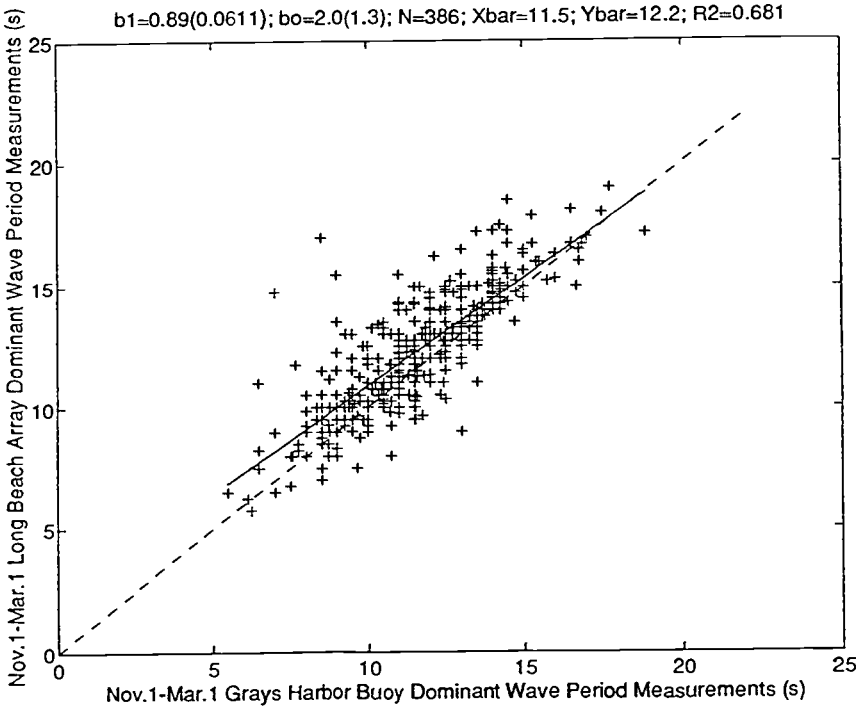

Figure 23 (A/B). A regression of Long Beach, Wa, CDIP array dominant wave periods in 11.5 meters depth versus the Grays Harbor, Wa, buoy measurements for A) ALL DATA and B) WINTER (Nov.-Feb.).

C)

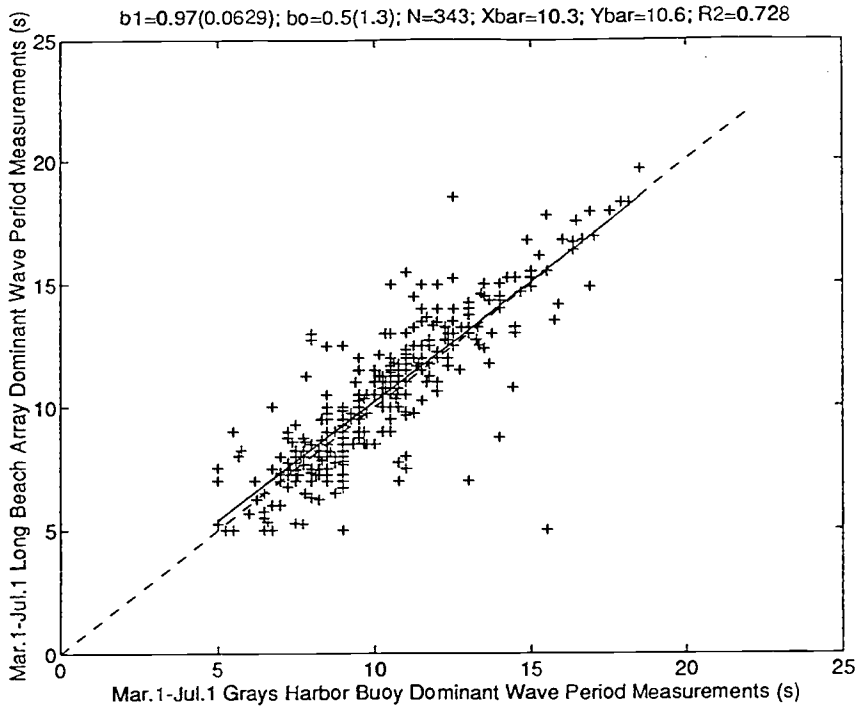

D)

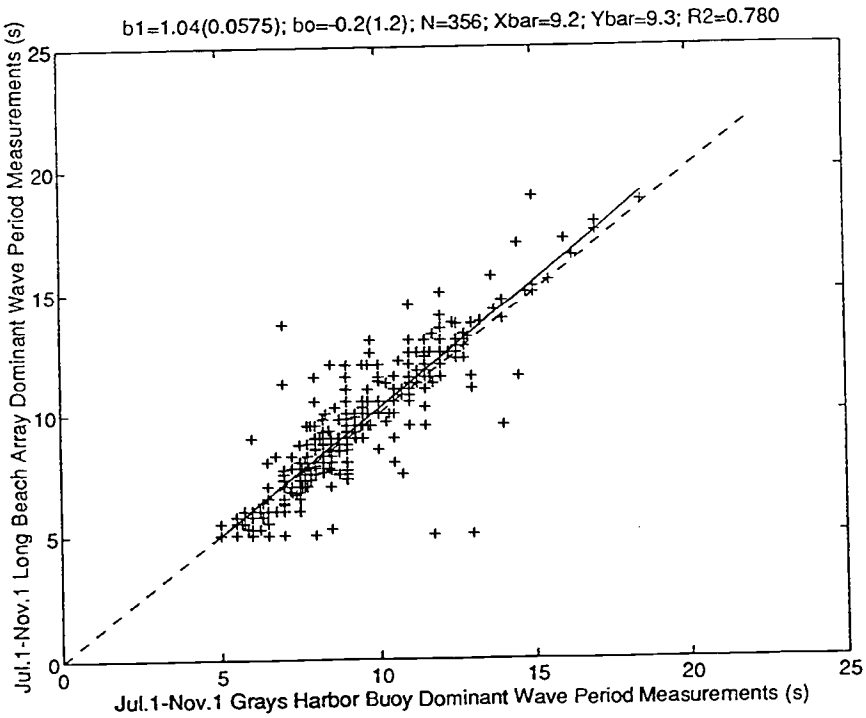

Figure 23 (C/D). A regression of Long Beach, Wa, CDIP array dominant wave periods in 11.5 meters depth versus the Grays Harbor, Wa, buoy periods for C) SPRING (Mar.-Jun.) and D) SUMMER (Jul.-Oct.).

and R-squared values (scatter) of the wave height and period regressions are closer to unity on average between array and offshore buoy than are the same parameters between offshore buoys (see sections above). Period 1 (November 1 to March 1) regressions typically have the largest scatter in wave heights and periods, and correspond to a more broad banded wave signal than seen in Periods 2 or 3. In conclusion, the array/buoy comparisons agree more favorably than do the buoy/buoy comparisons.

Distributions of Array Data

Distributions of Coquille Bay and Long Beach pressure-sensor array data are shown in Figures 24a and 24b. These distributions represent all individual wave height measurements made by each array since deployment. Both distributions have the same shape (skewed towards smaller wave heights with rare large wave heights), indicating similar wave climates. The distributions are shifted right of zero since each point in the distribution is a significant wave height, and not likely to be near zero. Though the significant wave height measurements appear to be Rayleigh distributed, they fail the statistical goodness-of-fit test.

As with the buoy data, array wave height distributions were then plotted log-normally. Figures 25a and b show the log-normal distributions of all significant wave height measurements for the Coquille Bay and Long Beach arrays. Although both distributions fail the Chi-squared goodness-of-fit test, they appear log-normally distributed. The distributions appear to be equally broad-banded, indicating similar overall wave variability measured at each location.

The distributions were separated into the three four-month segments used above to examine any seasonality in the wave climate at each location. Figures 26a, b, and c show the log-normal distributions of mean daily significant wave height measured by the Coquille array for the periods November 1-March 1 (period 1 (a)), March 1- July 1 (period 2 (b)), and July 1- November 1 (period 3 (c)), respectively. Figure 27 (a, b, and c) shows similar distributions for the Long Beach array. The numbers of observations in each distribution are shown in the plots. Though none of the array wave height distributions pass the Chi-squared goodness-of-fit test, they appear log-normally distributed. Again, the Chi-squared test is highly sensitive to the number of observations and width of bins used in the distributions, and its significance should be considered accordingly.

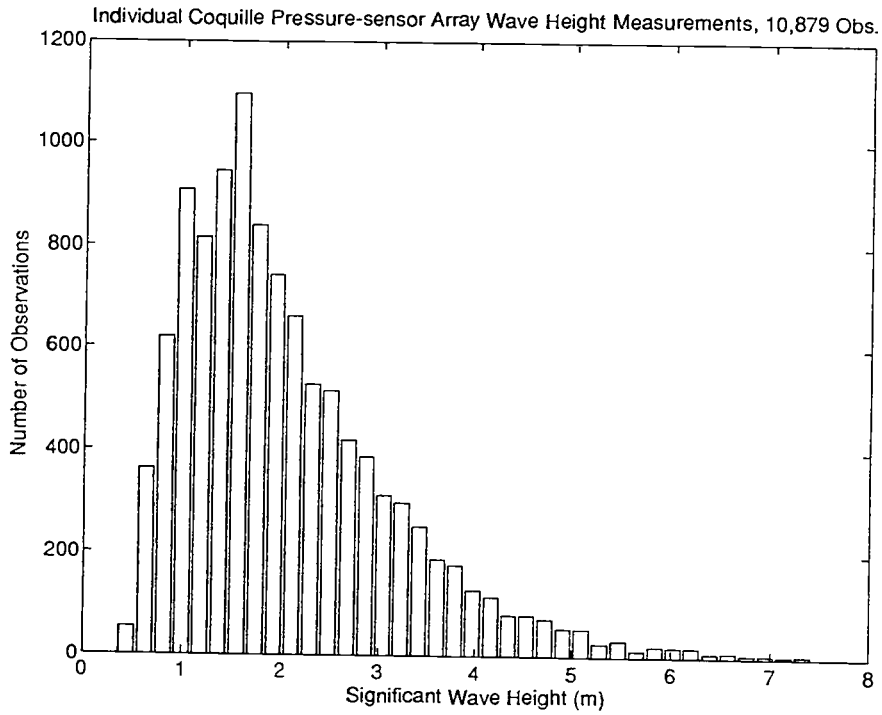

Figure 24A. Histogram of all CDIP Bandon, Oregon, pressure-sensor array significant wave height measurements.

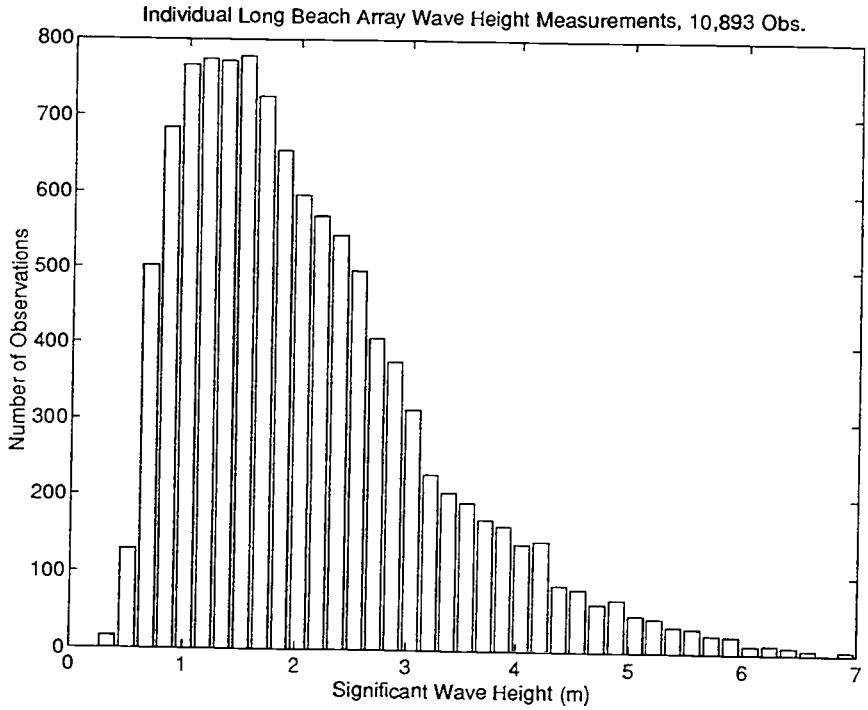

Figure 24B. Histogram of all CDIP Long Beach, Washington, pressure-sensor array significant wave height measurements.

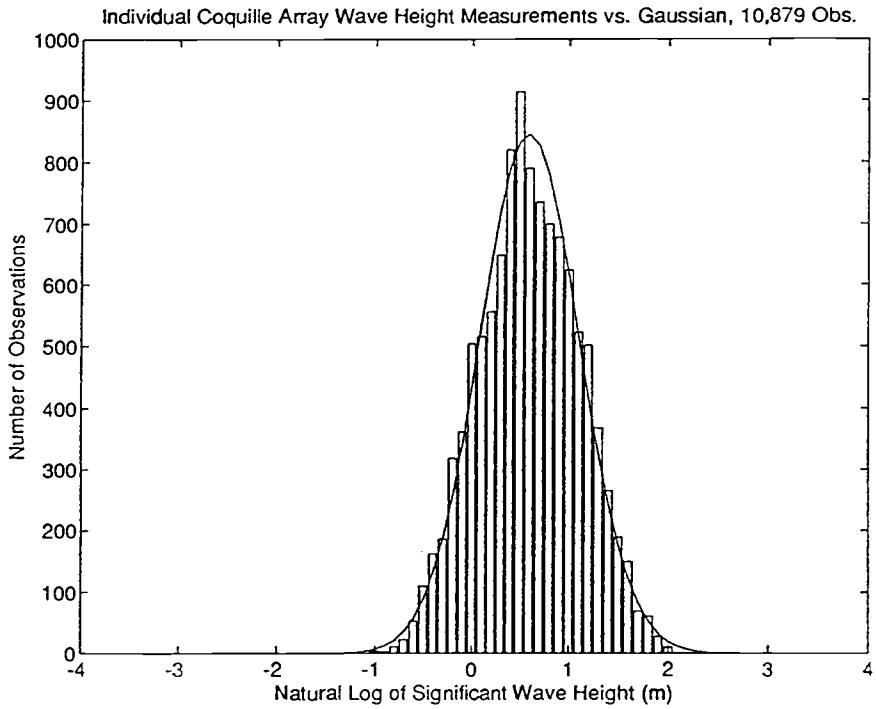

Figure 25A. The log-normal distribution of all CDIP Bandon, Oregon, pressure-sensor array significant wave height measurements versus the Gaussian distribution.

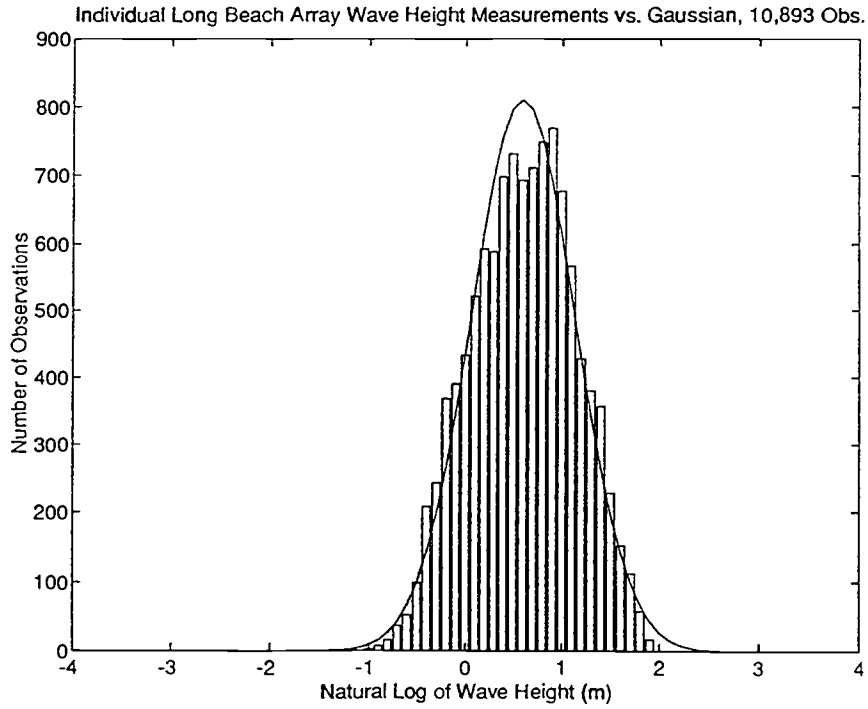

Figure 25B. The log-normal distribution of all CDIP Long Beach, Wa, pressure-sensor array significant wave height measurements versus the Gaussian distribution.

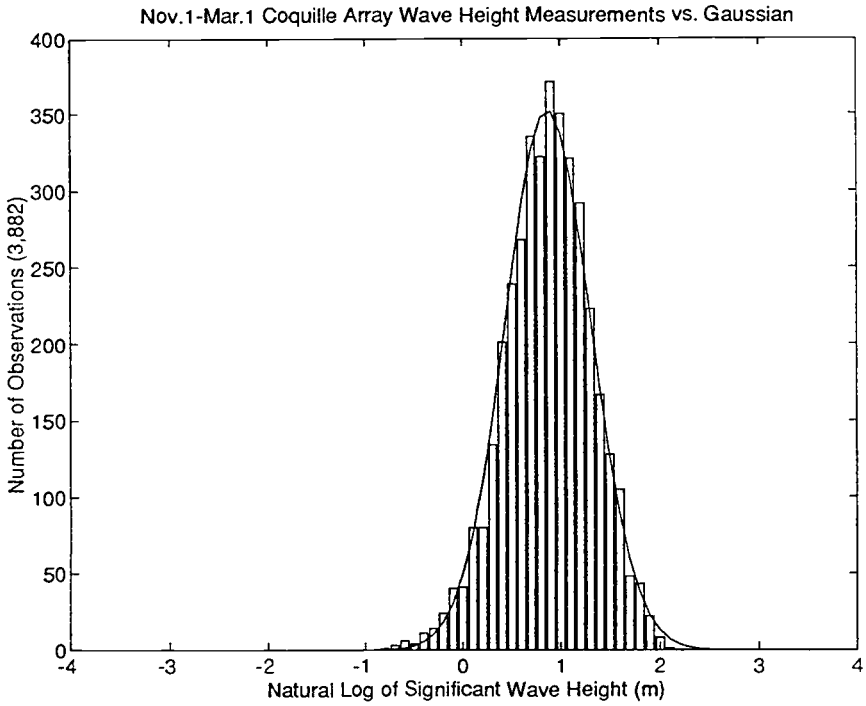

Figure 26A. The log-normal distribution of Winter (Nov.-Feb.) CDIP Bandon, Or pressure-sensor array significant wave heights versus the Gaussian distribution.

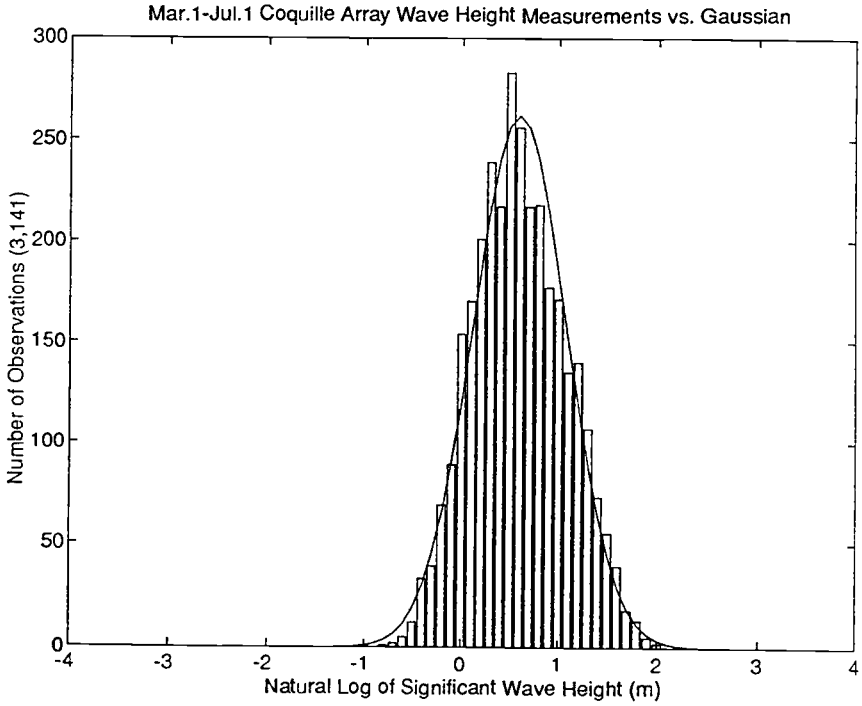

Figure 26B. The log-normal distribution of Spring (Mar.-Jun.) CDIP Bandon, Or pressure-sensor array significant wave heights versus the Gaussian distribution.

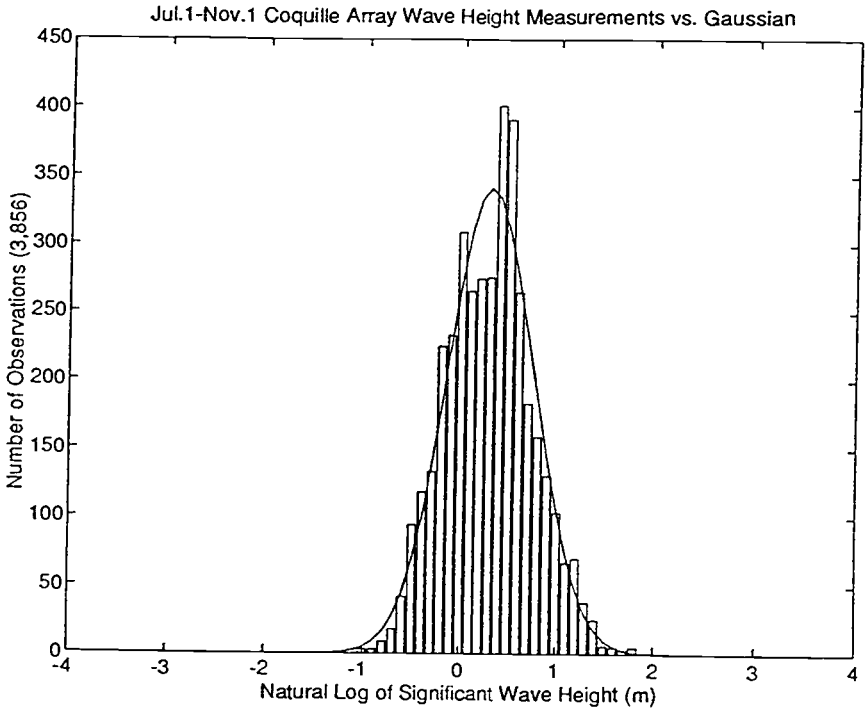

Figure 26C. The log-normal distribution of Summer (Jul.-Oct.) CDIP Bandon, Or pressure-sensor array significant wave heights versus the Gaussian distribution.

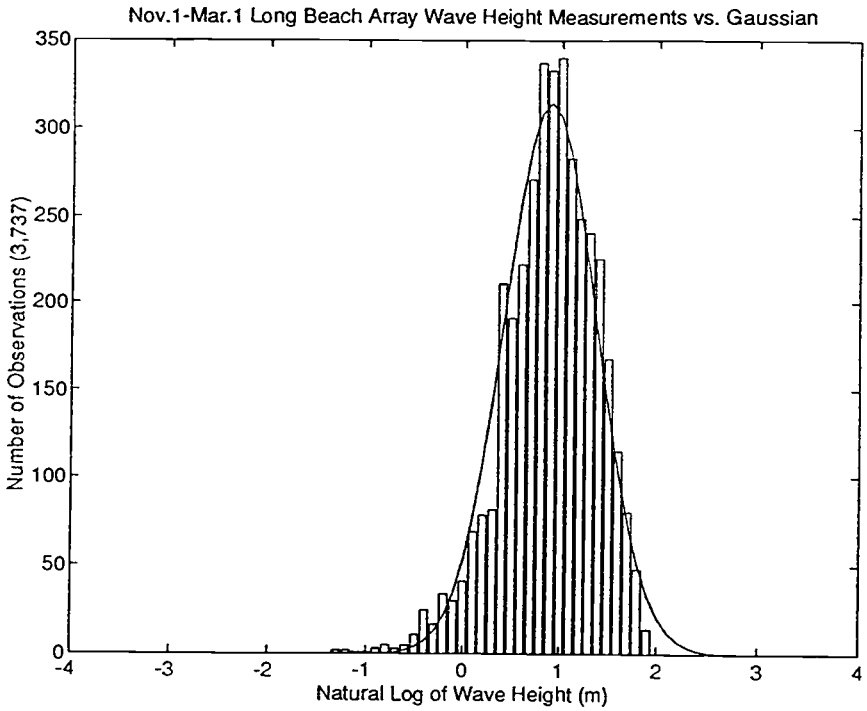

Figure 27A. The log-normal distribution of Winter (Nov.-Feb.) Long Beach, Wa pressure-sensor array significant wave heights versus the Gaussian distribution.

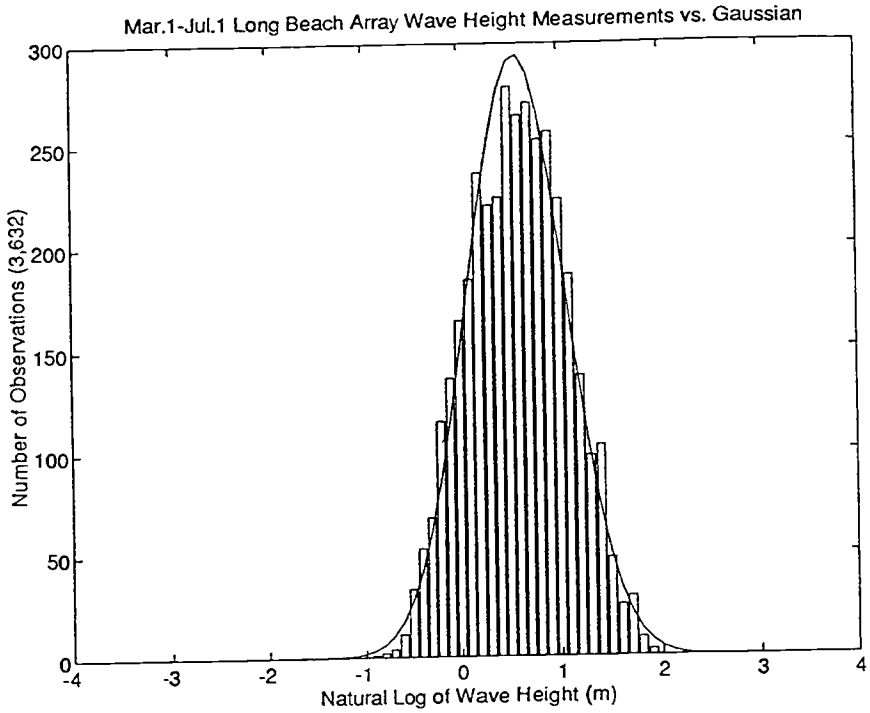

Figure 27B. The log-normal distribution of Spring (Mar.-Jun.) Long Beach, Wa pressure-sensor array significant wave heights versus the Gaussian distribution.

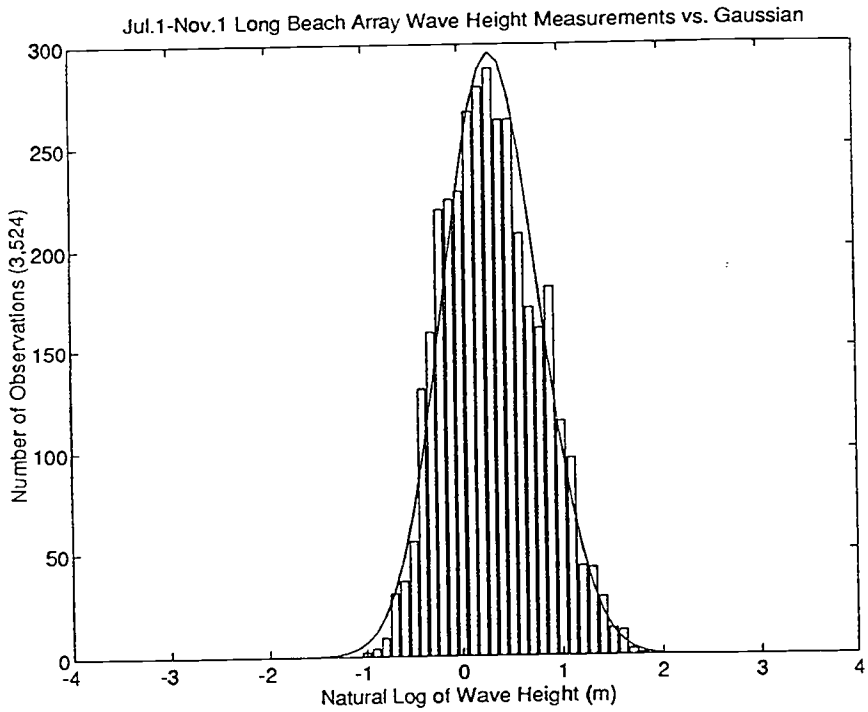

Figure 27C. The log-normal distribution of Summer (Jul.-Oct.) Long Beach, Wa pressure-sensor array significant wave heights versus the Gaussian distribution.

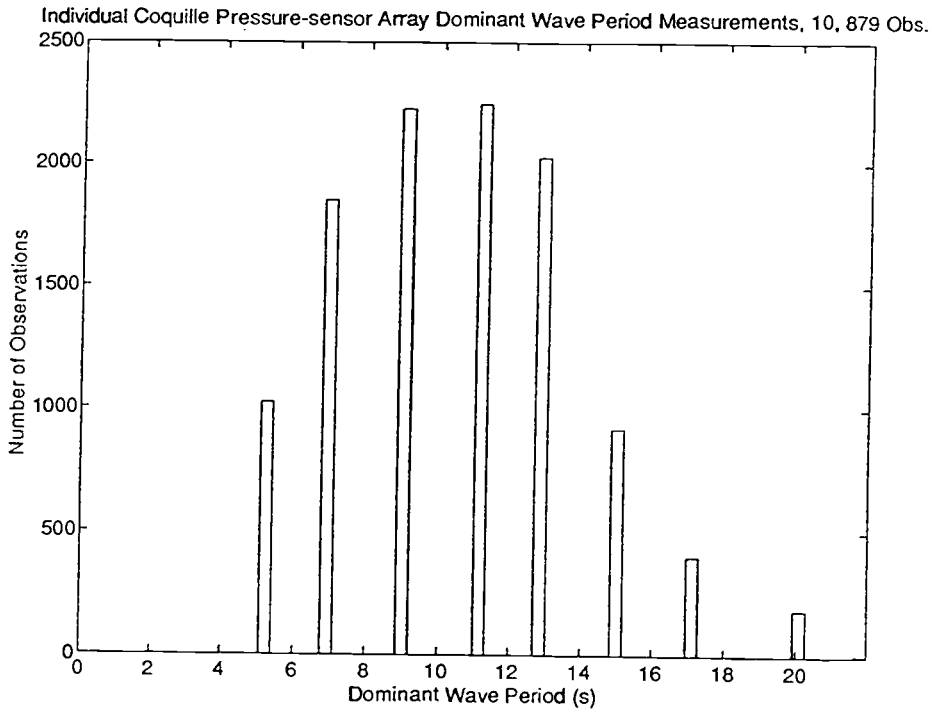

Figure 28A. Histogram of all CDIP Bandon, Oregon, pressure-sensor array dominant wave period measurements.

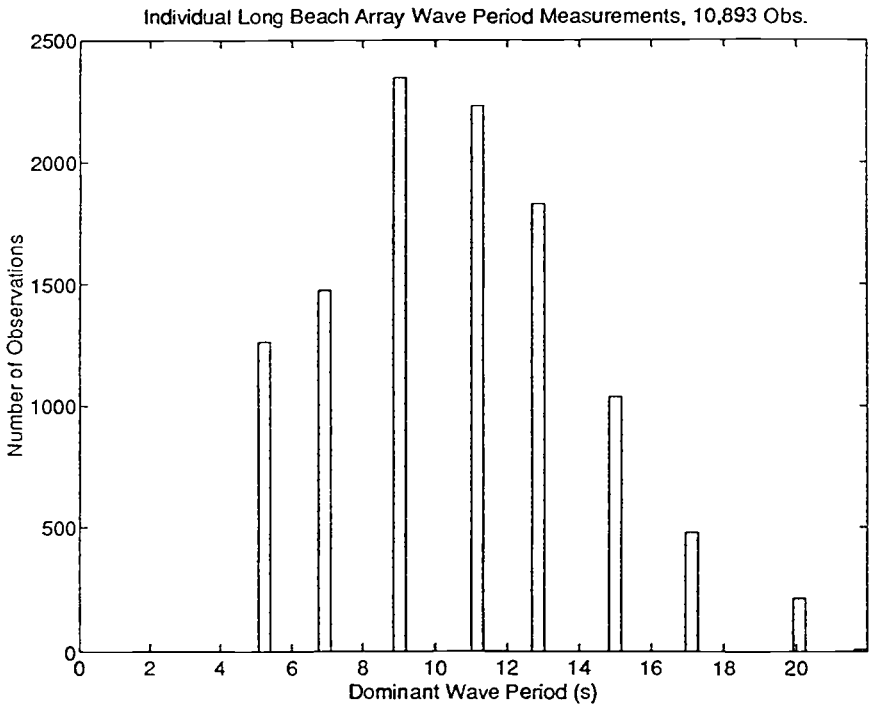

Figure 28B. Histogram of all CDIP Long Beach, Washington, pressure-sensor array dominant wave period measurements.

Figures 28a and 28b show the distributions of all dominant wave period measurements for the two arrays. The lack of detail in the distributions (their large bin width) is an artifact of the spectral calculation of dominant wave period. No attempts were made to fit these distributions to theoretical probability distributions.

Calculations of Wave Breaker Heights

Of interest to analyses of coastal processes are assessments of breaking wave conditions on sloping beaches. Particularly useful is knowing the heights of the waves as they break. Since direct measurements are unavailable, monthly mean and maximum wave breaker heights (H_b) were calculated from each offshore buoy data set according to the formulation of Komar and Gaughan (1973):

$$H_b = 0.39g^{1/5}(H^2T)^{2/5} \qquad (5)$$

where H is the deep-water significant wave height and T is wave period. The 0.39 coefficient is empirical, based on the fit to laboratory and field data. Figures 29a, b, and c show monthly mean and maximum calculated wave breaker heights respectively for the Coquille Bay buoy, the Newport (NDBC) buoy, and Grays Harbor Buoy. One standard deviation about the mean is shown in each plot. The results from the CDIP buoy offshore from the Coquille River indicate that the mean breaker heights reach about 3.5 meters during the winter, decreasing to 1.5 to 2.0 meters during the summer. Individual winter storms generate breaking waves in the nearshore having significant wave heights up to 9 to 10 meters (Figure 29a). Mean and maximum monthly wave breaker heights are compared in Figures 30a and 30b. NDBC buoy mean and maximum Hb calculations are predictably higher (O(1m)) than the Coquille or Grays Harbor Hb calculations, given the larger wave parameters measured by that buoy. All three sets of annual Hb calculations agree very well in annual trends.

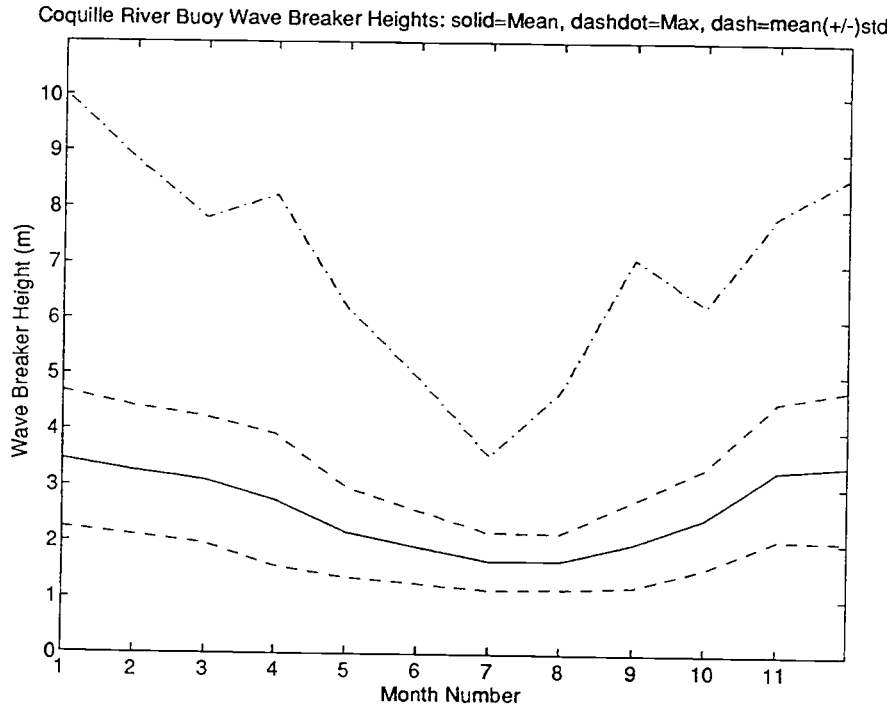

Figure 29A. Monthly variations in wave breaker heights, calculated with equation (4) from the deep-water measurements of the CDIP buoy near Bandon, Or.

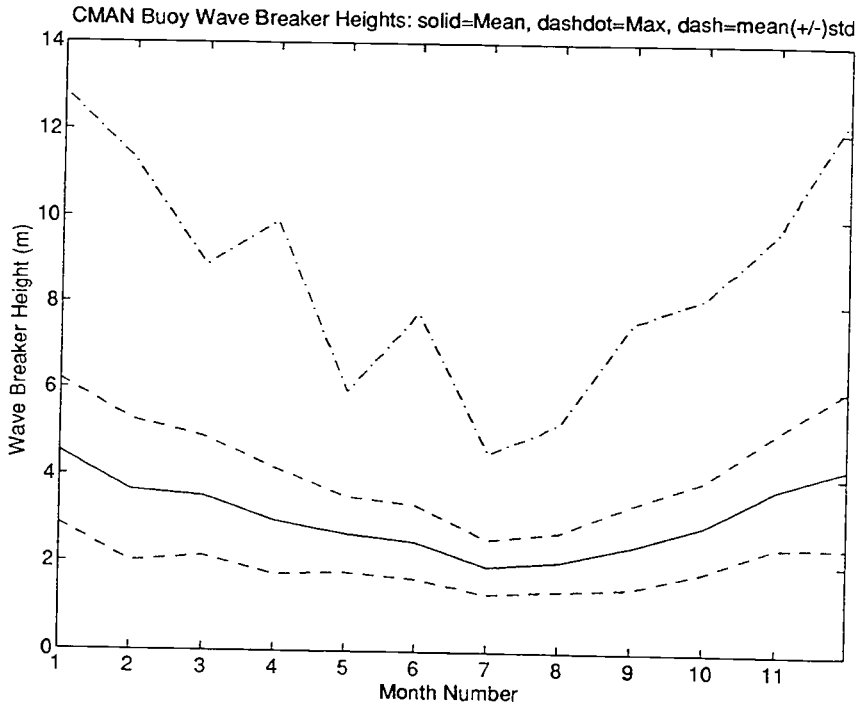

Figure 29B. Monthly variations in wave breaker heights, calculated with equation (4) from the deep-water measurements of the NDBC buoy off Newport, Or.

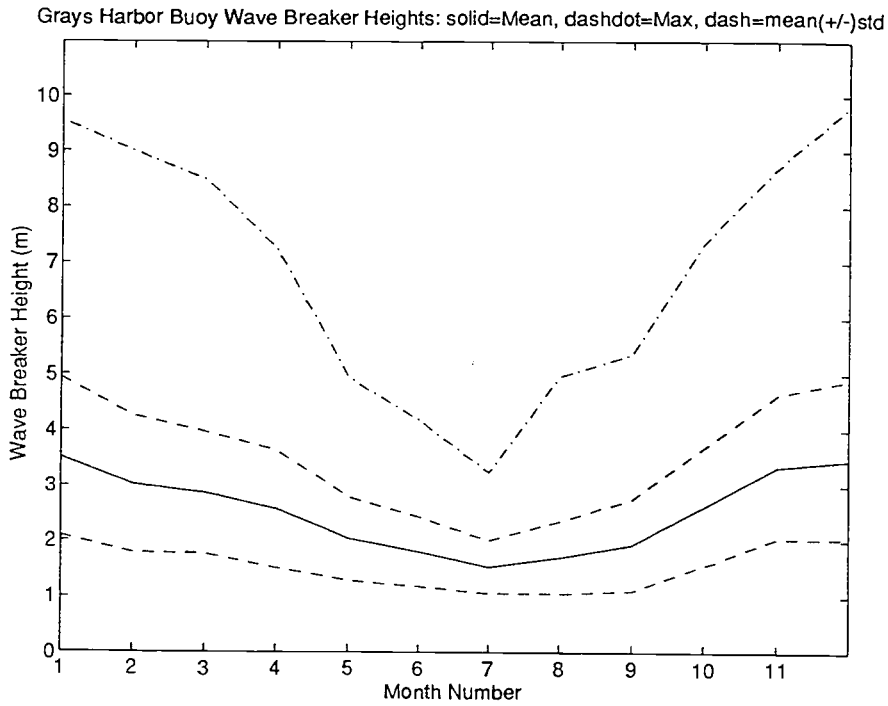

Figure 29C. Monthly variations in wave breaker heights, calculated with equation (4) from the deep-water measurements of the CDIP buoy near Grays Harbor, Wa.

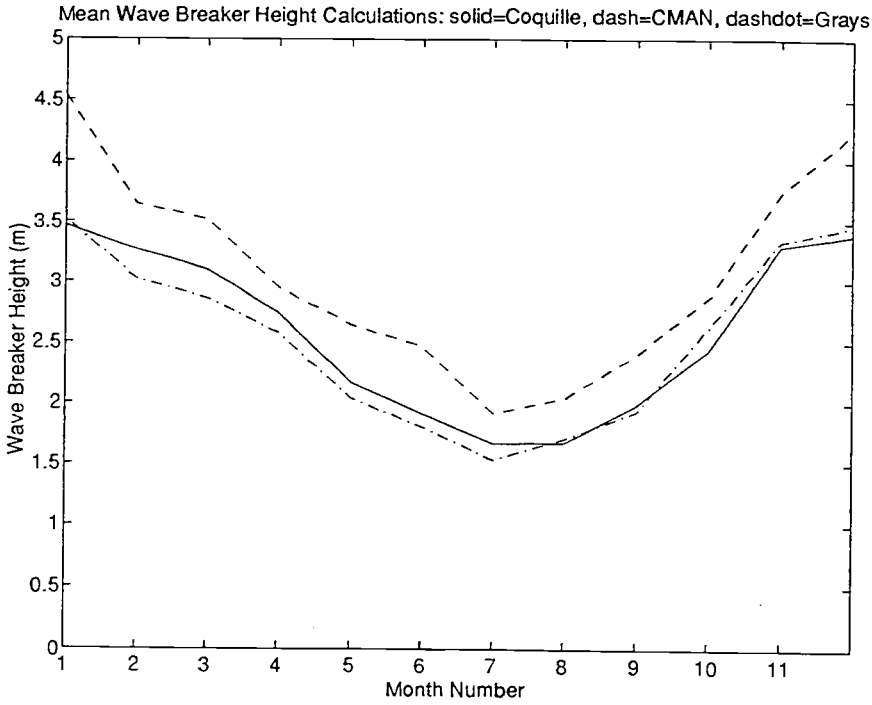

Figure 30A. Comparisons of mean wave breaker heights for the CDIP and NDBC buoys.

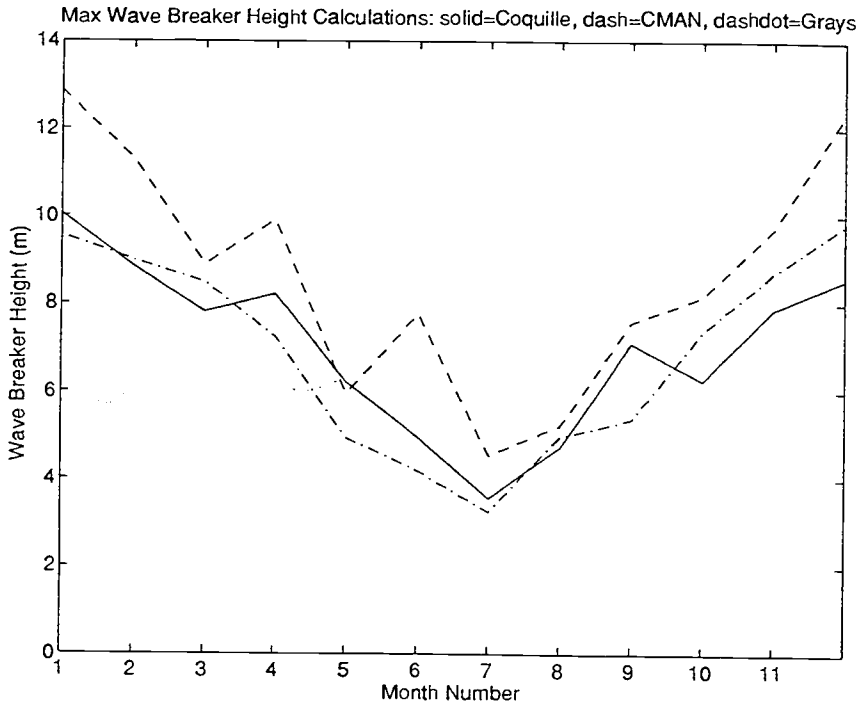

Figure 30B. Comparisons of maximum wave breaker heights for the CDIP and NDBC buoys.

CHAPTER 4
MICROSEISMOMETER DATA

The microseismometer system is important in establishing the wave climate of the Pacific Northwest, since it contains 23 years of daily wave measurements. This chapter discusses comparisons of the microseismometer wave gage data with deep-water buoy measurements. Wave heights and periods from manually analyzed seismometer records collected in Newport, Oregon, are directly compared with data from the deep-water buoys located offshore from Newport, and Bandon, Oregon. Monthly means and maxima are compared, statistical tests are performed, and linear regressions are presented as in Chapter 3. The data collected after automation of the microseismometer system are presented and compared with the deep-water buoys, and a re-calibration of the system is performed.

Comparison of Strip-Chart Microseismometer Data (1972-92) With Offshore Buoys

Microseismometer wave gage records that have accumulated on strip-charts since 1981 were analyzed manually to yield estimates of significant wave heights and zero-crossing periods using the procedure described in Chapter 2. In those analyses it has been assumed that the larger waves in a record approximate the average height of the 10% highest waves. This representative height is determined manually from the chart paper using a transparent template. The measured height is then multiplied by 0.8 to give an estimate of the significant wave height, based on the assumption of a Rayleigh distribution of wave heights. The zero-crossing wave period is estimated from the ratio of record length to number of zero-crossing waves in the 10 minute record. The average zero-crossing interval is then multiplied by 2 because of the 2-to-1 relationship of microseism frequency to ocean wave frequency, as predicted by Longuet-Higgins (1950).

Data from the microseismometer wave gage, recorded every six hours, were first analyzed to produce mean daily significant wave heights and mean daily zero-crossing wave periods. This produced data spanning six years of measurements for comparison with the NDBC buoy (located nearly directly offshore from the wave gage), and 12 years of data for comparison with the CDIP buoy off Bandon, Oregon. The rationale behind comparing mean daily parameters rather than individual measurements was given in

Chapter 3. Mean daily statistics were averaged to produce mean monthly statistics over the entire record of overlapping measurements made by the various instruments.

Figures 31a and 31b compare monthly mean and maximum values of significant wave heights derived from the strip-chart microseismometer data with NDBC buoy data. These two sensors agree very well in mean heights, and reasonably well in maximum heights, both with similar annual trends. Plots comparing mean and maximum microseismometer zero-crossing periods with NDBC spectrum-determined dominant wave periods show poor agreement (Figures 31c and 31d). In fact, the annual trend shown by the two curves have an inverse relationship for most of the annual cycle. During the summer months in which the microseismometer records long wave periods, the NDBC buoy reports short periods. The agreement between the two systems is best during winter, perhaps suggesting that the microseismometer is best at resolving periods when wave energy levels are high.

An identical comparison of monthly mean and maximum wave heights and periods is made between the microseismometer wave gage and CDIP buoy off Bandon, Oregon. In Figures 32a-d it can be seen that the microseismometer reports larger mean and maximum wave heights and periods throughout most of the year (except July and August when seismometer wave heights are smaller). The annual trends are similar for wave heights, but again quite dissimilar for wave periods. Tables 13 and 14 (a, b) list basic statistics of monthly mean and maximum (mean daily) significant wave heights and wave periods upon which Figures 31 and 32 are based. Wave height and period variances are included as well as the numbers of observations (days) upon which each monthly measurement is based.

F-test (variances) and t-test (means) comparisons were made between mean monthly significant wave heights and periods for the microseismometer strip-chart measurements versus data from the two buoys. In the NDBC comparison, wave height means and variances test below or near the critical test value, and wave period variances test below the critical value, whereas wave period means test as statistically different. In the CDIP comparison, only wave height variances test below the critical value, though wave height means and wave period variances are close. Again, the CDIP/microseismometer wave period means test as statistically different. On the basis of the above tests it appears that the strip-chart seismometer wave heights agree best with the NDBC buoy located nearly directly offshore.

Table 13a. NDBC deep-water buoy wave statistics for comparison with strip-chart microseism data.

Month	MD Hs (m)	Hs Variance (m*m)	Max MD Hs (m)	MD Td (s)	Td Variance (s*s)	Max MD Td (s)	Observations
January	3.44	1.74	7.61	12.73	5.73	18.83	118
February	2.62	1.32	5.76	11.83	6.51	17.82	99
March	2.64	1	5.76	11.42	4.18	16.35	100
April	2.14	0.68	5.33	10.77	3.72	15.78	109
May	2.04	0.38	4.13	10.09	4.72	17.98	99
June	1.85	0.39	5.04	9.69	3.81	15.9	146
July	1.47	0.23	2.95	8.42	3.12	16.6	150
August	1.53	0.24	3.76	8.63	3.13	14.8	144
September	1.75	0.42	4.56	10.24	6.18	20.07	139
October	2.08	0.55	4.35	10.99	3.63	16.7	148
November	2.81	0.88	4.52	11.87	4	18	89
December	3.14	2.34	7.34	13.09	3.18	18.38	60

Table 13b. Microseismometer strip-chart wave statistics for comparison with the NDBC buoy.

Month	MD Hs (m)	Hs Variance (m*m)	Max MD Hs (m)	MD Tz (s)	Tz Variance (s*s)	Max MD Tz (s)	Observations
January	3.78	0.88	6.1	14.16	3.57	18.5	118
February	2.89	0.85	5.1	14	3.36	18.25	99
March	2.67	1.2	5.7	13.74	6.02	17.72	100
April	2.13	0.75	5.64	13.83	4.47	21.58	109
May	1.84	0.43	3.86	14	5.87	22.45	99
June	1.63	0.49	4.88	14.3	5.1	21.5	146
July	1.12	0.19	2.74	15.61	8.44	24.35	150
August	1.25	0.29	2.97	14.91	5.8	22.22	144
September	1.71	0.72	5.18	14.46	4.99	21.8	139
October	2.18	0.45	4.34	13.5	2.96	18.95	148
November	2.83	0.89	5.41	12.04	10.28	18.82	89
December	3.48	2.03	6.1	13.76	6.06	19.57	60

Linear regressions of mean daily significant wave heights and periods were used to further compare the data sets. Tables 15 through 18 give the calculated least-squares regression slopes and y-intercepts for wave height and period correlations between the microseismometer and NDBC (Newport) buoy (Tables 16 & 18), and the microseismometer and CDIP (Bandon) buoy (Tables 15 & 17). Also shown are the R-squared (goodness-of-fit) values, and the numbers of points (days) used in each

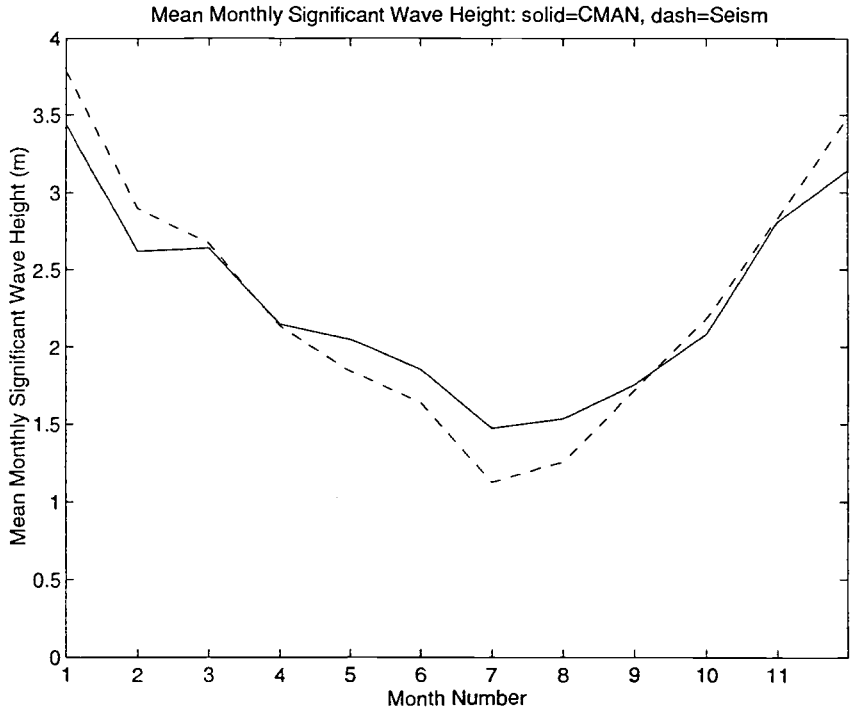

Figure 31A. Comparison of mean monthly significant wave heights between strip-chart microseismometer and NDBC buoy data.

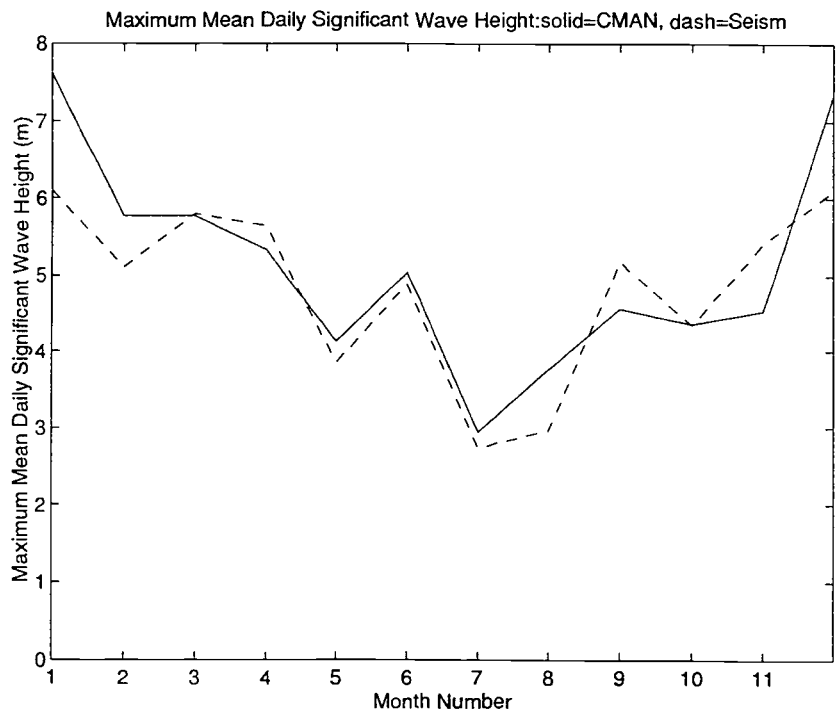

Figure 31B. Comparison of maximum monthly significant wave heights between strip-chart microseismometer and NDBC buoy data.

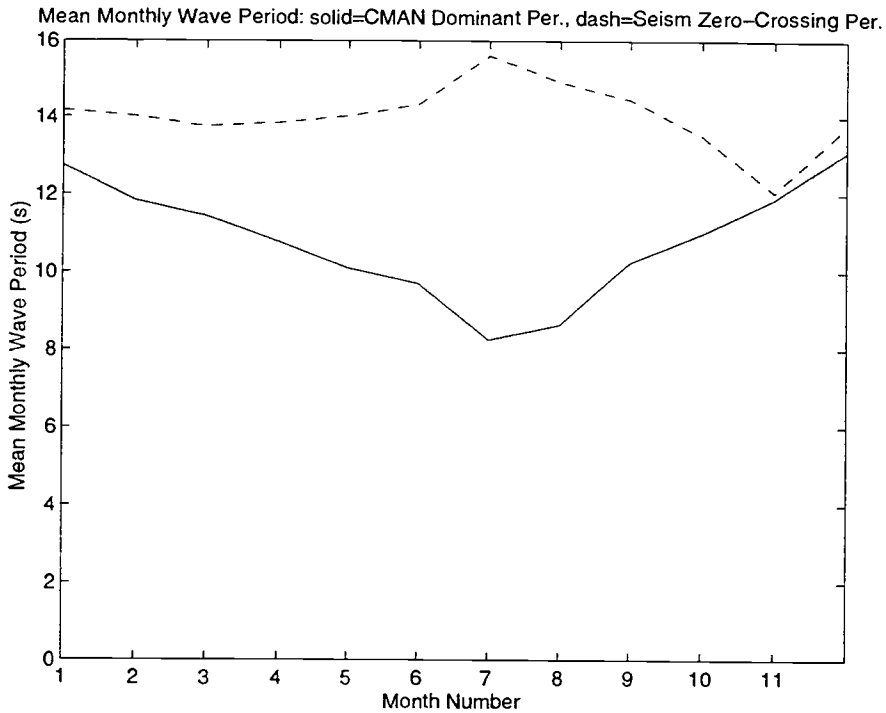

Figure 31C. Comparison of mean monthly zero-crossing/dominant wave periods between strip-chart microseismometer and NDBC buoy data.

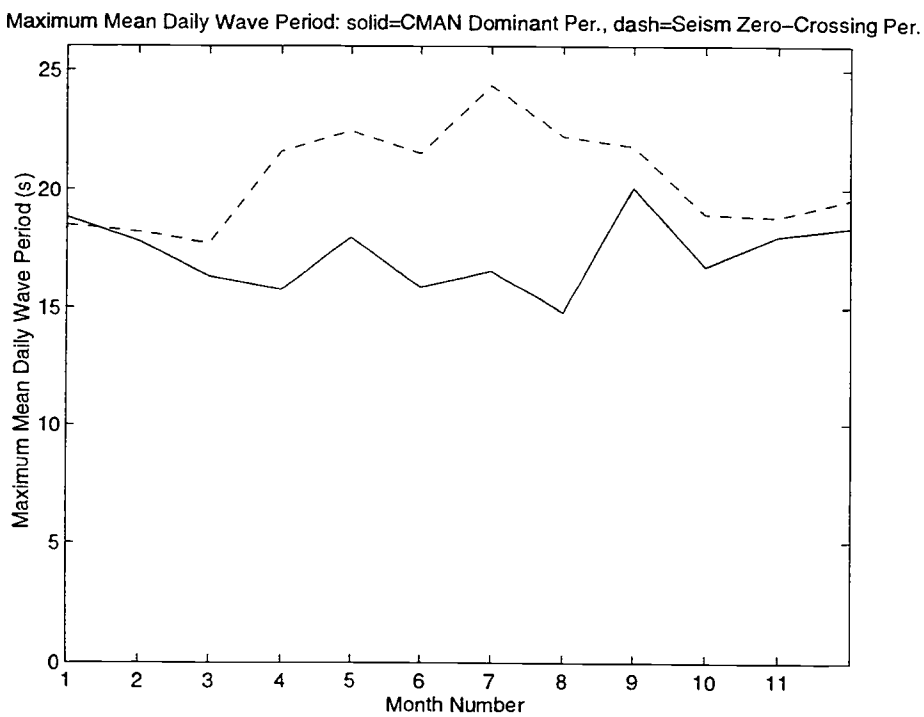

Figure 31D. Comparison of maximum monthly zero-crossing/dominant wave periods between strip-chart microseismometer and NDBC buoy data.

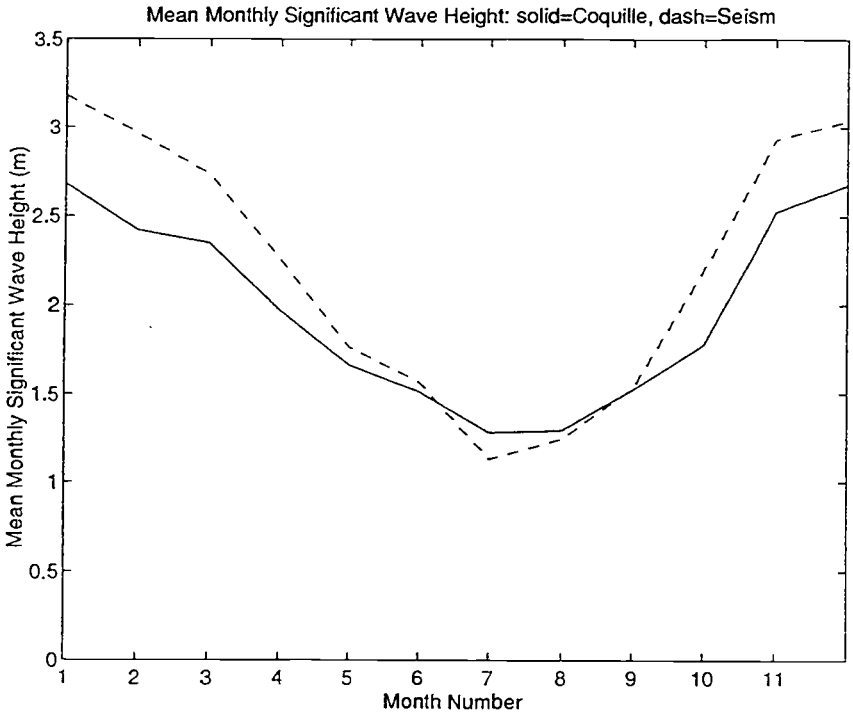

Figure 32A. Comparison of mean monthly significant wave heights between strip-chart microseismometer and CDIP (Bandon) buoy data.

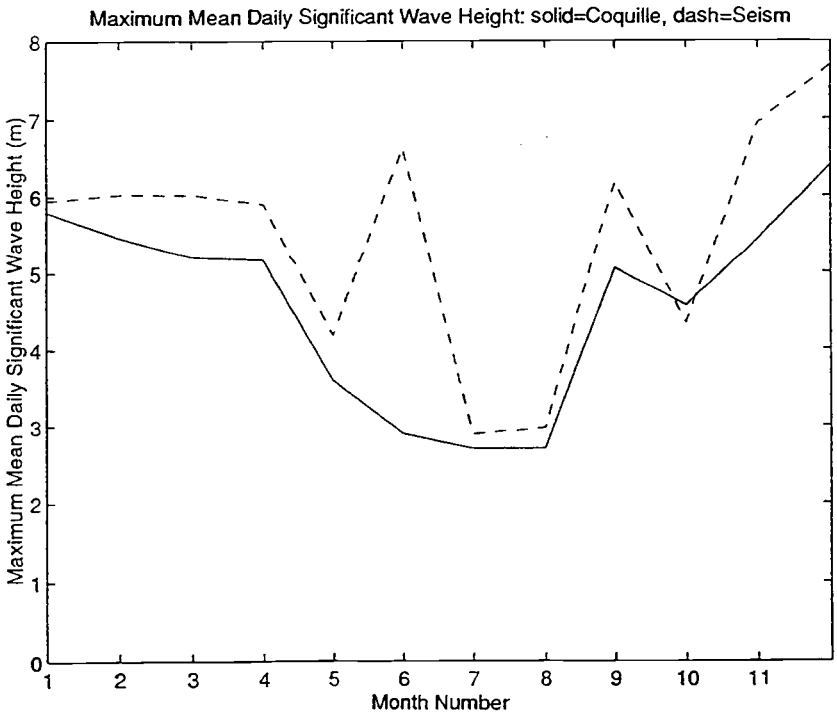

Figure 32B. Comparison of maximum monthly significant wave heights between strip-chart microseismometer and CDIP (Bandon) buoy data.

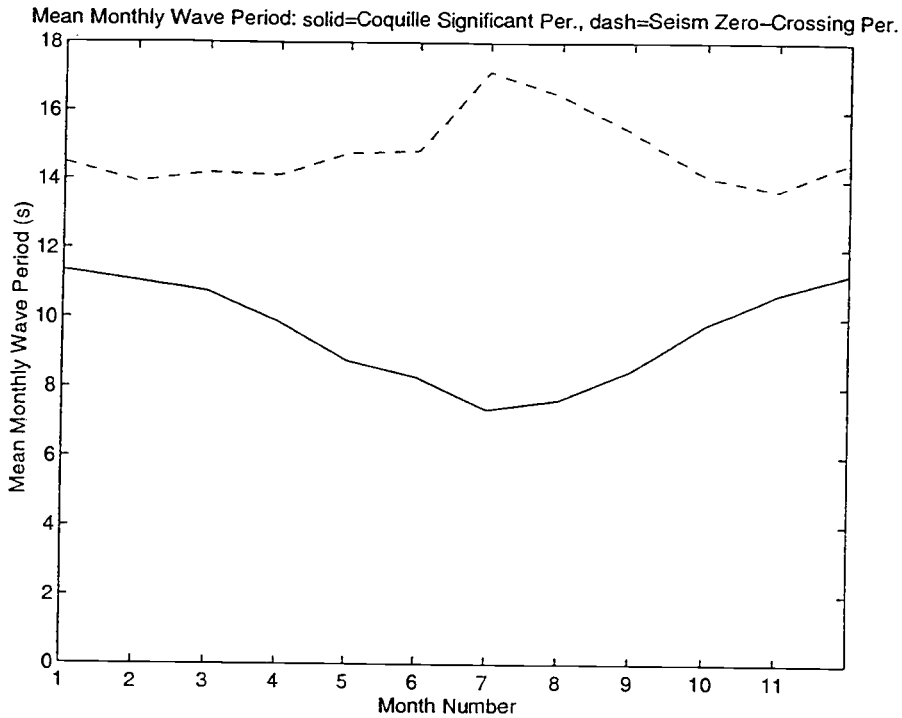

Figure 32C. Comparison of mean monthly zero-crossing/dominant wave periods between strip-chart microseismometer and CDIP (Bandon) buoy data.

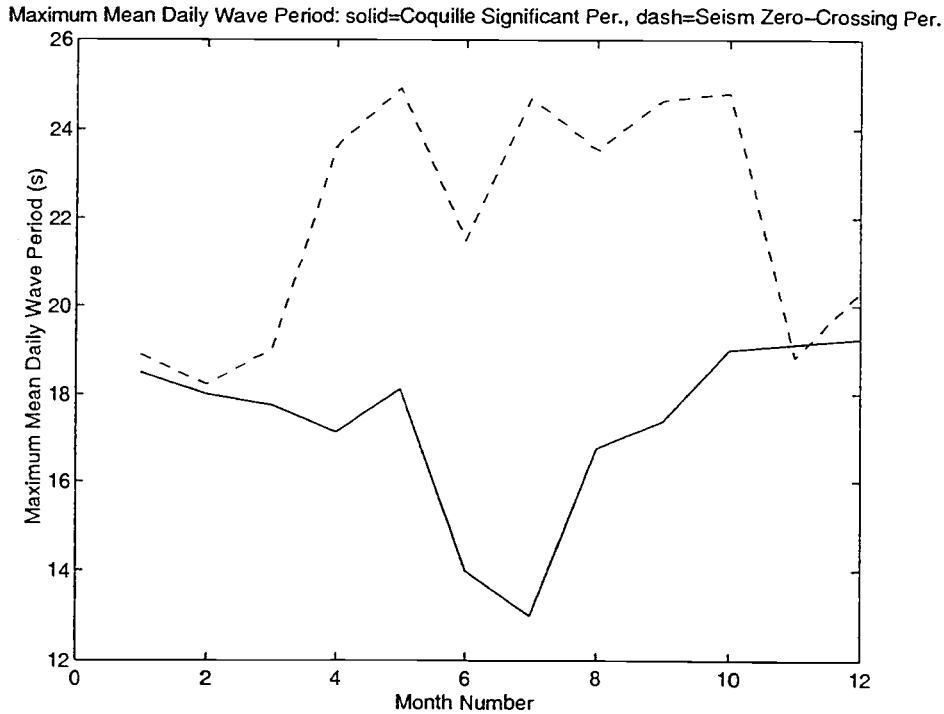

Figure 32D. Comparison of maximum monthly zero-crossing/dominant wave periods between strip-chart microseismometer and CDIP (Bandon) buoy data.

Table 14a. CDIP Coquille (Bandon, Oregon) deep-water buoy wave statistics for comparison with microseismometer records.

Month	MD Hs (m)	Hs Variance (m*m)	Max MD Hs (m)	MD Td (s)	Td Variance (s*s)	Max MD Td (s)	Observations
January	2.68	0.92	5.79	11.34	5.82	18.5	175
February	2.41	0.71	5.46	11.06	5.46	18	210
March	2.35	0.64	5.2	10.74	4.8	17.75	231
April	1.96	0.6	5.16	9.87	4.11	17.12	224
May	1.66	0.31	3.6	8.74	3.74	18.12	210
June	1.51	0.26	2.9	8.27	3.14	14	164
July	1.28	0.18	2.7	7.35	1.63	13	176
August	1.29	0.15	2.7	7.62	2.7	16.75	207
September	1.52	0.36	5.05	8.47	5.62	17.37	223
October	1.77	0.43	4.57	9.78	5.46	19	204
November	2.52	0.83	5.43	10.67	6.15	19.12	173
December	2.67	1.29	6.4	11.26	6.01	19.25	224

Table 14b. Microseismometer strip-chart wave statistics for comparison with the CDIP deep-water buoy off Bandon, Oregon.

Month	MD Hs (m)	Hs Variance (m*m)	Max MD Hs (m)	MD Tz (s)	Tz Variance (s*s)	Max MD Tz (s)	Observations
January	3.17	1.26	5.94	14.48	2.35	18.9	175
February	2.96	1.03	6.02	13.92	2.96	18.22	210
March	2.73	0.99	6.02	14.18	4	19	231
April	2.26	1.01	5.89	13.99	6.36	23.62	223
May	1.77	0.44	4.19	14.55	7.67	24.99	208
June	1.56	0.58	6.62	14.83	5.56	21.5	164
July	1.14	0.16	2.89	16.37	10.21	24.7	166
August	1.27	0.25	2.97	15.26	6.79	23.53	193
September	1.53	0.6	6.17	15.02	8.07	24.65	217
October	2.2	0.56	4.34	13.99	4.41	24.8	202
November	2.93	1.21	6.93	13.68	4.83	18.82	173
December	3.03	1.74	7.69	14.53	4.58	20.32	224

regression. As in Chapter 3, the data were separated into three four-month segments roughly representing winter, spring, and summer.

The NDBC/microseismometer strip-chart regressions are shown in Figures 33 (wave heights) and 34 (wave periods) a-d. Least-squares regression slopes are near unity, though there is moderate scatter in the data. The NDBC buoy tends to yield somewhat greater wave heights, particularly during the most extreme storm conditions. Some data

Table 15. Significant wave height regression statistics between the CDIP (Bandon, OR) buoy and microseismometer strip-chart data.

Period	Least Squares Slope (Confidence Interval)	y-intercept (Confidence Interval)	R-Squared	Number of Points
All	0.93(0.0344)	0.4(0.1)	0.543	2386
Nov.1-Mar.1 (period 1)	0.71(0.0657)	1.2(0.2)	0.367	782
Mar.1-Jul.1 (period 2)	0.86(0.0670)	0.5(0.2)	0.436	826
Jul.1-Nov.1 (period 3)	0.96(0.0624)	0.1(0.1)	0.539	778

Table 16. Significant wave height regression statistics between the NDBC (Newport, OR) buoy and microseismometer strip-chart data.

Period	Least Squares Slope (Confidence Interval)	y-intercept (Confidence Interval)	R-Squared	Number of Points
All	0.87(0.0348)	0.2(0.1)	0.635	1400
Nov.1-Mar.1 (period 1)	0.59(0.0673)	1.5(0.3)	0.446	365
Mar.1-Jul.1 (period 2)	0.84(0.0692)	0.2(0.2)	0.559	454
Jul.1-Nov.1 (period 3)	0.93(0.0589)	0(0.2)	0.624	581

Table 17. Wave period regression statistics between the CDIP (Bandon, OR) buoy significant wave period and microseismometer strip-chart zero-crossing period.

Period	Least Squares Slope (Confidence Interval)	y-intercept (Confidence Interval)	R-Squared	Number of Points
All	0.11(0.0387)	15.6(0.4)	0.012	2386
Nov.1-Mar.1 (period 1)	0.18(0.0551)	12.2(0.6)	0.05	782
Mar.1-Jul.1 (period 2)	0.11(0.0748)	15.4(0.7)	0.01	826
Jul.1-Nov.1 (period 3)	.28(0.0879)	17.4(0.8)	0.047	778

Table 18. Wave period regression statistics between the NDBC (Newport, OR) buoy dominant wave period and microseismometer strip-chart zero-crossing period.

Period	Least Squares Slope (Confidence Interval)	y-intercept (Confidence Interval)	R-Squared	Number of Points
All	0.04(0.0518)	14.6(0.6)	0.002	1400
Nov.1-Mar.1 (period 1)	0.35(0.1102)	9.2(1.5)	0.096	365
Mar.1-Jul.1 (period 2)	0.08(0.1003)	13.2(1.1)	0.005	454
Jul.1-Nov.1 (period 3)	0.15(0.0872)	16(0.9)	0.019	581

points in these regressions show the NDBC buoy measuring waves 6 to 7 meters high, while the microseismometer concurrently yields heights on the order of 1 meter. Since no comparable disagreements are found in the microseismometer/CDIP comparison, this probably represents spurious measurements by the NDBC buoy. R-squared values of wave height regressions range from 0.44 to 0.63. Regressions of microseismometer zero-crossing periods and NDBC dominant periods lend confirmation to the earlier comparisons, showing no significant correlation. The microseismometer typically yields longer periods, centered near 15 seconds. Further, there is no discernible trend in the periods measured by the two systems.

The CDIP/microseismometer strip-chart comparison is shown in Figures 35 (wave heights) and 36 (wave periods) a-d. Wave height regressions are similar to the NDBC results, though there is even more scatter in these regressions based on R-squared values. The R-squared value is low, with a value of 0.54 in the comparison of all mean daily values (Figure 35a). The same seasonal trends are evident, showing best statistical agreement in the summer. Again, the wave period regressions were not significant.

These observations confirm earlier findings by Thompson et. al. (1985) and Howell and Rhee (1990) which showed good agreement in wave heights, but poor agreement in wave periods between microseismometer wave gages and offshore sensors. The latter study compared microseismometer wave gage data collected at the Chetco River, Oregon, with the CDIP Bandon buoy and array data. Their published comparison time series of significant wave heights shows the microseismometer wave gage usually reports larger wave heights than the other sensors. Of interest is the fact that the data appear to be best correlated in the summer, an observation in disagreement with an earlier study by Thompson et. al. (1985). Following the regressions from winter through summer, the R-squared value increases (less scatter), and the least-squares regression slope approaches unity (better correlation). Thompson's study, limited to two months of data (one summer and one winter month), found that best agreement occurred during the winter characterized by large waves. However, in these figures it can be seen that the data are least correlated when the mean daily significant wave height measured by either sensor exceeds 4 meters. The results obtained here indicate that the overall wave climate at Bandon and Newport are very similar, though the daily wave conditions at these sites could differ substantially as suggested by Thompson et. al., especially during the summer when more locally generated waves are prevalent.

A)

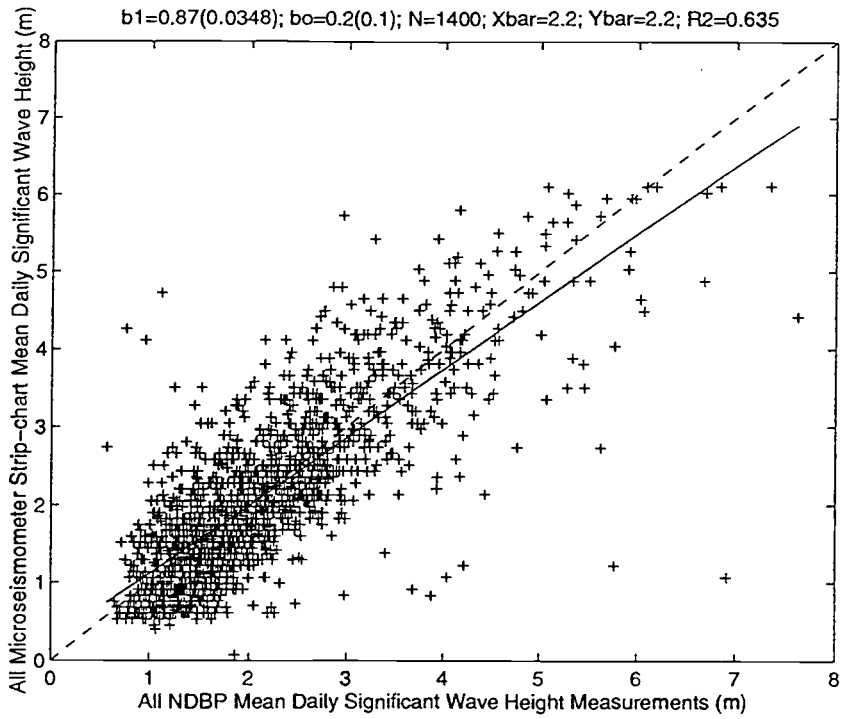

B)

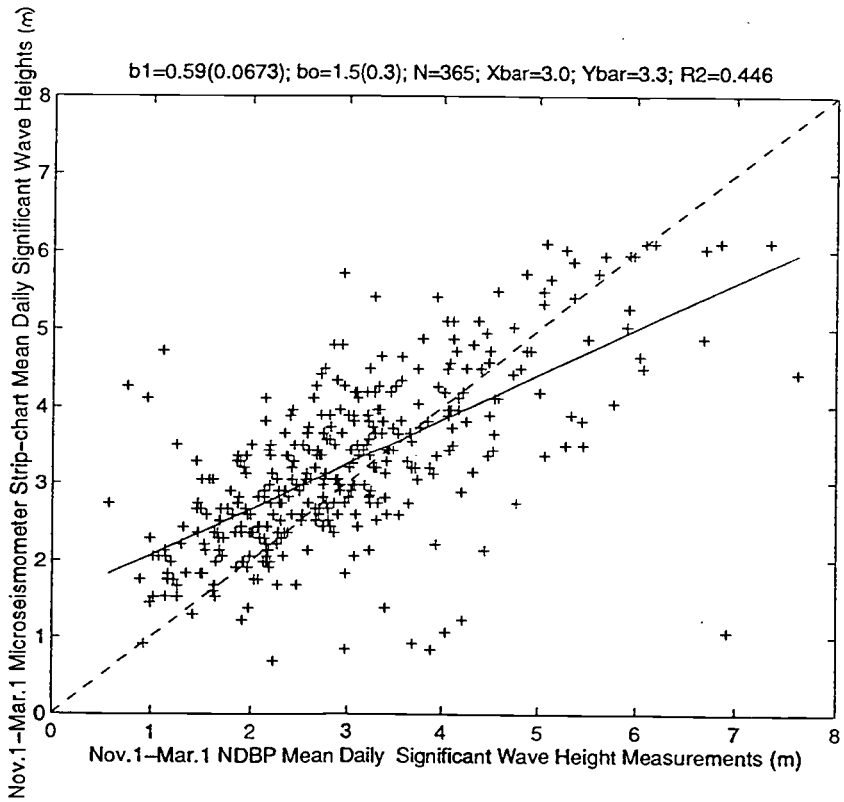

Figure 33 (A/B). A regression of NDBC deep-water buoy and strip-chart microseismometer significant wave height measurements for A) ALL DATA, and B) WINTER (Nov.-Feb.). The solid line is the best-fit least-squares regression line, and the dashed line is 1:1.

C)

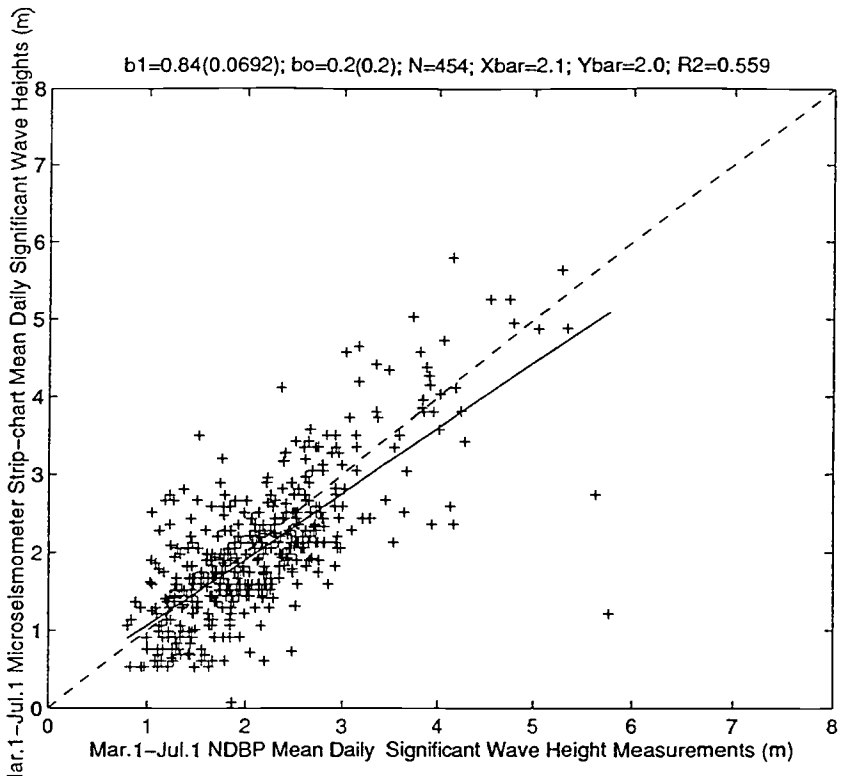

D)

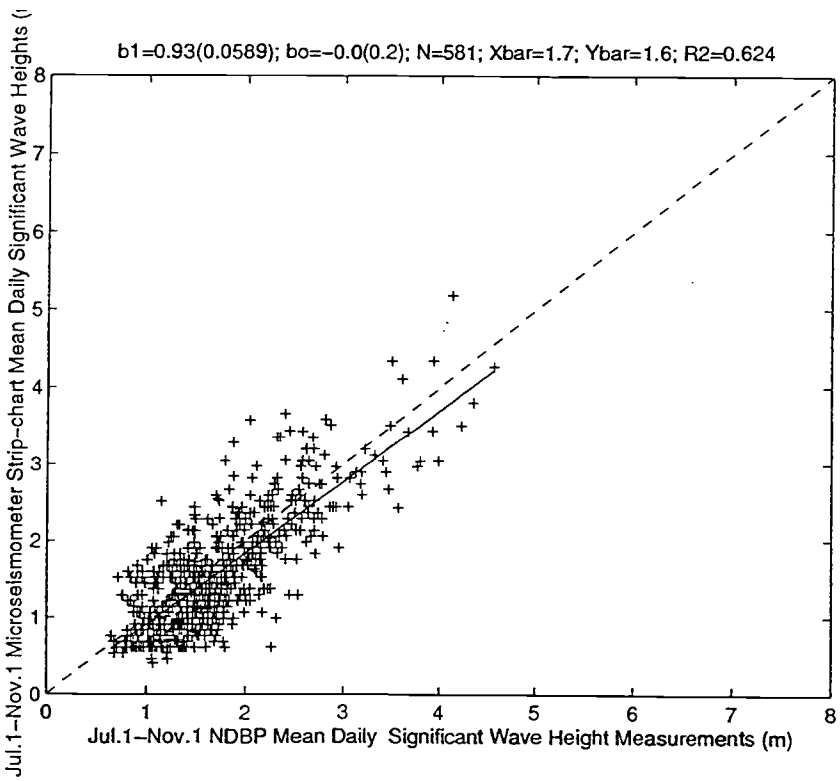

Figure 33 (C/D). A regression of NDBC deep-water buoy and strip-chart microseismometer significant wave height measurements for C) SPRING (Mar.-Jun.), and D) SUMMER (Jul.-Oct.). The solid line is the best-fit least-squares regression line, and the dashed line is 1:1.

A)

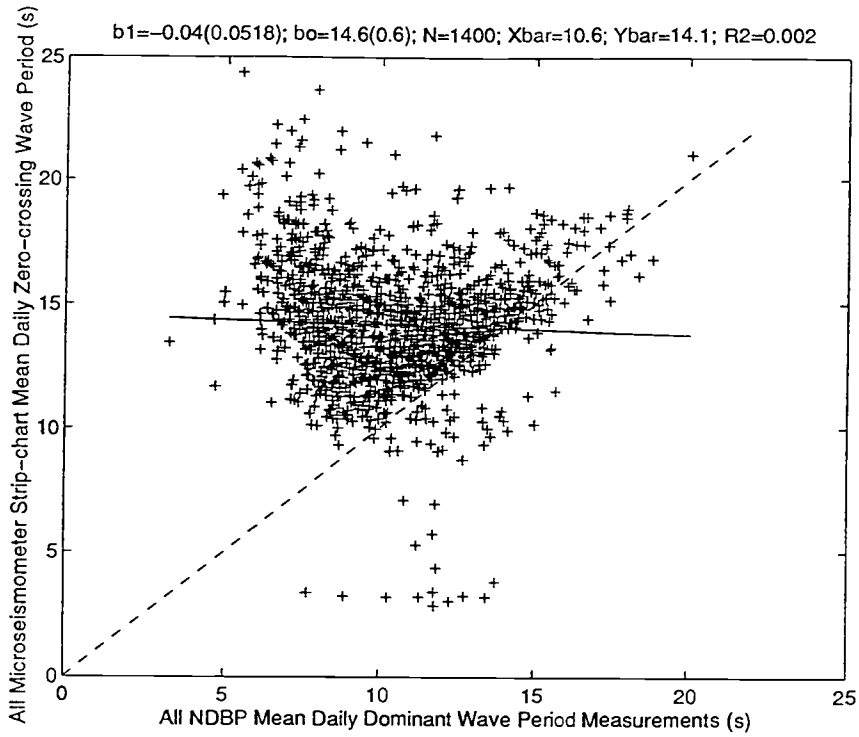

B)

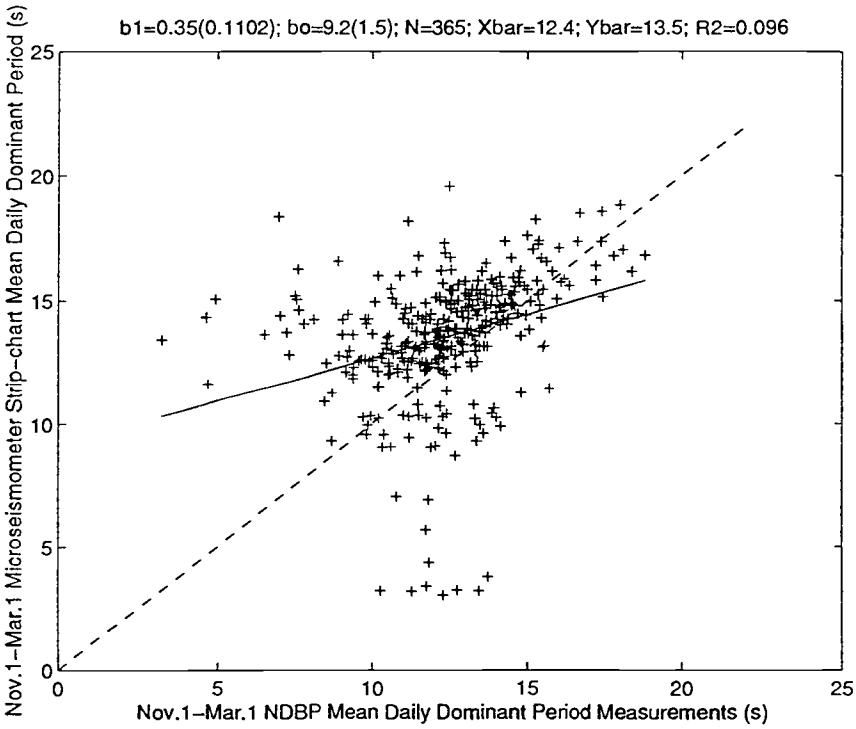

Figure 34 (A/B). The poor agreement between measurements of wave periods by strip-chart microseismometer records and NDBC buoy data for A) ALL DATA and B) WINTER (Nov.-Feb.). The solid line is the best-fit least-squares regression line, and the dashed line is 1:1.

C)

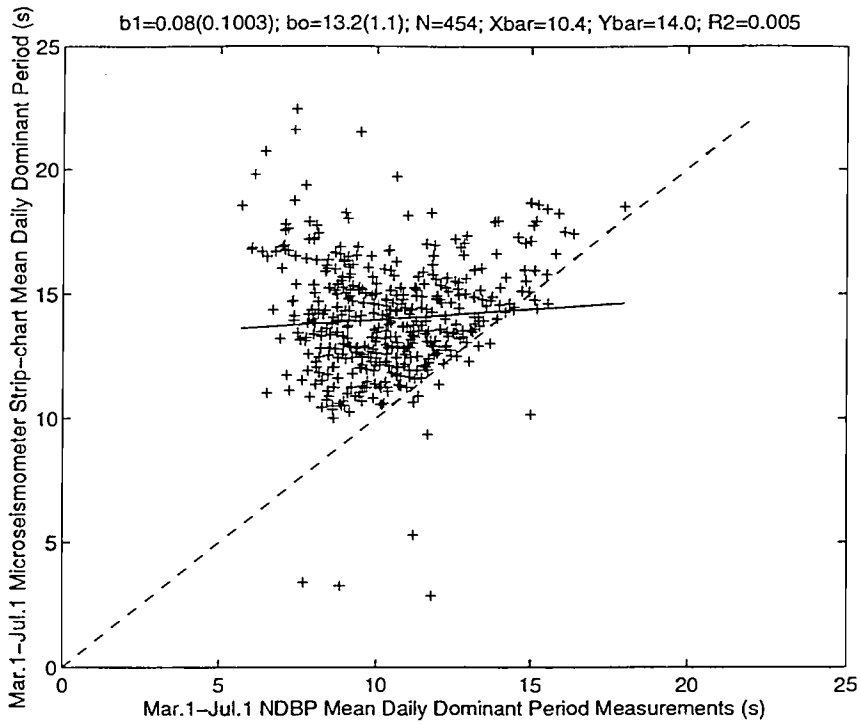

D)

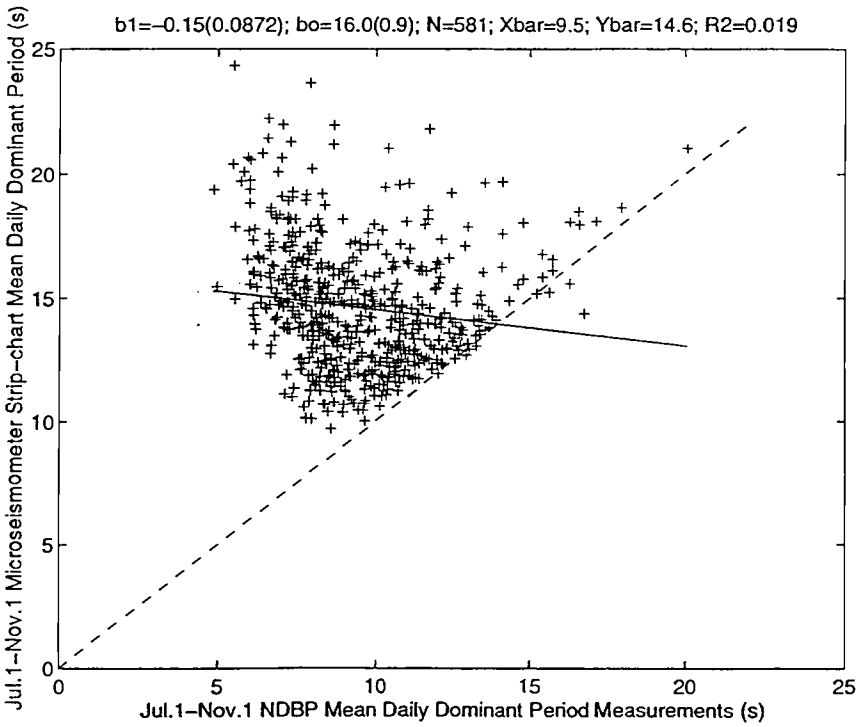

Figure 34 (C/D). The poor agreement between measurements of wave periods by strip-chart microseismometer records and NDBC buoy data for C) SPRING (Mar.-Jun) and D) SUMMER (Jul.-Oct). The solid line is the best-fit least-squares regression line, and the dashed line is 1:1.

A)

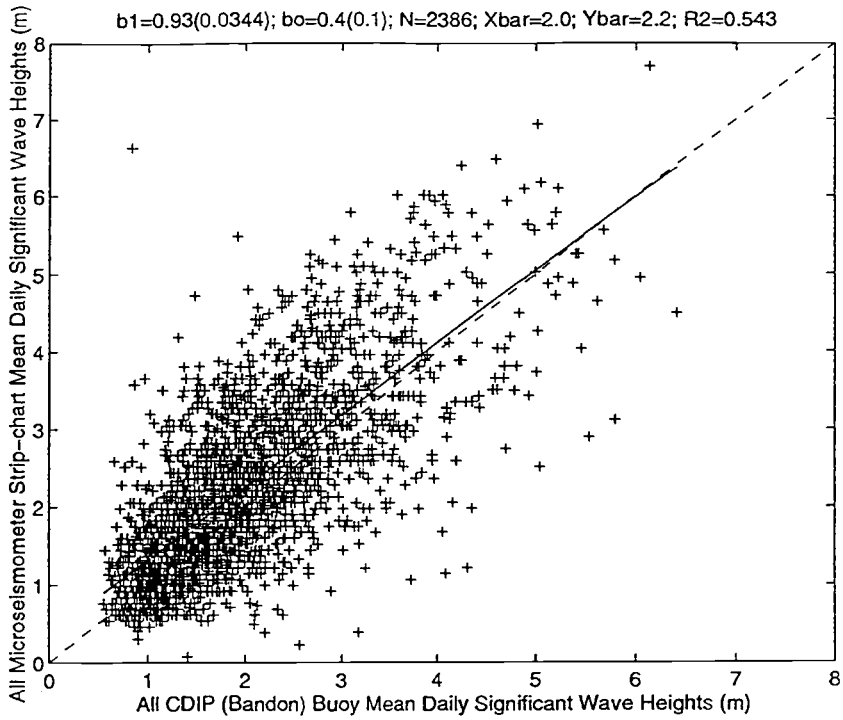

B)

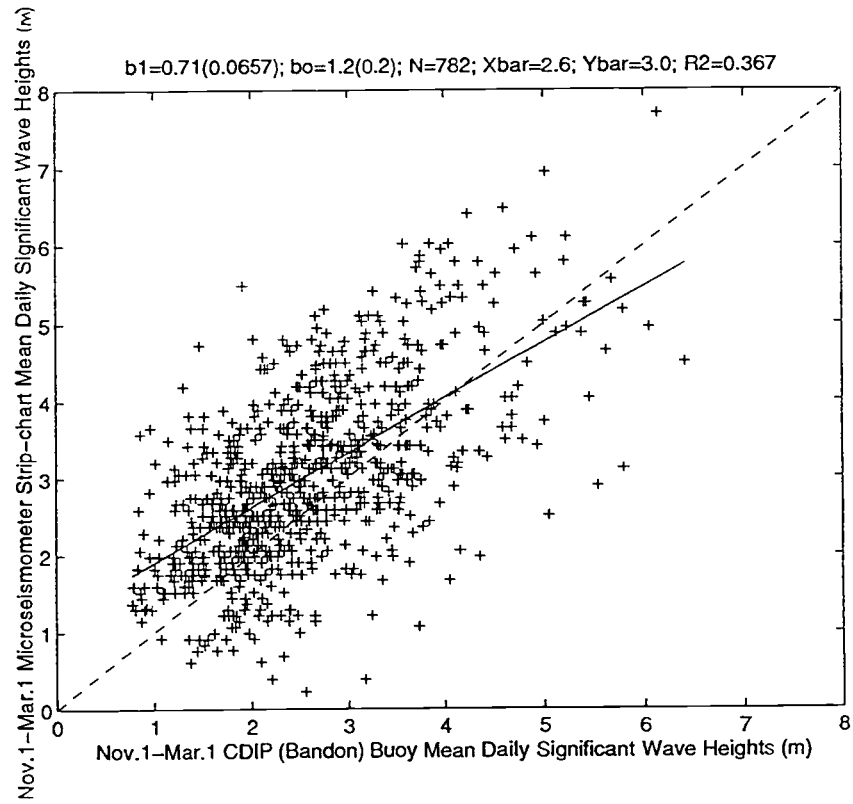

Figure 35 (A/B). A regression of CDIP (Bandon) deep-water buoy and strip-chart microseismometer significant wave height measurements for A) ALL DATA, and B) WINTER (Nov.-Feb.). The solid line is the best-fit least-squares regression line, and the dashed line is 1:1.

C)

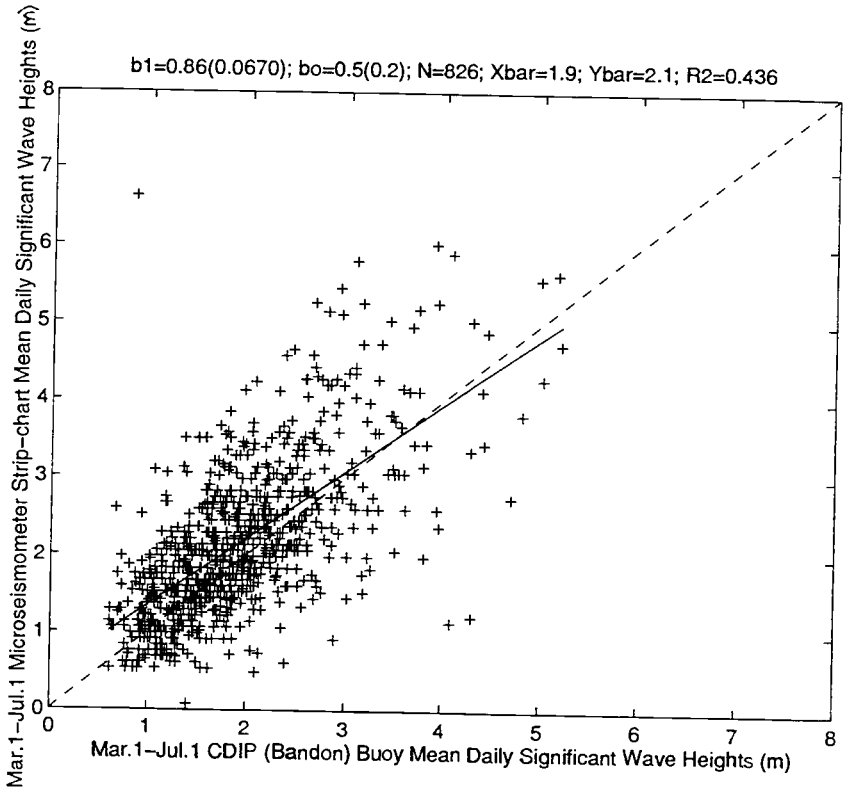

D)

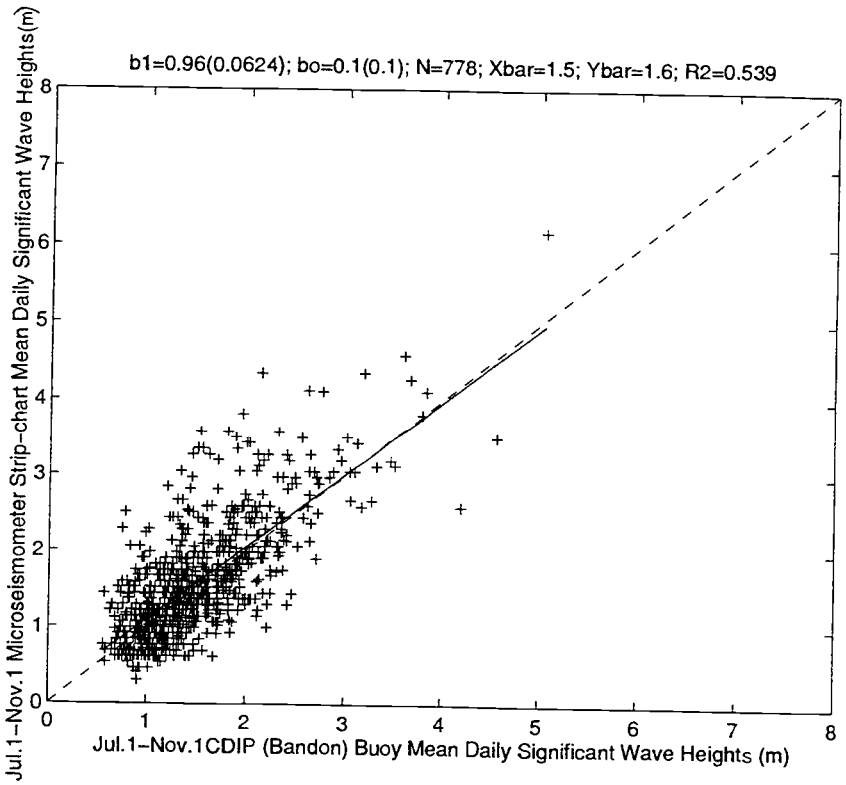

Figure 35 (C/D). A regression of CDIP (Bandon) deep-water buoy and strip-chart microseismometer significant wave height measurements for C) SPRING (Mar.-Jun.), and D) SUMMER (Jul.-Oct.). The solid line is the best-fit least-squares regression line, and the dashed line is 1:1.

A)

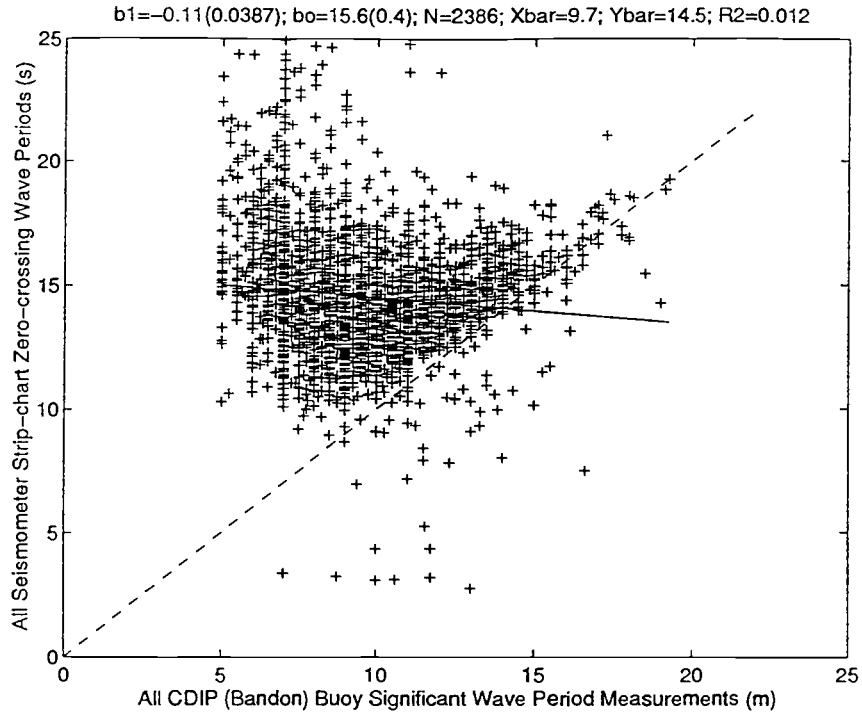

B)

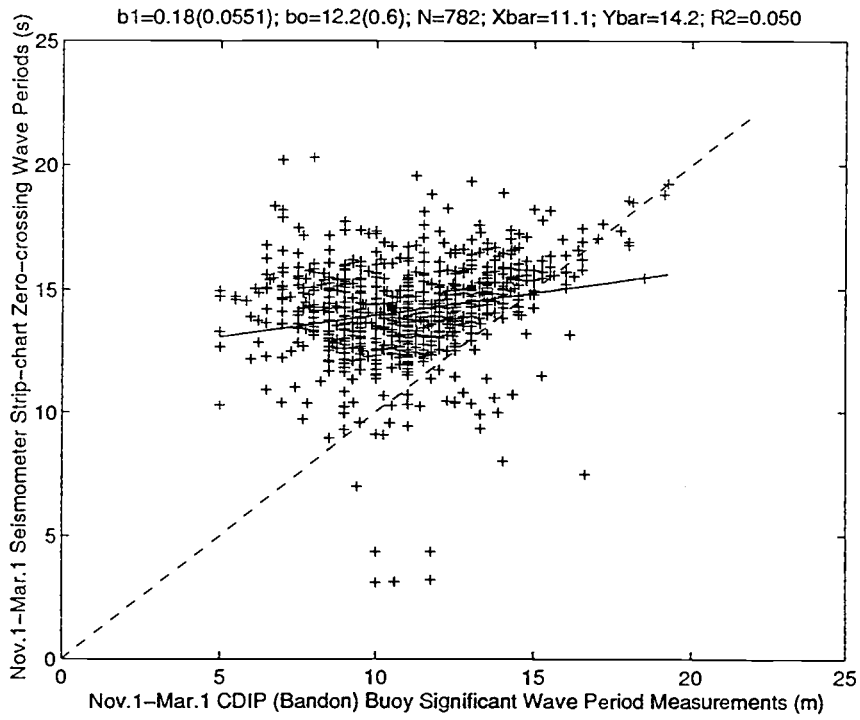

Figure 36 (A/B). The poor agreement between measurements of wave periods by strip-chart microseismometer records and CDIP (Bandon) buoy data for A) ALL DATA and B) WINTER (Nov.-Feb.). The solid line is the best-fit least-squares regression line, and the dashed line is 1:1.

C)

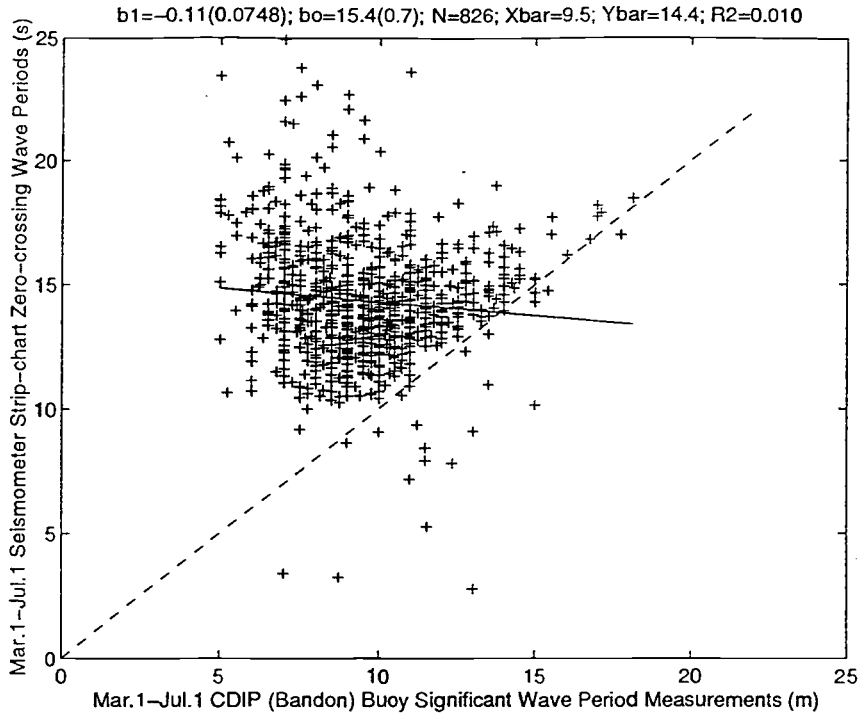

D)

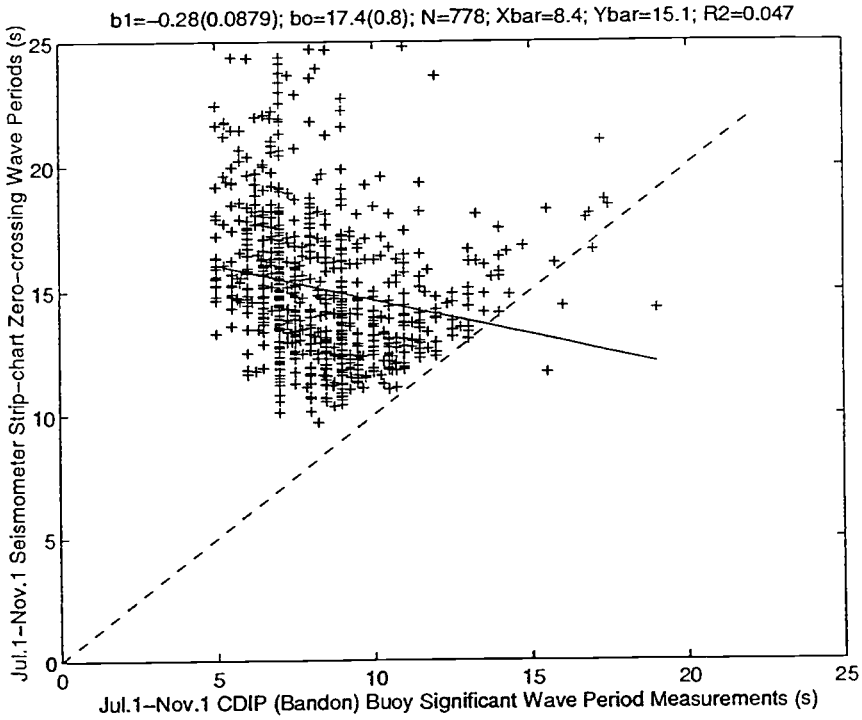

Figure 36 (C/D). The poor agreement between measurements of wave periods by strip-chart microseismometer records and CDIP (Bandon) buoy data for C) SPRING (Mar.-Jun) and D) SUMMER (Jul.-Oct). The solid line is the best-fit least-squares regression line, and the dashed line is 1:1.

A joint frequency distribution of significant wave heights and zero-crossing periods for all microseismometer strip-chart measurements from 1971-1992 is shown in Figure 37. The contour lines in the figure represent the numbers of observations of significant wave heights and periods, and the dashed lines denote wave steepness. The greatest concentration of microseismometer observations centers on significant wave heights of about 2 meters, and corresponding zero-crossing periods around 14 seconds. The joint distribution of microseismometer data has features similar to the distributions of deep-water buoy data, in both the tongue of larger steep waves seen in NDBC data and the tongue of long period small waves seen in the CDIP data. The microseismometer data has characteristics of both local wave generation and distantly generated swell.

Figure 38 shows the distribution of significant wave heights measured by the microseismometer wave gage. The distribution has the same shape as the deep-water buoy data (skewed towards smaller wave heights with rare large wave heights). This distribution was then plotted log-normally by season in Figures 39 a-d. The data fail the Chi-squared goodness-of-fit test, and do not appear as well log-normally distributed as the deep-water buoy data (Chapter 3). All distributions do, however, show similar broad-bandedness, though there is little seasonal dependence. Figure 40 shows the distribution of all zero-crossing wave period measurements by the microseismometer wave gage. No attempts were made to try and fit this distribution to theoretical probability distributions.

Comparison of Computerized Microseismometer Data ('92-93) With Offshore Buoys

The microseismometer system was computerized in 1992 so that raw time-series of microseism amplitude are now stored in a data base at Oregon State University. These data consist of 15-minute time-series recorded four times a day at six hour intervals. The raw time-series are automatically analyzed by computer and converted into significant wave height, zero-crossing wave period, and dominant wave period.

A 386-16 MHz microprocessor with a 12 bit analog-to-digital (A/D) card now records the signal from the microseismometer. The recorded time-series data are in A/D units of microseism amplitude vs. time. The RMS (root-mean-square) of the time-series data is calculated and then converted to significant wave height by a polynomial generated from the transparent template for manual analysis of the strip-chart microseism records. The zero-crossing wave period is calculated by dividing the length of the record

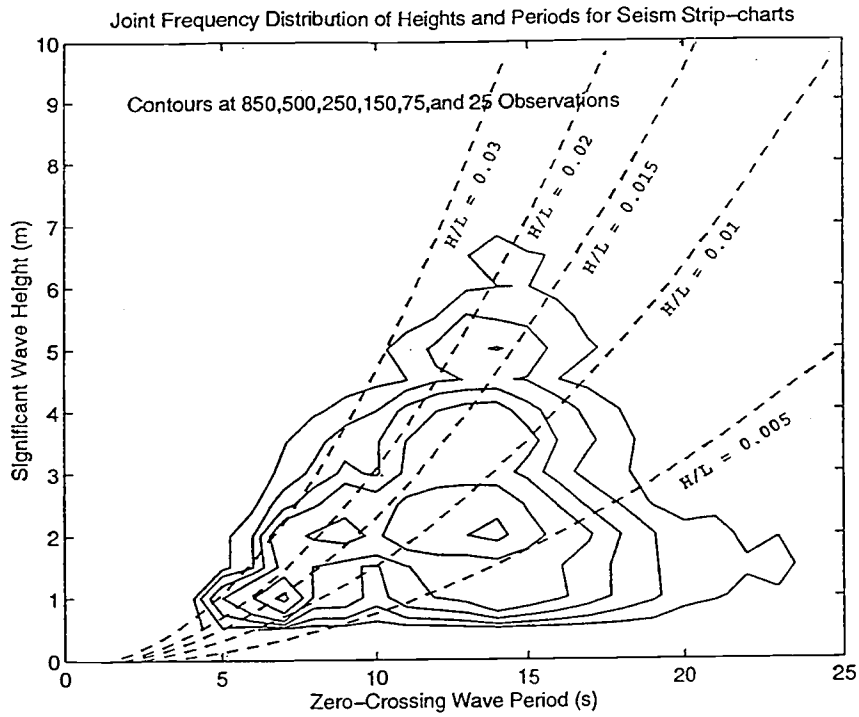

Figure 37. The joint frequency plot of significant wave heights versus zero-crossing wave periods for the measurements derived from strip-chart microseismometer data.

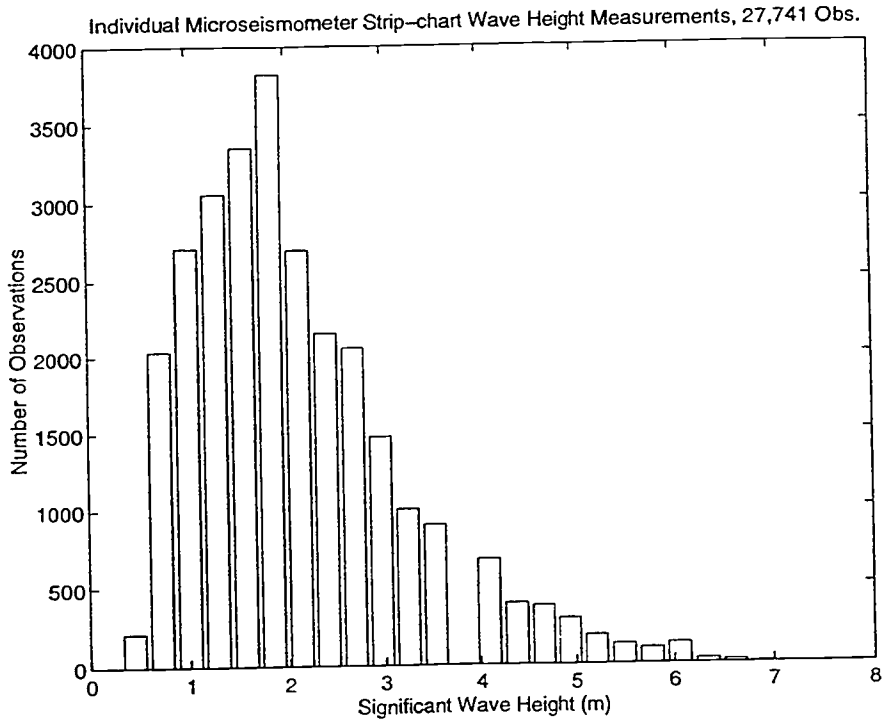

Figure 38. Histogram of all microseismometer strip-chart significant wave height measurements.

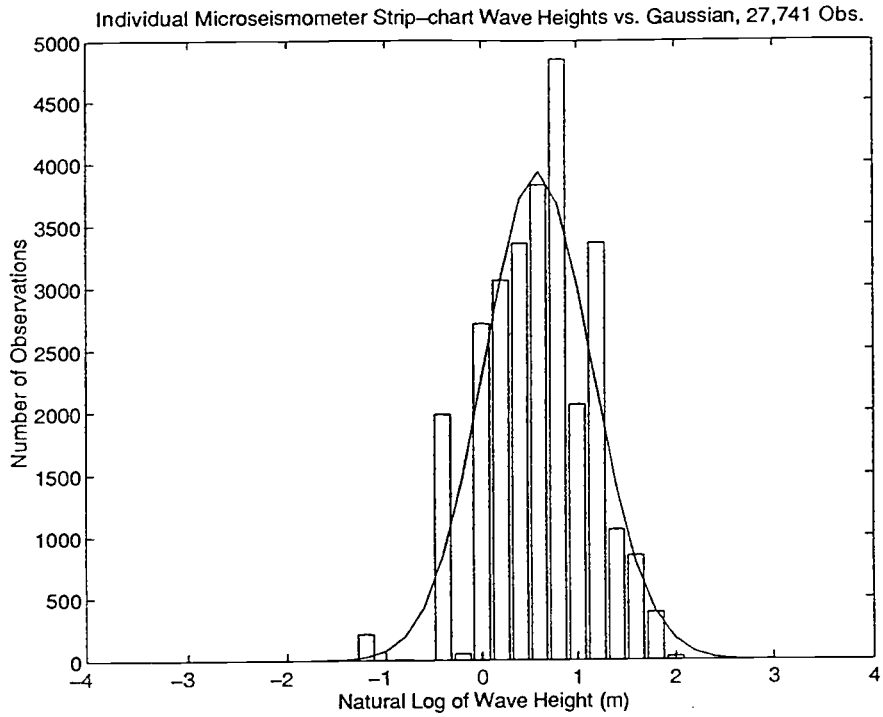

Figure 39A. The log-normal distribution of all microseismometer strip-chart significant wave height measurements versus the Gaussian distribution.

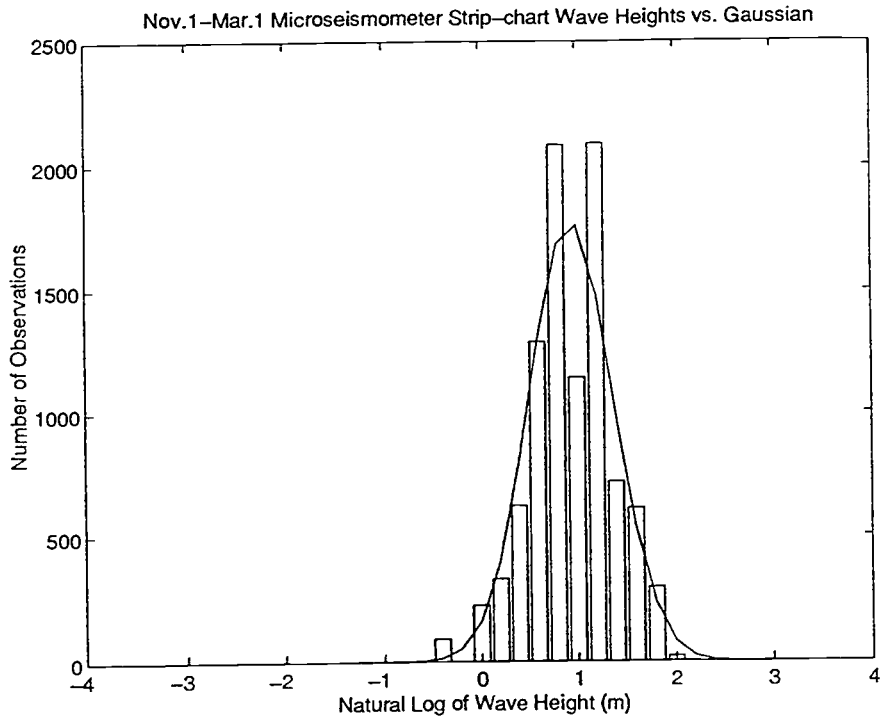

Figure 39B. The log-normal distribution of Winter (Nov.-Mar.) microseismometer strip-chart significant wave height measurements versus the Gaussian distribution.

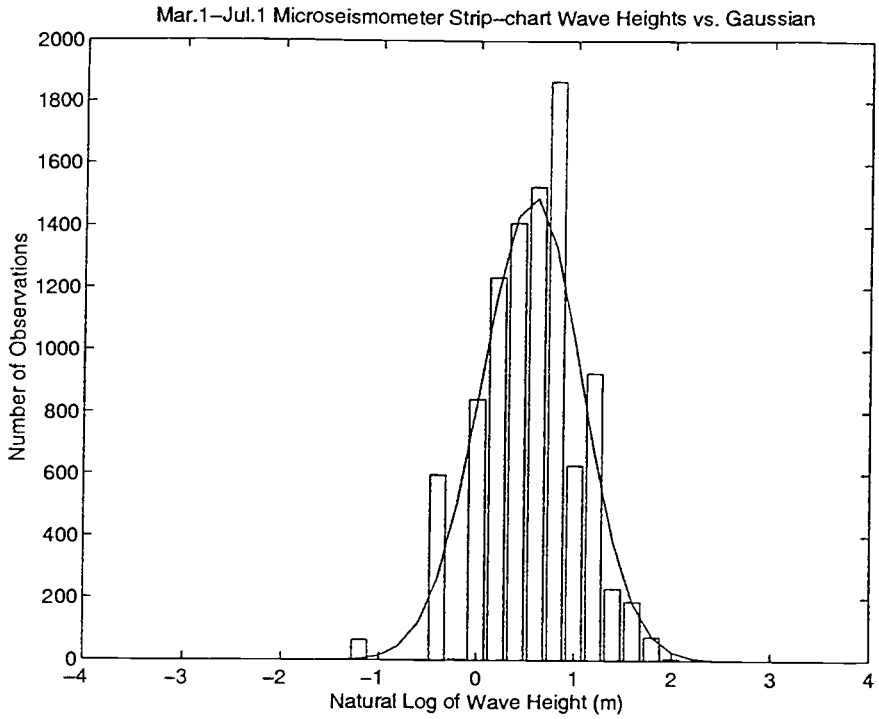

Figure 39C. The log-normal distribution of Spring (Mar.-Jun.) microseismometer strip-chart significant wave height measurements versus the Gaussian distribution.

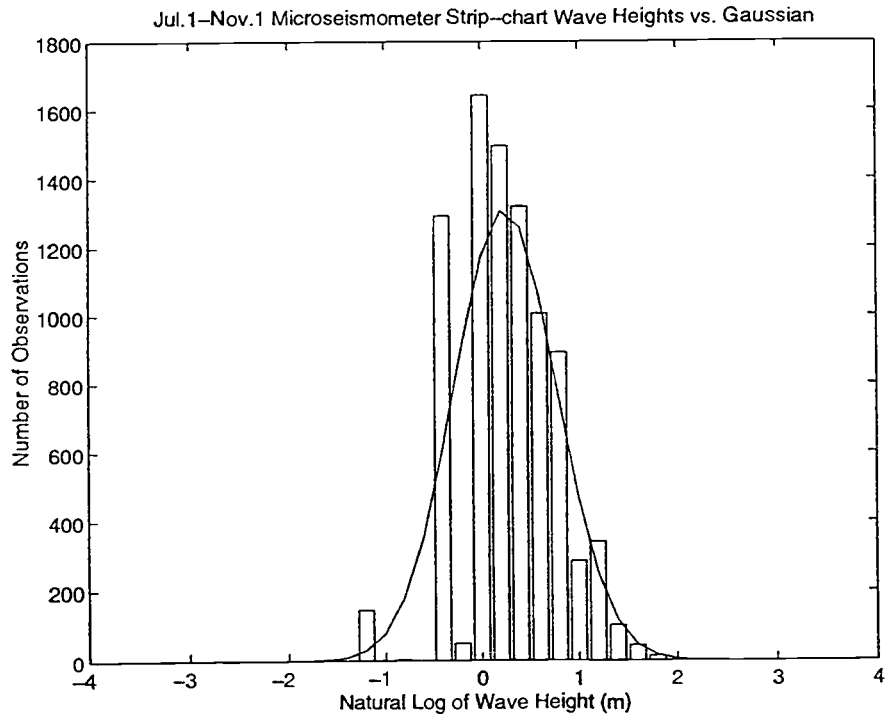

Figure 39D. The log-normal distribution of Summer (Jul.-Oct.) microseismometer strip-chart significant wave height measurements versus the Gaussian distribution.

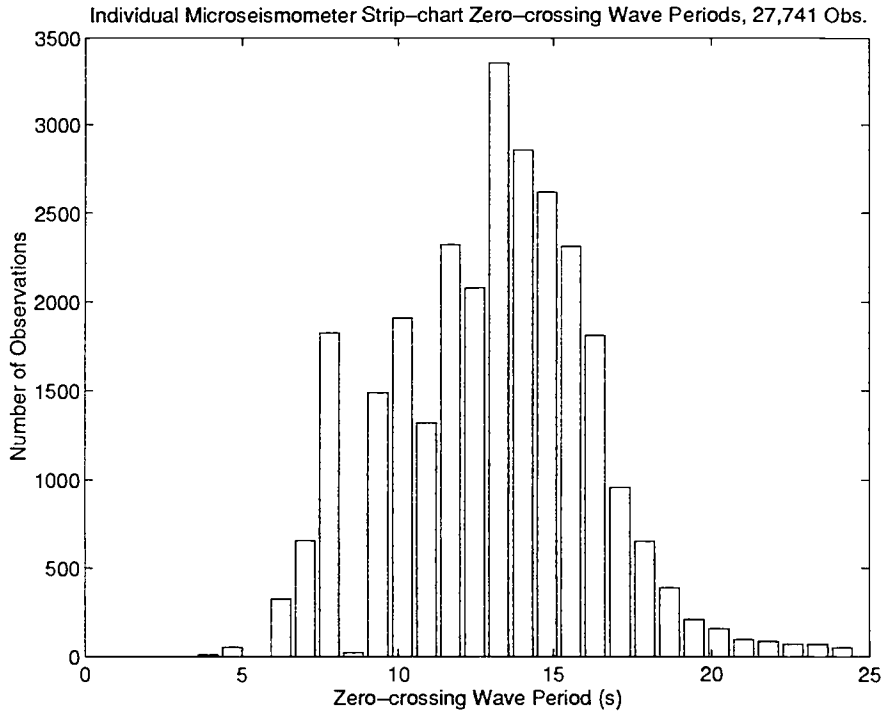

Figure 40. Histogram of all microseismometer strip-chart zero-crossing wave period measurements.

by the number of times the wave signal crosses the mean signal level. The algorithm which calculates zero-crossing wave period skips ahead 3 seconds after each zero-crossing to avoid noise problems in the signal. This insures that no zero-crossing wave period can be less than six seconds (3 data seconds).

An algorithm was written to spectrally determine dominant wave period from the microseism signal. The dominant period is calculated using the method of Fast Fourier Transform (FFT). This results in spectra of wave energy vs. frequency from which the frequency of peak wave energy is extracted and multiplied by 2 (because of the 2-to-1 relationship of microseisms and ocean waves).

Data from the computerized microseismometer wave gage were first analyzed to produce mean daily significant wave heights, mean daily zero-crossing wave periods, and mean daily dominant wave periods. This produced data spanning nearly two years of measurements for comparison with the NDBC and CDIP (Bandon) buoys. Mean daily statistics were averaged to produce mean monthly statistics over the entire record of overlapping measurements made by the various instruments.

As with the strip-chart data, comparisons of calculated zero-crossing and dominant periods from the microseismometer with dominant wave periods from the buoys were found not to be significant. Zero-crossing and dominant wave periods from the seismometer were found to be universally larger than buoy dominant periods, and no linear relationship was found in comparisons of mean daily measurements. As a result, no comparison results are presented.

Mean daily significant wave heights measured by the computerized microseismometer system were compared with wave heights measured by the buoys, showing poor agreement at first. The microseismometer wave gauge was therefore re-calibrated using simultaneous NDBC data as control. The NDBC buoy was chosen because it is directly offshore from the seismometer in Newport, Oregon. The NDBC buoy also gives higher significant wave heights than the other buoys (Chapter 3), preferred in conservative engineering calculations. Figures 41a and 41b compare recalibrated monthly mean and maximum values of significant wave heights from the microseismometer with the NDBC control data. Differences in monthly means are less than 0.5 meters, and differences in maxima are on the order of 1 meter. Figures 42a and 42b compare recalibrated microseismometer wave heights with data from the CDIP buoy

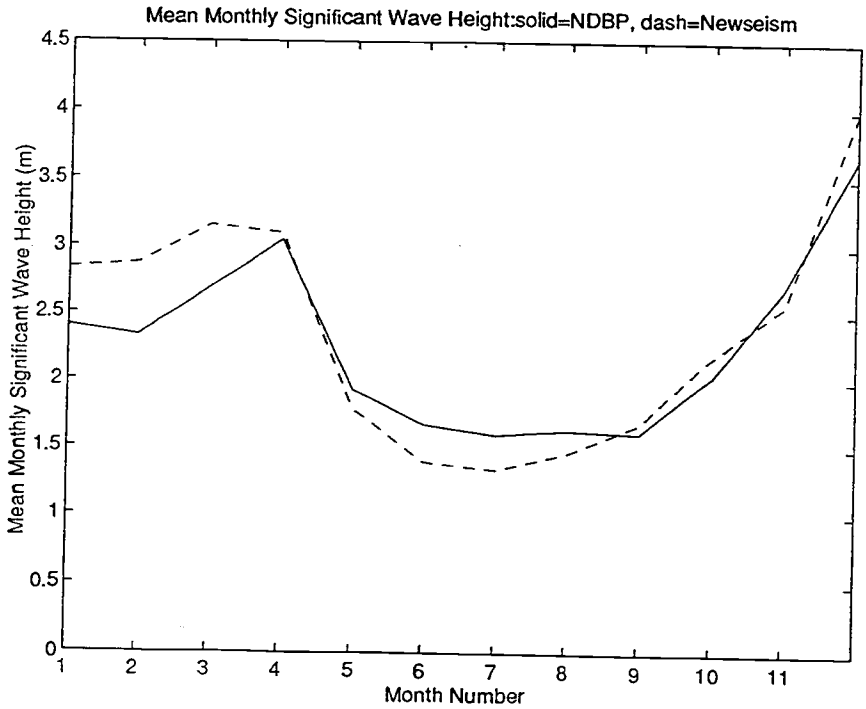

Figure 41A. Comparison of mean monthly significant wave heights between computerized microseismometer and NDBC buoy data.

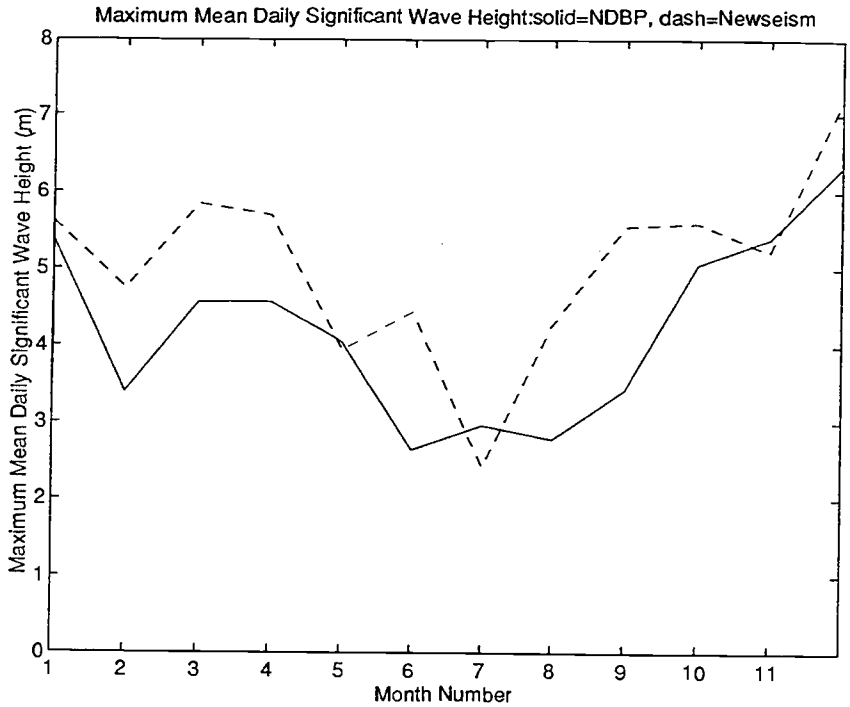

Figure 41B. Comparison of maximum monthly significant wave heights between computerized microseismometer and NDBC buoy data.

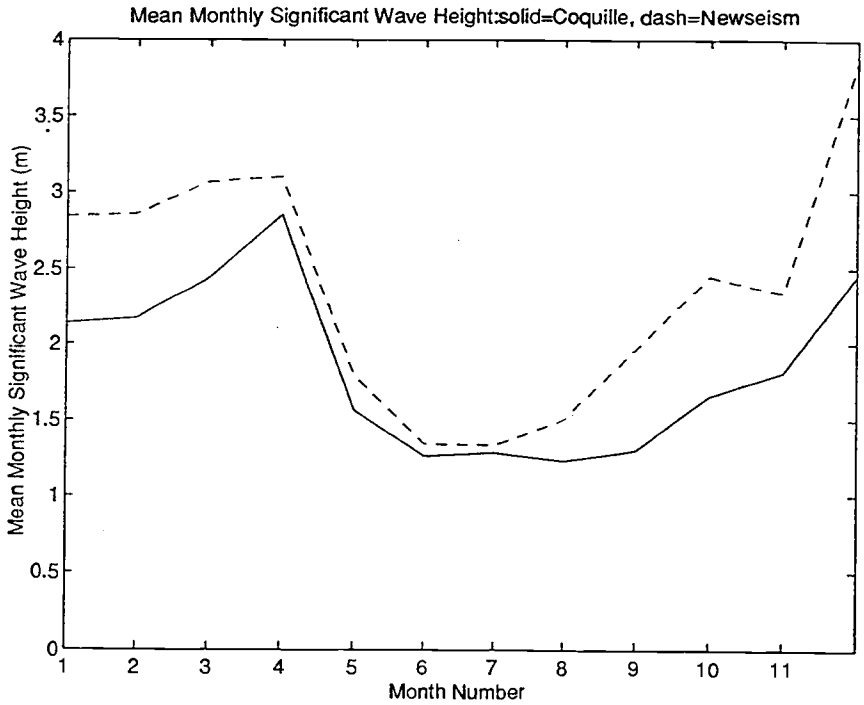

Figure 42A. Comparison of mean monthly significant wave heights between computerized microseismometer and CDIP (Bandon) buoy data.

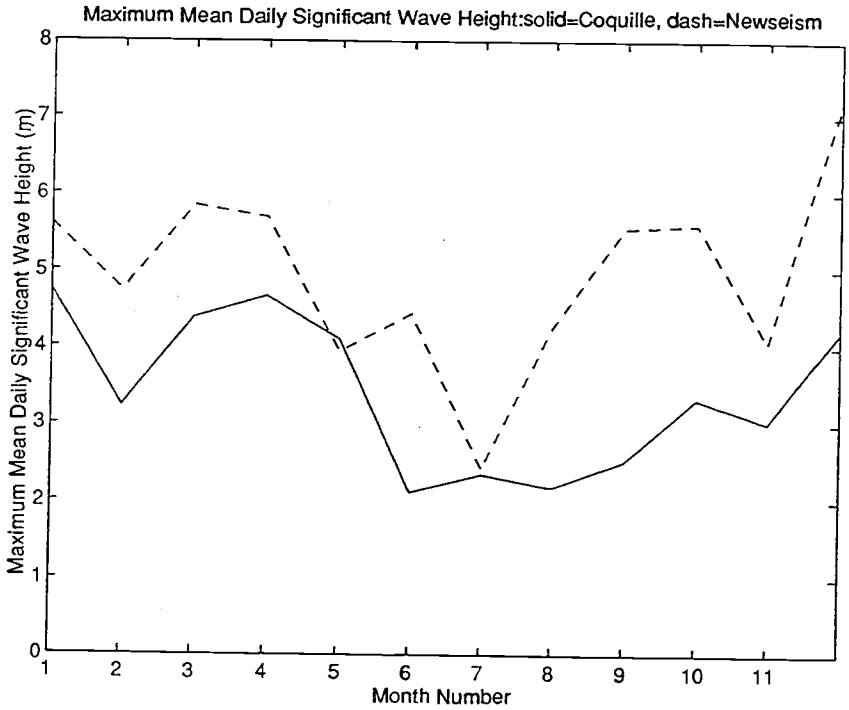

Figure 42B. Comparison of maximum monthly significant wave heights between computerized microseismometer and CDIP (Bandon) buoy data.

off Bandon, OR. Not surprisingly, the microseismometer wave heights are systematically larger than the CDIP measurements, given that the NDBC wave heights are larger than CDIP wave heights (Chapter 3). Differences in monthly means are on the order of 1 meter, and differences in maxima are on the order of 2 meters (though in September the microseismometer maximum mean daily wave height is 3 meters higher than the CDIP measurement!).

Figures 43a-d show the re-calibrated microseismometer wave heights versus the NDBC buoy wave heights. There is excellent agreement between the two sensors, with reasonably high R-squared values except during the summer when the seismometer reports some spuriously large wave heights. In fact, there is a marked improvement over the manually-analyzed records.

Figures 44a-d compare computerized microseismometer wave heights with CDIP (Bandon) buoy wave heights. As expected, the mean daily microseismometer wave heights are larger than the CDIP measurements, though there is an excellent trend in each regression.

A joint frequency table was created for all data from the microseismometer (strip-chart and computerized), shown in Figure 45. The contour lines represent the numbers of observations of significant wave heights and periods for the entire length of record measured by the microseismometer (23 years). The dashed lines in the figures denote significant wave steepness. The distribution shows the expected overall increase in wave period with increasing wave height. The greatest concentration of microseismometer observations centers on wave heights of about 2 meters and corresponding periods around 13 seconds. The distribution has features similar to those found in both buoy distributions (Chapter 3).

Figure 46 shows the distribution of significant wave height measurements for the microseismometer. This distribution represents all individual wave height measurements made by the seismometer since deployment. The distribution has the characteristic Rayleigh shape (skewed towards smaller wave heights with rare large wave heights). The distribution is shifted right of zero since each point in the distribution is a significant wave height which is not likely to be near zero.

Though the significant wave height measurements look Rayleigh distributed, they fail the statistical goodness-of-fit test. Wave heights were plotted log-normally in Figure 47. Although the distribution fails the Chi-squared goodness-of-fit test, it appears quite irregular. The distribution appears as equally broad-banded as the buoy distributions (Chapter 3), indicating similar overall wave height variability at each location. A distribution of all microseismometer zero-crossing wave periods is shown in Figure 48. No attempt was made to try and fit this distribution to theoretical probability distributions.

The above comparisons further confirm the usefulness of the microseismometer system for the routine collection of wave data on high energy coastlines. Measurements of wave heights are nearly as reliable as those measured by deep-water buoys, though wave periods are unreliable. In finding a good correlation between microseismometer-inferred wave heights and offshore wave heights, further confirmation is made of the theory by Longuet-Higgins (1950) as to the association of microseisms with reflected ocean waves.

A)

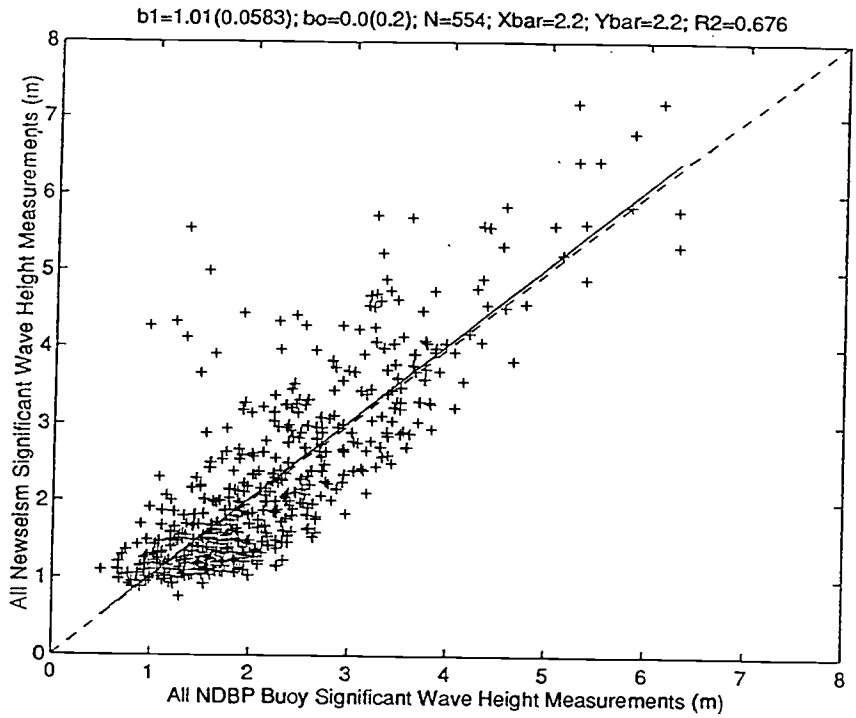

B)

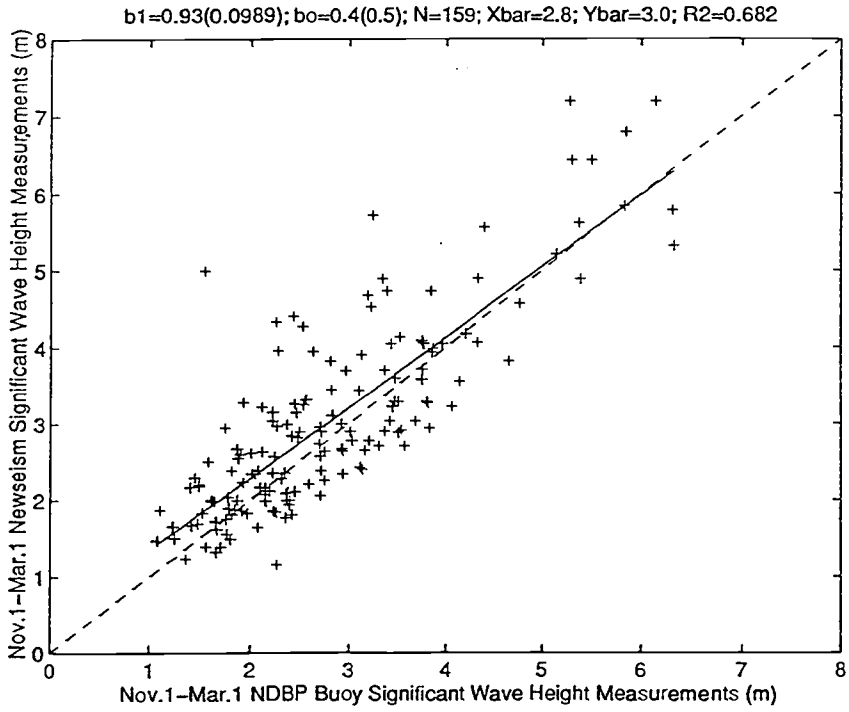

Figure 43 (A/B). A regression of NDBC deep-water buoy and computerized microseismometer significant wave height measurements for A) ALL DATA, and B) WINTER (Nov.-Feb.). The solid line is the best-fit least-squares regression line, and the dashed line is 1:1.

C)

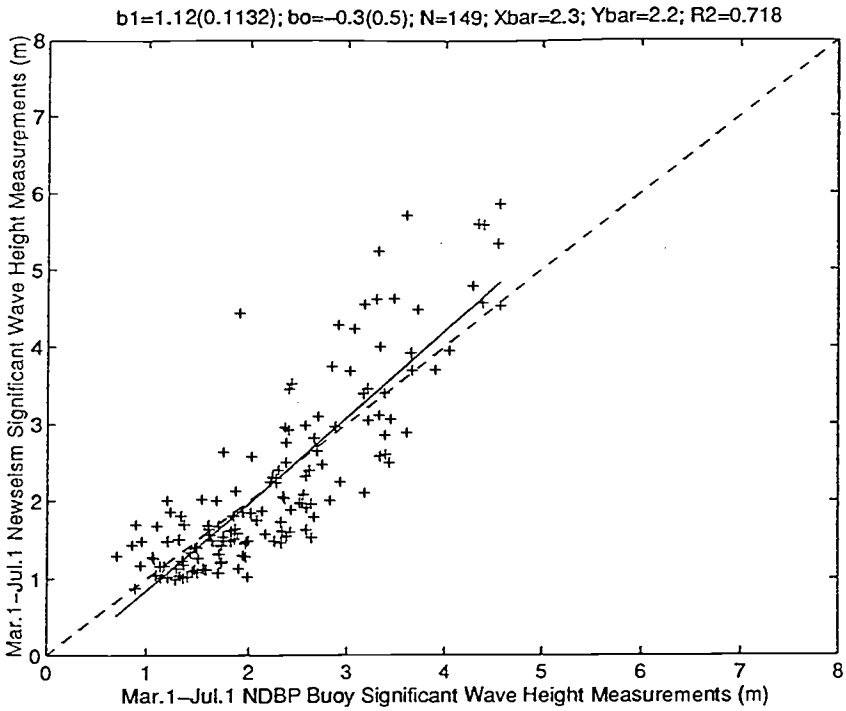

D)

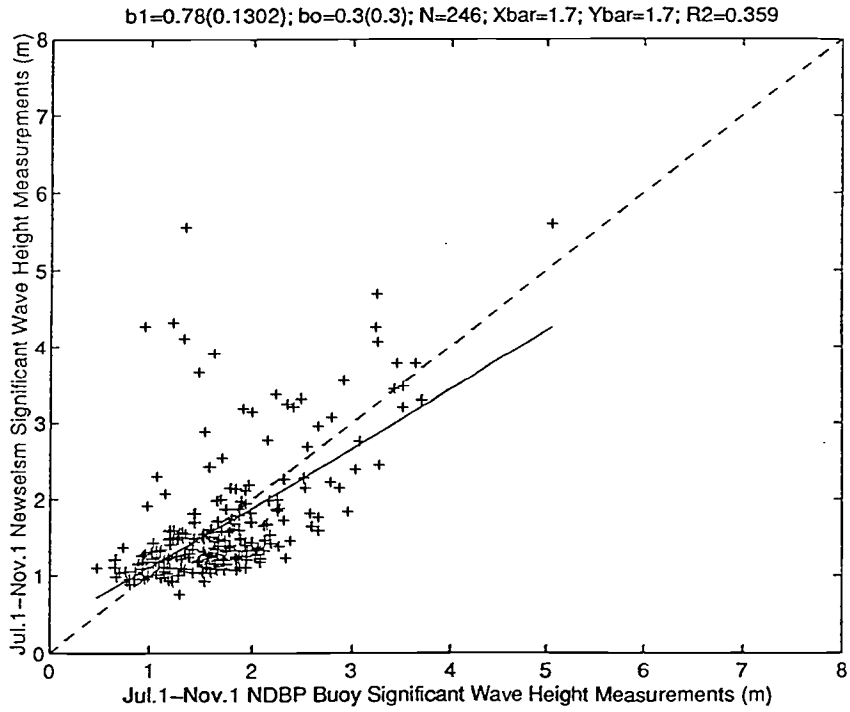

Figure 43 (C/D). A regression of NDBC deep-water buoy and computerized microseismometer significant wave height measurements for C) SPRING (Mar.-Jun.), and D) SUMMER (Jul.-Oct.). The solid line is the best-fit least-squares regression line, and the dashed line is 1:1.

A)

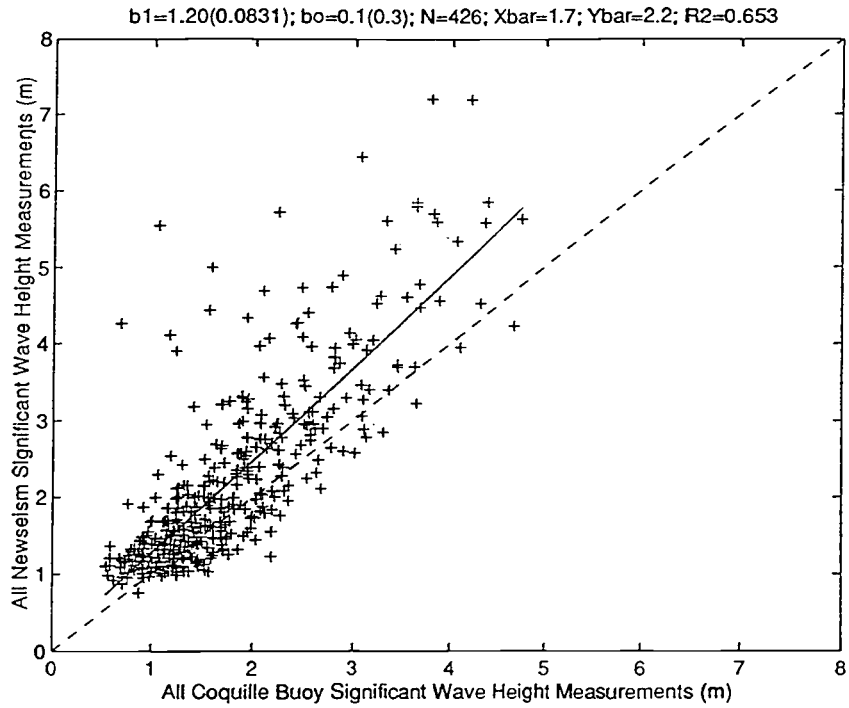

B)

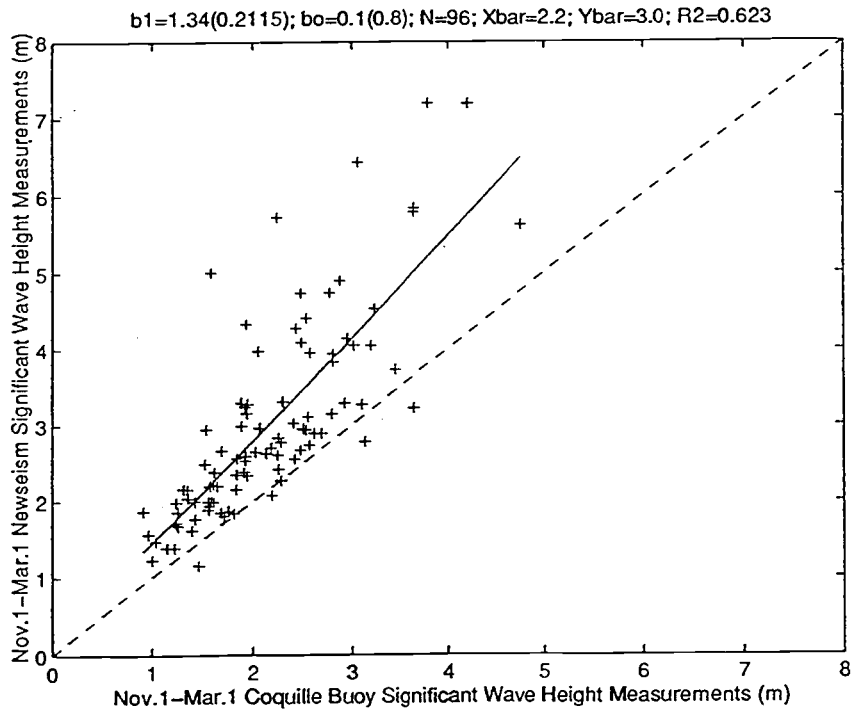

Figure 44 (A/B). A regression of CDIP (Bandon) deep-water buoy and computerized microseismometer significant wave height measurements for A) ALL DATA, and B) WINTER (Nov.-Feb.). The solid line is the best-fit least-squares regression line, and the dashed line is 1:1.

C)

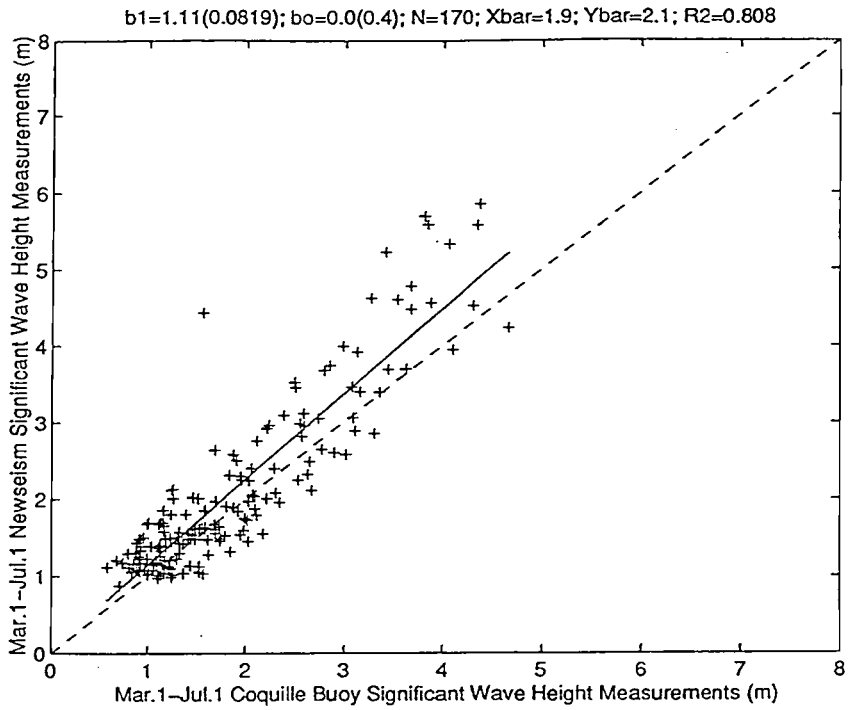

D)

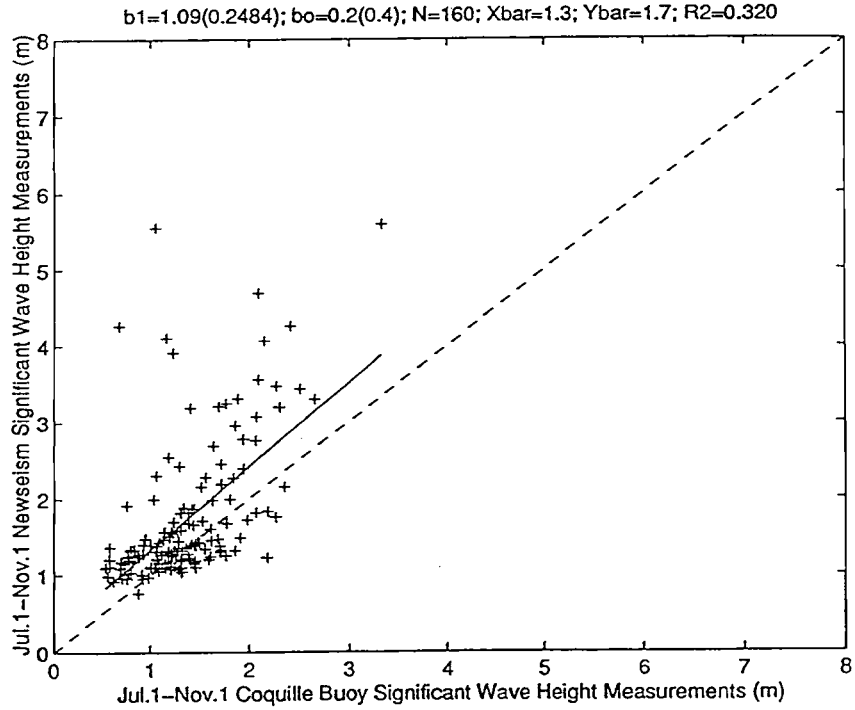

Figure 44 (C/D). A regression of CDIP (Bandon) deep-water buoy and computerized microseismometer significant wave height measurements for C) SPRING (Mar.-Jun.), and D) SUMMER (Jul.-Oct.). The solid line is the best-fit least-squares regression line, and the dashed line is 1:1.

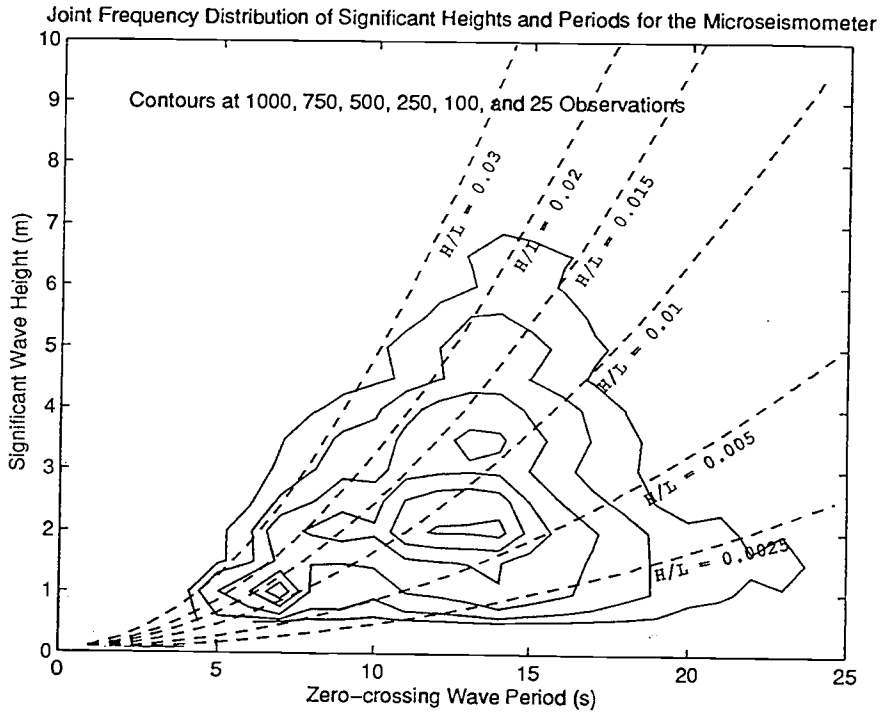

Figure 45. The joint frequency plot of all significant wave heights versus zero-crossing wave periods for the measurements derived from the microseismometer (strip-charts and computerized).

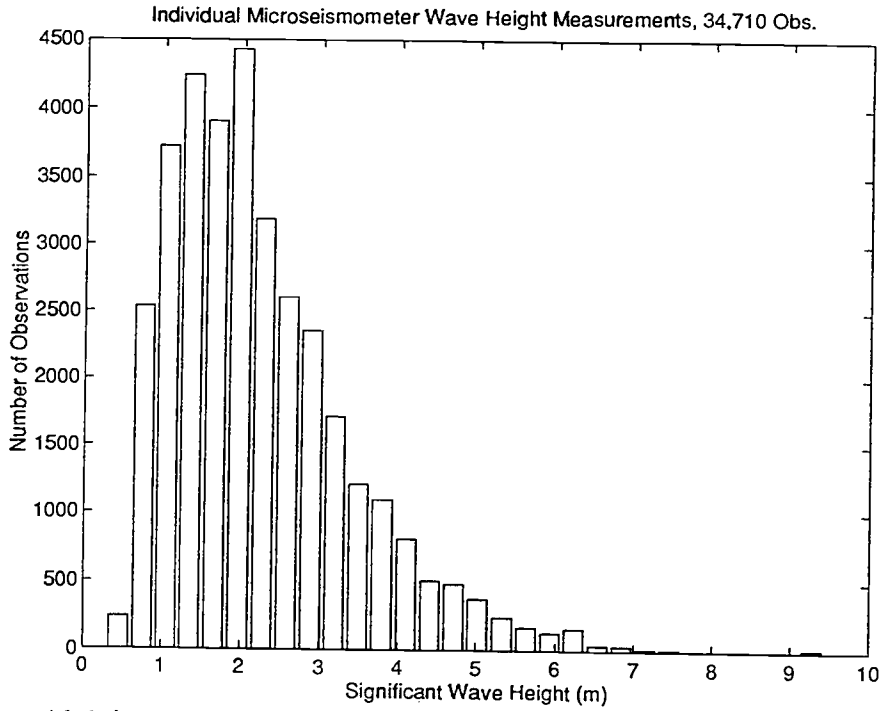

Figure 46. Histogram of all microseismometer (strip-chart and computerized) significant wave height measurements.

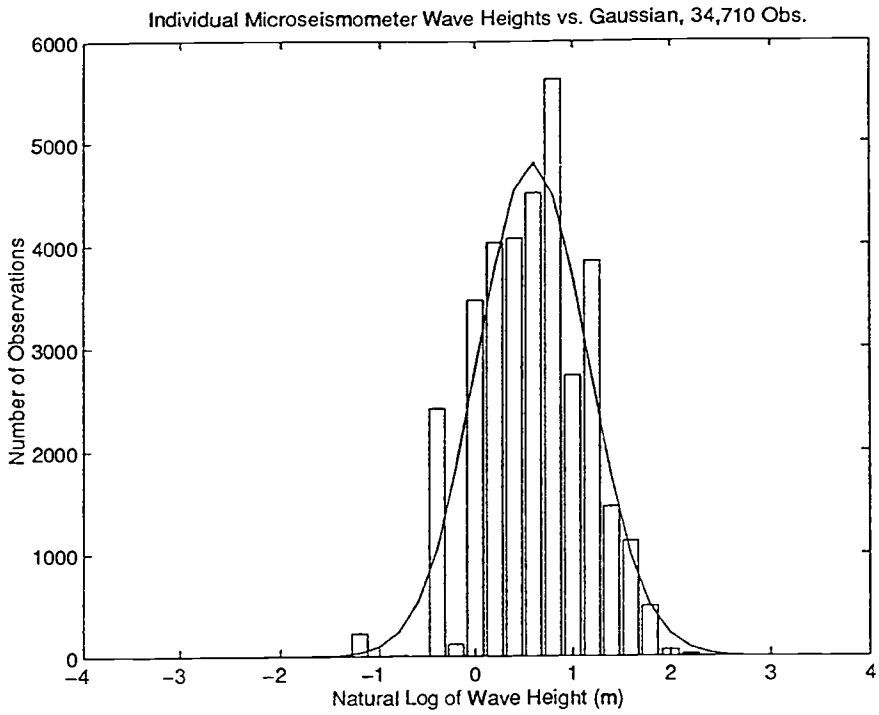

Figure 47. The log-normal distribution of all microseismometer (strip-chart and computerized) significant wave heights versus the Gaussian distribution.

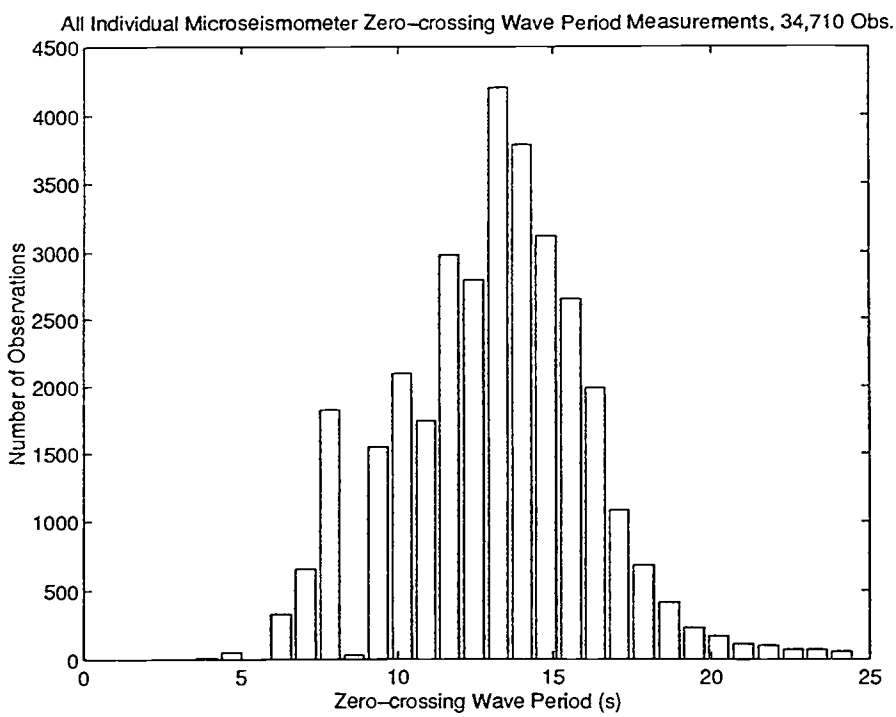

Figure 48. The log-normal distribution of all microseismometer (strip-chart and computerized) zero-crossing wave periods versus the Gaussian distribution.

CHAPTER 5
WIS HINDCAST DATA

The Wave Information Study of the U.S. Army Corps of Engineers has produced daily wave hindcast data for the period 1956-1975. This provides no overlap with the available buoy and array data from which to make comparisons, but there are four years of overlap (1971-75) with the microseismometer data. This chapter discusses comparisons of the WIS hindcast data with microseismometer wave measurements. Monthly means and maxima are compared, statistical tests are performed, and linear regressions are presented as in previous chapters. A recalibration of the WIS hindcast estimates for the Pacific Northwest is suggested from the comparisons.

Comparison of WIS Hindcast Data With Microseismometer Data (1971-75)

The Wave Information Study (WIS) of the US Army Corps of Engineers was undertaken to generate 20 years of hindcast wave data spanning the period 1956 to 1975 (Hemsley and Brooks, 1989). The three phases of WIS hindcast data, and the hindcasting technique are described briefly in Chapter 2. Phase II wave estimates are available for 17 stations along the ocean coasts of Oregon and Washington. Station 42 positioned in deep-water offshore from Newport, Oregon (Figure 2), is used in the present comparison because it is closest to the microseismometer.

Phase II hindcast deep-water wave data for Station 42, recorded every three hours, were first analyzed to produce mean daily significant wave heights and mean daily peak wave periods. Mean daily statistics were averaged to produce mean monthly statistics over the entire record of overlapping measurements made by the two systems. This produced data spanning roughly three years of measurements for comparison with the microseismometer data. This overlap allows an examination of how reliably the WIS hindcast procedures predict significant wave heights and periods on the high-energy Northwest coast.

Figures 49a and 49b compare mean and maximum (mean daily) values of significant wave heights derived from the WIS hindcast data with strip-chart microseismometer measurements. The same annual trend is evident in both figures,

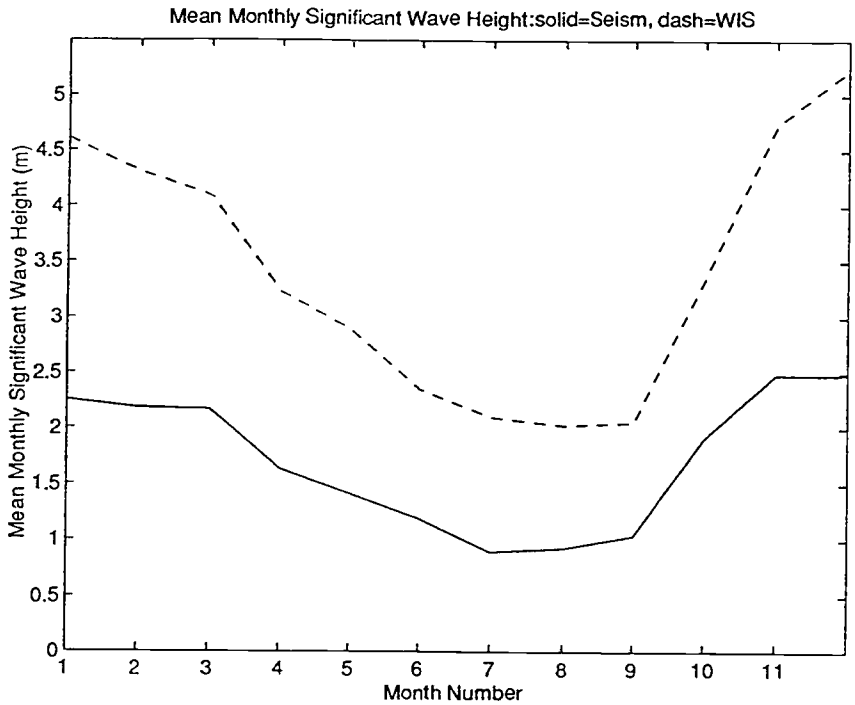

Figure 49A. Comparison of mean monthly significant wave heights between the microseismometer and WIS Station 42 data.

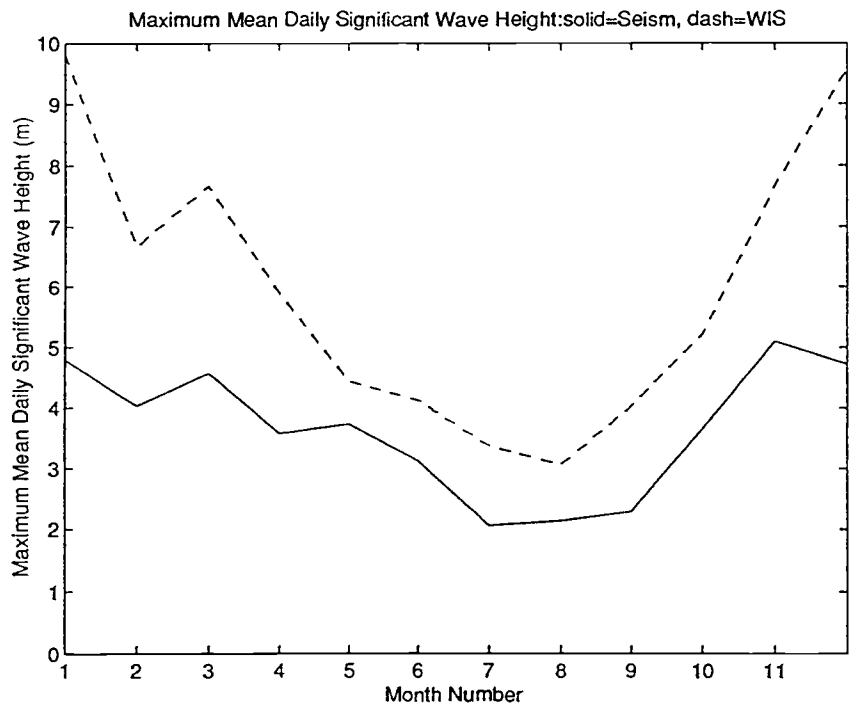

Figure 49B. Comparison of maximum monthly significant wave heights between the microseismometer and WIS Station 42 data.

though the WIS wave heights are substantially larger than the microseismometer heights. Differences in monthly means range from 1 to 2.5 meters, while differences in monthly maximum wave heights range from 0.8 to 5 meters.

F-test and t-test comparisons of mean monthly significant wave heights were made between the WIS hindcast data and microseismometer strip-chart measurements. The results of these tests indicate that wave height means are statistically different, but there is no reason to suspect that wave height variances are different.

Linear regressions of mean daily significant wave heights were used to further compare the data sets. Table 19 gives the calculated least-squares regression slopes and y-intercepts for wave height correlations between the WIS hindcast data and microseismometer measurements. Also shown are the R-squared (goodness-of-fit) values, and the numbers of points (days) used in each regression. As in Chapters 3 and 4, the data were separated into four-month segments roughly representing winter, spring, and summer.

Table 19. Significant wave height regression statistics between WIS hindcasts and microseismometer data.

Period	Least Squares Slope (Confidence Interval)	y-intercept (Confidence Interval)	R-Squared	Number of Points
All	1.31(0.0601)	1.2(0.2)	0.637	1034
Nov.1-Mar.1 (period 1)	1.13(0.1233)	2.1(0.4)	0.521	301
Mar.1-Jul.1 (period 2)	0.98(0.1061)	1.6(0.3)	0.475	364
Jul.1-Nov.1 (period 3)	0.91(0.0957)	1.3(0.2)	0.484	369

The WIS/microseismometer regressions are shown in Figures 50 a-d. There is a good trend in the data, with an R-squared = 0.637 value in the regression of all data (Figure 50a). The regressions performed by season (Figures 50 b-d) are similar, though with lower R-squared values. The significant wave heights derived from the WIS hindcasts are roughly 30% larger than those measured by the microseismometer. It has been shown in Chapter 4 that the microseismometer provides good estimates of deep-water significant wave heights when compared with buoy data. Therefore, the WIS hindcast significant wave heights at Station 42 must be systematically higher than those derived from buoy measurements. In some cases the hindcast wave heights reach nearly 10 meters, with many greater than 7 meters. This does not agree with the wave climate determined by any of the other measurement systems used in this study. Further,

A)

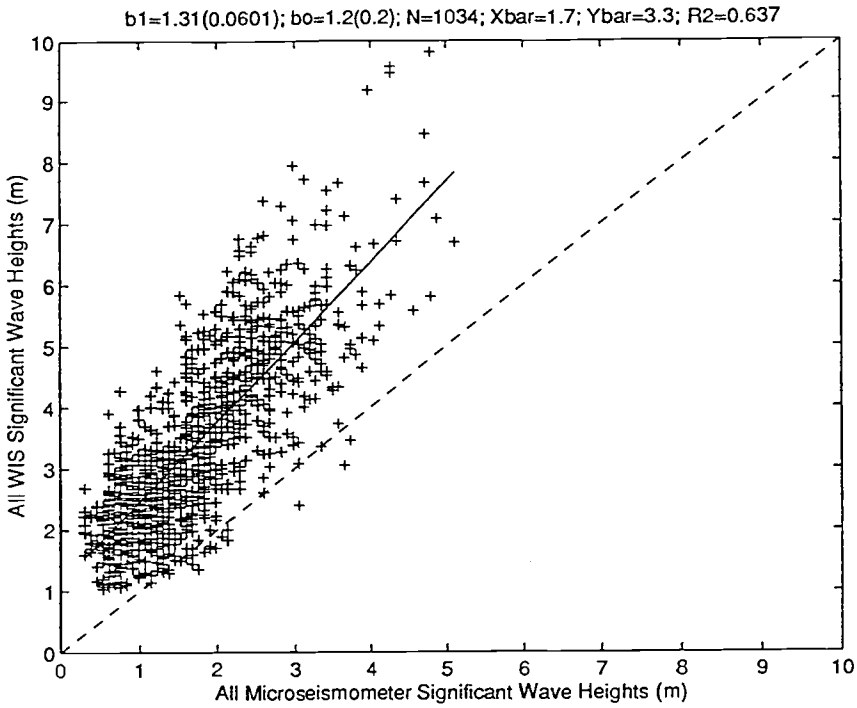

B)

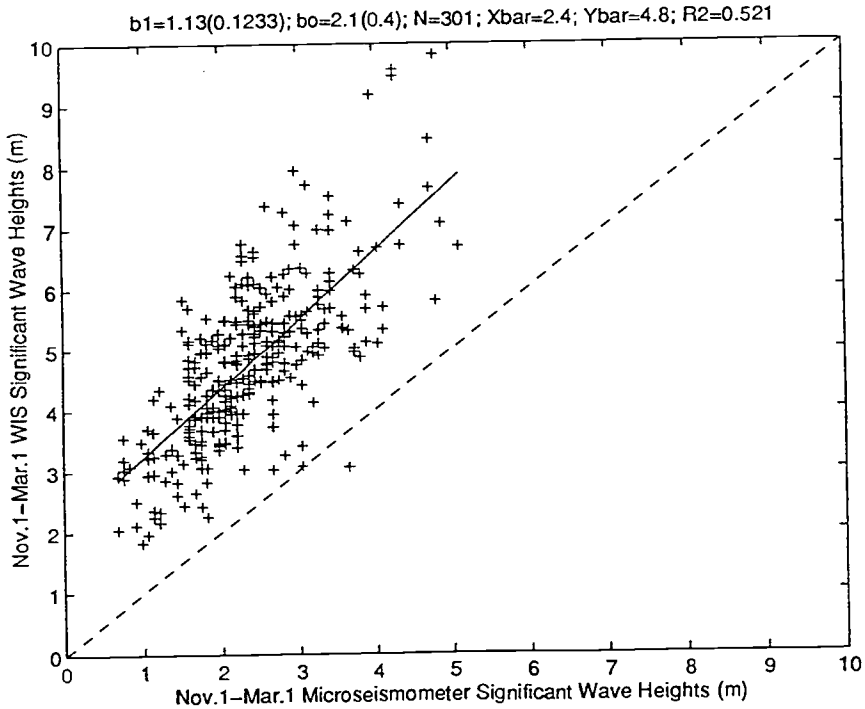

Figure 50 (A/B). Significant wave heights derived from WIS hindcast analyses for the years 1973-75, compared with simultaneous measurements from the microseismometer system for A) ALL DATA, and B) WINTER (Nov.-Feb.). The solid line is the best-fit least-squares regression line, and the dashed line is 1:1.

C)

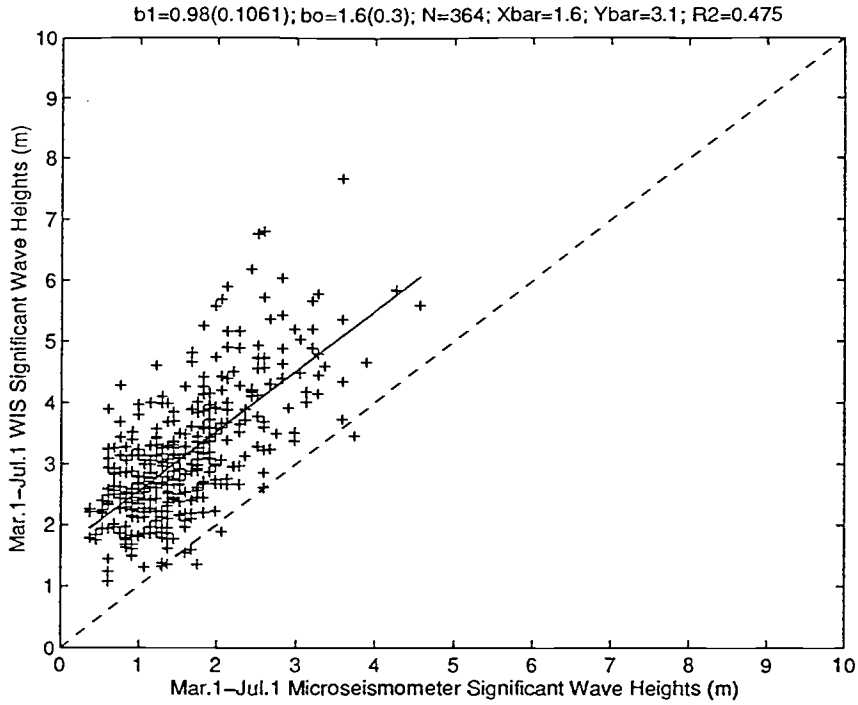

D)

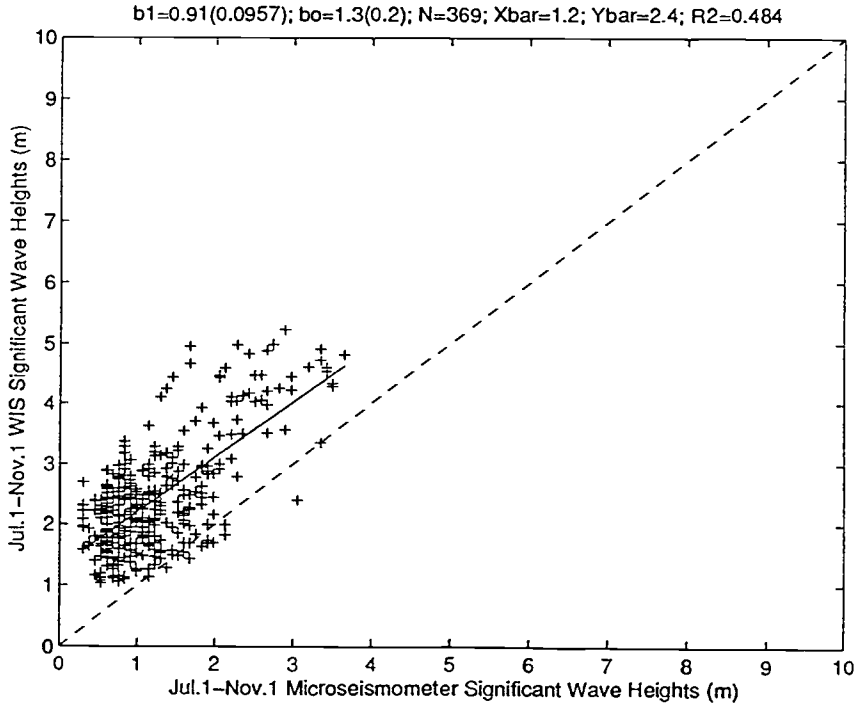

Figure 50 (C/D). Significant wave heights derived from WIS hindcast analyses for the years 1973-75, compared with measurements from the microseismometer system for C) SPRING (Mar.-Jun.), and D) SUMMER (Jul.-Oct). The solid line is the best-fit least-squares regression line, and the dashed line is 1:1.

comparing WIS monthly mean values of significant wave heights with those from the buoys (Chapter 3, Figure 3) confirms that the WIS values are too high, assuming the wave climate has not changed in the 38 years of measurements.

As shown in Chapter 4, the microseismometer does not provide reliable estimates of wave periods. Consequently, there are no reliable wave period data available with which to compare directly with the WIS hindcast data. The mean period for the entire WIS data set is 10.98 seconds (Table 20), which is reasonably close to the mean periods derived from the buoy measurements, indicating that the WIS hindcast techniques are defining effectively the same wave period climate. A histogram of all Station 42 peak wave periods is shown in Figure 51. Comparing this distribution with those from the deep-water buoys (Chapter 3, Figures 15 a,b,c) shows that the WIS periods best resemble the NDBC buoy significant wave periods, which are slightly larger than those measured by the two CDIP buoys.

Table 20. Means and standard deviations of all significant wave heights and periods measured by the various systems.

Data Source	Mean(Hs)	Std(Hs)	Mean(Td)	Std(Td)	Observations
CDIP Coquille Buoy	1.94	0.93	9.69	3.04	17764
CDIP Grays Harbor Buoy	1.92	1.01	9.95	3.04	14924
NDBC Buoy	2.19	1.14	10.54	3.14	35651
Microseismometer	2.05	1.14	12.95*	4.98	29154
WIS (Station 42)	3.25	1.47	10.98	2.47	39921

MD-Mean Daily; Td-Dominant Period; Hs-Significant Wave Height; * Zero-crossing

Hubertz. et. al. (1992), analyzed WIS hindcast data for the Pacific coast of the United States (including Alaska and Hawaii), and found results in general agreement with this study. They compared hindcast wave conditions for 1988 using standard WIS techniques to the measured data from nearby buoys. WIS hindcast data were also compared in a climatological sense with buoy and array data collected during the early 1980's (due of the lack of measured wave conditions available during the WIS time period). Hubertz et. al. found that hindcast significant wave heights were higher than

measured by an RMS value of 1.3 meters, though no bias was found comparing peak wave periods, in agreement with the present study. At present there are no plans by the Corps of Engineers to recalibrate the Pacific coast hindcast data, and the data must therefore be used with caution.

WIS hindcast data for the U.S. Atlantic coast have been analyzed in previous studies, though not with concurrent measurements. Miller and Jensen (1990) compared wave climate statistics from five years of WAVERIDER buoy data and one year of pressure-sensor array data with WIS hindcast data off Duck, North Carolina. Good agreement was found between wave height distributions larger than 0.5 meters, but agreement between wave period distributions was poor. In fact, Miller and Jensen report WIS hindcast peak periods 3-4 seconds smaller on average than buoy and array derived peak periods, opposite to the results found in this study. The best agreement in wave heights was found for values greater than 1 meter. Hubertz, et. al. (1994) compared wave climate statistics derived from WIS hindcasts with those from NOAA buoys at five sites along the Atlantic coastline, and re-calibrated the hindcast parameters using more recent advances in hindcasting techniques and direct comparisons with 1990 weather conditions.

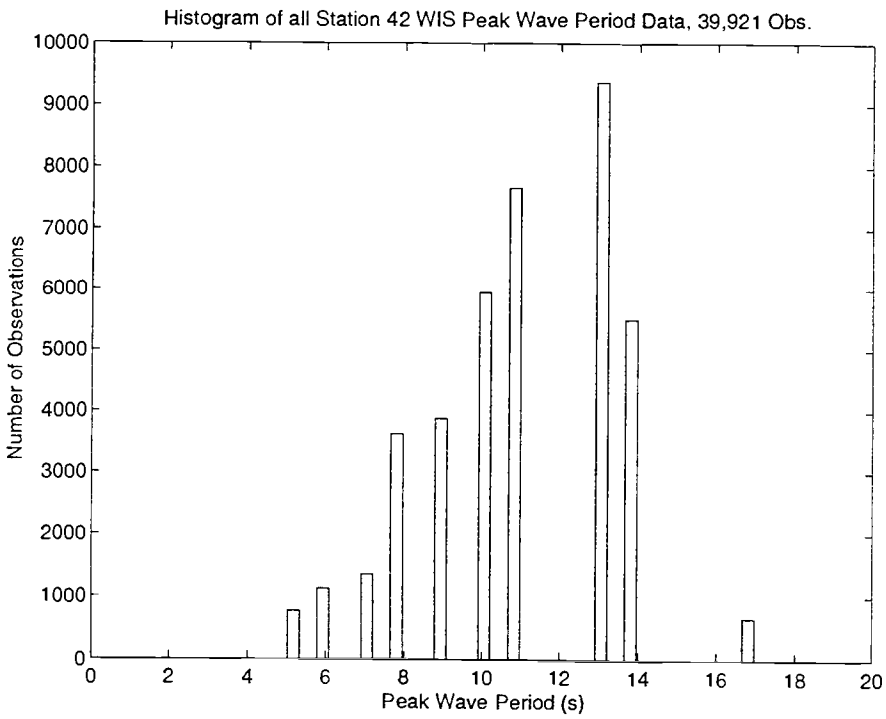

Figure 51. Histogram of all WIS Station 42 peak wave period data.

They found that mean and maximum values of wave heights and peak periods from the 20-year hindcast (1956-1975) agreed well with values measured by the buoys over various lengths of time during the 1980's. They report that root-mean-square differences in wave heights were 0.5 meters, and rms differences in peak periods were 2-3 seconds. Of interest is that mean monthly WIS peak periods were smaller, and maximum monthly periods were larger than the buoy measurements. They concluded that hindcast values of wave heights and peak periods accurately represent these wave parameters along the Atlantic coast, though the hindcast analyses tend to overestimate wave heights as found in this study, but not to the same degree. Finally, Hubertz, et. al. (1991) present a 32-year hindcast of WIS wave data for the Great lakes and use data from NOAA buoys for calibration and validation. They found good agreement in wave heights and periods between buoy-measured and hindcast-predicted measurements, expected since they used the buoy data to calibrate the WIS analyses.

One objective of the present study was to join the various data sources available for the Northwest into one 38-year data set from which to predict extreme-wave parameters. To do this, in light of the above comparison, it was necessary to re-calibrate the Station 42 WIS wave height measurements. This was done in a least-squares sense by multiplying all hindcast wave heights by 0.76 (reciprocal of calculated least-squares slope) and subtracting 1.2 meters (y-intercept of least-squares slope). This produces a few negative hindcast wave heights under low wave conditions. Although only the extreme storm events were of interest in the extreme-wave analyses, the above recalibration produced wave heights that are too small in there being too few storms with significant wave heights larger than 6 meters.

CHAPTER 6
EXTREME WAVE ANALYSIS

An extreme wave height analysis involves the estimation of the largest wave height expected in some time interval due to a rare storm event. The main objective of this analysis is to provide reliable wave statistics for the sound design and engineering of coastal structures. The return period is one of the basic parameters of extreme wave statistics and represents the average time period between storm wave heights exceeding some threshold value (Herbich, et. al., 1990). In this chapter, extreme significant wave heights are calculated for various return periods using data from the two Scripps deep-water buoys (Coquille Bay, OR, and Grays Harbor, WA), the microseismometer system, and the WIS hindcast data. The data sets are then joined to produce 23-years of wave measurements from which to reliably predict the 69-year extreme significant wave height. Also, calculations of extreme run-up and wave power characterizations are presented for various data sets.

Calculation of Extreme Significant Wave Heights from Deep-Water Wave Heights

Since record lengths from which extreme significant wave heights are estimated are usually short compared with return periods of interest, the extreme wave heights cannot be estimated directly from the data. The typical procedure is to fit the data to a theoretical probability distribution and then extrapolate the distribution to probabilities corresponding to return periods of interest (Earle and Bishop, 1984). This usually involves the projection of the 50- to 100-year extreme-wave conditions, based on measurements obtained over a much shorter time span (Wang and Le Mehaute, 1983; Goda, 1990; Herbich, 1990). Only the peak values of significant wave heights from discrete storms are used because individual storms are considered independent, and a series of wave heights at the peaks of storms constitute a set of samples from independent random variables (necessary for the use of most statistical theories) (Herbich, et. al., 1990). There are several sources of uncertainty in estimating extreme wave heights in this manner. They include, but are not limited to: measurement uncertainties in the input data, errors due to the choice of the theoretical probability distribution, and errors due to extrapolating long return periods

from short data series. A review of these and other uncertainties has been made by Borgman and Resio (1977).

Extreme significant wave heights were calculated by the computer program included in ACES (Automated Coastal Engineering System), provided by the Army Corps of Engineers. The program utilizes the method developed by Goda (1988) to fit the input data to five frequently-used probability distributions (the Fisher-Tippett Type I, and Weibull with exponents ranging from 0.75 to 2.0). Information is provided to assist the user in determining the distribution which best fits the data in the form of a correlation coefficient and the sum of squares of the residuals. The general assumptions used by the Extremal Significant Wave Height Analysis program are: (1) that all input wave heights come from a single statistical population of storm events (e.g. extra-tropical storms in the Northern Hemisphere), (2) that wave height properties at a location are reasonably represented by the significant wave height, and (3) that extreme wave heights are not limited by physical factors (i.e. limiting water depth). The input significant wave heights are assumed to represent the maxima from storm events, and the user is left to determine a threshold value above which waves are considered to represent storm events. The total number of storm events expected over the length of record must be estimated, though the results are fairly insensitive to the chosen value. The ACES Technical Reference states that, "as a general rule-of-thumb, (extreme) heights can be extrapolated to return periods up to 3 times the length of record" (Leenknecht et. al., 1992). Confidence intervals (as a function of return period) are calculated and provided by ACES using the method of Goda (1988), since return periods are typically longer than the duration of the wave record. The confidence intervals are a function of the chosen best-fit distribution (independent of how well the data fit the distribution) and the number of input storm wave heights.

CDIP Deep-Water Buoy Extreme Significant Wave Heights

Extreme significant wave heights were calculated and plotted using the program ACES for storm waves recorded by the two CDIP deep-water buoys (Coquille and Grays Harbor). Since the length of record at each of these stations is 12 years, calculated extreme heights are only reliable to return periods of 36 years. As the choice of the wave height threshold value for input data is up to the scientist or engineer, two different thresholds were selected for each station to determine the sensitivity of the program to that choice. Figures 52a and 52b are return period plots for the Coquille buoy for

threshold values of 6 and 5 meters respectively. Storm waves greater than the threshold value were considered independent if four or more days separated measurements; otherwise, if measurements were closer in time, the greater value was selected in order to not violate the above assumptions. The choice of the threshold determines the number of storms over the record length (a program input), which affects the width of the confidence interval around the projected wave heights. A 6 meter threshold value for the Coquille buoy results in 18 storms over 12 years. The Weibull k=1.0 best-fit distribution gives a 36-year return significant wave height of 7.56 meters. A 5 meter threshold for the same data results in 41 storms, the Weibull k=1.4 best-fit distribution, and a 36-year return wave height of 7.75 meters (0.19 meters difference). The confidence interval bounds can be seen to be larger in Figure 52a (the 6 meter cutoff), dependent on the type of distribution and number of input storm waves. Tables 21a and 21b accompany Figures 52a and 52b, and list specifics of the analyses and values from the plots at various return periods.

Figures 53a and 53b are plots derived from analyses of the Grays Harbor buoy data. Tables 22a and 22b accompany the plots. A 6 meter threshold value for the Grays Harbor buoy results in 17 storms over 12 years, the Weibull k=2.0 best-fit distribution, and a 36-year return significant wave height of 7.34 meters. A 5 meter threshold for the same data results in 43 storms, the Weibull k=1.4 best-fit distribution, and a 36-year return wave height of 7.85 meters (0.51 meters difference). It can be seen that the choice of threshold is of some importance, though differences in extreme significant wave heights predicted using either Coquille data or Grays Harbor data are no more than 0.22 meters, depending on threshold. This points to a similarity in storm wave conditions measured at both stations.

Microseismometer System Extreme Significant Wave Heights

Extreme significant wave heights were calculated and plotted using the program ACES for storm waves recorded by the microseismometer wave gage. Since the length of the microseismometer record is 23 years, calculated extreme heights are reliable to return periods of 69 years. Both 5 and 6 meter thresholds were chosen to select storm events from the record. Storm waves greater than the threshold value were considered independent if four days or more separated measurements; otherwise, if measurements

A)

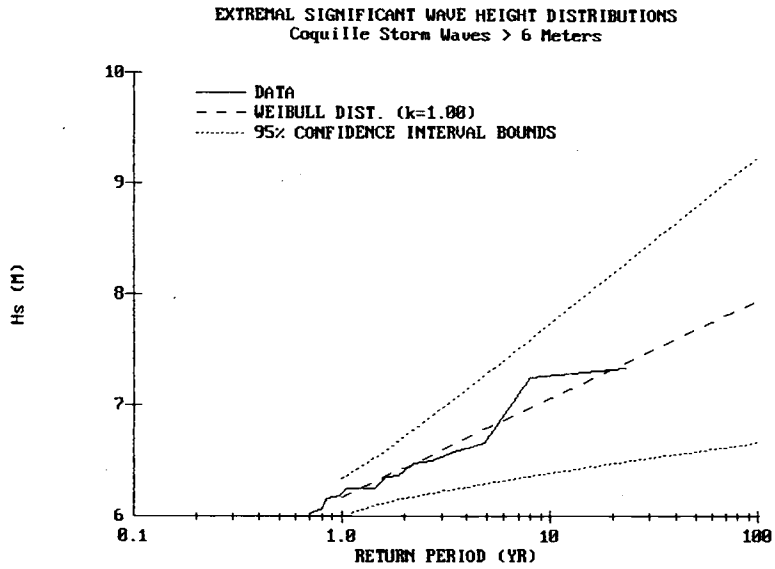

B)

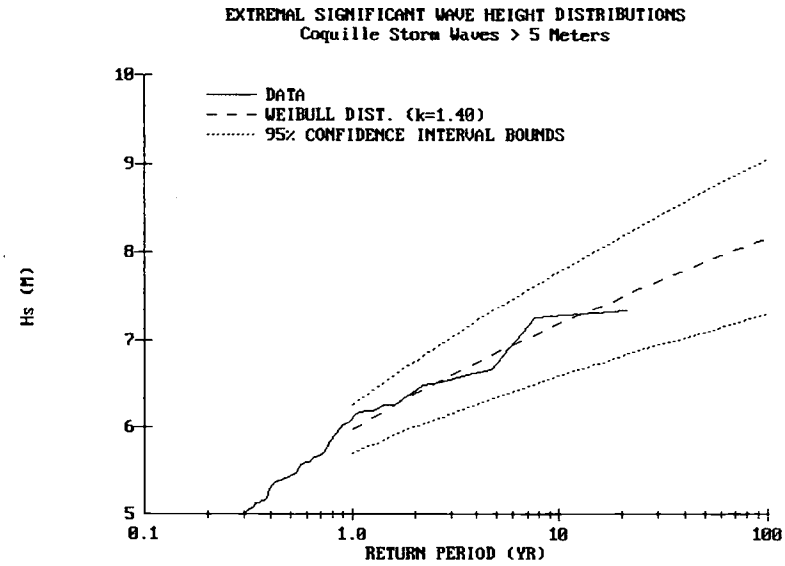

Figure 52 (A/B). Extreme significant wave heights based on the occurrence of storms in excess of A) 6 meters, and B) 5 meters, for data from the CDIP (Bandon) deep-water buoy. The Weibull theoretical curve has been fitted to the measured storm data, and used to project the 50- and 100-year extreme wave conditions.

Table 21a. Extremal significant wave height return period table for the Coquille deep-water buoy. The extreme wave heights are based on the occurrence of storms with deep-water significant wave heights in excess of 6.0 meters.

Return periods calculated from best-fit Weibull distribution w/ k=1.0(Correlation=0.9752)
Number of Storms = 18
Duration of Wave Record = 12 years
Mean of Sample Data = 6.402
Standard Deviation of Sample = 0.370

Return Period (Yr)	Hs (M)	SIGR (M)	(Hs-1.96*SIGR) (M)	(Hs+1.96*SIGR) (M)
2	6.44	0.14	6.16	6.72
5	6.8	0.25	6.3	7.29
10	7.06	0.34	6.39	7.74
25	7.42	0.47	6.5	8.34
36*	7.56	0.5	6.55	8.57
50	7.69	0.56	6.58	8.79
100	7.95	0.66	6.67	9.24

Hs = Significant Wave Height
SIGR = Standard Error of Significant Wave Height With Return Period R
(1.96*SIGR) = Confidence Interval Bounds at the 95% Confidence Level
* Heights can be extrapolated to return periods up to 3 times the record legth (rule-of-thumb)

Table 21b. Extremal significant wave height return period table for the Coquille deep-water buoy. The extreme wave heights are based on the occurrence of storms with deep-water significant wave heights in excess of 5.0 meters.

Return periods calculated from best-fit Weibull distribution w/ k=1.4 (Correlation=0.992)
Number of Storms = 41
Duration of Wave Record = 12 years
Mean of Sample Data = 5.746 m
Standard Deviation of Sample = 0.6 m

Return Period (Yr)	Hs (M)	SIGR (M)	(Hs-1.96*SIGR) (M)	(Hs+1.96*SIGR) (M)
2	6.38	0.19	6	6.76
5	6.85	0.26	6.35	7.36
10	7.18	0.3	6.59	7.78
25	7.59	0.36	6.88	8.31
36*	7.75	0.38	6.99	8.5
50	7.88	0.41	7.09	8.68
100	8.17	0.45	7.29	9.05

Hs = Significant Wave Height
SIGR = Standard Error of Significant Wave Height With Return Period R
(1.96*SIGR) = Confidence Interval Bounds at the 95% Confidence Level
* Heights can be extrapolated to return periods up to 3 times the record legth (rule-of-thumb)

A)

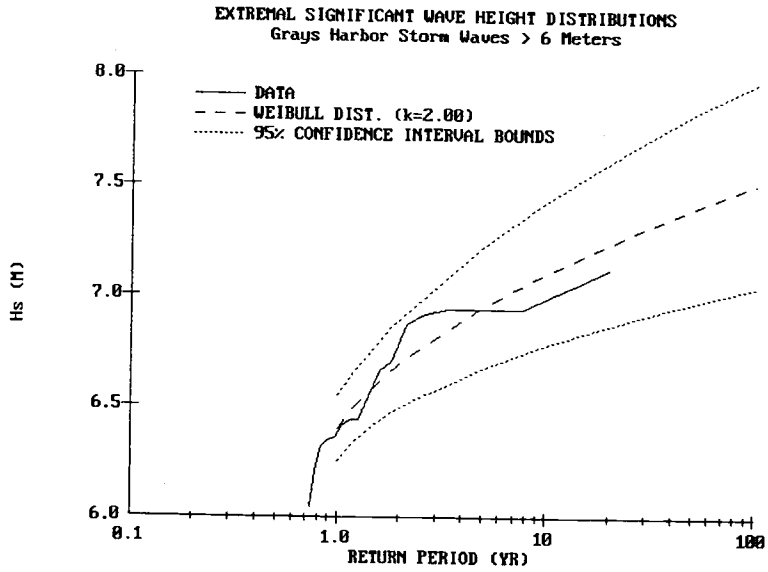

B)

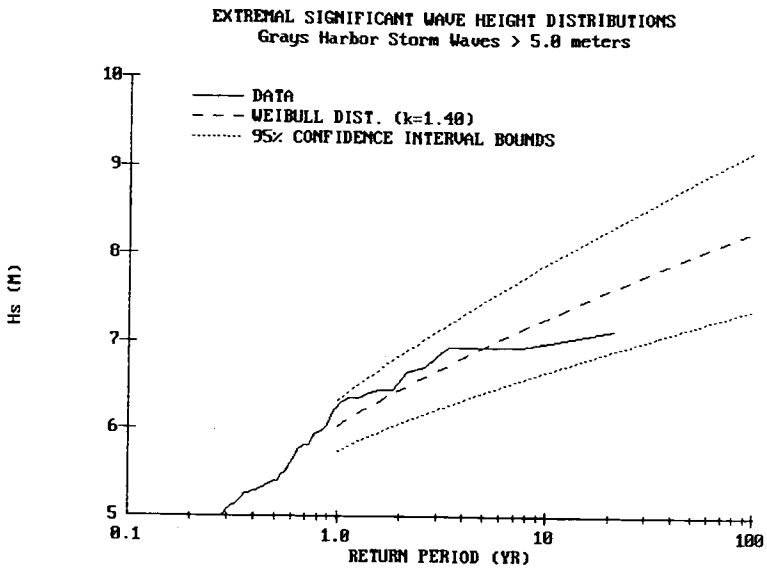

Figure 53 (A/B). Extreme significant wave heights based on the occurrence of storms in excess of A) 6 meters, and B) 5 meters, for data from the CDIP (Grays Harbor) deep- water buoy. The Weibull theoretical curve has been fitted to the measured storm data, and used to project the 50- and 100-year extreme wave conditions.

Table 22a. Extremal significant wave height return period table for the Grays Harbor deep-water buoy. The extreme wave heights are based on the occurrence of storms with deep-water significant wave heights in excess of 6.0 meters.
Return periods calculated from best-fit Weibull distribution w/ k=2.0 (Correlation=0.9676)
Number of Storms = 17
Duration of Wave Record = 12 years
Mean of Sample Data = 6.602 m
Standard Deviation of Sample = 0.311 m

Return Period (Yr)	Hs (M)	SIGR (M)	(Hs-1.96*SIGR) (M)	(Hs+1.96*SIGR) (M)
2	6.69	0.1	6.49	6.89
5	6.95	0.14	6.68	7.22
10	7.1	0.17	6.78	7.43
25	7.28	0.2	6.9	7.66
36*	7.34	0.21	6.94	7.75
50	7.4	0.22	6.97	7.82
100	7.51	0.24	7.04	7.97

Hs = Significant Wave Height
SIGR = Standard Error of Significant Wave Height With Return Period R
(1.96*SIGR) = Confidence Interval Bounds at the 95% Confidence Level
* Heights can be extrapolated to return periods up to 3 times the record legth (rule-of-thumb)

Table 22b. Extremal significant wave height return period table for the Grays Harbor deep-water buoy. The extreme wave heights are based on the occurrence of storms with deep-water significant wave heights in excess of 5.0 meters.
Return periods calculated from best-fit Weibull distribution w/ k=1.4 (Correlation=0.976
Number of Storms = 43
Duration of Wave Record = 12 years
Mean of Sample Data = 5.77 m
Standard Deviation of Sample = 0.628 m

Return Period (Yr)	Hs (M)	SIGR (M)	(Hs-1.96*SIGR) (M)	(Hs+1.96*SIGR) (M)
2	6.45	0.2	6.06	6.84
5	6.93	0.27	6.41	7.45
10	7.27	0.31	6.66	7.88
25	7.69	0.37	6.96	8.42
36*	7.85	0.39	7.07	8.63
50	7.99	0.42	7.17	8.81
100	8.28	0.46	7.38	9.18

were closer in time, the greater value was selected in order not to violate the assumptions discussed in Chapter 3. Figure 54a is a return period plot for microseismometer data with wave heights greater than 5 meters as input. This threshold value results in 126 storms over 23 years. The Weibull k=1.0 best-fit distribution gives a 69-year significant wave height of 9.16 meters. A 6 meter threshold value (Figure 54b) results in 64 storms over 23 years, the Weibull k=0.75 best-fit distribution, and a 69-year return significant wave height of 9.27 meters. Tables 23 a and b accompany these figures, and list the specifics of the analysis and values from the plots at various return periods.

Table 23a. Extremal significant wave height return period table for the microseismometer wave gage at Newport, OR. The extreme wave heights are based on the occurrence of storms with deep-water significant wave heights in excess of 5.0 meters.
Return periods calculated from best-fit Weibull distribution w/ k=1.0 (Correlation=0.978)
Number of Storms = 126
Duration of Wave Record = 23 years
Mean of Sample Data = 5.97 m
Standard Deviation of Sample = 0.65 m

Return Period (Yr)	Hs (M)	SIGR (M)	(Hs-1.96*SIGR) (M)	(Hs+1.96*SIGR) (M)
2	6.87	0.18	6.52	7.22
5	7.46	0.25	6.97	7.95
10	7.91	0.31	7.31	8.51
25	8.5	0.38	7.76	9.24
50	8.95	0.43	8.1	9.8
69*	9.16	0.45	8.25	10.1
100	9.4	0.49	8.44	10.36

Hs = Significant Wave Height
SIGR = Standard Error of Significant Wave Height With Return Period R
(1.96*SIGR) = Confidence Interval Bounds at the 95% Confidence Level
* Heights can be extrapolated to return periods up to 3 times the record legth (rule-of-thumb)

WIS Hindcast Extreme Significant Wave Heights

WIS hindcast storm wave heights were used to calculate extreme significant wave heights using the program ACES. Since the length of the WIS data record is 20 years, calculated extreme heights are reliable to return periods of 60 years. The largest 34 storm wave heights from the original WIS data were used to calculate extreme statistics;

A)

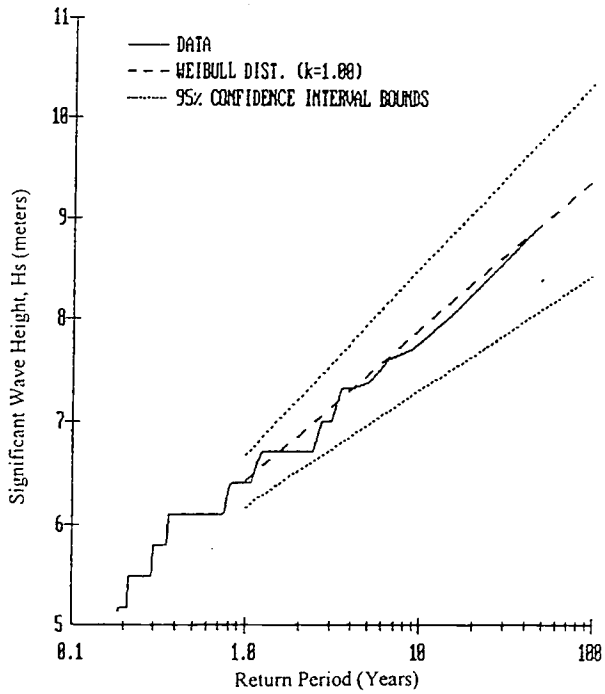

B)

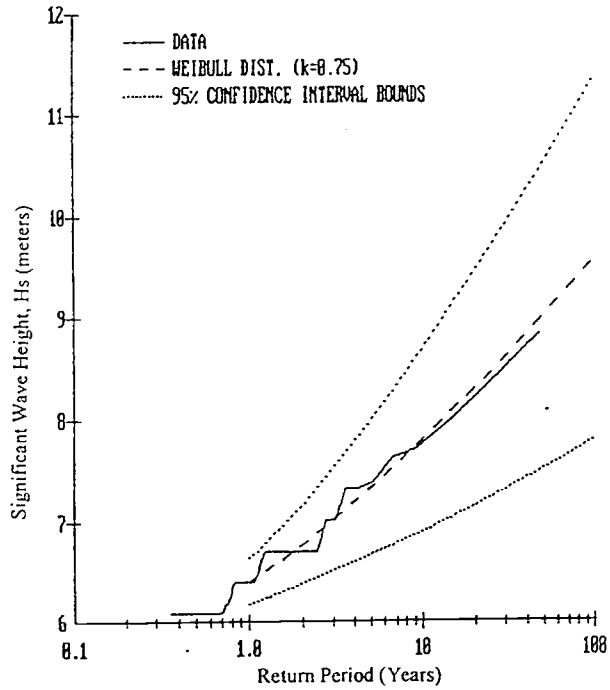

Figure 54 (A/B). Extreme significant wave heights based on the occurrence of storms in excess of A) 5 meters, and B) 6 meters, for data from the microseismometer system. The Weibull theoretical curve has been fitted to the measured storm data, and used to project the 50- and 100-year extreme wave conditions.

Table 23b. Extremal significant wave height return period table for the microseismometer wave gage at Newport, OR. The extreme wave heights are based on the occurrence of storms with deep-water significant wave heights in excess of 6.0 meters.
Return periods calculated from best-fit Weibull distribution w/ k=0.75 (Correlation=0.989)
Number of Storms = 64
Duration of Wave Record = 23 years
Mean of Sample Data = 6.46 m
Standard Deviation of Sample = 0.55 m

Return Period (Yr)	Hs (M)	SIGR (M)	(Hs-1.96*SIGR) (M)	(Hs+1.96*SIGR) (M)
2	6.77	0.2	6.38	7.16
5	7.33	0.34	6.67	7.98
10	7.79	0.46	6.9	8.69
25	8.47	0.63	7.24	9.69
50	9.01	0.73	7.51	10.51
69*	9.27	0.83	7.64	10.9
100	9.58	0.91	7.79	11.36

Hs = Significant Wave Height
SIGR = Standard Error of Significant Wave Height With Return Period R
(1.96*SIGR) = Confidence Interval Bounds at the 95% Confidence Level
* Heights can be extrapolated to return periods up to 3 times the record legth (rule-of-thumb)

Figure 55a is the return period plot. These data give a 60-year return significant wave height of 11.6 meters, clearly too large. The recalibrated wave heights (Chapter 5) were then used as input. A threshold value of 5 meters results in 34 storms over 20 years. The Weibull k=1.0 best-fit distribution gives a 60-year significant wave height of 7.6 meters (Figure 55b). This value is significantly smaller than calculations based on the other data sets. Choosing a 6 meter threshold value results in too few storms to reliably predict extreme wave heights (6 storms/20 years).

Joint Microseismometer/CDIP Extreme Significant Wave Heights

The WIS data were judged too unreliable to generate extreme statistics. Further, it is believed that the deep-water buoys provide more reliable wave height and period information than the microseismometer system. Therefore, the microseismometer and CDIP (Bandon) deep-water buoy data were joined to create the longest reliable wave

A)

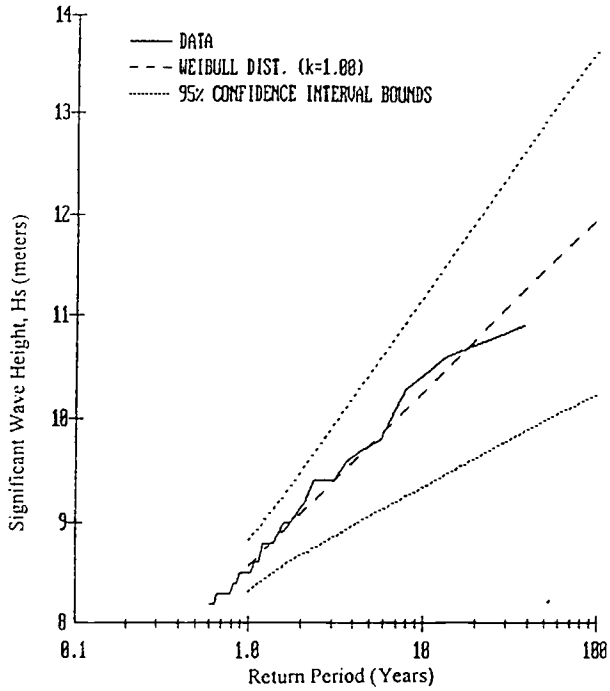

B)

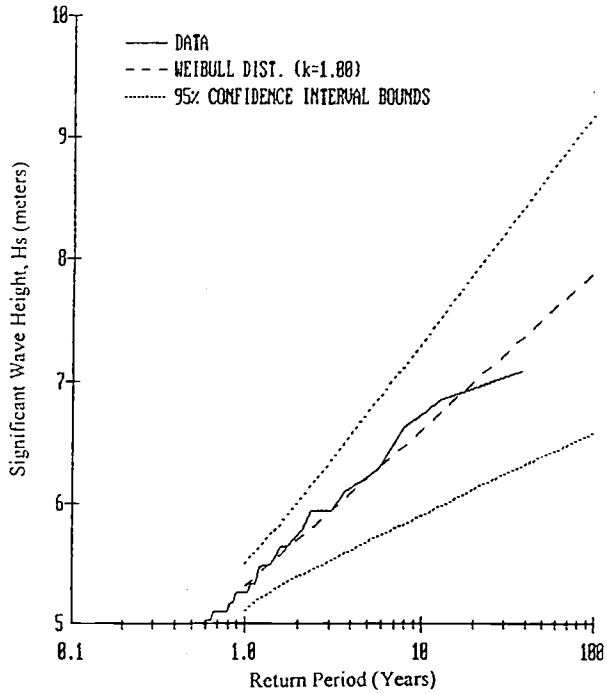

Figure 55 (A/B). Extreme significant wave heights based on the occurrence of storms in A) Un-calibrated WIS heights, and B) heights in excess of 5 meters, for WIS Station 42 data. The Weibull theoretical curve has been fitted to the measured storm data, and used to project the 50- and 100-year extreme wave conditions.

record from which to calculate extreme wave heights, with preference given to the buoy data for periods of overlapping measurements. This produces a 23-year wave record, from which a 69-year return wave height can be extrapolated. Figures 56 a and b are return period plots for the joint Microseismometer/CDIP data set for threshold values of 5 and 6 meters respectively. A threshold value of 5 meters results in 68 storms over 23 years The Weibull k=1.0 best-fit distribution gives a 69-year significant wave height of 8.4 meters. A threshold value of 6 meters results in 24 storms over 23 years, the Weibull k=1.0 best-fit distribution, and a 69-year significant wave height of 8.0 meters. Tables 24 a and b accompany these figures, and list the specifics of the analyses and values from the plots at various return periods.

Table 24a. Extremal significant wave height return period table for the microseismometer/CDIP joint data set. The extreme wave heights are based on the occurrence of storms with deep-water significant wave heights in excess of 5.0 meters.
Return periods calculated from best-fit Weibull distribution w/ k=1.0 (Correlation=0.979)
Number of Storms = 68
Duration of Wave Record = 23 years
Mean of Sample Data = 5.771 m
Standard Deviation of Sample = 0.604 m

Return Period (Yr)	Hs (M)	SIGR (M)	(Hs-1.96*SIGR) (M)	(Hs+1.96*SIGR) (M)
2	6.24	0.17	5.91	6.58
5	6.8	0.26	6.29	7.31
10	7.22	0.33	6.58	7.87
25	7.78	0.42	6.95	8.6
50	8.2	0.49	7.23	9.16
69*	8.39	0.52	7.36	9.43
100	8.62	0.56	7.51	9.72

Hs = Significant Wave Height
SIGR = Standard Error of Significant Wave Height With Return Period R
(1.96*SIGR) = Confidence Interval Bounds at the 95% Confidence Level
* Heights can be extrapolated to return periods up to 3 times the record legth (rule-of-thumb)

A)

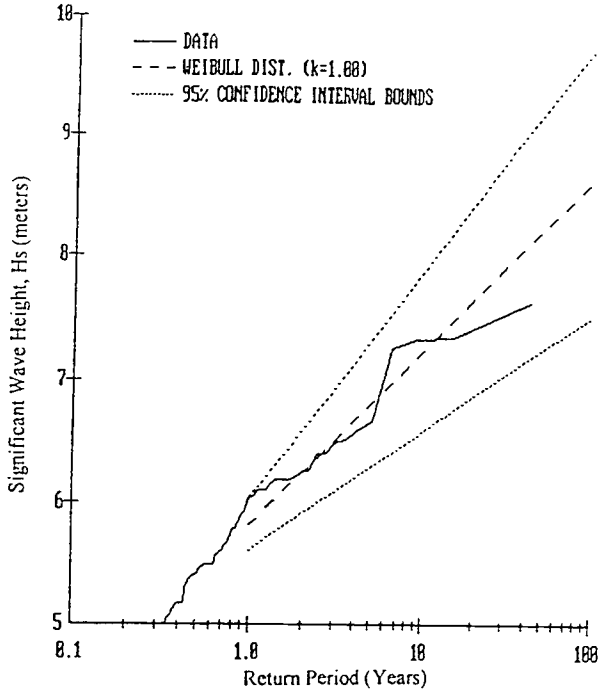

B)

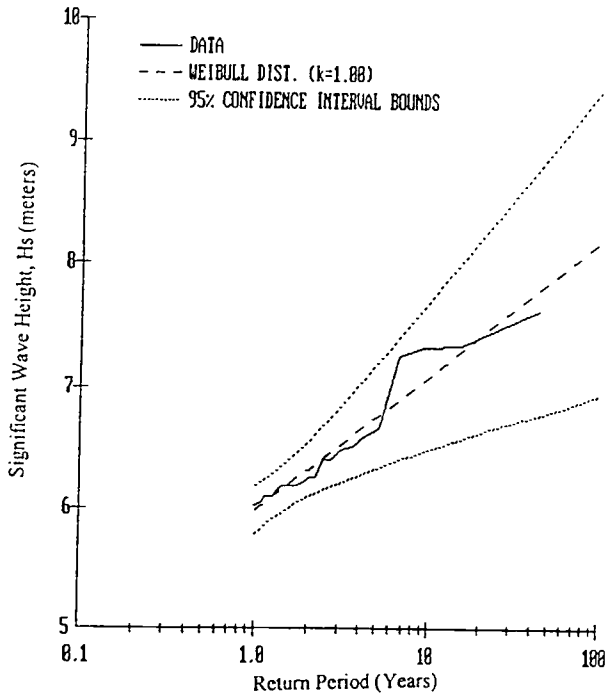

Figure 56 (A/B). Extreme significant wave heights based on the occurrence of storms in excess of A) 5 meters, and B) 6 meters, for data from the microseismometer/CDIP joint data set. The Weibull theoretical curve has been fitted to the measured storm data, and used to project the 50- and 100-year extreme wave conditions.

Table 24b. Extremal significant wave height return period table for the microseismometer/CDIP joint data set. The extreme wave heights are based on the occurrence of storms with deep-water significant wave heights in excess of 6.0 meters.
Return periods calculated from best-fit Weibull distribution w/ k=1.0 (Correlation=0.969)
Number of Storms = 24
Duration of Wave Record = 23 years
Mean of Sample Data = 6.443 m
Standard Deviation of Sample = 0.465 m

Return Period (Yr)	Hs (M)	SIGR (M)	(Hs-1.96*SIGR) (M)	(Hs+1.96*SIGR) (M)
2	6.32	0.11	6.1	6.54
5	6.75	0.22	6.33	7.18
10	7.08	0.31	6.48	7.69
25	7.52	0.44	6.67	8.38
50	7.85	0.53	6.8	8.9
69*	8	0.57	6.86	9.14
100	8.18	0.63	6.94	9.42

Hs = Significant Wave Height
SIGR = Standard Error of Significant Wave Height With Return Period R
(1.96*SIGR) = Confidence Interval Bounds at the 95% Confidence Level
* Heights can be extrapolated to return periods up to 3 times the record legth (rule-of-thumb)

Characterizations of Extreme Run-up and Wave Power from Deep-Water Buoy Data

Of interest to analyses of potential coastal erosion during storms is the characterization of extreme run-up and wave power. Holman and Sallinger (1985) found that wave set-up on a beach, η, (the superelevation of the mean water level above the still water level of the sea) could be written:

$$\eta/H = 0.35\ \xi_o \qquad (6)$$

where ξ_o is the iribarren number:

$$\xi_o = S/(H/L)^{1/2} \qquad (7)$$

where S is the beach slope, H is the deep-water significant wave height, T is the wave period, and L_o is the deep-water wave length given by:

$$L_o = (g/2\pi)T^2 \qquad (8)$$

where g is the acceleration of gravity. Combining the equations above gives an empirical formula for set-up based on beach slope, deep-water significant wave height, and wave period:

$$\eta = 0.14\ S\ \{g^{1/2}\ H^{1/2}\ T\} \qquad (9)$$

Similarly, defining the run-up of waves on the beach above the mean set-up level as the 2% exceedence, Holman (1986) found:

$$R_{2\%}/H = 0.55\ \xi_o \qquad (10)$$

by substituting (7) and (8) one obtains:

$$R_{2\%} = 0.22\ S\ \{g^{1/2}\ H^{1/2}\ T\} \qquad (11)$$

This suggests that set-up and run-up during storms can be characterized using $\{g^{1/2}\ H^{1/2}\ T\}$. The extreme significant wave height program in ACES was again used, this time with the characterization of storm run-up waves as input. This approach was felt valid, as the program simply fits a data set to known mathematical distributions, and extrapolates extreme values from the best-fit distribution. A threshold value was chosen such that 20 independent storm run-up events occurred over the 12 year record length of the Coquille buoy. Figure 57 is a plot of extreme $\{g^{1/2}\ H^{1/2}\ T\}$ based on the characterization above. The data fit the Weibull k=1.0 distribution very well, having a correlation of 0.9807. The values of extreme run-up characterization (without beach slope or 0.22 coefficient) for various return periods are shown in Table 25. This information can be used for site-specific extreme set-up or run-up estimates where the beach slope is known.

Wave power (or wave energy flux), the rate at which energy is transmitted in the direction of wave propagation, can be written:

$$P = \rho\ g^2\ H^2\ T/(32\ \pi) \qquad (12)$$

where ρ is water density (1000 Kg/m^3), H is deep-water wave height, and T is wave period (CERC, 1984). This characterization of storms emphasizes wave height more than

Table 25. Extreme run-up characterization return period table based on $[g^{1/2} H^{1/2} T]$ using Coquille deep-water buoy data.

Return periods calculated from best-fit Weibull distribution w/ k=1.0 (Correlation=0.9807)
Number of Storms = 20
Duration of Wave Record = 12 years
Mean of Sample Data = 132.42
Standard Deviation of Sample = 12.51

Return Period (Yr)	{g^0.5 H^0.5 T} (M)	SIGR (M)	(g^0.5 H^0.5 T-1.96*SIGR) (M)	(g^0.5 H^0.5 T+1.96*SIGR) (M)
2	135.1	4.8	125.7	144.6
5	147.1	8.4	130.7	163.6
10	156.2	11.3	134.1	178.3
25	168.2	15.2	138.4	198
36*	173	16.1	140.1	205.8
50	177.3	18.2	141.7	212.9
100	186.3	21.2	144.9	227.8

{g^0.5 H^0.5 T} = Characterization of Extreme Run-up
SIGR = Standard Error of Run-up With Return Period R
(1.96*SIGR) = Confidence Interval Bounds at the 95% Confidence Level
* Heights can be extrapolated to return periods up to 3 times the record legth (rule-of-thumb)

Table 26. Extreme wave power return period table based on $[\rho g^2 H^2 T/(32 \pi)]$ using Coquille deep-water buoy data.

Return periods calculated from best-fit Weibull distribution w/ k=1.0 (Correlation=0.9955)
Number of Storms = 20
Duration of Wave Record = 12 years
Mean of Sample Data = 61.913 (*10^4)
Standard Deviation of Sample = 13.583 (*10^4)

Return Period (Yr)	Power *10^4 (J/s)	SIGR (J/s)	(Power-1.96*SIGR) (J/s)	(Power+1.96*SIGR) (J/s)
2	64.9	5.24	54.63	75.18
5	78.12	9.12	60.24	96
10	88.12	12.26	64.09	112.15
25	101.34	16.49	69.01	133.66
36*	106.6	17.79	70.94	142.3
50	111.34	19.72	72.68	149.99
100	121.33	22.96	76.32	166.34

Power*10^4 = {1/(32*pi) * rho*g^2*H^2*T}
SIGR = Standard Error of Power With Return Period R
(1.96*SIGR) = Confidence Interval Bounds at the 95% Confidence Level
* Heights can be extrapolated to return periods up to 3 times the record legth (rule-of-thumb)

wave period, whereas run-up is characterized more by wave period. Again, the extreme significant wave height program in ACES was used, this time with the characterization of storm wave power as input. A threshold value was chosen such that 20 independent storm wave power events occurred over the 12 year record length of the Coquille buoy. Figure 58 is a plot of extreme wave power based on the characterization above. The data fit the Weibull k=1.0 distribution very well, having a correlation of 0.9955. The values of extreme wave power for various return periods are shown in Table 26. This information could presumably be used as a prediction of extreme storm wave power for return periods up to 36 years.

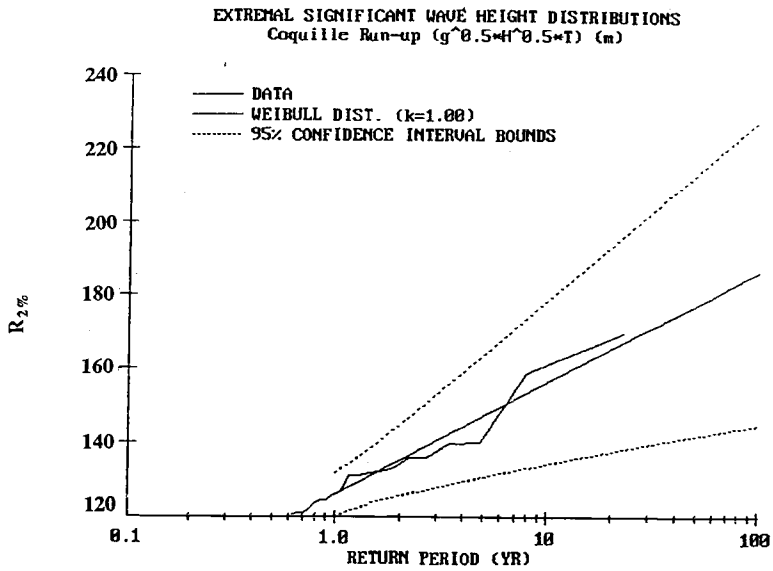

Figure 57. Characterization of extreme run-up height based on the largest 20 run-up calculations from CDIP (Bandon) deep-water buoy measurements.

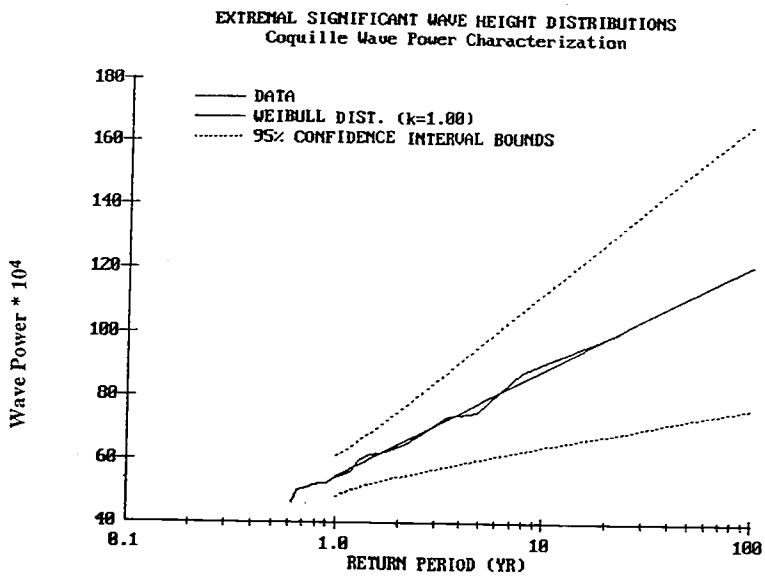

Figure 58. Characterization of extreme wave power based on the largest 20 wave power calculations from CDIP (Bandon) deep-water buoy measurements.

CHAPTER 7
CONCLUSIONS

The research presented in this thesis has been directed toward two major goals: to directly compare wave measurements from the various instruments and to derive a representative wave climate and extreme statistics for the Pacific Northwest coast based on those measurements. Accomplishing these goals has been complicated by the multiplicity of data sets available, including direct measurements since the 1980's by the NDBC and CDIP deep-water buoys and shallow-water arrays, remote sensing measurements by a microseismometer system since the 1970's, and hindcast data from the Wave Information Study (1956-1975). The measurements overlapped sufficiently to allow direct comparisons of the various data sets. The main conclusions derived in the study are:

(1) The deep-water wave climate is essentially uniform along the length of the Pacific Northwest coast, the ocean shores of Oregon and Washington. Wave measurements derived from the various systems may vary at any particular time due to local effects, but daily and monthly means agree very well. Means and standard deviations of all measurements of significant wave heights and periods for the various measurement systems have been compiled in Table 20.

(2) The NDBC buoy yields wave heights that are approximately 8% higher than those measured by the two CDIP buoys, while measurements of wave periods are statistically the same. Due to the location of the NDBC buoy, mid-way between the two CDIP buoys, differences in measured heights must be due to instrumentation differences since the analysis procedures are the same.

(3) Wave measurements obtained by the CDIP shallow-water pressure-sensor arrays in 11 meters water depth agree with the deep-water buoy measurements when transformed to deep-water using linear wave theory. This indicates the reliability of the deep-water buoy data, and indicates that the use of linear theory to transform wave measurements is an acceptable approximation.

(4) The microseismometer system yields good measurements of significant wave heights when compared to the deep-water buoys, but no trend is found when comparing wave periods which are systematically too high when derived from the microseismometer system. An attempt to resolve wave periods spectrally using raw microseism time series resulted in little success, in part because of the large number of spurious low-frequency signals in the microseism record.

(5) Significant wave heights derived from WIS hindcast techniques are approximately 30-60% higher than measurements by the deep-water buoys. Though no direct comparisons of WIS wave periods were possible, the mean period for the entire WIS data set is consistent with the buoy measurements (Table 20), indicating that the WIS hindcast techniques are defining a similar wave period climate.

(6) There is a marked seasonality in the annual wave climate of the Pacific Northwest, with mean-monthly significant wave heights in the summer months ranging from 1.25 to 1.75 meters, increasing to 2 to 3 meters in the winter months, with individual storms yielding significant wave heights from 6 to 7 meters. The corresponding mean-monthly dominant wave periods range from 7 to 9 seconds during summer months, increasing to 11-13 seconds in winter months.

(7) Calculations of wave breaker heights for Pacific Northwest beaches yield significant wave heights of 9 to 10 meters for the storm conditions.

(8) The largest storm waves measured during the 23-years of microseismometer and deep-water buoy measurements had a deep-water significant wave height of 7.3 meters. The projection of the 50- and 100-year extreme wave heights for storms with heights exceeding 5 meters yields deep-water significant wave heights of 8.2 and 8.8 meters respectively.

(9) The WIS hindcast data could not be used in the extreme-wave analyses even after wave heights were re-calibrated to yield the same average wave climate as the direct measurements. The hindcast wave heights are much too high before re-calibration, and are truncated for the most extreme storms after re-calibration.

The microseismometer wave measurement system has been computerized and automated as a result of this study. The significant wave height and zero-crossing wave period are calculated and recorded four times daily at Newport, Oregon, replacing the need for strip-chart recording and manual analyses of the data. Also, the raw microseism time-series are now stored for future use. This study has further demonstrated that the microseismometer wave gage is an effective, low-maintenance measurement system for obtaining reliable wave height information.

The results of the analyses in this study further establish the extreme nature of the wave climate of the Pacific Northwest. Quantifying the wave climate, including the sound prediction of extreme storm-wave conditions, will lead to a better understanding of the potential for erosion and flooding of properties backing beaches. The wave data presented here will be useful in coastal management decisions, and in the design of engineered coastal structures.

BIBLIOGRAPHY

Bodvarsson, G.M., 1975. *Ocean wave-generated microseisms at the Oregon Coast:* M.S. thesis, Oregon State University, Corvallis, 83 p.

Borgman, L.E., and Resio, D.T., 1977. Extremal prediction in wave climatology: in *Ports '77*, 394-412.

Brown, E.P.M., 1991. Wave Power Measurements in New Zealand: *Coastal Engineering - Climate for Change*, 10th Australasian Conference on Coastal and Ocean Engineering, p.79-84.

CERC, 1984. *Shore Protection Manual*: Coastal Engineering Research Center, U.S. Army Corps of Engineers.

Corson, W.D.; Abel, C.E.; Brooks, R.M.; Farrar, P.D.; Groves, B.J.; Payne, J.B.; McAneny; and Tracy, B.A., 1987. Pacific Coast Hindcast Phase II Wave Information: WIS Report 16, Coastal Engineering Research Center, U.S. Army Corps of Engineers, Vicksburg, Mississippi.

Creech, C., 1981. *Nearshore wave climatology, Yaquina Bay, Oregon (1971-1981):* Oregon State University Sea Grant Program, Report ORESU-T-81-002.

Earle, M.D., and Bishop, J.M., 1984. A Practical Guide to Ocean Wave Measurement and Analysis, Endeco, Inc., 78 p.

Enfield, D.B., 1973. *Prediction of hazardous Columbia River bar conditions*: Ph.D. thesis, Oregon State University, Corvallis, 204 p.

Ewans, K.C., 1984. *Ocean waves, microseisms and their interrelations*: Ph.D. thesis, University of Aukland, New Zealand.

Goda, Y., 1988. On the methodology of selecting design wave height, *Proceedings of the Twenty-first Coastal Engineering Conference*, American Society of Civil Engineers, pp. 899-913.

Hasselman, K., 1963. A statistical analysis of the generation of microseisms, *Review of Geophysics*, vol.1, no.2, 177-210.

Hemsley, J.M., and Brooks, R.M., 1989. Waves for coastal design in the United States: *Journal of Coastal Research*, 5, 639-663.

Herbich, J. B., et. al., 1990. Handbook of Coastal and Ocean Engineering, Vol. 1, Gulf Publishing Co, 372-406.

Holman, R.A., 1986. Extreme values statistics for wave run-up on a natural beach: *Coastal Engineering*, v.9, 527-544.

Holman, R. A., and Sallinger, A.H., 1985. Setup and Swash on a Natural Beach: *Journal of Geophysical Research*, v.90, no.c1, 945-953.

Howell, G.L., and Rhee, J.P., 1990. Investigation of seismic wave gage analysis techniques and comparative evaluation of the seismic wave gage at Chetco River, Oregon, CERC Misc. Paper CERC-90-3, 19 p.

Hubertz, J.M, Brooks, R.M., Brandon, W.A., and Tracy, B.A., 1994. Hindcast wave information for the U.S. Atlantic coast: *Journal of Coastal Research*, v.10, no.1, 79-100.

Hubertz, J.M, Driver, D.B., and Reinhard, R.D., 1991. Wind waves on the Great Lakes: a 32-year hindcast: *Journal of Coastal Research*, v.7, no.4, 945-967.

Hubertz, J.M., Tracy, B.A., Payne, J.B., and Cialone, A., 1992. Verification of Pacific Ocean deepwater hindcast wave information. WIS Report 29, Coastal Engineering Research Center, U.S. Army Corps of Engineers, Vicksburg, Mississippi.

Kibblewhite, A.C., and Brown, E.P.M., 1991. The use of shore-based seismometers for wave energy resource assessment in New Zealand: *Oceans '91*, p.1-5.

Kibblewhite, A.C., and Ewans, K.C., 1985. Wave-wave interactions, microseisms and infrasonic ambient noise in the ocean: *Journal of the Acoustic Society in America*, 78: 981-994.

Komar, P.D., 1978. Wave conditions on the Oregon coast during the winter of 1977-78 and the resulting erosion of Nestucca Spit: *Shore & Beach*, 44, 3-8.

Komar, P.D., 1983. The erosion of Siletz Spit, Oregon: In *Coastal Processes and Erosion*, CRC Press, Boca Raton, Florida.

Komar, P.D., 1986. The 1982-83 El Nino and erosion on the coast of Oregon: *Shore & Beach,* 54, 3-12.

Komar, P.D., et. al., 1976. Wave conditions and beach erosion on the Oregon coast: *The Ore Bin*, 38, 103-112.

Komar, P.D., et. al. (in press). Wave run-up on Oregon beaches and the erosion of sea cliffs: *Proceedings 24th International Conference on Coastal Engineering*, Amer. Soc. Civil Engrs.

Komar, P.D., and Gaughan, M.K., 1973. Airy wave theory and breaker height prediction: *Proceedings of the 13th Coastal Engineering Conference*, 405-418.

Komar, P.D. and McKinney, B.A.,1977. The spring 1976 erosion of Siletz Spit, Oregon, with an analysis of the causative storm conditions: *Shore & Beach*, 45, 23-30.

Komar, P.D., Neudeck, R.H., and Kulm, L.D., 1972. Observations and significance of deep-water oscillatory ripple marks on the Oregon Continental Shelf. In: *Shelf Sediment Transport*, Duane and Pilkey (eds.), Dowden, Hutchinson & Ross, Stroudsburg, PA, p.601-619.

Komar, P.D., and Rhee, C.C., 1976. Erosion of Siletz Spit, Oregon: *Shore & Beach*, 44, 9-15.

Komar, P.D., and Shih, S.M., 1993. Cliff erosion along the Oregon coast; A tectonic sea-level imprint plus local controls by beach processes: *Journal of Coastal Research*, 9, 747-765.

Leenknecht, D. A., et. al., 1992. *Automated Coastal Engineering System (ACES), Users Guide*: Coastal Engineering Research Center, U.S. Army Corps of Engineers.

Longuet-Higgins, M.S., 1950. A theory of the origin of microseisms, *Transactions of the Royal Society (London)*, Series A, vol.243, p.1-35.

Miller, H.C., and Jensen, R.E., 1990. Comparison of Atlantic Coast Wave Information Study Hindcasts with Field Research Facility Gage Measurements. CERC Technical Report CERC-90-17, 32 p.

NDBC, 1992. National Data Buoy Center 1992 Annual Report: U.S. Dept. of Commerce, NOAA, 34 p.

Quinn, W.H., Creech, H.C., and Zoph, D.O., 1974. Coastal Wave Observations via seismometer. Mariners Weather Log, 18: 367-369.

Ross, D.B., 1979. On the use of aircraft in the observation of one- and two-dimensional ocean wave spectra: In *Ocean Wave Climate*, edited by M.D. Earle and A. Malahoff, Plenum Press, 253-267.

Seymour, R.J., Sessions, M.H., and Castel, D., 1985. Automated remote recording and analysis of coastal data: *Journal of Waterway, Port, Coastal and Ocean Engineering*, Amer. Soc. Civil Engrs., 111, 388-400.

Shih, S.M., and Komar, P.D., 1994. Sediments, beach morphology and sea cliff erosion within an Oregon coast littoral cell: *Journal of Coastal Research*, 10, 144-157.

Steele, K., and Johnson, A., 1979. Data buoy wave measurements: *Ocean Wave Climate*, edited by M.D. Earle and A. Malahoff, Plenum Press, New York, p.301-316.

Thompson et. al., 1985. Evaluation of the seismometer wave gage and comparative analysis of wave data at Yaquina and Coquille Bays, Oregon. CERC Misc. Paper CERC-85-12, 24 p.

Wang, S., and Le Mehaute, B., 1983. Duration of measurements and long-term wave statistics: Journal of Waterway, Port, Coastal and Ocean Engineering, Amer. Soc. Civil Engrs., 109: 236-249.

Zoph, D.O., Creech, C., and Quinn, W.H., 1976. The wavemeter: A land-based system for measuring nearshore ocean waves: *MTS Journal*, 10, 19-25.